

Aerodynamic engineering of a pulmonary prime-pull vaccine against Tuberculosis

A thesis presented for the degree of
Doctor of Philosophy
from the Institute of Pharmacy and Pharmaceutical Sciences
at the University of Strathclyde

by

Carla Belen Roces Rodriguez

Declaration of Authenticity

'This thesis is the result of the author's original research. It has been composed by the author and has not been previously submitted for examination which has led to the award of a degree.' *'The copyright of this thesis belongs to the author under the terms of the United Kingdom Copyright Acts as qualified by University of Strathclyde Regulation 3.50. Due acknowledgement must always be made of the use of any material contained in, or derived from, this thesis.'*

Signed: Carla B. Roces

Date: 22/10/2018

Acknowledgements

I have so many people to thank that I do not know where to begin. I guess I will do it in chronological order. First, I would like to thank Dennis Christensen from Statens Serum Institut (SSI) for making my Ph.D possible in the first place, and I would also to take the chance to thank Signe, Rune, Jane and Gabriel for the help with the *in vivo* studies. I would like to thank my colleagues from Aston University (Birmingham) where I began my Ph.D. In particular, Jiteen Ahmed for his technical support and for being always available whenever I needed his help. Mandeep and Shital, although we were in different groups you made my life easier at Aston, thank you.

After almost a year at Aston University, we moved up to Glasgow, where I am now, to the University of Strathclyde and we were only 4 people from the group making this move: Maryam, Swapnil, Giulia and myself. I think probably this has been one of the best things that could have happened to me. We, as a group became closer, as it is not easy to start from zero in a new University. They have proved to me that they are good colleagues and better friends. Also, Maryam thanks a lot for the help with the cell work. Besides, during my stay at Strathclyde I met fantastic people, like Maribel. It is not possible to describe how much fun we both had during the few months she did the placement here. Gustavo and Neil joined later making the lab a better place. Especially Neil, my boyfriend, who has been my rock and my best friend. He has seen me going through all the lows and highs during the last two years and remained by my side through all.

I would like to thank my supervisor Professor Yvonne Perrie for all the help, support and fun during my studies. She has been always a great supervisor, sharing good ideas and advice inside and outside the University. So many memories and adventures lived during the past 3 years, including karaokes and unforgettable conferences. Thanks to her I am where I am now.

A mis amigas, Lo Máximo de Gijón, que siempre están ahí para lo bueno y para lo malo, apoyando en la distancia como buenas amigas. Curru, Mari, Luci, Mer, Palo, Bit, Isa y Cami, son ya muchos años juntas y por mucho que pase el tiempo sé que siempre podré contar con vosotras, gracias chicas.

Por último, tengo que agradecer a mi familia, mi madre, mi padre y mi hermana. Sin ellos NADA hubiese sido posible. Ellos son mi verdadero apoyo. No importa la hora ni el día, siempre disponibles para mí, dispuestos a escuchar todos mis problemas y todas mis alegrías. Ellos me han dado la fuerza necesaria para seguir cuando más lo he necesitado, siempre positivos. Millones de gracias por ser así, sois los mejores y os quiero. No podría terminar sin mencionar a mi sobri, que me alegra los días con sus videos y fotos, y sobre todo cuando me llama PIA.

University of Strathclyde

Aerodynamic engineering of a prime-pull vaccine against pulmonary Tuberculosis

Carla B. Roces Rodriguez

Abstract

Tuberculosis (TB) remains the infectious disease with the highest mortality alongside HIV. Despite the existence of the Bacillus Calmette–Guérin (BCG) vaccine there is an unmet need for an effective vaccine against pulmonary TB, the most common form of TB. Traditional vaccines were based on live-attenuated organisms, but nowadays the development of subunit vaccines is attracting the attention of researches largely as a result of the improved safety profile. However, many subunit vaccines lack potent immunogenicity, therefore the inclusion of an adjuvant within the subunit vaccine formulation may be required. Due to the optimal biological properties of the lipids, liposomes are extensively studied as delivery systems along with polymer-based particulate systems such as the well-known poly(lactic-co-glycolic acid) family (PLGA). The cationic liposomal adjuvant formulation (CAF) 01, which is based on the cationic surfactant dimethyldioctadecylammonium (DDA) bromide and the immunopotentiator trehalose 6,6'-dibehenate (TDB) from *Mycobacterium tuberculosis*, has previously been shown to be a strong adjuvant system against several diseases such as TB. CAF01 is commonly prepared by the thin film method which has several drawbacks including scale-up and reproducibility. In contrast, controllable technologies such as microfluidics have advantages in material preparation such as uniform flow and mixing, high efficiency, continuous operation, easy control and low cost. Therefore, initial studies were focused towards method optimisation of CAF01 through microfluidics, followed by *in vivo* evaluation of the optimised formulation (biodistribution and immunisation studies). The second part of the thesis was based in the formulation PLGA nano- and microparticles using microfluidics and the double emulsion method respectively. All formulations were characterised according to their size, polydispersity and surface charge as empty particulate systems and incorporating either ovalbumin (OVA) as a model antigen or the vaccine candidate Ag85B-ESAT6-Rv2660c (H56). Selected PLGA particles were formulated as dry powders for inhalation and for the delivery of the H56 tuberculosis antigen into the deep lungs (alveoli). *In vitro* deposition within the lungs was evaluated using a Pharmacopoeia approved airway simulator, while cell viability, particle uptake and antigen processing was assessed in three macrophages cell lines. Finally, a prime-pull vaccine approach for protection against pulmonary TB was investigated. An immunisation protocol consisting of parenteral (subcutaneous) priming with the TB vaccine candidate H56 alongside CAF01 followed by respiratory mucosal boosting of the H56 within PLGA nano- and microparticles was carried out in order to elucidate if intranasal administration of the H56 antigen produces the desired immunological responses for the protection against pulmonary TB. The immune responses generated indicate the retention of the immunogenicity of the antigen encapsulated within a lyophilised PLGA delivery system, demonstrating the successful scale independent manufacture of polymer based delivery systems encapsulating antigens for inhalation/aerolisation delivery to the lung mucosa.

Keywords: Tuberculosis, prime-pull, vaccine adjuvant, pulmonary delivery

List of Publications

C. B. Roces and Y. Perrie (2018) Fabrication of poly(lactic-co-glycolic acid) (PLGA) particulate delivery systems (in preparation).

C. B. Roces, D. Christensen and Y. Perrie (2018) Scale-independent manufacture of the cationic adjuvant formulation (CAF) 01 retains the immunogenicity of the formulation *in vivo* (in preparation).

A. Wilkinson, E. Lattmann, **C. B. Roces**, G. K. Pedersen, D. Christensen and Y. Perrie (2018). Lipid conjugation of TLR7 agonist Resiquimod ensures co-delivery with the liposomal Cationic Adjuvant Formulation 01 (CAF01) but does not enhance immunopotentiality compared to non-conjugated Resiquimod+CAF01. *Journal of Control Release* (accepted)

S. Joshi, M. T. Hussain, **C. B. Roces**, G. Anderluzzi, E. Kastner, S. Salmaso, D. J. Kirby, Y. Perrie (2016). Microfluidics based manufacture of liposomes simultaneously entrapping hydrophilic and lipophilic drugs. *International Journal of Pharmaceutics*.

C. B. Roces, E. Kastner, P. Stone, D. Lowry and Y. Perrie (2016). Rapid quantification and validation of lipid concentrations within liposomes. *Pharmaceutics*.

Y. Perrie, E. Kastner, S. Khadke, **C. B. Roces**, P. Stone (2015). Manufacturing methods for liposomes. *MiMB, Vaccine adjuvants: methods and protocols*. Springer.

List of Posters and Oral Presentations

C. B. Rocés, D. Christensen and Y. Perrie (**2018**) Scale-independent manufacture of liposomal vaccine adjuvants. 9th APS International PharmSci Conference, Glasgow, United Kingdom. (Best poster prize award)

Internal meeting Work Package 1 (WP 2) Tuberculosis Vaccine Initiative (TBVAC). 7th-8th June **2018** Toulouse, France. (Oral presentation)

C. B. Rocés, D. Christensen and Y. Perrie (**2017**) A comparative study of manufacturing methods for the production of cationic liposomal adjuvants. International Liposome Society, Athens, Greece. Page 89.

C. B. Rocés, D. Christensen and Y. Perrie (**2017**) Formulation and *in vitro* aerosolisation of PLGA nano- and micro-particles for the delivery of TB antigens in the lungs. 8th APS International PharmSci Conference, Hatfield, United Kingdom. Abstract #23

C. B. Rocés, D. Christensen and Y. Perrie (**2017**) Development of an inhaled polymeric antigen carrier systems against pulmonary TB. 44th Controlled Release Society, Boston, United States. Abstract ID 3355. (Poster presentation)

Internal meeting Work Package 1 (WP 2) Tuberculosis Vaccine Initiative (TBVAC). 6th -7st July **2017** Brussels, Belgium. (Oral presentation)

C. B. Rocés, D. Christensen and Y. Perrie (**2017**) Poly(lactic-co-glycolic acid) based micro- and nano-particles for pulmonary delivery of the H56 TB vaccine candidate. United Kingdom and Ireland Controlled Release Society, Cardiff, United Kingdom. Accepted 26th April 2017. (Poster presentation)

C.B. Rocés and Y. Perrie (**2016**) Microfluidics: and easy method for manufacturing of PLGA nanoparticles. 7th APS International PharmSci Conference, Glasgow, United Kingdom. Abstract #141. Accepted 13.06.16 (Poster presentation)

C.B. Rocés and Y. Perrie (**2016**) Characterisation and lipid quantification of liposomal adjuvants using HPLC-ELSD. 7th APS International PharmSci Conference, Glasgow, United Kingdom. Abstract #87. Accepted 13.06.16 (Poster presentation)

C. B. Rocés, D. Christensen and Y. Perrie (**2016**) Microfluidics as a method for preparation of liposomal adjuvants. 43rd Controlled Release Society, Seattle, United States. Abstract #511. Accepted 22.04.16 (Poster presentation)

Internal meeting Work Package 1 (WP 2) Tuberculosis Vaccine Initiative (TBVAC). 30th June-1st July **2016** Ulm, Germany. (Oral presentation)

C. B. Rocés, D. Christensen and Y. Perrie (**2016**) Manufacturing of PLGA nanoparticles as vaccine adjuvants by using microfluidics. Modern Vaccine Adjuvant Formulations, Copenhagen, Denmark. Abstract #106. Accepted 25.04.16 (Poster presentation)

C. B. Rocés, D. Christensen and Y. Perrie (**2016**) Engineering of liposomes as vaccine adjuvants using microfluidics. United Kingdom and Ireland Controlled Release Society, Cardiff, United Kingdom. Accepted 07.03.15 (Poster presentation)

TBVAC Symposium: TB vaccines and immunity, Work Package 1 (WP 1). 1st-5th February **2016**, Les Diablerets, Switzerland. (Oral presentation)

C. B. Roces, D. Lowry, L. Marshall and Y. Perrie (**2015**) Preparation of liposomal adjuvants using microfluidics. International Liposome Society, London, United Kingdom. Accepted 20.11.15 (Poster presentation)

C. B. Roces and Y. Perrie (**2015**) Microfluidics as manufacturing method for polymer-based delivery systems. RPS Pharmaceutical Science Poster event, London (UK). (Poster presentation)

C. B. Roces and Y. Perrie (**2015**) Manufacturing of nanoparticles as adjuvants for vaccine delivery. Enhancing Nanoparticle Formulation and Scale Up, Microfluidics user group meeting, Birmingham (UK) (Poster and oral presentation)

Table of Contents

Acknowledgements.....	2
Abstract.....	3
List of Publications	4
List of Posters and Oral Presentations.....	5
Table of contents	7
List of Tables	15
List of Figures	18
Abbreviations.....	29
Chapter 1: General Introduction	33
1.1 Tuberculosis (TB).....	34
1.1.1 The pathogen: <i>Mycobacterium tuberculosis</i> (Mtb)	35
1.1.2 TB transmission: airborne infection.....	35
1.1.3 TB histological structure: Granulomas.....	36
1.1.4 Immunity to TB.....	36
1.1.4.1 Innate immune response to TB.....	36
1.1.4.2 Adaptive immune response to TB.....	37
1.1.5 TB vaccine: Bacilli–Calmette–Guerin (BCG)	37
1.2 Vaccine approaches for TB.....	38
1.2.1 Modification, boosting or replacement of BCG	41
1.2.2 Vaccine design: live attenuated, inactivated or subunit vaccines	42
1.2.3 Vaccine targeting disease stage: pre- or post-exposure and therapeutic vaccination.....	42
1.3 TB vaccine candidate: Hybrid 56 (H56)	43
1.4 Methods for enhancing immunogenicity: ADJUVANTS	44
1.4.1 Lipid-based adjuvants: Liposomes	45
1.4.1.1 The Cationic Adjuvant Formulation (CAF) 01.....	46
1.4.2 Biodegradable polymer-based adjuvants: Poly lactic-co-glycolic acid (PLGA)	48
1.4.2.1 Effect of the PLGA composition: degradation rate and release profile	49
1.5 Pulmonary delivery	50

1.5.1	Particle deposition in the lungs: Impaction, sedimentation and diffusion.....	51
1.5.2	Alveolar macrophages (AM) particle uptake: endocytosis.....	52
1.6	Hypothesis and general objectives	53
Chapter 2: Scale-Independent manufacture of liposomal cationic adjuvants.....		54
2.1	Introduction	55
2.2	Aim and objectives.....	55
2.3	Materials and methods.....	56
2.3.1	Material used for the preparation of liposomal formulations.....	56
2.3.2	Methods for manufacturing liposomes	57
2.3.2.1	Lipid film hydration method (LH).....	57
2.3.2.2	High shear mixing (HSM).....	58
2.3.2.3	Microfluidics (MF)	59
2.3.3	Purification of the liposomal formulations	60
2.3.3.1	Dialysis purification	60
2.3.3.2	Ultracentrifugation	61
2.3.4	Gas chromatography (GC) for quantification of residual solvent.....	61
2.3.5	Determination of the particle size, polydispersity and zeta potential by dynamic light scattering (DLS)	63
2.3.6	Quantification of antigen loading and lipid recovery by High Performance Liquid Chromatography using an Evaporative Light Scattering Detector (HPLC-ELSD).....	64
2.3.7	Sodium dodecyl sulfate (SDS) polyacrylamide gelelectrophoresis (PAGE) for the qualitative analysis of the protein loaded	66
2.3.8	Statistical analysis	67
2.4	Results and discussion	67
2.4.1	Production of CAF01 liposomes using the microfluidics technique Nanoassemblr™	67
2.4.1.1	Effect of the lipid concentration	67
2.4.1.2	Effect of the total flow rate (TFR) and flow rate ratio (FRR).....	70
2.4.2	Quantification of the residual solvent after purification of the formulation	73
2.4.3	Evaluation of the impact of the manufacturing technique on the production of CAF01 and CAF01-based liposomes.....	74

2.4.4 Loading of ovalbumin (OVA) as a model antigen onto the preformed liposomal adjuvant formulations.....	80
2.4.4.1 Quantification of the lipid concentration using HPLC-ELSD	84
2.4.4.2 Quantification of the individual lipid recovery after process manufacture	90
2.5 Conclusions	92
Chapter 3: <i>In vivo</i> biodistribution and immunogenicity of CAF01 liposomal formulations manufactured by different methods.....	93
3.1 Introduction	94
3.2 Aim and objectives.....	94
3.3 Materials and methods.....	95
3.3.1 Material used for the preparation of liposomal formulations.....	95
3.3.2 Material used for the radiolabelling of the vaccine components and biodistribution study ...	95
3.3.3 Material used for the immunisation studies	95
3.3.4 Biodistribution studies in mice of radiolabelled vaccine components.....	96
3.3.4.1 Radiolabelling of the tuberculosis antigen H56.....	96
3.3.4.2 Radiolabelling of the liposomal formulations.....	97
3.3.4.3 Pontamine blue injection.....	98
3.3.4.4 Organ and tissue processing for the quantification of the radioactive isotopes.....	98
3.3.4.5 Stability of liposomes in simulated <i>in vivo</i> conditions.....	100
3.3.5 Immunisation studies in mice	100
3.3.5.1 Preparation of the vaccine formulations.....	100
3.3.5.2 Dynamic light scattering	100
3.3.5.3 Quantification of H56 antigen loading by HPLC-UV.....	101
3.3.5.4 Animal ethics and immunisation protocol.....	102
3.3.5.5 Antibody analysis	102
3.3.5.6 Re-stimulation of the splenocytes and lymph nodes.....	104
3.3.5.7 Cytokine analysis of restimulated splenocytes, lymphocytes and at the injection site	105
3.3.5.8 Processing of the site of injection.....	106

3.3.6	Statistical analysis	106
3.4	Results and discussion	107
3.4.1	Physicochemical characterisation of the CAF01:H56 adjuvant formulations prepared for biodistribution	107
3.4.2	Interaction of liposomes with serum proteins in simulated <i>in vivo</i> condition	108
3.4.3	The effect of the manufacturing method on the pharmacokinetic profile of the DDA:TDB formulation <i>in vivo</i>	110
3.4.3.1	Detection of the vaccine components at the site of injection (SOI)	110
3.4.3.2	Detection of the vaccine components at the lymph nodes (POP, ILN and MLN)	113
3.4.4	Effect of the manufacturing method on the immunogenicity of the formulation	115
3.4.4.1	Physicochemical characterisation of the liposomal formulations for immunisation	115
3.4.4.2	Antigen specific antibody secretion detected in serum	116
3.4.4.3	Cytokine secretion analysis from restimulated splenocytes and lymphocytes	117
3.4.4.4	Cytokine detection at the injection site	118
3.5	Conclusions	119
	Chapter 4: Manufacture of PLGA particulate delivery systems	120
4.1	Introduction	121
4.2	Aim and objectives	121
4.3	Materials and methods	122
4.3.1	Materials	122
4.3.2	Methods for the manufacture of poly(lactic-co-glycolic acid) particles for antigen delivery: ..	122
4.3.2.1	Manufacturing of poly(lactic-co-glycolic acid) nanoparticles by using microfluidics (Nanoassemblr™)	122
4.3.2.2	Manufacturing of poly(lactic-co-glycolic acid) microparticles using the double emulsion (w/o/w) solvent evaporation method	123
4.3.3	Characterisation of the PLGA particles by dynamic light scattering (DLS)	124
4.3.3.1	Malvern nano ZS	124
4.3.3.2	Mastersizer 2000	125
4.3.3.3	Malvern AT-line	125
4.3.4	Stability test: The effect of PVA content	126

4.3.5	Purification of the PLGA nanoparticles: solvent removal and non-encapsulated antigen	126
4.3.5.1	Dialysis for removal of organic solvent	126
4.3.5.2	Tangential Flow Filtration (TFF) for removal of non-encapsulated antigen	126
4.3.6	Quantification of the residual solvent by gas chromatography (GC)	127
4.3.7	High Performance Liquid Chromatography (HPLC).....	127
4.3.7.1	HPLC-UV for antigen quantification	127
4.3.7.2	HPLC-ELSD for quantification of polymer recovery	128
4.3.8	Bicinchoninic acid assay (BCA) for the quantification of polymer recovered after purification of the nanoparticles using TFF	129
4.3.9	Release studies at different temperatures	129
4.3.10	Morphological characterisation of the nanoparticles	129
4.3.10.1	Scanning electron microscopy (SEM).....	129
4.3.10.2	Cryogenic transmission electron microscopy (CryoTEM)	130
4.3.11	Statistical analysis	130
4.4	Results and discussion	131
4.4.1	Microfluidics manufacturing of PLGA nanoparticles: the effect of process parameters.....	131
4.4.2	Continuous processing of nanoparticles: AT-line particle size analysis.....	135
4.4.3	Quantification of the residual solvent within the formulation after purification of the nanoparticles by dialysis and effect of the purification method on the physicochemical characteristics of the PLGA-NPs.....	137
4.4.4	Quantification of the polymer recovered after manufacturing of PLGA nanoparticles	140
4.4.5	The effect of microfluidic process parameters on the physicochemical characteristics and loading efficiencies of the PLGA-NPs.	142
4.4.5.1	Effect of the Flow Rate Ratio (FRR) in the physicochemical characteristics and encapsulation efficiency of the PLGA nanoparticles	143
4.4.5.2	Effect of the Total Flow Rate (TFR) on the physicochemical characteristics and encapsulation efficiency of the PLGA nanoparticles	146
4.4.6	Effect of the initial antigen concentration loaded in the physicochemical characteristics and encapsulation efficiency of the PLGA nanoparticles	148
4.4.7	Varying the antigen incorporated within the nanoparticles.....	150

4.4.8	The effect of the addition of a stabiliser into the PLGA nanoparticles.....	152
4.4.9	Morphological characterisation of the PLGA nanoparticles	154
4.4.10	PLGA nanoparticles: Antigen release studies	155
4.4.11	Manufacture of microspheres	161
4.5	Conclusions	163
Chapter 5: Aerodynamic engineering of a PLGA antigen delivery system for pulmonary delivery 165		
5.1	Introduction	166
5.2	Aim and objectives.....	166
5.3	Materials and methods.....	167
5.3.1	Materials	167
5.3.2	Preparation of PLGA nanoparticles.....	167
5.3.3	Purification of the PLGA nanoparticles: removal of non-encapsulated antigen	168
5.3.4	Preparation of PLGA microparticles by the double emulsion method.....	168
5.3.5	Freeze drying of nano- and microparticles.....	168
5.3.6	Antigen release study of PLGA reconstituted nanoparticles	169
5.3.7	HPLC-UV for antigen quantification.....	169
5.3.8	HOT-stage microscopy	170
5.3.9	Dynamic Light Scattering	170
5.3.9.1	Malvern nano ZS	170
5.3.9.2	Mastersizer 2000	170
5.3.10	Scanning electron microscopy	171
5.3.11	Pharmacopoeia airway simulator: Next Generation Impactor (NGI)	171
5.3.12	Bicinchoninic acid assay (BCA) for the quantification of polymer recovered after NGI	172
5.3.13	<i>In vitro</i> studies.....	172
5.3.13.1	Cell viability	173
5.3.13.2	Particle uptake	174
5.3.13.3	DQ-OVA processing.....	174
5.4	Results and discussion	175

5.4.1	Selection of the adequate cryoprotectant.....	175
5.4.1.1	Effect of sucrose.....	176
5.4.1.2	Effect of leucine	179
5.4.1.3	The effect of combining both sucrose and leucine within a dried nanoparticle product ..	181
5.4.2	Characterisation of the PLGA particulate delivery systems (nano- and microparticles) after Freeze-drying	183
5.4.3	Antigen release profiles from PLGA nanoparticles	188
5.4.4	Thermal analysis of the dry powder PLGA formulations using HOT-Stage microscopy	191
5.4.5	Morphological characterisation of the antigen loaded PLGA nano- and micro-particles	197
5.4.6	Aerosol performance of the dried powder PLGA particles.....	200
5.4.7	<i>In vitro</i> studies in different cell lines.....	204
5.4.7.1	Cell viability studies.....	204
5.4.7.2	<i>In vitro</i> uptake studies in macrophages cell lines	204
5.4.7.3	DQ-OVA processing of PLGA particulate delivery systems	209
5.5	Conclusions	212
	Chapter 6: An <i>in vivo</i> model: prime-pull vaccination by priming with CAF01:H56 and boosting with PLGA:H56	213
6.1	Introduction	214
6.2	Aim and objectives.....	214
6.3	Materials and methods.....	215
6.3.1	Materials	215
6.3.2	Preparation of PLGA nanoparticles for nasal delivery	215
6.3.3	Preparation of PLGA microparticles for nasal delivery	215
6.3.4	Immunisation protocol	216
6.3.5	Organ processing	217
6.3.5.1	Lungs	218
6.3.5.2	Spleens	218
6.3.6	Antibodies ELISA	218

6.3.7	Cytokines ELISA	218
6.3.8	Intracellular FACs staining (icFACS).....	219
6.4	Results and discussion	219
6.4.1	Preparation of PLGA nano- and microparticles for the nasal delivery of H56 vaccine candidate: rational design	220
6.4.2	Prime-pull vaccination: immunological responses	221
6.4.2.1	Humoral immune responses: IgG quantification	221
6.4.2.2	Cellular mediated immune responses: cytokine production and T cell location.....	222
6.4.2.3	Specific location of the T-cell responses.....	226
6.5	Conclusions	232
Chapter 7: Overall Conclusions and Future Work		233
7.1	The need for a new Tuberculosis (TB) vaccine.....	234
7.2	The use of microfluidics as a tool for the manufacture of CAF01	234
7.3	<i>In vivo</i> studies with CAF01 liposomal formulation manufactured by microfluidics retains its biodistribution profile and immunogenicity	236
7.4	Scale independent production of PLGA delivery systems	236
7.5	Aerodynamic engineering of a TB vaccine for lung delivery.....	238
7.6	Prime-pull immunisation stimulates cytokine production in the lung parenchyma	239
7.7	Concluding remarks and future work	240
References.....		241

List of Tables

Chapter 1: General Introduction

Table 1.1 TB vaccine candidate pipeline currently in clinical trials. Data source: Tuberculosis Vaccine Initiative (TBVI) website (www.tbvi.com)..... 39

Table 1.2 TB vaccine candidates currently in clinical trials and classified according to the targeted vaccine stage [53]. 43

Chapter 2: Scale-Independent manufacture of liposomal cationic adjuvants

Table 2.1: Information about the lipids used for the formulation of liposomal adjuvants..... 57

Table 2.2 Methods used for solvent and protein removal..... 61

Table 2.3 General classification of residual solvents according to ICH guidelines. Only some examples are shown [169] 62

Table 2.4 Boiling points of the organic solvents used during the microfluidic formulation of the liposomal adjuvants and the selected internal standard..... 63

Table 2.5 HPLC methods: **(A)** Gradient elution method for the quantification of cholesterol, DMPC, TDB and DDA. Gain was adjusted for each lipid, being Gain 12 for TDB and Gain 3 for the rest of the lipids; **(B)** Method used for the quantification of OVA loading efficiency. Retention time 12.2 min. Gain 10. 65

Table 2.6 Lipid concentrations (mg/mL) used for the formulation of the four liposomal formulations: DDA and TDB concentrations were fixed at 2.5 mg/mL and 0.5 mg/mL (CAF01) respectively and cholesterol was added to the CAF01 formulation at two different concentrations (low = 0.4 mg/mL and high = 0.8 mg/mL). In the fourth formulation, DDA was completely replaced by 1,2-dimyristoyl-sn-glycero-3-phosphocholine (DMPC) and kept at the original concentration..... 75

Table 2.7 Calculated LOQ and LOD values for each lipid. TDB was the most difficult compound to quantify due to the low concentrations used within the liposomal formulations which was depicted by the intensity peaks obtained from the chromatogram. The determined LOD and LOQ were 0.11–0.36 mg/mL, 0.02–0.08 mg/mL, 0.06–0.20 mg/mL, and 0.05–0.16 mg/mL for DDA, cholesterol, DMPC and TDB respectively..... 87

Chapter 3: *In vivo* biodistribution and immunogenicity of CAF01 liposomal formulations manufactured by different methods

Table 3.1 List of liposomal formulations selected for the biodistribution studies in mice. The lipid concentrations correspond to the initial concentration used in order to have equal final lipid composition in all the formulations..... 98

Table 3.2 Liposomal formulations selected for the immunisation study. Lipid concentrations correspond to the initial concentrations used for the preparation of the liposome adjuvants..... 100

Chapter 4: Manufacture of PLGA particulate delivery systems

Table 4.1 DLS Instrument parameters for particle size measurements using dynamic light scattering (DLS). 125

Table 4.2 HPLC-UV method followed for the quantification of encapsulated antigen within the polymer nano- and micro-particles using 210 nm UV wavelength [215, 216]. 128

Table 4.3 Gradient method used for the quantification of the polymer recovered after microfluidics using HPLC-ELSD [217]. 128

Table 4.4 Effect of the initial antigen concentration loaded on the physicochemical characteristics and antigen loaded of the PLGA NPs produced using microfluidics at FRR 1:1 and TFR 10 mL/min. Results represent mean \pm SD of triplicate measurements. 151

Chapter 5: Aerodynamic engineering of a PLGA antigen delivery system for pulmonary delivery

Table 5.1 Type and concentration of cryoprotectant used for the formulation of PLGA nanoparticles in powder format. 169

Table 5.2 Cut-off diameters of the Next Generation Impactor stages at flow rate $60 \pm 5\%$ L/min. .. 172

Table 5.3 Physicochemical characteristics of the empty and antigen loaded PLGA nanoparticles manufactured using microfluidics TFR 10 mL/min, FRR 1:1 containing 10% (w/v) sucrose and 1% LEU (w/v) before freeze drying and after reconstitution of the dried powders. All results represent the mean \pm SD of at least 3 different batches. 185

Table 5.4 Physicochemical characteristics of the empty and antigen loaded PLGA microparticles manufactured using microfluidics TFR 10 mL/min, FRR 1:1 containing 10% (w/v) sucrose and 1% LEU (w/v) before freeze drying in and after reconstitution of the dried powders. All results represent the mean \pm SD of at least 3 different batches. 186

Table 5.5 Results from the release study carried out on PLGA NPs loading OVA before freeze drying and described in Chapter 4. 188

Table 5.6 The table shows the calculated aerolisation parameters of the PLGA powders prepared using freeze drying: fine particle dose (FPD), fine particle fraction (FPF), emitted dose (ED) and respirable fraction (FR), after Next Generation Impactor (NGI). 203

Chapter 6: An *in vivo* model: prime-pull vaccination by priming with CAF01:H56 and boosting with PLGA:H56

Table 6.1 Methods used for increase the recovery of the antigen after concentration using Vivacon 2 (MWCO 50,000) 216

Table 6.2 Vaccines administered to the CB6F1 female mice for the immunisation study following a prime-pull protocol. All mice were parenterally primed twice with CAF01:H56 except for the unvaccinated group. Each group was boosted with the same H56 antigen dose encapsulated in either PLGA NPs (50:50, 75:25 and 85:15) or PLGA 85:15 MPs. 217

List of Figures

Chapter 1: General Introduction

- Figure 1.1** World map showing the estimated incidence of TB in 2016 (WHO report 2017)[1]. 34
- Figure 1.2** Schematic representation of the main characteristics related to liposomes in terms of characterisation. 46
- Figure 1.3** Molecular structure of (A) the cationic surfactant DDA and (B) the immunopotentiator TDB, the two components of the CAF01 formulation. 47
- Figure 1.4** Poly lactic-co-glycolic acid (PLGA) molecular structure (x = number of units PLA; y = number of units of PGA). 49

Chapter 2: Scale-Independent manufacture of liposomal cationic adjuvants

- Figure 2.1** Schematic representation of thin film method: (A) lipids dissolved in organic solvent, (B) formation of the lipid film, (C) addition of the buffer above T_m and under agitation to form MLVs, (D) Incorporation of antigen/protein post liposome formulation..... 58
- Figure 2.2** Representation of HSM method: (A) lipids dissolved in organic solvent, (B) formation of the lipid film, (C) addition of the buffer, formulation mounted in a water bath and immersion of the HSM probe, (D) formation of SUVs, (E) antigen loading after liposome formation..... 59
- Figure 2.3** Representation of microfluidics cartridge: Aqueous phase (inlet 1) and lipids in solvent (inlet 2) are injected into the microfluidics system and liposomes are formed by a nanoprecipitation reaction and collected in the outlet. 60
- Figure 2.4** Dialysis process: (1) pre-treatment of the dialysis membrane to remove any contaminant, (2) close one of the ends and introduce the sample, (3) close the other end, (4) dialyse the sample against the adequate amount of buffer under stirring and exchange the buffer according to the method selected. 61
- Figure 2.5** Schematic representation of the mechanism of an evaporative light scattering detector (ELSD). First, the chromatographic effluent passes through the nebulizer and mixes with the nebulizing gas (N_2) causing dispersion of droplets. Subsequently, droplets enter into the nebulizing chamber where the mobile phase evaporates and condense, being removed as waste. Finally, the analyte crosses an optical cell, a laser beam penetrates the particles and the scattered light is detected and converted into a signal..... 64
- Figure 2.6** Simplified representation of SDS-PAGE technique: Gels are placed within the apparatus and samples are loaded on the top of it. Then proteins move through the porous gel from the top to the bottom due to an electrical current. The speed at which particles are drawn through the matrix depends on their mass..... 66

Figure 2.7 Physicochemical characteristics of the CAF01 adjuvant formulations manufactured using microfluidics at TFR 10 mL/min, FRR 3:1 and varying the initial concentration from 0.3 to 24 mg/mL (A) Particle size (B) PDI and (C) Zeta potential. Results represent the mean \pm SD from at least 3 independent experiments.....	69
Figure 2.8 The impact of the different parameters adopted during microfluidics formulation of CAF01 liposomes. The (A) particle size (bars) and PDI (dots) and (B) zeta potential of the CAF01 liposomes manufactured by using microfluidics at flow rate ratios of 1:1, 3:1 and 5:1 and flow rates of 5, 10 and 15 mL/min. Results represent the mean \pm SD from at least 3 independent experiments.	71
Figure 2.9 Gas chromatography: (A) 2-propanol calibration curve and (B) Concentrations (%) of solvent in the liposomal samples produced using microfluidics after the different 1 and 4 hours dialysis. Results represent the mean \pm SD from at least 3 independent experiments.	74
Figure 2.10 Physicochemical characteristics (size, PDI and ZP) of the empty CAF01 and CAF01-based liposomal formulations manufactured using (A, D) the traditional LH method, (B, E) HSM and (C, F) MF. Particle size (bars) and PDI (dots). Results represent the mean \pm SD of at least 3 independent batches.....	79
Figure 2.11 Physicochemical characteristics (size, PDI and ZP) of the OVA loaded CAF01 and CAF01-based liposomal formulations manufactured using (A, D) the traditional LH method, (B, E) HSM and (C, F) MF. Particle size (bars) and PDI (dots). Results represent the mean \pm SD of at least 3 independent batches.....	81
Figure 2.12 Percentage of antigen (OVA) loaded onto the liposomal adjuvants manufactured using (A) lipid film hydration methods (LH), (B) high shear mixing (HSM) and (C) microfluidics. Results represent the mean \pm SD of at least 3 independent batches. (D) SDS-Page gel of the liposomal formulations after preparation by LH method. Protein is attached to the cationic liposomes as we can see it is in the pellet (P) whereas in the neutral liposomes the protein is not attached to them and therefore it appears in the supernatant (S).	83
Figure 2.13 HPLC-ELSD chromatogram showing the four lipids used for the preparation of liposomal formulations: DDA (1.5 mg/mL), DMPC (1.5 mg/mL), cholesterol (2 mg/mL) and TDB (1 mg/mL). The ELSD gain was 3 for DDA, DMPC and cholesterol whereas TDB was quantified at gain 12.	85
Figure 2.14 Calibrations curves of (A) DDA (from 0.125 – 2.5 mg/mL) (B) TDB (from 0.2 – 1 mg/mL) (C) Cholesterol (from 0.125 – 1 mg/mL) and (D) DMPC (0.25 to 2.5 mg/mL) obtained from the HPCL-ELSD using gain 3 for DDA, DMPC and cholesterol and gain 12 for TDB. Results represent the mean \pm SD of at least 3 independent batches.	86
Figure 2.15 Method validation for cholesterol as a model compound (reproducibility and repeatability): (A) Intraday (same day) and (B) interday (different days) reproducibility. Cholesterol	

concentration range used from 0.25 to 1 mg/mL. Results represent the mean \pm SD of at least 3 independent batches. 88

Figure 2.16 Method validation for cholesterol (robustness): (A) elution peaks at different column temperatures and (B) elution peaks at different flow rates. 89

Figure 2.17 Lipid recovery quantification for the four liposomal formulations manufactured using the lipid film hydration (LH), high shear mixing (HSM) and microfluidics at FRR 1:1, 3:1 and 5:1 (A) CAF01 (DDA-TDB) (B) CAF01 + 18mol% cholesterol, (C) CAF01 + 31mol% cholesterol and (D) DMPC-TDB. .. 91

Chapter 3: *In vivo* biodistribution and immunogenicity of CAF01 liposomal formulations manufactured by different methods

Figure 3.1 Diagram showing the incorporation of ¹²⁵I into amino acid residues of proteins during the radiolabelling procedure. 96

Figure 3.2 Overlay plots of the BCA assay (white) and beta counts (black) for the separation of the non-labelled H56 antigen for the biodistribution study. BCA assay was carried out in order to quantify where the H56 antigen was located within the aliquots whereas the beta counting was performed for the confirmation of radiolabelling of the antigen. Aliquots containing both antigen and Iodine were pooled together and diluted for future use. 97

Figure 3.3 Calibration curve with different volumes of iodine to eliminate the iodine overspill in the tritium region. Counts per minute A (CPM) which correspond to the region A (0 – 18.6 KeV) was plotted on the y-axis against the CPM B (x-axis) which correspond to the region (0 – 80 keV). 99

Figure 3.4. (A) Calibration curve for the H56 antigen in 50% IPA/Tris (1:1 v/v) and (B) HPLC-UV setting used for its quantification. Results represent the mean value of at least 3 independent experiments \pm SD. 101

Figure 3.5 Scheme of the immunisation protocol followed in this study. Three intramuscular injections containing CAF01:H56 manufactured using either the lipid film hydration or microfluidics were administered with 2 week interval in between. Blood was collected at days 7, 21 and 49 whereas organs were isolated and processed at the end of the study on day 49. 102

Figure 3.6 Outline of the ELISA plate set-up used for the antibody analysis study and schematic representation of direct ELISA protocol followed. 103

Figure 3.7 Schematic representation of the haemocytometer grid for the cell count and equation followed for calculation of the viable cells. 104

Figure 3.8 Outline of the ELISA plate set-up used for the cytokine analysis study. Samples were plated in duplicate. ConA was used at a concentration of 5 μ g/mL as a positive control RPMI media was used as a negative control and H56 antigen for the quantification of antigen-specific responses. 105

Figure 3.9 Schematic representation of sandwich ELISA protocol followed for the quantification of cytokines in the spleen, popliteal lymph node and site of injection.	106
Figure 3.10 Physicochemical attributes (A) size (bars), PDI (dots), ZP (values) and (B) loading efficiency (as percentage) of the formulations selected for the biodistribution study. Non-radiolabelled formulations were prepared in triplicate using the same lipid stock as for the biodistribution study. Results represent the mean value of at least 3 independent experiments \pm SD.	108
Figure 3.11 Stability study of the liposomal formulations under simulated <i>in vivo</i> conditions. Physicochemical characteristics of CAF01 LH under simulated <i>in vivo</i> conditions (50% FCS and 37°C). (A) Particles size (B) polydispersity and (C) zeta potential. Results represent the mean value of at least 3 independent experiments \pm SD.....	109
Figure 3.12 Biodistribution study: Percentage of (A) liposomes and (B) antigen retained at the site of injection (SOI). Dual labelling of liposomes and antigen by incorporating either ^3H or ^{125}I was used for the detection of the individual components of the vaccine at different time points. Results represent the mean of 3 mice \pm standard deviation.	111
Figure 3.13 Pictures of the site of injection from all four groups at selected time points. Mice were injected with pontamine blue 3-4 days prior the start of the experiment as a marker to detect the monocytes influx and to visualise the lymph nodes by dying the macrophages.	112
Figure 3.14 Biodistribution study: Percentage of liposomes and antigen detected in the (A, D) ILNs, (B, E) POP and (C, F) MLNs. Dual labelling of liposomes and antigen by incorporating either ^3H or ^{125}I was used for the detection of the individual components of the vaccine at different time points. Results represent the mean of 3 mice \pm standard deviation.....	114
Figure 3.15 Physicochemical characteristics of the liposomal adjuvant formulations used for the immunisation study in mice (A) Particle size (bars), PDI (dots) and ZP (values), (B) antigen loading and (C) lipid recovery. (D) Average mice weight. Results represent the mean value of at least 3 independent experiments \pm SD.	115
Figure 3.16 Antigen-specific (A) IgG1 and (B) IgG2c responses. C57BL/6 mice were intramuscularly immunised with H56 combined with different adjuvants and humoral response was analysed in blood. H56-specific IgG1 serum response detected by ELISA on sera collected (A) 7, (B) 21 and (C) 49 days after i.m. immunization. Antibody titres were expressed as the reciprocal of the highest dilution with an OD value ≥ 0.1 after background subtraction.....	116
Figure 3.17 Cytokine production in splenocyte and lymph node (POP) culture supernatants (A) IL-5 (B) IL-17 and (C) IFN-γ. C57BL/6 mice were intramuscularly immunized with H56 combined with different and spleens were collected 3 weeks after the last immunization. Values, expressed as	

picograms per milliliter, are reported as the mean value \pm SD of H56-stimulated of five animals per group..... 118

Figure 3.18 Cytokine production at the injection site (A) IFN- γ (B) IL-5 and (C) IL-17. C57BL/6 mice were intramuscularly immunized with H56 combined with different adjuvants and site of injections were excised 3 weeks after the last immunization. Values, expressed as picograms per miligram, are reported as the mean value \pm SD of H56-stimulated of five animals per group. 119

Chapter 4: Manufacture of PLGA particulate delivery systems

Figure 4.1 Schematic representation of microfluidics cartridge from Precision Nanosystems. There are two inlets where the aqueous (inlet 1) and organic phase (inlet 2) are injected in. Both fluids are mixed at the selected ratio (FRR) and speed (TFR) and by chaotic lamellar flow nanoparticles are formed and collected in the outlet..... 123

Figure 4.2 Schematic representation of double emulsion ($w_1/o/w_2$) solvent evaporation method. Initial primary water in oil (w_1/o) emulsion is formed by dispersion of an aqueous solution with or without antigen (w_1) into an organic polymer solution. This primary emulsion is then added into a secondary water phase solution containing 10% PVA and homogenised at high speed for 3 min. Solvent is evaporated overnight. Next day, samples are centrifuged and washed with ultrapure water 3 times to remove any non-incorporated trace of PVA. In the final centrifugation step, the pellet is reconstituted with the desired volume of buffer..... 124

Figure 4.3 Effect of the process parameters from the microfluidics system in the physicochemical characteristics of the PLGA nanoparticles (A) FRR 1:1, (B) FRR 3:1 and (C) FRR 5:1 and (D) zeta potential. Results represent the mean \pm SD of at least three independent batches..... 134

Figure 4.4 Comparative study of the size measurements obtained with Malvern OFF-line and AT-line in order to demonstrate the capability of the microfluidics method for continuous manufacturing of PLGA nanoparticles. Particle sizes and intensity graphs of the PLGA 85:15, 75:25 and 50:50 nanoparticles manufactured by using microfluidics at TFR 10 mL/min and FRR 1:1. 136

Figure 4.5 Gas chromatography results: (A) Calibration curve of the analyte of interest (acetonitrile) and (B) percentage of residual solvent after dialysis. Results represent mean \pm SD of triplicate measurements. 138

Figure 4.6 Physicochemical characteristics of the PLGA nanoparticles after microfluidics, dialysis and tangential flow filtration: (A) Particle size, (B) Particle size distribution and (C) Zeta potential. Results represent mean \pm SD of triplicate measurements..... 139

Figure 4.7 (A) HPLC-ELSD chromatogram showing the elution peaks for the copolymers 85:15, 75:25 and 50:50 and (B) their calibration curve with the calculated LOD and LOQ values for each polymer. Results represent mean \pm SD of triplicate measurements. 140

Figure 4.8 Polymer recovery of PLGA 85:15, 75:25 and 50:50 NPs manufactured through the microfluidics method: TFR 10 mL/min and FRR 1:1, 3:1, 5:1. Results represent mean \pm SD of triplicate measurements.	141
Figure 4.9 BCA assay for the quantification of PLGA within the nanoparticles after TFF: (A) Calibration curves obtained from the BCA assay using dialysed samples as standards and the LOQ and LOD values calculated for each polymer; (B) calculated recovery after TFF. Results represent mean \pm SD of triplicate measurements.	142
Figure 4.10 Effect of the flow rate ratio (FRR) on the physicochemical characteristics of the PLGA NPs produced using microfluidics at TFR 10 mL/min and encapsulating OVA as a model antigen: (A) Particle size and particles size distribution, (B) zeta potential and (C-D) encapsulation efficiency as percentage of PLGA NPs encapsulating 0.2 and 0.5 mg/mL OVA respectively. Results represent mean \pm SD of at least triplicate measurements.	145
Figure 4.11 Effect of the total flow rate (TFR) on the physicochemical characteristics of the PLGA NPs produced using microfluidics at FRR 1:1 and encapsulating OVA as a model antigen: (A) Particle size and particles size distribution, (B) zeta potential and (C) encapsulation efficiency. Results represent mean \pm SD of at least triplicate measurements.	147
Figure 4.12 Effect of the initial antigen concentration loaded on the physicochemical characteristics of the PLGA NPs produced using microfluidics at FRR 1:1 and TFR 10 mL/min: (A) Particle size and particles size distribution and (B) zeta potential. The encapsulation efficiency (solid line) vs amount of antigen loaded (dotted line) for (C) PLGA 50:50, (D) PLGA 75:25 and (E) PLGA 85:15. Results represent mean \pm SD of triplicate measurements.	149
Figure 4.13 Calibration curves calculated from the HPLC-UV responses: (A) Ovalbumin standards, (B) H56 TB antigen standards, (C) Bovine Serum Albumin standards and (D) calculated limit of detection and limit of quantification for each antigen. Results represent mean \pm SD of triplicate measurements.	150
Figure 4.14 Effect of the incorporation of different concentrations of PVA as stabiliser in the PLGA 75:25 nanoparticles formulated using microfluidics TFR 10 mL/min and FRR 1:1: (A) particle size (grey dots) and PDI (black dots) and (B) Zeta potential. A stability study of the particles was carried out for a month: (C) particle size and (D) size distribution of H56 loaded PLGA 75:25. Different amounts of PVA (0.5%, 1% and 2%) were added into the aqueous phase in order to compare the stability of the nanoparticles over the period of one month. Results represent mean \pm SD of triplicate measurements.	153

Figure 4.15 (A-B) CryoTEM micrographs of PLGA 75:25 nanoparticles manufactured using microfluidics at TFR 10 mL/min and FRR 5:1. Particles are in the nanometre range and show a regular and spherical shape..... 154

Figure 4.16 SEM micrographs (A) empty PLGA 75:25 NPs FRR 1:1 (B) empty PLGA 75:25 NPs FRR 3:1, (C) empty PLGA 75:25 NPs FRR 5:1, (D) antigen loaded PLGA 85:15 , (E) antigen loaded PLGA 75:25 FRR 1:1 after dialysis, (F) antigen loaded PLGA 50:50 FRR 1:1 after dialysis, (G) antigen loaded PLGA 85:15 FRR 1:1 after TFF, (H) antigen loaded PLGA 75:25 FRR 1:1 after TFF and (I) antigen loaded PLGA 50:50 FRR 1:1 after TFF. 155

Figure 4.17 Particle size and PDI of the PLGA (A) 50:50, (B) 75: 25 and (C) 85:15, (D-F) overlay intensity plots and (G) ZP values at the selected time points measured for the release study. (H) Release study at 37°C of the PLGA 85:15, 75:25 and 50:50 nanoparticles manufactured by using microfluidics at a TFR of 10 mL/min and FRR 1:1. Results represent mean ± SD of at least triplicate measurements. . 158

Figure 4.18 Particle size and PDI of the PLGA (A) 50:50, (B) 75:25 and (C) 85:15, (D-F) overlay intensity plots and (G) ZP values at the selected time points measured for the release study. (H) Release study at 37°C of the PLGA 85:15, 75:25 and 50:50 nanoparticles manufactured by using microfluidics at a TFR of 10 mL/min and FRR 5:1. Results represent mean ± SD of at least triplicate measurements. . 159

Figure 4.19 Particle size and PDI of the PLGA (A) 50:50, (B) 75:25 and (C) 85:15, (D-F) overlay intensity plots and (G) ZP values at the selected time points measured for the release study. (H) Release study at 4°C of the PLGA 85:15, 75:25 and 50:50 nanoparticles manufactured by using microfluidics at a TFR of 10 mL/min and FRR 1:1. Results represent mean ± SD of at least triplicate measurements..... 160

Figure 4.20 Physicochemical characteristics (A, D) Particle size, (B, E) SPAN, (C, F) Zeta potential and (G) encapsulation efficiency (EE %) of the (A-C) empty and (D-G) antigen loaded microspheres produced using the double emulsion method. Results represent mean ± SD of at least triplicate measurements. 162

Figure 4.21 SEM micrographs PLGA microparticles encapsulating ovalbumin as a model antigen: (A-A') PLGA 85:15, (B-B') PLGA 75:25 and (C-C') PGA 50:50 at two different magnifications for better examination of the MP surface..... 163

Chapter 5: Aerodynamic engineering of a PLGA antigen delivery system for pulmonary delivery

Figure 5.1 Particle size and particle size distribution of the empty PLGA (A) 50:50, (B) 75:25 and (C) 85:15 nanoparticles after addition of 3, 5, 7 and 10% w/v sucrose into the formulation prior freeze drying and reconstitution with ultrapure water. Results represent the mean ± SD of at least three independent batches. 178

Figure 5.2 ZP of all three copolymers after addition of 3, 5, 7 and 10% w/v sucrose into the formulation prior freeze drying and reconstitution with ultrapure water. Results represent the mean \pm SD of at least three independent batches.....	179
Figure 5.3 Particle size and particle size distribution of the empty PLGA (A) 50:50, (B) 75:25, (C) 85:15 nanoparticles after addition of 0.5, 0.7 and 1% w/v leucine into the formulation prior freeze drying and reconstitution with ultrapure water.....	180
Figure 5.4 ZP of all three copolymers after addition of 0.5, 0.7 and 1% w/v leucine into the formulation prior freeze drying and reconstitution with ultrapure water.....	181
Figure 5.5 Particle size and particle distribution of the empty PLGA (A) 50:50, (B) 75:25 (C) 85:15 nanoparticles and (D) ZP of all three copolymers after addition of: 3% sucrose in combination with 0.5% or 1% (w/v) leucine; 10% sucrose in combination with 0.5% or 1% leucine into the formulation prior freeze drying and reconstitution with ultrapure water.....	182
Figure 5.6 ZP of all three copolymers after addition of: 3% sucrose in combination with 0.5% or 1% (w/v) leucine; 10% sucrose in combination with 0.5% or 1% leucine into the formulation prior freeze drying and reconstitution with ultrapure water.....	183
Figure 5.7 Visual inspection of the antigen loaded PLGA nanoparticles and microparticles before freeze drying, after freeze drying (dry powder) and after reconstitution to the original volume with ultrapure water.....	187
Figure 5.8 Particle size and PDI of the PLGA (A) 50:50, (B) 75:25 and (C) 85:15, (D-F) overlay intensity plots and (G) ZP values at the selected time points measured for the release study. (H) Release study at 37°C of the PLGA 85:15, 75:25 and 50:50 nanoparticles manufactured by using microfluidics at a TFR of 10 mL/min and FRR 1:1 after FD and reconstitution with ultrapure water. Results represent mean \pm SD of triplicate measurements.....	190
Figure 5.9 Representative HSM micrographs of citric acid powder used as a control (magnification 10x).	191
Figure 5.10 Representative HSM micrographs of the cryoprotectants used for the production of dry powders using freeze drying: (A) sucrose and (B) leucine (magnification 10x).	192
Figure 5.11 Representative HSM micrographs of PVA used during the preparation of PLGA microspheres by the double emulsion method (magnification 4x).....	192
Figure 5.12 Hot-stage micrographs of the (A) PLGA 85:15 (starting material) (magnification 4x), (B) antigen loaded PLGA 85:15 microparticles after freeze drying with no cryoprotectant (magnification 10x), (C) antigen loaded PLGA 85:15 microparticles after freeze drying with a combination of sucrose (10% w/v) and leucine (1% w/v) (magnification 10x), (D) antigen loaded PLGA 85:15 nanoparticles after freeze drying with no cryoprotectant (magnification 4x) and (E) antigen loaded PLGA 85:15	

nanoparticles after freeze drying with a combination of sucrose (10% w/v) and leucine (1% w/v) (magnification 10x).	194
Figure 5.13 Hot-stage micrographs of the (A) PLGA 75:25 (starting material) (magnification 4x), (B) antigen loaded PLGA 75:25 microparticles after freeze drying with no cryoprotectant (magnification 10x), (C) antigen loaded PLGA 75:25 microparticles after freeze drying with a combination of sucrose (10% w/v) and leucine (1% w/v) (magnification 10x), (D) antigen loaded PLGA 75:25 nanoparticles after freeze drying with no cryoprotectant (magnification 4x) and (E) antigen loaded PLGA 75:25 nanoparticles after freeze drying with a combination of sucrose (10% w/v) and leucine (1% w/v) (magnification 4x).	195
Figure 5.14 Hot-stage micrographs of the (A) PLGA 50:50 (starting material) (magnification 10x), (B) antigen loaded PLGA 50:50 microparticles after freeze drying with no cryoprotectant (magnification 4x), (C) antigen loaded PLGA 50:50 microparticles after freeze drying with a combination of sucrose (10% w/v) and leucine (1% w/v) (magnification 10x), (D) antigen loaded PLGA 50:50 nanoparticles after freeze drying with no cryoprotectant (magnification 10x) and (E) antigen loaded PLGA 50:50 nanoparticles after freeze drying with a combination of sucrose (10% w/v) and leucine (1% w/v) (magnification 10x)	196
Figure 5.15 SEM micrographs of the OVA loaded PLGA nanoparticles (1) 85:15, (2) 75:25 and (3) 50:50 (a) powder state after freeze drying and after (b) reconstitution with ultrapure water.	198
Figure 5.16 SEM micrographs of the OVA loaded PLGA microspheres (1) 85:15, (2) 75:25 and (3) 50:50 (a) powder state after freeze drying and after (b) reconstitution with ultrapure water.	199
Figure 5.17 SEM micrographs of the OVA loaded PLGA microspheres (L) before freeze drying and (R) after reconstitution of the dry powder with ultrapure water.	200
Figure 5.18 Aerosol dispersion performance of the loaded freeze dried (A) PLGA nanoparticles particles and (B) PLGA microparticles with different copolymer ratios 85:15, 75:25 and 50:50, as percentage deposition on each stage of the Next Generation Impactor (NGI). Results represent mean \pm SD, n =3 of independent batches.	201
Figure 5.19 Aerosol dispersion performance of the freeze dried PLGA-loaded 85:15 TFR 10 FRR 1:1 nanoparticles as percentage deposition on each stage of the Next Generation Impactor (NGI). Results represent mean \pm SD, n =3 of independent batches. Different amounts of dry powder were filled into the size 3 capsule: 10 mg, 30 mg and 50 mg.	202
Figure 5.20 CTB assay for the quantification of nanoparticle and microparticle cell viability in three different cell lines: MH-S, RAW264.7 and THP-1. Results in collaboration with Maryam Hussain (Strathclyde Institute of Pharmacy and Biomedical Sciences).	206

Figure 5.21 Nanoparticle uptake in three different cell lines MH-S, RAW264.7 and THP-1 at 37°C and 4°C. Results in collaboration with Maryam Hussain (Strathclyde Institute of Pharmacy and Biomedical Sciences).	207
Figure 5.22 Microparticle uptake in three different cell lines: MH-S, RAW264.7 and THP-1 at 37°C and 4°C. Results in collaboration with Maryam Hussain (Strathclyde Institute of Pharmacy and Biomedical Sciences).....	208
Figure 5.23 DQ-OVA encapsulated in PLGA NPs and MPs as a percentage of amount cleavage after 48 hours exposure to MH-S cells, RAW264.7 and THP-1 cell for PLGA nanoparticles and microparticles. Results in collaboration with Maryam Hussain (Strathclyde Institute of Pharmacy and Biomedical Sciences).	210
Figure 5.24 DQ-OVA encapsulated in PLGA NPs and MPs as a percentage of amount cleavage after 48 hours exposure to MH-S cells, RAW264.7 and THP-1 cell. Results in collaboration with Maryam Hussain (Strathclyde Institute of Pharmacy and Biomedical Sciences).	211
Chapter 6: An <i>in vivo</i> model: prime-pull vaccination by priming with CAF01:H56 and boosting with PLGA:H56	
Figure 6.1 Immunisation protocol followed for the prime-pull immunisation of CB6F1 mice to investigate the production of antigen specific antibodies and cytokines for the development of a vaccine effective against pulmonary TB. Mice were immunised three times (2 x s.c. with CAF01:H56 and 1 x i.n. with PLGA:H56) with 2 weeks interval between immunisations and 2 weeks after the intranasal boosting they were terminated and data analysed.....	217
Figure 6.2 Percentage recovery of H56 antigen after using three different membrane treatments prior concentration of the antigen up to 10 mg/mL. Method 1 consisted in wetting the membrane with ultrapure water prior addition of the antigen. Method 2 consisted in addition of a surfactant to decrease binding affinity of the Ag to the membrane (passivation method) and Method 3 no treatment.....	221
Figure 6.3 Antigen-specific humoral immune responses in (A) serum and (B) supernatants from lung lymphocytes after prime-pull immunisation (2 x s.c. CAF01:H56 and 1 x i.n PLGA:H56). Serum samples from 6 individual mice in each vaccine group were isolated 2 weeks after the booster immunization. H56-specific serum production of immunoglobulin G (IgG) was measured by ELISA. ELISA OD ₄₅₀ values are represented as mean values ± S.D, n=6.....	224
Figure 6.4 Antigen-specific cellular immune responses in supernatants from re-stimulated splenocytes and lung lymphocytes after prime-pull immunisation (2 x s.c. CAF01:H56 and 1 x i.n PLGA:H56): IL-17 concentration in the (A) lungs and (B) spleen respectively; IFN-γ concentration in the (C) lungs and (D) spleen respectively. Individual spleens and lungs were isolated 2 weeks after the booster	

immunization. H56-specific cellular production of cytokines was measured by ELISA. Calculated mean concentration values (bars) \pm SD are represented. 225

Figure 6.5 Percentage of IFN γ ⁺CD4⁺CD44⁺ and IL-17⁺CD4⁺ producing T cells measured by intracellular staining in the lung parenchyma (negative) and lung vasculature (positive). T cell responses following vaccination 2 x s.c. CAF01:H56 and 1 x i.n PLGA:H56 in CB6F1 mice (n = 6). Two weeks after intranasal boosting of the antigen, the cells from the lungs were stimulated with H56 antigen and cytokine production was assessed by icFACS. **(A)** Percentage and **(B)** number of H56-specific CD4⁺ T cells producing IFN- γ in the lung parenchyma and **(C)** in the lung vasculature; **(D)** Percentage and **(E)** number of H56-specific CD4⁺ T cells producing IL-17 in the lung parenchyma and **(F)** in the lung vasculature..... 228

Figure 6.6 Percentage of CD4⁺CD44⁺ or CD4⁺CCR6⁺ T cells (IL-17 and IFN- γ) of the study by intracellular flow cytometry on the lung. T cell responses following vaccination 2 x s.c. CAF01:H56 and 1 x i.n PLGA:H56 in CB6F1 mice (n = 6). Two weeks after intranasal boosting of the antigen, the cells from the lungs were stimulated with H56 antigen and cytokine production was assessed by icFACS. **(A)** Percentage and **(B)** number of H56-specific CD4⁺ T cells producing IFN- γ /IL-17 and **(C)** CCR6 medium fluorescence intensity cytokine production in the lung parenchyma. 229

Figure 6.7 Percentage of IFN γ ⁺CD4⁺CD44⁺ and IL-17⁺CD4⁺ CD44⁺ producing T cells measured by intracellular staining in the splenocytes and lymph nodes of vaccinated mice. T cell responses following vaccination 2 x s.c. CAF01:H56 and 1 x i.n PLGA:H56 in CB6F1 mice (n = 6). Two weeks after intranasal boosting of the antigen, the cells from the lungs were stimulated with H56 antigen and cytokine production was assessed by icFACS: Percentage of **(A)** IFN- γ , **(B)** IL-17 and **(C)** CCR6 in the spleen. Percentage of **(D)** IFN- γ , **(E)** IL-17 and **(F)** CCR6 cytokines in the LNs..... 231

Abbreviations

ACN	Acetonitrile
AM	Alveolar macrophages
ANOVA	Analysis of variance
APC	Antigen presenting cell
BCA	Bicinchoninic acid assay
BCG	Bacillus Calmette-Guérin
BSA	Bovine Serum Albumin
CAF	Cationic adjuvant formulation
CCR6	Chemokine receptor 6
CFP-10	Culture filtrate protein of 10 kDa
Chol	Cholesterol
CMI	Cellular mediated immune response
ConA	Concanavalin A
CryoTEM	Cryogenic transmission electron microscopy
CTB	Cell Titer Blue
D10	Cumulative 10% point of diameter
D50	Cumulative 50% point of diameter
D90	Cumulative 90% point of diameter
DC	Dendritic cell
DDA	<i>N,N'</i> -dimethyl- <i>N,N'</i> -dioctadecylammonium
DF	Dilution factor
dH₂O	Ultrapure water
DiIc	1,1'-Dioctadecyl-3,3',3'-Tetramethylindocarbocyanine Perchlorate
DLS	Dynamic light scattering
DMPC	1,2-dimyristoyl-sn-glycero-3-phosphocholine
ECACC	European Collection of Authenticated Cell Cultures
ED	Emitted dose
EDTA	Ethylenediaminetetraacetic acid
EE	Encapsulation efficiency
ELISA	Enzyme-linked immunosorbent assay

ELSD	Evaporative light scattering detector
EMA	European Medicines Agency
ESAT-6	Early secreted antigen 6 kDa
EtOH	Ethanol
FBS	Foetal Bovine Serum
FD	Freeze drying
FDA	Food and Drug Administration
FPD	Fine particle dose
FPF	Fine particle fraction
FRR	Flow rate ratio
GC	Gas chromatography
H56	Hybrid 56
HBsAg	Hepatitis B antigen
HCl	Hydrochloric acid
HPLC	High performance liquid chromatography
HRP	Horseradish peroxidase enzyme
HSM	High shear mixing
ICH	International Conference of Harmonization
iFACS	Intracellular Flow cytometry staining
IgG	Immunoglobulin G
IL	Interleukin
ILN	Inguinal lymph node
INF-γ	Interferon gamma
IPA	2-Propanol or isopropyl alcohol
IS	Internal standard
LH	Lipid film hydration
LOD	Limit of detection
LOQ	Limit of quantification
LTBI	Latent Tuberculosis Infection
MeOH	Methanol
MF	Microfluidics
MHC	Major Histocompatibility Complex

MLN	Mesenteric lymph node
MLV	Multilamellar vesicles
MMAD	Mass median aerodynamic diameter
MP	Microparticle
mPES	Modified polyethersulfone
MPL	Monophosphoryl lipid A
Mtb	<i>Mycobacterium tuberculosis</i>
MTBC	Mycobacterium Tuberculosis Complex
Mw	Molecular weight
MWCO	Molecular Weight Cut Off
NaCl	Sodium chloride
NaN₃	Sodium azide
NaOH	Sodium hydroxide
NGI	Next Generator Impactor
NP	Nanoparticle
OD	Optical density
OVA	Ovalbumin
PAMP	Pathogen-associated molecular patterns
PBS	Phosphate buffered saline
PC	Phosphatidylcholine
PDI	Polydispersity index
PGA	Polyglycolic acid
pI	Isoelectric point
PLA	Polylactic acid
PLGA	Poly lactic-co-glycolic acid
POP	Popliteal lymph node
PRR	Pattern recognition receptor
PVA	Polyvinyl alcohol
RF	Respirable fraction
RPMI	Roswell Park Memorial Institute medium
SD	Standard deviation
SDS-PAGE	Sodium dodecyl sulfate polyacrylamide gel electrophoresis

SEM	Scanning electron microscopy
SHM	Staggered herringbone micromixer
SOI	Site of injection
SUV	Small unilamellar vesicles
TB	Tuberculosis
TBVI	Tuberculosis Vaccine Initiative
TDB	α, α' -trehalose 6,6'-dibehenate
TDM	Trehalose 6,6'-dimycolate
TFA	Trifluoroacetic acid
TFF	Tangential Flow Filtration
TFR	Total flow rate
Tg	Glass transition temperature
Th	T helper
TLR	Toll like receptor
T_m	Transition temperature from gel-to-liquid crystalline
TMB	Tetramethylbenzidine
TNF	Tumour necrosis factor
Tris	2-amino-2-(hydroxymethyl)-1,3-propanediol
UV	Ultraviolet
WHO	World Health Organisation
ZP	Zeta potential

Chapter 1

General Introduction

1.1 Tuberculosis (TB)

Tuberculosis (TB) is an infectious disease caused by a mycobacteria called *Mycobacterium tuberculosis* (Mtb). According to the World Health Organisation (WHO) it is the leading cause of death from a single infectious agent and it ranks as the 9th cause of death globally. It is estimated that a third of the global population is infected with it. The data from WHO's latest report (2017) shows a reduction in the mortality from 1.7 million in 2000 to 1.3 million in 2016 and approximately further 374,000 deaths among HIV-positive people [1]. More than 10 million people were estimated to be infected with TB and 90% of the affected population were adults. The majority of the people infected by Mtb do not develop the disease and they are recognised as having latent TB infection (LTBI) whereas people developing the disease are considered to have active TB. Among all the infected people, it is predicted that less than 10% of them develop the disease, which is enough to maintain the global epidemic. TB incidence (Figure 1.1) is mainly registered in African and Asian countries such as India, Pakistan, Indonesia and China [1]. There are specific initiatives and associations with focus on the control of the TB burden, which aim to achieve a 90% reduction in the deaths caused by TB and a TB incidence reduction of 80% by 2030 (e.g. Tuberculosis Vaccine Initiative (TBVI or TBVAC) which financially supported the work shown in this thesis). Regardless of all the research and efforts in controlling TB disease by vaccination, the vision of a world free of this disease remains out of reach due to several scientific barriers which include population genetics, the degree of exposure to the bacteria, the lack of understanding how Mtb works and the lack of well validated animal models since no obvious association of protection or immunity have been found in any of the animal models utilised.

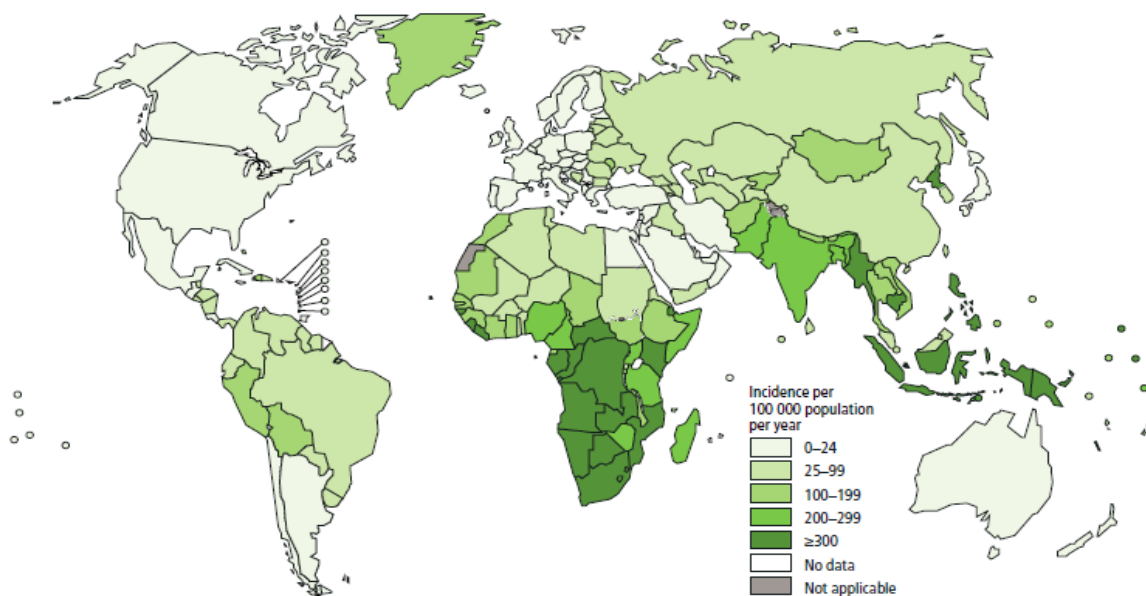


Figure 1 1 World map showing the estimated incidence of TB in 2016 (WHO report 2017)[1].

1.1.1 The pathogen: *Mycobacterium tuberculosis* (Mtb)

Mycobacterium tuberculosis (Mtb) is a mycobacteria belonging to the Actinomycete family which was first discovered by Robert Koch in 1882. It is an obligate aerobe and intracellular pathogen whose main phenotypic characteristic is considered to be its acid fastness properties [2]. Due to its waxy bacterial wall it resists the Gram staining method and therefore, it has to be characterised by other techniques [3]. It belongs to the Mycobacterium Tuberculosis Complex (MTBC) which is a group of mycobacterium that causes TB either in humans or animals. Members of the MTBC are: *Mycobacterium tuberculosis*, *Mycobacterium bovis*, *Mycobacterium africanum*, *Mycobacterium microti*, *Mycobacterium pinnipedii*, *Mycobacterium caprae*, *Mycobacterium mungii* and *Mycobacterium orygis*. Among all of these, Mtb is reported to be the causative agent of TB in humans although other members of the MTBC might also cause the disease in humans. Members of the MTBC able to cause disease, carry genes for the virulence factors: the early secreted antigen 6 kilodaltons (ESAT-6) and the culture filtrate protein of 10 kD (CFP-10) [4].

1.1.2 TB transmission: airborne infection

Mtb is transmitted through the air from a patient with pulmonary TB to another person and is the traditional example of an airborne infection [5]. It mainly affects the lungs (pulmonary TB) but it can spread and affect other organs (extrapulmonary TB). Only patients with pulmonary TB can be considered as infectious. Therefore, the mechanism of transmission is regarded to be any manoeuvre generating the ejection of aerosolised droplets. These aerosolised droplets containing bacteria are called 'droplet nuclei' and can be generated by any expiratory action such as coughing, yelling, singing, sneezing and so on. All these actions involve to some degree the production of watery secretions or disruption of mucus promoting the particle aerolisation. Once the droplet nuclei are expelled, these droplets can survive in the air for a prolonged time and thus, can be inhaled by another person resulting in a new infection [6]. Just a single TB bacillus is necessary to cause the disease. Three different situations can occur upon inhalation of the bacilli: (1) The bacteria do not cause infection and it is eliminated by the immune system, (2) the bacteria establish infection but it is in a latent or dormant state (LTBI) which do not produce any symptoms, or (3) the infection evolves from latent to active and thus, becomes symptomatic and the host is able to spread the infection [7]. It is estimated that 10% of the people with LTBI progress to active TB at some point of their lives and immunocompromised patients have a higher likelihood (e.g. HIV-positive) [8]. The symptoms associated with pulmonary TB are generally productive and chronic cough which might contain blood in sputum, fever, fatigue and weight loss.

1.1.3 TB histological structure: Granulomas

Once the droplet nuclei is inhaled and has reached the alveoli, the alveolar macrophages (AM) engulf the bacilli and the dendritic cells (DCs) and neutrophils take them up [9-11]. Gradually, uninfected and infected cells containing the bacteria assemble in an organised shape which commonly contains the dead cells and bacteria in the central core (this substance is called caseum) and the T cells surrounding in the periphery. This compacted structure is the characteristic TB tissue lesion [12-14]. Granulomas might contribute to spread the infection or to help the host containing the infection within them depending on the infection stage. During early infection, granulomas benefit the dissemination of the infection within macrophage aggregates and as the CD4⁺ T cells must be in direct contact with the pathogen in order to elicit a protective immune response, granulomas may restrict the T cell efficacy eradicating the bacteria [15, 16]. Besides, granulomas are dynamic structures, as opposed to what was commonly believed, which allow infected cells to move without restriction outside the structure [17]. During the late infection stages, granulomas protect the host from infection by confining the bacteria within the interior and thus, avoiding dissemination.

1.1.4 Immunity to TB

Factors affecting the possibility of acquiring the infection are related to the environment or the host immune system. The susceptibility of a person to become infected or not is not well understood. Mtb pathogen infects and replicates in phagocytic cells, disrupting the elimination mechanism typical of these cells [18, 19]. The majority of the people infected with Mtb eradicate or limit the infection and therefore the progression to disease, by means of the host's innate and adaptive immune response [20].

1.1.4.1 Innate immune response to TB

Innate immune responses are the first line of defence upon infection with Mtb but this response is not enough for TB control. Ligands expressed on the bacteria are recognised by the phagocytic cells (macrophages, DCs and neutrophils) and subsequently engulfed [21]. Besides, pattern recognition receptors (PRRs) elicit secretion of specific pro-inflammatory and anti-inflammatory cytokines due to recognition of some bacterial components [22]. Other cells such as natural killer T cells contribute to the cytokine secretion during early infection [23]. Among all the cytokines secreted, tumour necrosis factor (TNF), interferon gamma (IFN- γ) and interleukin 2 (IL-2) are crucial for the protection against Mtb infection during innate immune responses [24-30]. If the inhaled droplet nuclei are not small

enough to reach the alveoli, the mucosal-associated invariant T cells (MAITs) will be in charge of clearing these large particles.

1.1.4.2 Adaptive immune response to TB

Adaptive responses are delayed but they are necessary for the control of TB infection and thus, for the maintenance of the latency stage. The production of polyfunctional CD4⁺ and CD8⁺ T cell lymphocytes and the involvement of DCs are essential for the control of TB infection [31, 32]. Several *in vivo* studies have confirmed the importance of CD4⁺ T cells for the protection against TB. These cells secrete several cytokines, including TNF, IFN- γ and interleukines (IL) -2, -4, -17 and -22. Furthermore, CD4⁺ T cells can kill infected cells due to their cytolytic activity [33]. It has been reported that mice lacking CD4⁺ T cells [34], and patients co-infected with HIV (which involves CD4⁺ T cell depletion) [35] favour the lethal course of TB. The importance of CD8⁺ T-cell responses has not been defined in humans, but it has been shown in mice and cattle [36]. However, patients with rheumatoid arthritis and under anti-TNF medication show a higher likelihood to acquire TB [37].

1.1.5 TB vaccine: Bacilli–Calmette–Guerin (BCG)

Vaccination, which is defined as the administration of a specific pathogen in the body in order to stimulate a long-lasting immune response against a specific disease, protecting and preventing against it for life, is one of the most effective inventions in healthcare [38]. The first vaccine was discovered by Edward Jenner in 1798 when researching about smallpox he discovered that using the fluid from the cowpox pustules he could eradicate the disease. Thus, the origin of the word vaccine comes from the Latin word for cow ‘vacca’.

Mtb was discovered in 1882 but it was not until 1921 that a vaccine against this disease was discovered. It took over 13 years to discover it by Calmette and Guerin at the Pasteur Institut (France). The vaccine was obtained after serial passage of a virulent strain from *M. bovis* (*Mycobacterium bovis* Bacilli–Calmette–Guerin, BCG) and was first orally administered to a child at risk of infection. Few years later, BCG started being administered globally for the prevention against TB. Nowadays more than 100 million children each year are vaccinated with BCG. It is a live attenuated vaccine, which is intradermally administered in a single shot. BCG is safe, stable and low cost, but it is only effective in reducing the risk of disseminated TB in children [39]. Besides, its efficacy varies from 0 to 80% worldwide and it is unsuccessful in preventing pulmonary TB at any age [40]. There are several factors

attributed to the broad efficacy shown by BCG. One of the reason might be the differences in the strain used (there are currently 5 main strains used for the production of BCG vaccine: Danish, Pasteur, Glaxo, Tokyo and Moreau strains) and the method for preparation, as there is no standardised method for the production of the vaccine. Another explanation could be the variation in the population genetics and susceptibility. Environmental factors such as previous exposure to mycobacteria, and geographical factors contribute to the variation in efficacy as well [41, 42]. It has been reported that BCG efficacy increases at higher latitudes, so the possible differences among environmental mycobacteria could be involved in this [43]. Besides the influence of the above-mentioned factors in the efficacy of BCG, one of the main reasons that might restrict its efficacy is its antigenic composition which is not similar enough to Mtb, and many of the main antigens involved in infection (e.g. ESAT-6 and CFP-10) are deleted in BCG vaccine independently of the strain used [44]. Therefore, besides being the world's most administered vaccine it fails to protect against the most common form of TB, pulmonary TB.

1.2 Vaccine approaches for TB

As mentioned, there is still an unmet need for an efficacious TB vaccine. Thus, to overcome the limitations of BCG, a wide range of vaccination strategies are being develop to stop and control TB transmission and infection. Extensive research have been carried out on the vaccine development field, leading to a large number of preclinical and clinical candidates (Table 1.1). Different approaches can be followed depending on the target population. Besides, vaccines can be developed either as replacements of the current BCG vaccine or as boosters and depending on the backbone structure they can be classified as live, inactivated or subunit vaccines.

Table 1.1 TB vaccine candidate pipeline currently in clinical trials. Data source: Tuberculosis Vaccine Initiative (TBVI) website (updated October 2018, www.tbvi.com).

Research Phase	Vaccine	Type of vaccine	Developers	Technical or/and financial support	Target Population
Preclinical	H64 + CAF01	Subunit vaccine	Statens Serum Institut (SSI)	TBVI	Adolescents/adults
	rBCG Δ ais/zmp1	Live attenuated	University of Zurich	Aeras, TBVI	Infants/neonates
	BCG, ChAdOx/MVA PPE15-85A	Viral vector	University of Oxford	TBVI	Adolescents/adults
	CysVac2/Advax	Protein/Adjuvant	University of Sydney	TBVI	Adolescents/adults
	CMV-6Ag	Viral vector	Vir Biotech	Aeras	Adolescents/adults
	MVA multiphasic vaccine	Viral vector	Transgene	TBVI	Therapeutic
Phase I	MVA85A (aerosol)	Viral vector	University of Oxford	TBVI	Adolescents/adults
	ChAdOx1.85A	Viral vector	University of Oxford	TBVI (formerly)	Adolescents/adults
	Ad5 Ag85A	Viral vector	McMaster University, CanSino	Other	Adolescents/adults
	GamTBVac	Protein/Adjuvant	MoH Russia	Other	Adolescents/adults
	H56:IC31	Protein/Adjuvant	SSI and Valneva	Aeras	Therapeutic

	ID93 +GLA-SE	Protein/Adjuvant	Infectious Disease Research Institute (IDRI)	Aeras	Therapeutic
	RUTI	Mycobacterial (whole cell)	Archivel Pharma	TBVI	Therapeutic
Phase IIa	H4:IC31	Protein/Adjuvant	SSI, Sanofi Pasteur	Aeras	Adolescents/adults
	TB/FLU-04L	Viral Vector	Research Institute for Biological Safety Problems, Kazakhstan	Other	Therapeutic and adolescents/adults
	ID93 +GLA-SE	Protein/Adjuvant	IDRI	Aeras	Adolescents/adults
	BCG revaccination	Live attenuated	-	Aeras	Adolescents/adults
	MTBVAC	Live attenuated	Biofabri, University of Zaragoza	Aeras, TBVI	Infants/neonates
Phase IIb	H56:IC31	Protein/Adjuvant	SSI, Valneva	Aeras	Adolescents/adults
	M72 + AS01E	Protein/Adjuvant	Glaxo Smith Klein (GSK)	TBVI (formerly), Aeras	Adolescents/adults
	DAR-901	Mycobacterial (whole cell)	Darmouth	Aeras, TBVI	Adolescents/adults
Phase III	M. Vaccae	Mycobacterial (whole cell)	AnHui Longcom	Other	Adolescents/adults
	VPM1002	Live attenuated	SII, Max Planck, VPM	TBVI	Infants, adolescents, adults and therapeutic
	MIP	Mycobacterial (whole cell)	Cadila Pharma	Other	Adolescents/adults and therapeutic

Independently of the approach or category in which the vaccine falls, the same rational as for the developing of any vaccine should be followed in terms of production, cost, safety and efficacy [45]. A vaccine can be broadly defined as a preparation used to acquire immunological memory for a particular disease in order to allow effective defence to subsequent wild-type exposure. Aside from personal immunity, a successful vaccine would also incorporate the ability to fully prevent or limit the transmission ability, generating herd immunity to mitigate the damage of the disease. Thus, lifelong immune responses are crucial since contact with the disease pathogen may occur any time during life, and production of both humoral and cellular immune responses would be ideal. Vaccines have to be safe and efficacious, and for this reason, they undergo a large number of tests to prove that the number of doses and the vaccine itself produce little or no harm when administered to target populations. Knowledge of the pathogen causing the disease is necessary in order to determine the quality of the protective immunity developed [45]. The vaccine cost should be reduced, and the method of production should be reproducible and accessible in developing countries, as most of the diseases affect these countries [45]. The exclusion of the cold-chain requirement would contribute with the reduction of the vaccine cost and it would facilitate the stability of the vaccine during transit and storage. This problem can be overcome by the addition of stabilising agents or the preparation of dry powder vaccines using lyophilisation methods (e.g. freeze drying).

1.2.1 Modification, boosting or replacement of BCG

In order to address the variability found with regards to the efficacy of the current BCG vaccine, a number of vaccines are currently being developed based upon the improvement of the current model via modification or boosting. The modifications involve the addition of new, more relevant Mtb antigens or the overexpression of the current genes in order to enhance T cell mediated immune responses [46]. In contrast, improvement of the efficacy of the BCG can be achieved by maintaining the current BCG model but with the addition of a booster vaccine [47]. The aim of a booster vaccine is to improve an existing antigen specific immune response to achieve a more potent response. It may be possible to further enhance the efficacy of a booster immunization by testing a number of different routes of administration or boosting times. Another option is the development of a new vaccine able to prevent the disease or infection. This vaccine should be able to stimulate the T cell production besides helping in the production of antibodies which is a feature that lack in the current BCG model. Besides other routes of administration should be explored as recent studies highlight the importance of T cell production within the lungs.

1.2.2 Vaccine design: live attenuated, inactivated or subunit vaccines

Vaccines can be categorised into (1) subunit vaccines, which utilise the combination of a number of relevant antigens to achieve protective immunity (2) live attenuated vaccines, and (3) inactivated vaccines [48]. Attenuated vaccines use reduced infectivity of the pathogen, such as the BCG vaccine. By this means, the pathogen replicates within the host and stimulates specific pathogen immune responses by mimicking the replication of the wild type pathogen as would happen following natural infection, thus, protecting against the disease without causing it. These vaccines are generally considered as a single vaccination due to the fear of reversing the infectivity [49]. In contrast, inactivated vaccines lack of infectivity due to chemical or physical inactivation of the pathogen but maintaining its immunogenicity. Inactivation treatments may contribute to the damage of the antigen, reducing the vaccine efficacy. The most common agents used for inactivation are formalin and β -propiolactone. The former might contribute to the damage of the antigenic proteins to be inactivated, modifying or reducing their immunogenicity, whereas β -propiolactone does not damage proteins. Usually, more than one injection and high concentrations are necessary for the stimulation of the desired immune response. On the other hand, subunit vaccines, are based on highly purified antigens such as recombinant proteins or peptides which are safe but insufficiently immunogenic by themselves [38, 49]. Due to the lack of knowledge on the specific antigens necessary to elicit the adequate immune response in humans, it is more likely that the whole pathogen containing vaccines (live attenuated and inactivated) contain the crucial antigens for the appropriate protective immunity.

1.2.3 Vaccine targeting disease stage: pre- or post-exposure and therapeutic vaccination

The challenge for the development of a new and effective TB vaccine also relays on the development of a vaccine able to generate the adequate humoral and cellular immune responses to either kill the pathogen upon entry, hinder the progression of the infection or prevent reactivation. Therefore, the selection of the target population to be treated is necessary for the vaccine design and development. These vaccines can be classified as preventive or therapeutic vaccines (Table 1.2). Preventive vaccines can be further categorised as pre-exposure and post-exposure. The first ones, the so-called prophylactic or priming vaccines, are commonly designed for infants or new born child, as they have to be administered to people who have not been previously in contact or exposed to Mtb. This is the case of the BCG vaccine which is administered commonly after birth. Furthermore, vaccine candidates designed for the replacement of BCG or subunit vaccines to be used as BCG boosters fall within this category [50]. In contrast, post-exposure vaccines (also known as boosting vaccines) target patients with LTBI. The target population are adolescents and adults with LTBI. These vaccines can be used as

replacement of BCG or boosters, and they mainly consists on subunit vaccines containing Mtb antigens secreted during the latency stage [51]. Finally, therapeutic vaccines are designed for infected people with active TB and treated with TB drugs, specifically, those patients resistant to TB drugs [48, 52]. TB drug treatment is the first line of defence against active TB. It consists on the administration of several antiTB drugs for a prolonged period of time and therefore, it causes problems of compliance. Besides, Mtb has developed ways to resist the drug treatment, and patients may suffer from multidrug-resistant (MDR) or extensively drug resistant (XDR) TB depending on the drugs Mtb develops resistant to [52].

Table 1.2 TB vaccine candidates currently in clinical trials and classified according to the targeted vaccine stage [53].

Target vaccine stage	Vaccine	Type of vaccine
Pre-exposure vaccine: Prevent TB disease	MTBVAC	Live attenuated
	VPM1002	Live attenuated
	MVA85A	Viral vector
	H4/H56	Subunit vaccine
	M72	Subunit vaccine
	ID93	Subunit vaccine
	BCG-ZMP1	Live attenuated
Post-exposure vaccine: Prevent TB disease	BCG revaccination	Live attenuated
	ID93	Subunit vaccine
	H56	Subunit vaccine
Therapeutic vaccine: Cure TB disease	M72	Subunit vaccine
	RUTI	Mycobacterial (whole cell)
	H56	Subunit vaccine
	ID93	Subunit vaccine
	M. vaccae	Mycobacterial (whole cell)
	VPM1002	Live attenuated
MVA multiphasic	Viral vector	
TB/Flu04L	Viral vector	

1.3 TB vaccine candidate: Hybrid 56 (H56)

Within the research carried out for the development of a new TB vaccine focus has been paid to TB antigens expressed during different stages of the pathogen life cycle [51]. As a result, combination of Mtb immunodominant antigens fused to each other have been constructed. This is the case of the Hybrid 1 (H1) which is based on the fusion of the antigens Ag85B and ESAT-6 from Mtb and the Hybrid 56 (H56) which uses the H1 structure with the addition of the latency antigen Rv2660c [51, 54]. H56 is considered as a multistage vaccine, since it can be used for pre- and post-exposure vaccination, as

it contains antigens secreted during early infection and a latency antigen expressed during dormant stage [51]. ESAT-6 is one of the best characterised antigens secreted by Mtb, it is expressed during infection and some studies have demonstrated the production of ESAT-specific CD4⁺ T cell during early and late infection stage. Opposite to that, Ag85B is highly expressed during early infection in the lungs but its expression gets reduced over time. Therefore, the stimulation of Ag85B-specific CD4⁺ T cells is decreased. These findings highlight the importance of antigen selection for the development of a TB vaccine.

1.4 Methods for enhancing immunogenicity: ADJUVANTS

Due to the poor immunogenicity of highly purified peptides/antigens (subunit vaccine) and inactivated vaccines when administered by themselves, the inclusion of adjuvants in the vaccine formulation is necessary. Adjuvants are substances that enhance and modulate the immune response when combined with vaccine antigens. Adjuvants can act as delivery systems, immunopotentiators or a combination of both. Delivery systems carry the antigen to the antigen presenting cells (APCs) facilitating its uptake and cell activation and extending its release. Immunopotentiators increase the immune responses by stimulations of specific cell receptors. The use of adjuvants may contribute to dose spare, decreasing the amount of antigen needed and the number of doses. However, the mechanism of action varies between adjuvants as well as the chemical composition. The first adjuvants approved for human use were alum and MF59 which have been extensively used; however, these adjuvants are only effective eliciting humoral responses (antibodies) to the vaccine antigens. Combination of alum with immunopotentiators may enhance the humoral immune responses and stimulate cellular immune responses. This has been shown by the addition of a monophosphoryl lipid A (MPL) to alum, which promotes the secretion of IFN- γ due to interaction with Toll-like receptors (TLRs) expressed on the surface of the APCs. The combination of both alum and MPL was the first vaccine approved for human use containing a TLR and it is licensed as a vaccine against the human papilloma virus (HVP) and it is called Cervarix. On the other hand, MF59 which is a squalene oil-in-water emulsion is licensed as an adjuvant for influenza vaccine due to its high antibody production. Therefore, the importance of the adjuvant in the vaccine formulation is crucial in dictating the immune response produced. Consequently, the use of these adjuvants for the development of a TB vaccine is limited due to the necessity of cellular mediated immune responses (CMI) for the protection against this infection (as TB is an intracellular pathogen and antibody responses are not enough to eradicate it [42]). Thus, developing vaccines capable to elicit T cell responses are crucial against intracellular pathogens and for this reason, the use of liposomes and poly lactic-co-glycolic acid (PLGA) particles as adjuvant systems has grown in the last decade [49, 55].

1.4.1 Lipid-based adjuvants: Liposomes

Lipid-based particulate adjuvants have been extensively investigated due to their biocompatibility, biodegradability and fusogenic properties [56]. Liposomes were first discovered by Bangham et al. in 1965, but it was not until approximately 10 years later when Gregoriadis et al. used them as adjuvant systems [57, 58]. The amphiphilic character of the lipids leads to the formation of spherical self-assembled vesicles enclosing an aqueous compartment upon dispersion in an aqueous phase and under agitation. Lipids are composed of a hydrophilic head group and a lipophilic tail, and thus, they assemble in a way that the hydrophobic-water interactions are decreased. Therefore, the head group is oriented towards the water phase whereas the lipid hydrocarbon tails are protected from the aqueous phase. They can be classified according to their size and lamellarity. [59, 60]. Liposomes containing one lipid bilayer are classified as unilamellar whereas liposomes containing more than one concentric bilayer are classified as multilamellar. Within these groups, liposomes can be classified in subcategories depending on the particle size. Commonly liposomes containing one lipid bilayer and with a particle size up to approximately 100 nm are considered small unilamellar vesicles (SUVs), liposomes with sizes between 200 – 800 nm are called large unilamellar vesicles (LUVs) and liposomes in the micrometre range (>1000 nm) are called giant unilamellar vesicles (GUVs). On the other hand, multilamellar vesicles (MLVs) encompass a broad particle size range from 500 to 5000 nm. Lipids dispersed in aqueous environments can adopt different supramolecular structures depending on several internal and external factors. Internal factors such lipid concentration, head group size, lipid tail length and saturation and surface charge. Temperature, pressure and addition of other components into the formulations can dictate the packing process [61]. Packing process can be quantified by the critical packing parameter (CPP) of the lipids which determines the expected supramolecular structure of the lipids. Lipids expressing a CPP less than 1 but more than 0.5 are predicted to form bilayers vesicles, and therefore liposomes. Large head group size and two hydrocarbon chains are characteristic of liposome forming lipids [62].

Liposomes have also attracted the attention of many researchers due to the possibility of the incorporation of hydrophilic and lipophilic substances in the aqueous compartment or the lipid bilayer respectively (Figure 1.2). Liposomes offer protection from the host enzymes to the loaded antigen [63, 64], enhancing the delivery of the antigen and promoting its uptake by APCs due to their particulate nature [59, 65, 66]. Besides, lipids can be categorised according to their surface charge into neutral, anionic and cationic particles (Figure 1.2). Thus, hydrophilic antigens can be loaded/associated onto the liposome surface due to electrostatic interactions between the antigen and the liposomes. This quality represents an optimal platform for the use of liposomes as adjuvants for subunit vaccines, since the antigens can be loaded onto the liposomal surface by modification of the buffer pH and

liposomal charge, which will determine the level of adsorption. For this reason, cationic liposomes have been extensively studied as adjuvant system for subunit vaccines, as liposomes can act as delivery systems and immunopotentiators as well, modulating the immune responses produced. Studies have shown the improved antigen-specific immune responses obtained when using cationic liposomes compared to either neutral or anionic [67-69]. The pharmacokinetics of the liposomal adjuvants can be modified by changes in their physicochemical characteristics such as size, surface charge, and by variation of the lipid components of the formulation. Cationic liposomes when co-administered with antigens by parenteral route have shown to form a depot at the site of injection which enhances the antigen presentation and produces high antibody and cell mediated immune responses, opposite to neutral liposomes [70].

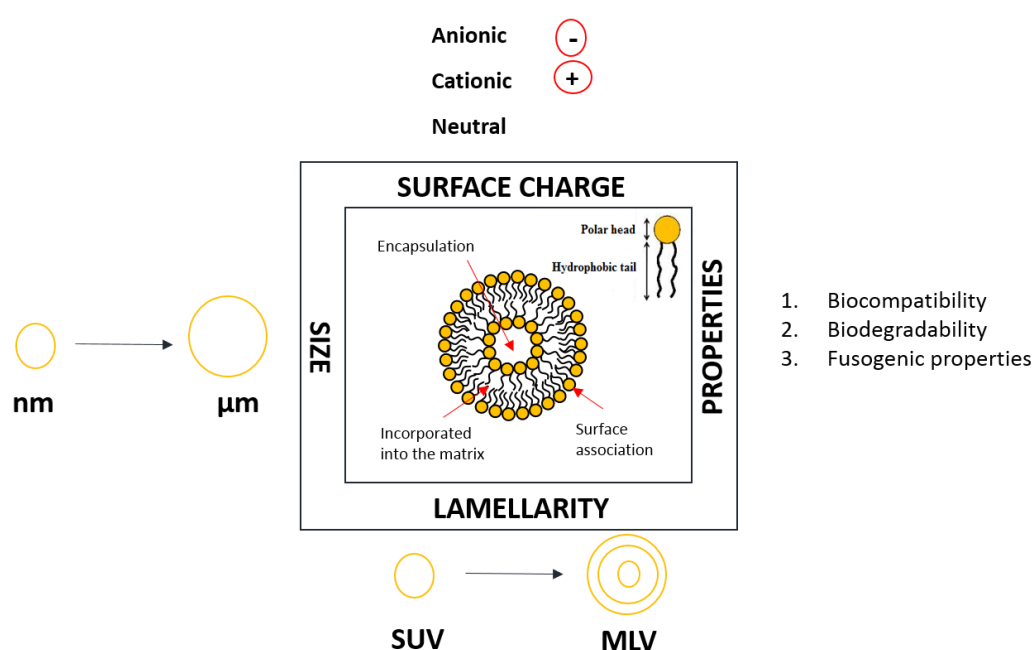


Figure 1.2 Schematic representation of the main characteristics related to liposomes in terms of characterisation.

1.4.1.1 The Cationic Adjuvant Formulation (CAF) 01

The cationic adjuvant formulation (CAF) 01 is a liposomal adjuvant formulation developed by Statens Serum Institut (SSI, Copenhagen, Denmark) based on the synthetic cationic surfactant N,N'-dimethyl-N,N'-dioctadecylammonium bromide (DDA) and the synthetic immunopotentiator α,α' -trehalose-6,6'-dibehenate (TDB) (Figure 1.3). DDA can form liposomes when dispersed in aqueous environment under agitation and at a temperature above its gel-to-liquid transition temperature (T_m 47°C) [71]. DDA contains a polar head group consisting of a quaternary ammonium attached to two methyl groups and carrying a bromide counter-ion, and two lipophilic saturated C_{18} hydrocarbon tails. [72, 73]. DDA

liposomes can be produced in a wide range of sizes from SUVs to MLVs depending on the method of preparation and the DDA concentration [74]. The main disadvantage is that this formulation is not stable and aggregates during storage [75]. The incorporation of TDB into the formulation in contrast, improves its stability besides enhancing the immunogenicity of the formulation. TDB is a synthetic analogue of trehalose 6,6'-dimycolate (TDM), the so-called cord factor, a mycolic acid from the mycobacterial cell wall from Mtb [76, 77]. Despite its strong immunonological features, its toxicity hinders its use in vaccine formulation [78, 79]. In contrast, TDB replaces the long mycolic acid branches found in TDM which are related to its toxicity, with 2 behenyl chains which are attached to the trehalose head group [71]. The head group increases the hydration of the liposomal membrane, favouring interaction with the aqueous environment and thus, preventing the aggregation of the formulation [80].

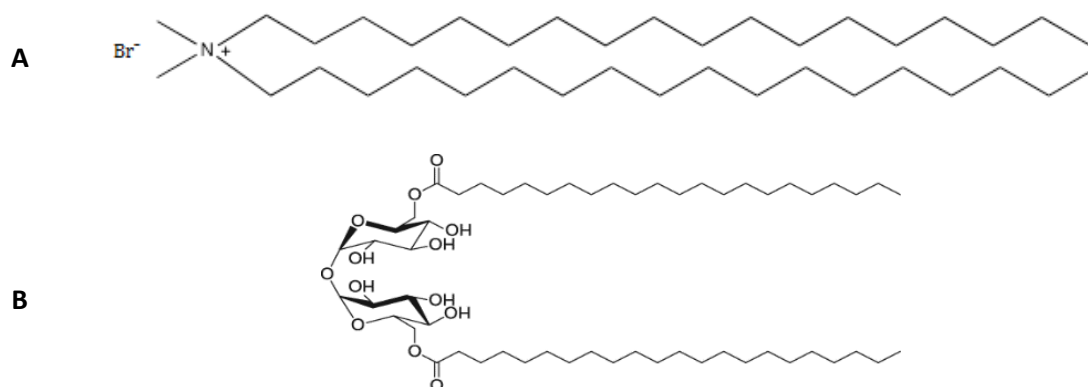


Figure 1.3 Molecular structure of (A) the cationic surfactant DDA and (B) the immunopotentiator TDB, the two components of the CAF01 formulation.

The traditional method for preparation of CAF01 is the lipid film hydration, a method developed by Bangham et al in 1965 which produces MLVs, at a weight ratio 5:1 (DDA:TDB). In order to reduce the size and lamellarity of the formulation, a size reduction method such as sonication or high shear mixing has to be applied to the preformed MLVs. This manufacturing process produces SUVs with a particle size of approximately 200 nm and a polydispersity between 0.2 and 0.4. CAF01 formulation is reported to be stable for up to 2 years when stored at 4 - 8°C [81]. Studies based on the lyophilisation of CAF01 using spray drying and freeze drying have been carried out in order to overcome the cold-chain problem, reduce the cost of the formulation and improve transit and storage [80, 82-85]. Moreover, the lyophilisation process also facilitates the sterilisation of the formulation using γ -radiation [86].

A wide variety of subunit vaccines, including HIV, TB, chlamydia and influenza, have been studied alongside CAF01 in order to elucidate its adjuvant effect (e.g. [73, 87-90]). The cationic surface charged

related to the quaternary ammonium of DDA has shown to be crucial for its immunological profile since by this means antigens are attached to the liposomal surface and thus, allows the co-delivery of both antigen and adjuvant to the APCs. The biodistribution of CAF01 *in vivo* has been studied by dual radiolabelling of the individual vaccine components (antigen and adjuvant). Results have shown the formation of a depot at the injection site (SOI) after parenteral vaccination [90, 91]. The depot effect has been proved to be related to the cationic nature of the formulation and the rigidity of the liposomal membrane at body temperature (CAF01 $T_m \sim 42^\circ\text{C}$). Hereby, APCs are recruited to the SOI where they engulf the vaccine components and become activated. These activated immune cells move to the draining lymph nodes for antigen presentation to the T cells and subsequently, activating them [91]. The depot formation is of utmost importance for the Th1/Th17 stimulation. Moreover, the inclusion of the immunopotentiator TDB results in an improved activation of APCs through interaction with the C-Lectin type receptor (CLR) Mincle which has been reported to activate the Syk-Card9 signalling pathway in mice and human [92-97]. Its immunological profile consists of strong production of cellular and humoral immune responses based on high IFN- γ and IL-17 secretion, low IL-5 production and high Immunoglobulin G (IgG) antibody production [98, 99]. The fusion proteins H1 and H56 have been widely investigated alongside CAF01 for development of a TB vaccine [54, 98]. H56 antigen as a standalone vaccine is less efficacious than BCG, however, studies in rodents have shown that administration of H56 adsorbed onto the CAF01 surface is more efficient than BCG.

1.4.2 Biodegradable polymer-based adjuvants: Poly lactic-co-glycolic acid (PLGA)

Biodegradable compounds degrade into non-toxic and biocompatible products upon *in vivo* administration. Subsequently, the degradation products are removed from the system by the normal metabolic pathways. These biodegradable compounds can be classified according to its origin into natural, synthetic, and semisynthetic polymers. Among the synthetic polymers, PLGA has attracted the attention of many researchers due to its advantages compared to other materials, due to its exceptional safety profile and its FDA and EMA approval for human use [55]. PLGA is a polyester which degrades by hydrolysis of the ester connections into its monomer components lactic (PLA) and glycolic acid (PGA) (Figure 1.4). Both PLA and PGA enter the tricarboxylic acid cycle and they are finally eliminated from the body as carbon dioxide and water. Moreover, glycolic acid can be eliminated by the kidney without previous modification [100].

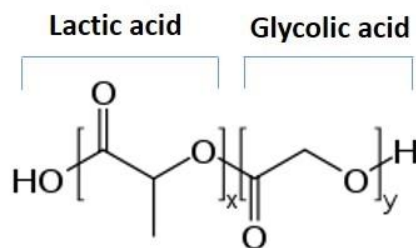


Figure 1.4 Poly lactic-co-glycolic acid (PLGA) molecular structure (x = number of units PLA; y = number of units of PGA).

These particulate delivery systems can be manufactured through a wide range of methods and therefore their physicochemical properties (size, morphology, surface charge) can be easily manipulated in order to achieve the adequate characteristics for the right interaction with biological cells [101-103]. In general, PLGA can be solubilised in broad range of solvents (e.g. acetone and chloroform) and PLGA particles can be manufactured by using methods such as double emulsion, coacervation, nanoprecipitation, extrusion or solvent evaporation [104-113]. Modification of the process parameters during the manufacturing method as well as the intrinsic PLGA properties dictates the size of the produced particles, which has been related to the type of immune responses obtained [114]. Commonly, PLGA particles are classified according to their particle size into nanoparticles (NPs) for particles smaller than 1000 nm and microparticles (MPs) for particles larger than 1000 nm. PLGA particles can either encapsulate or adsorb antigens onto their surface. However, due to their acidic interior environment, the manufacturing method or the solvent used for the dissolution of the polymer, the integrity of the antigens encapsulated into the PLGA NPs and MPs might be compromised and therefore, the antigen immunogenicity might be lost [115].

1.4.2.1 Effect of the PLGA composition: degradation rate and release profile

For the formulation design on PLGA as a vaccine delivery system, knowledge about its intrinsic properties is crucial in order to improve its efficacy. Several factors influence PLGA performance, among them, the monomer molar ratio, average molecular weight, crystallinity, size and shape are of absolute importance. PLGA polymer can be synthesized in wide variety of lactic to glycolic monomer ratios. The main PLGA copolymers used in research are 50:50, 65:35, 75:25 and 85:15, which in general contain higher lactic acid percentage. Varying the percentage of lactic or glycolic acid present in the polymer composition, influences the hydrophilicity of the polymer and thus, the degradation rate as reported in literature [116, 117]. The percentage of PGA influences greatly the hydrophilicity of the copolymer, therefore, PLGA copolymers with higher PGA content show accelerated degradation when compared to PLGA copolymers with higher PLA content. PLA has a methyl side group whereas PGA

lacks it, for that reason, PGA absorbs more water and hence degrades faster. For example, PLGA 50:50 shows the fastest degradation of all PLGA copolymers followed by PLGA 65:35, PLGA 75:15 and finally PLGA 85:15, which corresponds to the slowest degradation rate. Thus, the composition of PLGA plays a crucial role in the formulation of vaccine delivery systems as it will affect the antigen release [118]. The crystallinity and glass transition temperature (T_g) of the polymer also influences the degradation. In general the increase of PLA in the polymer composition results in lower copolymer crystallinity and thus, faster degradation due to increase hydrophilicity. Studies in literature disagree on this matter, as some groups have shown the increase of PLA accelerated the degradation rate due to the increase in polymer hydrophilicity, whereas other groups have shown that the opposite [119-121]. PLGA shows a rigid structure as its T_g is above 37°C. This temperature decreases with the PLA ratio and the molecular weight [122]. T_g and crystallinity also depend on another important characteristic of the PLGA impacting the degradation rate, which is the average molecular weight (Mw) of the copolymer. The copolymer Mw is inversely proportional to the degradation rates, thus, the higher the Mw the slower the polymer degradation due to the larger polymer chain [123].

It has been reported elsewhere that the release behaviour of PLGA generally follows either a biphasic or based on an initial burst release followed by a sustained release, or a triphasic profile (with an added final burst release) [124, 125]. It depends on the physical properties of PLGA and on the payload type and concentration, hence, the antigen release profile is commonly uncertain. This process takes place upon contact of the polymer with an aqueous environment, and it happens primarily as a consequence of water entering the polymer matrix, resulting in uniform bulk diffusion and erosion. Initial burst release is related to the antigen located near the polymer surface whereas the sustained release phase. Upon water entrance into the polymer matrix, PLGA degradation occurs resulting in the formation of channels for the release of the entrapped antigen until the polymer is totally solubilised.

1.5 Pulmonary delivery

The pulmonary route of administration is a prominent route for the delivery of drugs and vaccines due to numerous factors including ease of patient compliance, large surface area of the target site and an extensive vascular system supplying a rich amount of blood [126]. As a result of these beneficial attributes, the use of aerodynamic engineered delivery systems to carry small molecules and antigens to the lung for controlled release, deep lung deposition and higher systemic bioavailability has been previously used [127]. In particular, the use of micro- and nanometre delivery systems including

liposomes and polymers have been used to administer therapeutic payloads through this route of administration [128-131]

Lungs are the portal entry of Mtb, and for the bacteria in order to cause infection it must first overcome a number of barriers within the human body. Mtb droplet nuclei can enter the body both through the mouth or the nasal cavity, and upon entrance, it has to pass the trachea, bronchi and bronchioles in order to reach the AM which besides being the largest surface area in the lungs, serves as the host site of infection for Mtb. An understanding of these physical, chemical and biological challenges that Mtb faces is essential for future development of antigen delivery systems that aim to effectively vaccinate large populations [132].

1.5.1 Particle deposition in the lungs: Impaction, sedimentation and diffusion

When developing a particulate delivery system for pulmonary vaccination, a deep insight into the inner workings of the respiratory pathway is essential. An understanding of how micro and nanoscale particles interact within the various regions of the pathway and the challenges associated with these sections is crucial for effective particle deposition. Multiple factors influence this deposition including particle size, breathing patterns of the individual, mucocilliary clearance and the laws of physics that are at play within the lung space [133]. Therefore, the rational design of delivery systems has to consider physicochemical properties such as size and shape, geometry, charge and density of the particulate system for the deposition of the inhaled particles [134]. When discussing particle attributes in terms of particle size for inhalation, the mass median aerodynamic diameter (MMAD) is used and can be defined as the diameter at which 50% of the particles in a population are larger in mass than the other smaller 50% [135].

Particle deposition within the lungs can be classified into three mechanisms based primarily upon particle size: Impaction, sedimentation and diffusion. Impaction occurs for large particles, (above 10 μm MMAD) and the dominant force acting upon these particles during an inhale is momentum [132]. As the airflow moves down through the oesophagus, the larger particles cannot navigate through the twists and turns and largely are deposited onto the airway wall of the first ten bronchial generations as a result of centrifugal force [136, 137]. Therefore these particles largely cannot travel deep within the lungs as they are mainly cleared out by the mucociliary escalator where they then end-up deposited within the stomach. Generally, as the particle size decreases, the ability of the particulate delivery systems to permeate deeper within in the lung increases. Smaller particle undergo sedimentation after reaching the lung – a process which forces the build-up of the particles within the

lower bronchi due to gravity [137]. Within these sections of the airway system (the last 5 bronchial generations), the airflow is significantly less turbulent and therefore over time, gravitational forces encourage the particles to settle [136]. It is believed that this sedimentation process can therefore be enhanced by manipulating the breathing patterns of patients following administration. Finally, diffusion occurs for particles under a 0.5 microns threshold where they are typically exposed to Brownian motion laws, as a result of the lack of air speed within the alveolar spaces. Within these spaces, the particles are held in suspension and abnormally move around with limited contact to the tissue and a lack of deposition, thus the particles are generally exhaled back out [132, 133]. Understanding these mechanisms involved in particle deposition during inhalation treatment is thus essential for developing an effective delivery system. Design of particulates within the MMAD range of 0.5 – 5 μm could consequently prove to be the most promising approach based on the literature outlined. The use of an pharmacopoeia approved airway simulator selected according to the physical state of the particles (liquid or dry powder) such as Andersen Cascade Impactor (ACI), Next Generation Impactor (NGI) and Multi-stage Liquid Impinger (MSLI) is essential for the determination of the expected particle deposition within the lungs [138].

1.5.2 Alveolar macrophages (AM) particle uptake: endocytosis

Alveolar macrophages can be found in multiple locations as in the vasculature, parenchyma or airways and represent the first line of defence against Mtb. Recently, the importance of the recruitment of T cells to the lungs for the protection against TB infection has been demonstrated. The location of these T cells is crucial for the efficacy of the vaccine since the T cells have to be in direct contact with the Mtb infected macrophages [139-144]. Therefore, respiratory mucosal vaccination is believed to be the best way to teach the lung macrophages and DCs how to fight Mtb infection and to recruit antigen specific T cells to the site of infection [145, 146].

In order to achieve the satisfactory uptake by the AM, vaccine formulations have to be designed based on the understanding of how particles are engulfed. Consequently, physicochemical characteristics of the aerosol particle formulation such particle size, shape and charge (besides the composition of the particulate system) have to be modified in order to accomplish macrophages uptake. According to results reported in literature, aerosol particles with spherical shape are more efficiently taken up by AM than other shapes [147]. Besides, particle sizes in the nanometre and micrometre range are well taken up by macrophages, in general particles below 5 μm can be deposited in the deep lungs and be phagocytosed by AM [148, 149]. Regarding particle surface charge, positively charged particles show higher interaction with the cells due to the negatively cell surface charge. However, cationic particles

might show high toxicity and can damage the cells in the lungs due to the formation of reactive oxygen species (ROS) and the promotion of apoptosis [150, 151]. For this reason, the use of anionic and neutral particles for the delivery of small molecules and vaccines into the lungs has attracted the attention of the many researchers (e.g. [131, 152-155]). Additionally, it has been reported that particles based on hard material are better taken up than softer ones [156].

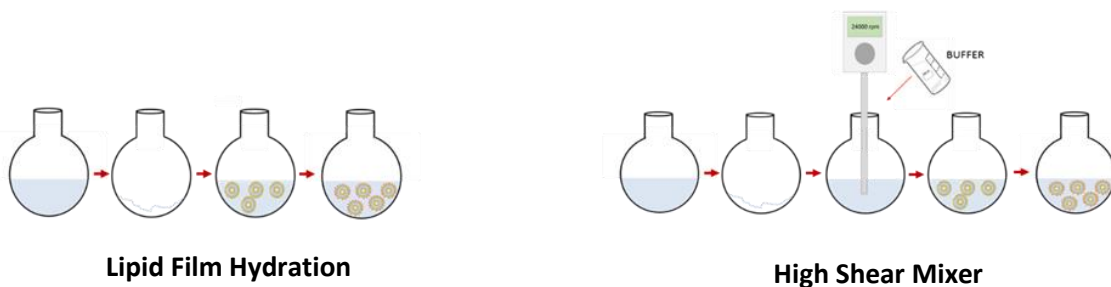
1.6 Hypothesis and general objectives

New approaches have to be taken into account for the development of a TB vaccine against pulmonary TB. Due to the intracellular nature of Mtb, recent research has focused on the design of adjuvants that “pull” T cells to the lungs, as T cells have to be in direct contact to the infected cells in order to be able to eradicate it. The proposal of the work reported in this thesis consists of an immunisation strategy based on the parenteral priming of a T cell helper (Th) -17 response followed by mucosal boosting. This strategy is built on data produced by Statens Serum Institut, showing that a parenteral priming of the H56 vaccine candidate in combination with the CAF01 adjuvant followed by mucosal boosting with H56 mediate local immunity without causing local vaccine induced side-effects (personal communication). Therefore, the primary objective of this project was to develop an inert delivery system that can deliver the H56 antigen into the lungs without potential side effects. The following objectives were set in order to accomplish this:

- Evaluation of a microfluidics method for the manufacturing of CAF01 as a scale-independent manufacturing method.
- *In vivo* evaluation of the CAF01 formulations manufactured using microfluidics and using the traditional liposomal manufacturing method of lipid film hydration.
- Evaluation of microfluidics as a manufacturing method for PLGA particles and comparison to the traditional double emulsion method.
- Investigate the effect of the microfluidics parameters and the PLGA properties on the production of PLGA as antigen delivery systems.
- Aerodynamic engineering of a PLGA particles for pulmonary delivery of H56 TB vaccine candidate via selection of an adequate cryoprotectant for the lyophilisation of PLGA particles and *in vitro* deposition, particle uptake, toxicity and antigen processing in macrophage cell lines.
- *In vivo* evaluation of a prime-pull approach by priming with CAF01:H56 and boosting with PLGA:H56 for the development of a TB vaccine effective against pulmonary TB.

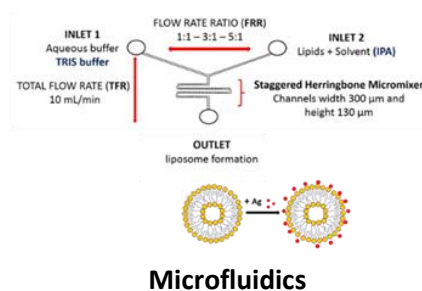
Chapter 2

Scale-independent manufacture of liposomal cationic adjuvants



Lipid Film Hydration

High Shear Mixer



Microfluidics

Papers related to this chapter:

Y. Perrie, E. Kastner, S. Khadke, **C. B. Roces**, P. Stone (2015). Manufacturing methods for liposomes. MiMB, Vaccine adjuvants: methods and protocols. Springer.

C. B. Roces, E. Kastner, P. Stone, D. Lowry and Y. Perrie (2016). Rapid quantification and validation of lipid concentrations within liposomes. Pharmaceutics.

2.1 Introduction

Liposomes are well reported for their activity as adjuvants, which are needed for the subunit vaccine formulation in order to induce potent and long-lasting immune responses. The physicochemical attributes of liposomal adjuvants have been associated with specific immunological responses, demonstrating that the design and development of vaccine adjuvants is of great importance in tailoring them to promote the desired immune responses. Indeed, pharmacokinetic studies have shown the importance of vesicle characteristics such as particle size and surface charge on the draining of the vaccine adjuvants to the lymph nodes and the recruitment of APCs to the injection site [157]. Lipid composition is a key factor controlling the characteristics of the liposomes produced. For example, membrane fluidity can be modified by inclusion of cholesterol within the liposomes, improving membrane stability [158]. Besides, hydrocarbon chain saturation and length can influence the rigidity of the liposomal membrane. In general, short chain lengths form disorganised and fluid membranes whereas rigid and ordered structures are obtained with long hydrocarbon chain lipids. The use of cationic lipids favours the absorption of subunit antigens onto the liposomal surface and promotes strong cell mediated immune responses due to better interaction with the negatively charged surface of the APCs [70]. In contrast, neutral lipids contribute to enhanced humoral responses [159]. Incorporation of immunopotentiator compounds can further enhance their immunological responses [75].

The manufacturing method used for the production of liposomes also has a big impact on their physicochemical characteristics. The traditional lipid film hydration method [57, 160, 161], which was the first technique used for the preparation of liposomes, is still in common practice. By this method it is difficult to control the particle size of the liposomes, producing highly polydisperse MLVs, thus, a second method to reduce the particle size is often needed. To address this, new techniques based on the controlled fluid mixing are emerging due to their easier scalability and tighter particle size production compared to traditional methods, allowing for large scale production. Therefore, all these factors should be taken into account when designing subunit vaccine adjuvants as they will to some extent dictate the adjuvant action [162].

2.2 Aim and objectives

The cationic liposomal adjuvant formulation (CAF) 01 which is based on the cationic surfactant DDA bromide and the immunopotentiator TDB from Mtb has previously been shown to be a strong adjuvant system against several diseases such as tuberculosis [75]. CAF01 is commonly prepared by

the thin film method [57] which has several drawbacks including scale-up and reproducibility. In contrast, controllable technologies such as microfluidics have advantages in material preparation such as uniform flow and mixing, high efficiency, continuous operation, easy control and low cost [163]. Therefore, the aim of this study was to investigate the use of microfluidics as a manufacturing method for CAF01. To achieve this, the objectives of this study were to:

1. Study the key parameters associated with the microfluidic liposome production, including choice of lipid and lipid concentration, flow rate ratio, total flow rate and residual solvent.
2. Develop and validate an analytical method for quantification of lipids within liposomal adjuvants.
3. Evaluate and compare the use of different liposome manufacturing techniques in terms of physicochemical characterisation, lipid recovery and antigen loading.
4. Assess the impact of incorporating cholesterol into the CAF01 bilayer and the substitution of the cationic DDA for the neutral lipid 1,2-dimyristoyl-*sn*-glycero-3-phosphocholine (DMPC) on the physicochemical attributes of the liposomal formulations produced.

2.3 Materials and methods

2.3.1 Material used for the preparation of liposomal formulations

The cationic surfactant dimethyldioctadecylammonium (DDA) bromide, the immunopotentiator trehalose 6,6'-dibehenate (TDB) and 1,2-dimyristoyl-*sn*-glycero-3-phosphocholine (DMPC) were purchased from Avanti Polar Lipids Inc. (Alabaster, USA) (Table 2.1). Albumin from chicken egg (ovalbumin), cholesterol and ethylenediaminetetraacetic acid (EDTA) were purchased from Sigma-Aldrich Company Ltd. (Poole, UK). 2-amino-2-(hydroxymethyl)-1,3-propanediol (Tris-base) was obtained from IDN Biomedical Inc. (Aurora, OH, USA) and used to make 10 mM Tris buffer and adjusted to pH 7.4 using hydrochloric acid (HCl). All other reagents were of analytical grade and were purchased from commercial suppliers.

Table 2.1: Information about the lipids used for the formulation of liposomal adjuvants.

Lipids	T _m (°C)	M _w (g/mol)	Structure
DDA	47°C	630.952	
TDB		987.433	
DMPC	24°C	677.933	
Cholesterol		386.65	

2.3.2 Methods for manufacturing liposomes

Three different techniques for the production of liposomes were applied and compared: the lipid film hydration method (LH), high shear mixing (HSM) and microfluidics (MF). Four liposomal formulations were prepared: DDA and TDB concentrations were fixed at 2.5 mg/mL and 0.5 mg/mL respectively and cholesterol was added to the CAF01 formulation at two different concentrations (0.4 mg/mL and 0.8 mg/mL) in order to increase the fluidity of the membrane bilayer. In the fourth formulation, DDA was replaced by DMPC and kept at the original concentration (2.5 mg/mL DMPC and 0.5 mg/mL TDB respectively).

2.3.2.1 Lipid film hydration method (LH)

Liposomes were prepared by a modification of the Bangham method [57]. Weighed amounts of DDA, TDB, cholesterol and DMPC were dissolved in the appropriate ratios in a mixture of chloroform and methanol (9:1 v/v). The required amount of lipid solution was transferred to a round bottom glass to reach the appropriate final concentration (2.5 mg/mL DDA or DMPC, 0.5 mg/mL TDB, 0.4 or 0.8 mg/mL

cholesterol). Organic solvent was removed under vacuum with a rotary evaporator during 15 min at 200 revolutions per minute (rpm). Afterwards, the lipid film was dried with a gentle stream of nitrogen (N_2) in order to remove any trace of organic solvent. Then, lipid film was hydrated with the appropriate amount of 10 mM Tris buffer (pH 7.4). Lipid suspensions were heated above transition temperature (60°C) for 20-30 min and vortexed for 1-2 min every 5 min (Figure 2.1). Liposomes were stored at $2-8^\circ\text{C}$ for further experiments. Ovalbumin (OVA) was added in a concentration of $2\ \mu\text{g}$ per vaccine dose ($50\ \mu\text{L}$) to the preformed liposomes and samples were vortexed for few minutes during 30 min. Samples were allowed to stand for 10-15 min for an effective adsorption on the liposomal surface.

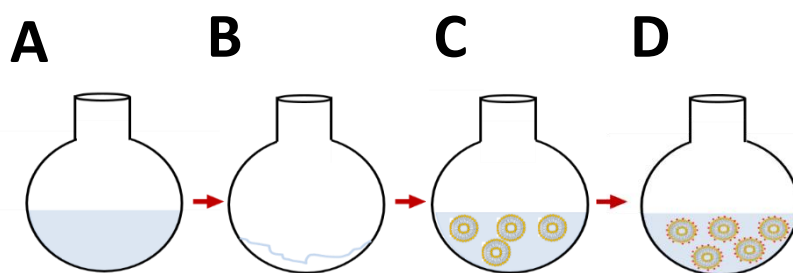


Figure 2.1 Schematic representation of thin film method: (A) lipids dissolved in organic solvent, (B) formation of the lipid film, (C) addition of the buffer above T_m and under agitation to form MLVs, (D) Incorporation of antigen/protein post liposome formulation.

2.3.2.2 High shear mixing (HSM)

High shear mixing is a size-reduction technique for the preparation of homogeneous sample population of SUVs from either preformed liposomes (MLVs) or by hydration of lipid powders [164, 165]. The principle behind this method is based on the rotor-stator theory. By this means, liposomal solutions are reduced in size due to the rotor speed which pushes the formulation towards the stator and shears off the outer layers of the liposomes [164-166]. Conducting this procedure at high speeds and at temperatures above the T_m of the lipid system results in the production of homogeneous liposomal formulations [164, 165]. Liposomal size and size distribution depend on the time and rotational speed at which the samples are manufactured. By this method, SUVs can be formed from either preformed MLVs or from the thin lipid film prepared as described in before. Thus, after preparation of the thin lipid film, formation of SUVs was done by hydration of the film with Tris buffer (10 mM, pH 7.4) and high shear mixing above transition temperature of the lipid mixture (at 60°C). The head of the HSM (Silent crusher M, Heidolph Instruments, Schwabach, Germany) was immersed in the formulation and samples were homogenized at high speed ($125,000 \times g$) during 15 minutes (Figure 2.2). Temperature was kept constant throughout the process. OVA was added in a concentration of $2\ \mu\text{g}$ per vaccine dose ($50\ \mu\text{L}$) to the preformed liposomes and samples were vortexed

for few minutes during 30 min. Samples were allow to stand for 10-15 min for an effective adsorption on the liposomal surface.

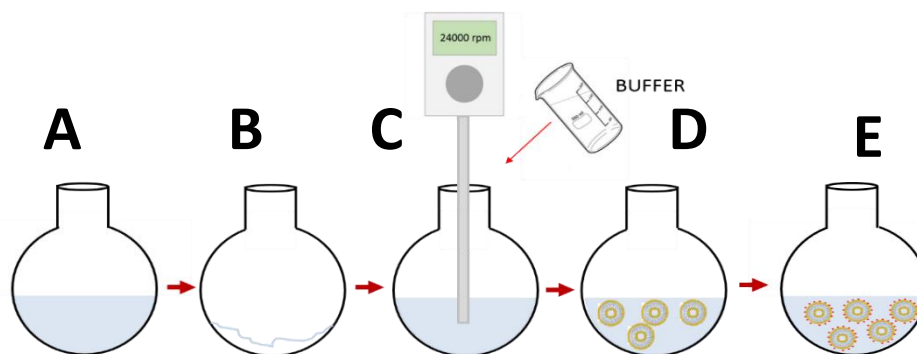


Figure 2.2 Representation of HSM method: (A) lipids dissolved in organic solvent, (B) formation of the lipid film, (C) addition of the buffer, formulation mounted in a water bath and immersion of the HSM probe, (D) formation of SUVs, (E) antigen loading after liposome formation

2.3.2.3 Microfluidics (MF)

Microfluidics is a technology which manipulates the mixing of liquid flows in micro-sized channels and allows the formation of size-controlled nanoparticles [163]. The preparation of liposomal formulations was carried out using the staggered herringbone micromixer (SHM) from Precision Nanosystems (Nanoassemblr™, Vancouver, Canada) (Figure 2.3) [167]. SHM is based in the pass of two different fluid streams through the herringbone structures located in the middle of the channel (300 μm width and 130 μm height). Lipids dissolved in an adequate solvent (i.e. compatible with the chip) and an aqueous buffer are injected into the system. Streaming of the fluids is controlled by the micromixer's software. Therefore, the software controls the flow rate ratio (FRR) (ratio between the two stream fluids), the total flow rate (TFR) of both streams, and the total amount of sample to be produced [167]. The formation of nanoparticles is due to the increasing advection, diffusion and the chaotic low profile which provoke an increase of polarity and therefore, a nanoprecipitation reaction [168].

Stocks of DDA, TDB, cholesterol and DMPC were prepared in 2-propanol (IPA) and mixed to the desired concentration. Lipids dissolved in IPA were injected into the right inlet whereas the aqueous phase was injected into the left microfluidics inlet (Figure 2.3). Selected speeds (TFRs) and ratios between the aqueous and organic phase were adopted in order to analyse the importance of these parameters in the production of liposomes. Thus, TFRs of 5 – 10 – 15 mL/min were chosen as well as FRRs of 1:1, 3:1 and 5:1. In general a total sample volume of 1 mL was prepared, with a start and end waste volume fixed at 0.3 and 0.05 mL respectively. The heating block was set at 60°C.

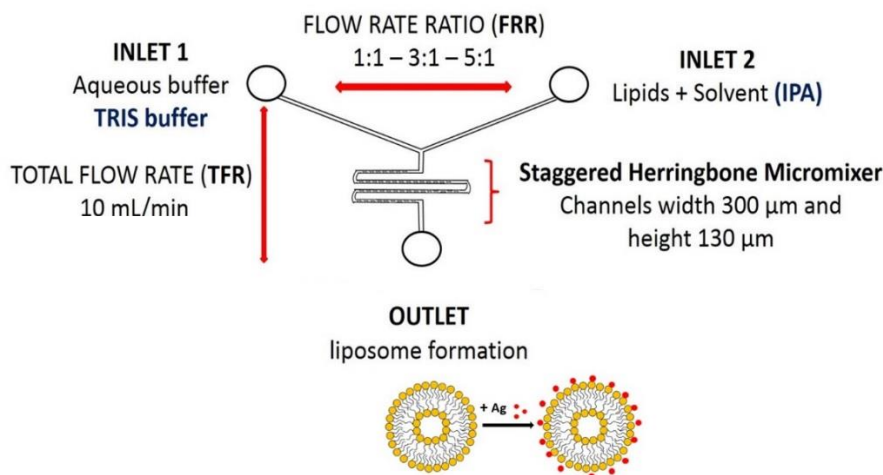


Figure 2.3 Representation of microfluidics cartridge: Aqueous phase (inlet 1) and lipids in solvent (inlet 2) are injected into the microfluidics system and liposomes are formed by a nanoprecipitation reaction and collected in the outlet.

OVA was added in a concentration of 2 μg per vaccine dose (50 μL) to the preformed liposomes and samples were vortexed for few minutes during 30 min. Samples were allowed to stand for 10-15 min for an effective adsorption on the liposomal surface.

2.3.3 Purification of the liposomal formulations

2.3.3.1 Dialysis purification

Dialysis tubing (Mw 12,000-14,000 Da, Sigma Aldrich, Poole, UK) for solvent removal was pre-treated during 2 h at 80°C in a solution containing 1 mM EDTA and 2% sodium bicarbonate in order to remove the sulphites and glycine contained in the membrane. Afterwards, the membrane was washed with deionised water and stored in 20% ethanol solution containing 1 mM EDTA. For 300,000 Da MWCO membrane (Spectra-Por®, Spectrum Labs, Breda, The Netherlands) manufacturer instructions were followed. Samples were loaded into the dialysis tubing with the appropriate MWCO (<14,000 Da and 300,000 Da for solvent or protein removal respectively) and dialysed against 200 mL Tris buffer (Figure 2.4). Buffer exchange was carried out at different intervals depending on the aim of the dialysis (Table 2.1).

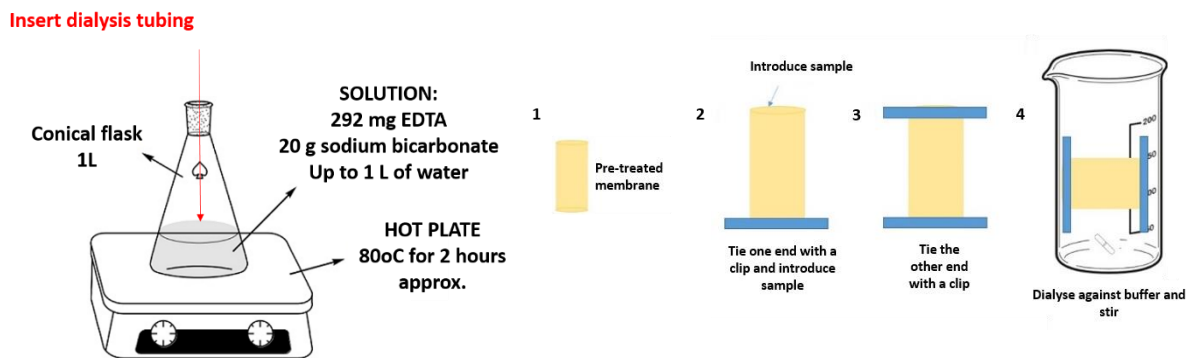


Figure 2.4 Dialysis process: (1) pre-treatment of the dialysis membrane to remove any contaminant, (2) close one of the ends and introduce the sample, (3) close the other end, (4) dialyse the sample against the adequate amount of buffer under stirring and exchange the buffer according to the method selected.

Table 2.2 Methods used for solvent and protein removal.

Method	Duration	Buffer exchange
<u>Dialysis tubing <14,000 Da</u>		
Solvent removal (fast)	1 h	After 30 min
Solvent removal (slow)	4 h	Every hour
<u>Dialysis tubing 300,000 Da</u>		
Protein removal	24 h	Every 2 h during the first 6 hours and 2 h before stop dialysis.

2.3.3.2 Ultracentrifugation

For the removal of unbound protein from the liposomal formulations prepared through the LH method samples were centrifuged at 125,000 x g during 30 min at 4°C in order to sediment liposomes. The supernatant was discarded and liposomes re-suspended in the appropriate amount of Tris buffer.

2.3.4 Gas chromatography (GC) for quantification of residual solvent

One of the main disadvantages of the microfluidics method is the use of organic solvents and therefore their removal from the formulation. The International Conference of Harmonization (ICH) of technical

requirements for registration of pharmaceuticals for human use has established limits for the organic solvents may contain formulations intended for human use. The guideline Q3C(R5) for residual solvents divides organic solvents into three classes (Table 2.3). Thus, organic solvent used during microfluidics process has to be within these limits, otherwise these adjuvant formulations are not allowed to be clinically tested because of the dangers they may cause [169].

Table 2.3 General classification of residual solvents according to ICH guidelines. Only some examples are shown [169]

Class	Compound	Concentration limit (ppm)
<i>Class I</i>	Benzene	2
Solvents to be avoided	Carbon tetrachloride	4
<i>Class II</i>	Acetonitrile (ACN)	410
Solvents to be limited	Methanol (MeOH)	3000
<i>Class III</i>	Ethanol (EtOH)	5000
Solvents with low toxic potential	1-Propanol	5000
	2-Propanol (IPA)	5000

Standards were prepared with different volumes of the analyte of interest (IPA) while keeping constant the internal standard (IS) volume (1-Propanol). For sample preparation, samples were diluted (1:20) in ultrapure water (type I) and the same percentage of the internal standard used for the calibration curves was included in the sample preparation (1% v/v 1-Propanol). The internal standard, 1-Propanol, was chosen as it is not contained in the samples and has a different boiling point (Table 2.4) which allows the separation of the volatile analyte mixture in two well separated peaks (no coelution). GC instrument (CSi 200 Gas chromatography, Cambridge Scientific Instruments Ltd., Cambridge, UK) temperatures were set as follows: 55°C oven temperature, 200°C and 230°C injector and detector temperatures, and helium 15 psi was used as a carrier gas. Calibration curve of IPA was made plotting the area ratio of the analyte/IS of triplicate results against the concentration.

Table 2.4 Boiling points of the organic solvents used during the microfluidic formulation of the liposomal adjuvants and the selected internal standard.

Organic Solvent	Boiling point (°C)
1-Propanol	97
2-Propanol	83
Acetonitrile	82
Methanol	65
Ethanol	78

2.3.5 Determination of the particle size, polydispersity and zeta potential by dynamic light scattering (DLS)

Determination of the particle size, and polydispersity index (PDI) is generally carried out using dynamic light scattering (DLS), which is a non-invasive technique that measures these parameters by quantification of the variation of the intensity of the scattered light as a function of time at a fixed scattering angle (Θ) (typically is 90°) [170, 171]. The particle size is determined by measuring the velocity of the particles in a sample going through Brownian motion, which is defined as the random movement of particles in a liquid due to collisions with molecules that surround them [172]. The velocity is defined by the translational diffusion coefficient (D) which by Stokes-Einstein equation is converted into particle size (Equation 2.1) [172]:

$$d_H = \frac{kT}{3\eta\pi D} \quad (\text{Equation 2.1})$$

Where d_H is the hydrodynamic diameter, k is the Boltzmann's constant and η is the viscosity of the sample. The hydrodynamic diameter refers to the diameter of a sphere as DLS assumes that the particles in the sample are spherical-shaped [173]. The size range that DLS can measure ranges from few nanometres to several microns [171]. To measure the particle charge at the slip plane of the particle surface (zeta potential) and electrophoretic mobility of the particles in solution, electrophoretic light scattering is used [172].

The size of liposomes was determined by DLS (Zetasizer nano ZS, Malvern PANalytical Ltd., Worcestershire, UK) approximately one hour after preparation. Three measurements at 25°C were conducted on the samples, which were previously diluted in filtered Tris buffer (10 mM, pH 7.4) to

achieve the optimal vesicle concentration (1:10 v/v) and vortexed to provide a homogeneous solution. Square single-use cuvettes were filled in with 1 mL of sample and were placed into the instrument which uses a 4-mW He-Ne 633 nm laser to analyse the samples [170]. For zeta potential measurement, samples were diluted in the same fashion as for the size (10-fold dilution). Three measurements of each sample at 25°C were taken. For collection and data analysis Malvern Dispersion Technology Software v.7.11 (Malvern PANalytical, Worcestershire, UK) was used.

2.3.6 Quantification of antigen loading and lipid recovery by High Performance Liquid Chromatography using an Evaporative Light Scattering Detector (HPLC-ELSD)

Evaporative light scattering detector (ELSD) or evaporative mass detector is used for the quantification of non-volatile components dissolved in volatile solvents. By this means, a nebuliser evaporates the solvent whereas the non-volatile compound becomes a mist of small particles which scatter a light beam and thus, the detector can quantify the amount of sample according to the scattered light detected (Figure 2.5) [174]. ELSD is generally used with a gradient elution analysis. Gradient elution is based on the change of the mobile phase composition during analysis. Commonly, mobile phase A contains the weaker solvent which usually is water with 0.1% trifluoroacetic acid (TFA), whilst mobile phase B contains the stronger solvent (ACN or MeOH) [174].

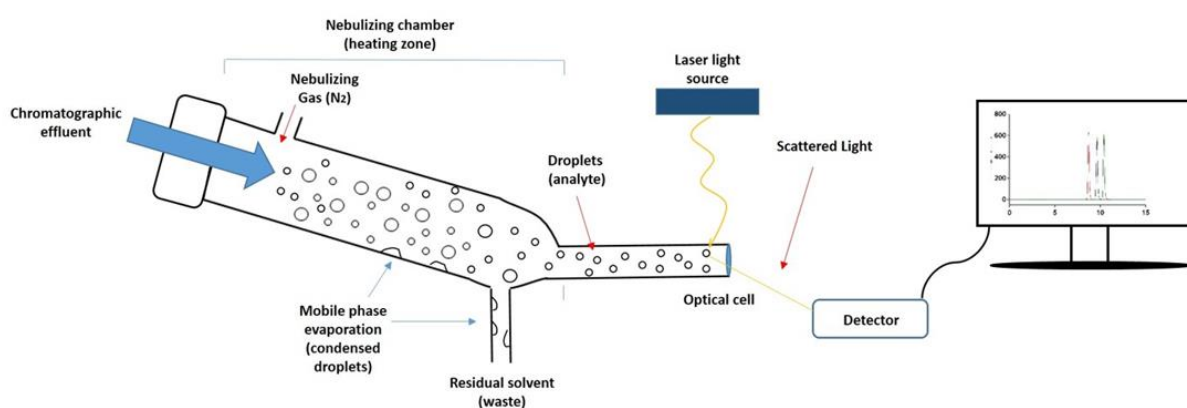


Figure 2.5 Schematic representation of the mechanism of an evaporative light scattering detector (ELSD). First, the chromatographic effluent passes through the nebulizer and mixes with the nebulizing gas (N₂) causing dispersion of droplets. Subsequently, droplets enter into the nebulizing chamber where the mobile phase evaporates and condense, being removed as waste. Finally, the analyte crosses an optical cell, a laser beam penetrates the particles and the scattered light is detected and converted into a signal.

Quantification of the lipid recovery and antigen loading was performed by high performance liquid chromatography (HPLC, YL Instruments Co. Ltd. Korea) using an SEDEX 90LTD ELSD detector (Sedex

Sedere, Alfortville, France). A Luna 5 μ C18(2) column (Phenomenex, Cheshire, UK), pore size of 100Å, was used for lipid quantification whereas a Jupiter 5 μ C18(2) column (Phenomenex, Cheshire, UK) pore size 300Å was used for antigen quantification. A C18 column (stationary phase) increases the retention of non-polar analytes. Lipids were dissolved in chloroform:methanol (9:1 v/v) and the antigen (OVA) was dissolved in buffer. Liposomal samples were injected without previous preparation. HPLC-ELSD settings were kept constant as follows: 30 μ L injection volume in a partial loopfill injection mode, 100 μ L loop volume and 15 μ L tubing volume. Column temperature was maintained at 35°C whereas the ELSD temperature was set at 52°C in all the runs. Analysis time, flow rate and mobile phases were changed depending on the nature of the sample measured (Table 2.5). Nitrogen was used as a carrier gas at 3.5 psi inlet pressure. Clarity DataApex version 4.0.3.876 was used for data analysis.

Table 2.5 HPLC methods: (A) Gradient elution method for the quantification of cholesterol, DMPC, TDB and DDA. Gain was adjusted for each lipid, being Gain 12 for TDB and Gain 3 for the rest of the lipids; (B) Method used for the quantification of OVA loading efficiency. Retention time 12.2 min. Gain 10.

A	Time	% Eluent A	% Eluent B	Flow rate
	(min)	(0.1% TFA in dH ₂ O)	(MeOH)	(mL/min)
	0	15	85	1.5
	6	0	100	1.5
	25	0	100	1.5
	26	15	85	1.5
	35	15	85	1.5
B	Time	% Eluent A	% Eluent B	Flow rate
	(min)	(0.1% TFA in dH ₂ O)	(MeOH)	(mL/min)
	0	100	0	1
	10	0	100	1
	15	0	100	1
	15.1	100	0	1
	20	100	0	1

Quantification of the lipid recovery for liposomal formulations prepared by the thin film method or HSM was done following Equation 2.2. Calculation of the recovery of the samples manufactured through microfluidics was performed according to Equation 2.3. Basically, the area of the peak given by the HPLC-ELSD was converted into concentration by using the appropriate calibration curve previously carried out. This result was divided by the initial concentration in the stock solution and

multiplied by 100%. In the case of the microfluidics samples, as the dilution is unavoidable through this method, the theoretical final lipid concentration after microfluidics was considered instead of the lipid concentration in the stock solution. The same calculations were performed for antigen quantification.

$$\frac{\text{concentration of the sample } \left(\frac{\text{mg}}{\text{mL}}\right)}{\text{concentration stock solution } \left(\frac{\text{mg}}{\text{mL}}\right)} \times 100 = \% \text{ recovery} \quad (\text{Equation 2.2})$$

$$\frac{\text{concentration of the sample } \left(\frac{\text{mg}}{\text{mL}}\right)}{\text{theoretical final concentration } \left(\frac{\text{mg}}{\text{mL}}\right)} \times 100 = \% \text{ recovery} \quad (\text{Equation 2.3})$$

2.3.7 Sodium dodecyl sulfate (SDS) polyacrylamide gelelectrophoresis (PAGE) for the qualitative analysis of the protein loaded

Gel electrophoresis was carried out in order to determine whether the protein was adsorbed onto the liposomal surface. Prior to load the samples into the 12% Tris-Glycine gels, samples were centrifuged at 272,000 x g during 30 min in order to get pellet and supernatant for each sample. Loading buffer was added to each of this fractions and then heated at 90°C during 3 min in order to denature the protein present in the sample. A volume of 10 µL of each sample pellet and supernatant was added onto the gels and compared with 10 µL of a known amount of the protein (40 µg/mL of OVA). Running buffer (Tris, Glycine, SDS and dH₂O) previously prepared was poured into the Novex Mini Cell gel apparatus (Bio-rad Laboratories, Herfordshire, UK) and let run until the dye reached the end of the gel at a constant 30 mA per gel. Afterwards, the gel was stained overnight with Coomassie blue and destained the day after for several hours. GeneFlash gel photoimager (Syngene bioimaging) was used to take a picture of the gels (Figure 2.6).

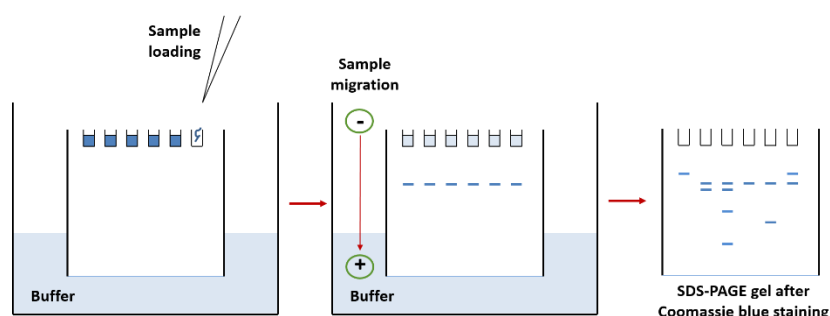


Figure 2.6 Simplified representation of SDS-PAGE technique: Gels are placed within the apparatus and samples are loaded on the top of it. Then proteins move through the porous gel from the top to the bottom due to an electrical current. The speed at which particles are drawn through the matrix depends on their mass.

2.3.8 Statistical analysis

One-way ANOVA or two-way ANOVA followed by Tukey's multiple comparison tests were used for data analysis. All the experiments were carried out at least in triplicate unless otherwise stated. Results are the mean of 3 measurements \pm standard deviation (SD) which is plotted as error bars.

2.4 Results and discussion

2.4.1 Production of CAF01 liposomes using the microfluidics technique Nanoassemblr™

The use of microfluidics as a technique for the production of liposomes has emerged during the last two decades. The Benchtop Nanoassemblr™ from Precision Nanosystems Inc., is a computerised system which controls the mixing of fluids within the micromixer. The micromixer is specially designed with microchannels containing a SHM in the middle which contains grooves that help with the mixing. It offers several advantages over the traditional methods, such as reduced time due to the fast mixing of the fluids within the micromixer and the ease of preparation of the sample. Besides, tight size control, reproducibility and scalability of liposomes and nanoparticles can be achieved [168, 175]. Lipids dissolved in solvent and aqueous phase converge at the centre of the channel where, due to lamellar flow, the polarity is increased and consequently the liposomes are formed due to a nanoprecipitation reaction and collected at the outlet of the micromixer. The speed at which the polarity increases is controlled by changes on the microfluidics parameters adopted [168, 176]. Moreover, Precision Nanosystems, Inc. has developed a system for scale up production through parallelisation of the micromixers (www.precisionnanosystems.com).

Based on the possibility of variation of the microfluidics parameters and the intrinsic properties of the formulation, the optimisation of the manufacturing of CAF01 using microfluidics was evaluated by alteration of a range of factors: the lipid concentration, the ratio between aqueous and organic phase (FRR) and the speed at which the liposomes are produced (TFR).

2.4.1.1 Effect of the lipid concentration

Lipids were dissolved in IPA and injected into the Nanoassemblr™ alongside the buffer (Tris 10 mM, pH 7.4) at a specific TFR and FRR. IPA was selected as solvent for microfluidics due to the failure of other solvents to dissolve TDB and the incompatibility of chloroform with the microfluidics cartridge, which is made of the thermoplastics Cyclic Olefin Polymer (COP) and Cyclic Olefin Copolymer (COC).

The aim of this experiment was to establish the minimum lipid concentration needed for the preparation of CAF01 liposomes and thus, reduce the cost of the method optimisation. Previous studies carried out by Davidsen et al. showed that CAF01 immunological responses were improved when the DDA:TDB molar ratio was fixed at 8:1 (5:1 weight ratio)[75]. Therefore, variation of the initial lipid concentration whilst keeping the DDA:TDB molar ratio constant was examined. Initial liposomes concentrations of 0.3, 1, 2, 3, 4, 6 and 24 mg/mL were formulated at constant microfluidics parameters TFR of 10 mL/min and FRR of 3:1. Figure 2.7A depicts the size of the liposomes at different initial total lipid concentrations. Results were highly variable although it is possible to observe that at low concentrations such as 0.3 mg/mL the size of the CAF01 liposomes was significantly ($p < 0.05$) smaller compared to the other concentrations tested. When increasing lipid concentration, the particle size reached a plateau where no significant changes were observed in the range from 1 to 24 mg/mL. CAF01 liposomes were heterogeneous in nature, showing PDIs > 0.2 (Figure 2.7B). Polydispersity indexes were highly variable at low DDA:TDB concentrations (0.3, 1 and 2 mg/mL). The variability was reduced when concentrations of 3 mg/mL or higher were used (PDIs ~ 0.3). In terms of zeta potential, all formulated liposomes were highly cationic with values between +60 to +75 mV for initial lipid concentrations from 1 to 24 mg/mL whereas CAF01 liposomes formulated with an initial concentration of 0.3 mg/mL showed significantly ($p < 0.05$) lower surface charge (from +43 to +52 mV) (Figure 2.7C).

These results suggest that 3 mg/mL appears to be the critical point, thereafter the variability in particle size, PDI and zeta potential is reduced. The *in vivo* adjuvant dose for DDA:TDB is a final concentration of 6 mg/mL following microfluidic production (24 mg/mL initial lipid concentration at FRR 3:1); however, this adjuvant formulation has a very high financial cost, therefore 3 mg/mL was selected for physicochemical characterisation studies. It has been previously reported in literature that the optimal DDA:TDB molar ratio is 8:1, for the stabilisation of DDA and thus, avoiding aggregation upon storage [75]. Thus, the use of 3 mg/mL for the microfluidic manufacture of liposomes is acceptable in order to assess the physicochemical characteristics of this adjuvant formulation, and to compare to other manufacturing methods as the lipid molar ratio is locked and no significant differences were observed when compared to the *in vivo* dose. In consequence, the final concentration of DDA:TDB can be increased to the required dose for immunisation studies without modification of the liposomal physicochemical attributes. Initial concentrations below 3 mg/mL are hypothesised to be too low for the formation of stable liposomes, as the dilution factor offered from the microfluidics technology when using FRR 3:1 is 4-fold lower than the initial concentration.

Previous studies carried out by Kastner et al. using the same microfluidics system but with different microchannel dimensions, demonstrated the possibility of producing phosphatidylcholine (PC)

liposomes including cholesterol at high and low concentrations without affecting the characteristics of the liposomes obtained when FRR 3:1 was applied [177]. However, only two lipid concentrations were compared in those studies. Furthermore, Joshi et al. studied in detail the effect of the initial lipid concentration for PC:chol liposomes and showed that concentrations above 3 mg/mL did not change the physicochemical characteristics of the formed liposomes [178].

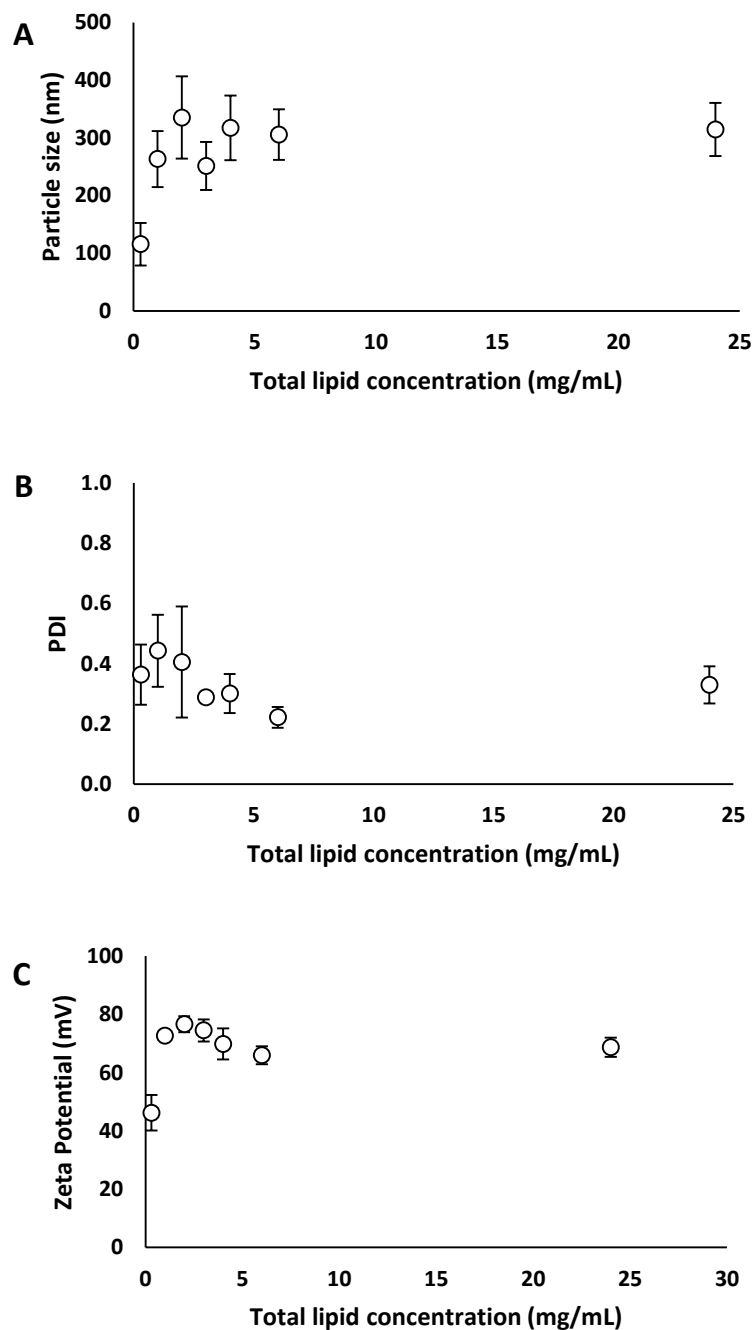


Figure 2.7 Physicochemical characteristics of the CAF01 adjuvant formulations manufactured using microfluidics at TFR 10 mL/min, FRR 3:1 and varying the initial concentration from 0.3 to 24 mg/mL (A) Particle size (B) PDI and (C) Zeta potential. Results represent the mean \pm SD from at least 3 independent experiments.

2.4.1.2 Effect of the total flow rate (TFR) and flow rate ratio (FRR)

After optimisation of the initial DDA:TDB concentration for the production of CAF01, the effect of the TFR as well as FRR was evaluated. In order to get an overview of the effect of the speed at which the liposomes are produced, TFRs of 5, 10 and 15 mL/min and FRRs 1:1, 3:1 and 5:1 were selected. The total initial lipid concentration was fixed at 3 mg/mL as a consequence of the results obtained in section 2.4.1.1. Figure 2.8 shows the impact of the variation of the TFR and flow rate ratio FRR in terms of liposomal physicochemical characterisation. CAF01 liposomes formulated at 1:1 FRR and TFRs 5 and 10 mL/min resulted in particles within the micrometre range, whereas liposomes formulated at higher speed (TFR 15 mL/min) were significantly ($p < 0.001$) smaller in size (approx. 600 nm). All formulated liposomes were highly polydisperse irrespective of the TFR applied. When CAF01 liposomes were formulated at a fixed 3:1 FRR (Figure 2.8), results showed smaller liposome sizes at all of the TFRs tested; all liposomal formulations were in the nanometre range with a flow rate of 15 mL/min again showing the smallest liposome size (~300 nm). PDI values were also lower than for FRR 1:1 but still above 0.2, which is often set as a limit for clinical manufacture of liposome products. Further increases in the flow rate ratio to 5:1 again reduced the size across all three total flow rates tested with particle sizes below 200 nm. However, PDI values were still high at around 0.4 to 0.5 representing a polydisperse formulation. In general, highest PDIs and largest sizes were shown by the FRR 1:1 independent of the TFR tested. The smallest liposomes were obtained with FRR 3:1 and 5:1, being similar in size except for the liposomes formulated at TFR 10 mL/min where significant ($p < 0.05$) differences between FRR 3:1 and 5:1 were observed. Mainly, liposomes formulated at low speed were larger than those formulated at higher speed. This observation suggests that the increase in the mixing speed favours the formation of liposomes. However, the ratio between the aqueous and organic phase showed the biggest impact in terms of vesicle size, in general, increasing the FRR decreased the particle size. From these results, the optimal parameters for the CAF01 formulation were therefore TFR 10 mL/min and FRR 3:1.

The indirect quantification of the liposomal surface charge by means of the zeta potential demonstrate the cationic nature of this adjuvant formulation due to the positively charged head group from the DDA molecule. All CAF01 formulations, independent of the microfluidics parameter used for their production, resulted in highly cationic formulations with ZP values from +65 to +75 mV (Figure 2.8B).

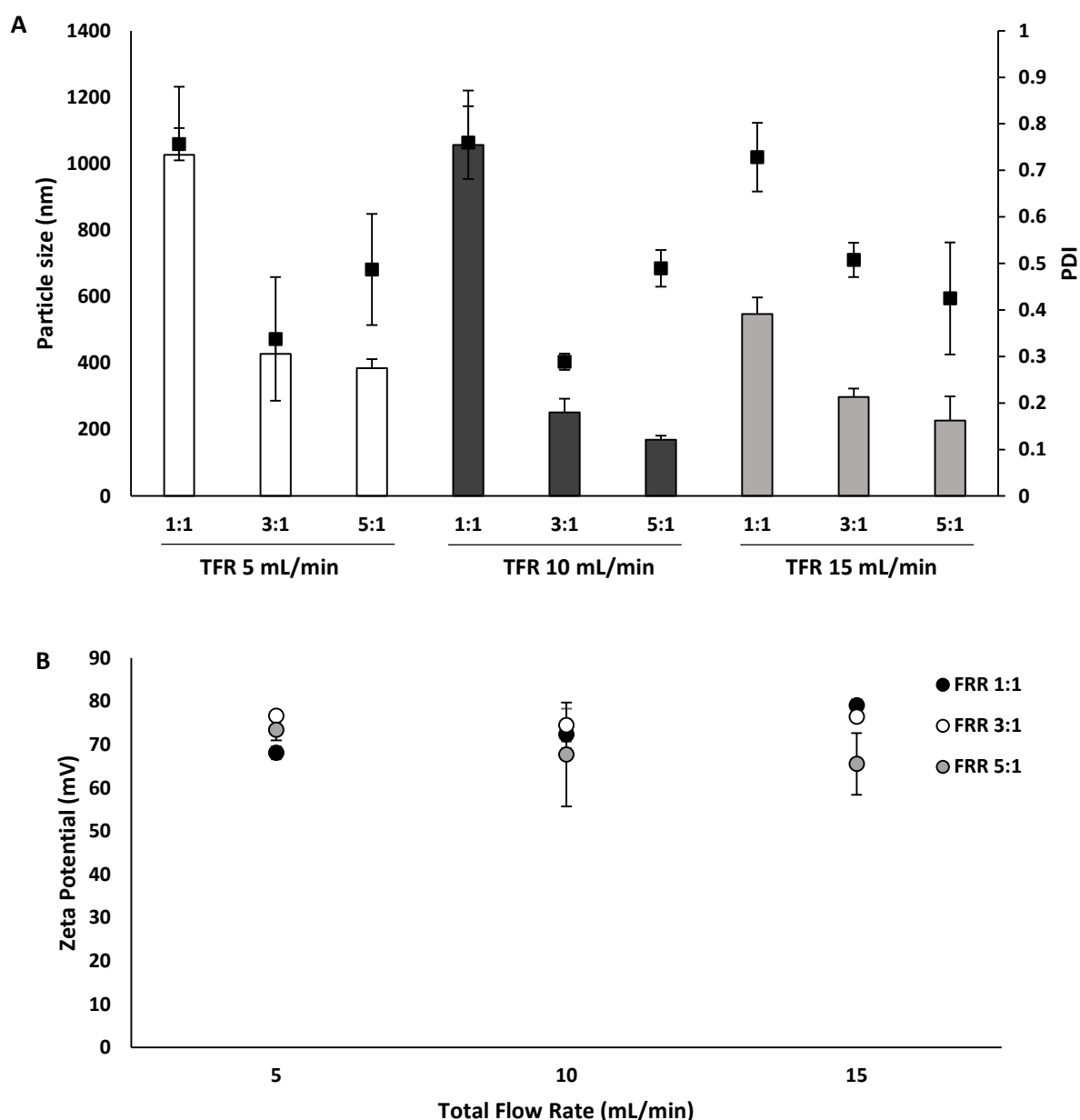


Figure 2.8 The impact of the different parameters adopted during microfluidics formulation of CAF01 liposomes. The (A) particle size (bars) and PDI (dots) and (B) zeta potential of the CAF01 liposomes manufactured by using microfluidics at flow rate ratios of 1:1, 3:1 and 5:1 and flow rates of 5, 10 and 15 mL/min. Results represent the mean \pm SD from at least 3 independent experiments.

The TFR and FRR are important factors to consider when producing liposomes as they impact on the polarity of the organic solvent-aqueous phases when mixing within the micromixer and therefore, affect the physicochemical attributes of the produced liposomes [177, 179]. The influence of the FRR has been reported previously by many researchers. The increase in the aqueous phase during the liposome production creates a narrow solvent stream which consequently favours the production of small size particles due to reduced particle fusion [180]. Kastner et al. showed the impact of the FRR

when producing the neutral PC:Chol liposomes using the same microfluidic technology from Precision Nanosystems [177]. Reported results are in correlation with the results obtained for CAF01 as liposomes produced at 1:1 FRR showed the largest particle size and increased FRR resulted in a decrease of liposome size. Besides, despite the reduction on the particle size, the PDI was increased at 5:1 FRR [177]. Results from another study from Kastner et al. where 1,2-dioleoyl-3-trimethylammonium-propane (DOTAP) containing liposomes were manufactured by microfluidics as well, were in agreement with these findings [167]. The polarity is influenced by the volume of organic solvent in contact with the aqueous phase and therefore, increases with increasing the FRR. The theory behind the influence of the FRR is related to the Ostwald ripening effect, the lower amount of organic solvent concentration reduces the likelihood of particle fusion and subsequently, formation of larger particles, resulting in the production of small particles [167, 168]. Studies carried out with different microfluidics technology are in line with these results, reporting the effect of the FRR on the particle size [167, 168, 181, 182]. Regarding PDI, the high values obtained for 5:1 FRR might be explained by the further dilution which in consequence results in a reduced lipid concentration, lower diffusion rate and incomplete nucleation [167, 183].

The speed at which the particles are manufactured through the system was altered to examine the capability of MF as a high-throughput method for CAF01 production. Opposite to what it is broadly reported in literature, the variation in the TFR showed an impact on the liposomal production, decreasing the particle size at high speeds [183, 184]. Maeki et al. showed the influence of the initial lipid concentration impacted upon the particle size of the produced lipid particles when produced at different TFRs using a chaotic micromixer. The higher the TFR the smaller the lipid nanoparticles when concentrations of 10 and 20 mg/mL were used, but when lower concentration (5 mg/mL) were used, no differences were observed on the particle size of the formed NPs [185]. These results were explained by the rapid mixing of both aqueous and organic phases within the micromixer. Organic solvent gets diluted very quickly, hindering the formation of large particles [185]. On the other hand, low TFRs enable both phases to interact for a prolonged period of time, favouring the lipid fusion and thus, formation of larger liposomes [182].

These results highlight the importance of the liposome composition in the MF production, as the influence of the MF parameters on the liposome production mainly depend on the nature of the lipid composition. In consequence, the particle size of CAF01 liposomes was controlled by the FRR and TFR applied during manufacture. From these results, the TFR 10 mL/min was selected for further experiments due to the reduced variability in the liposomal physicochemical attributes (size and PDI).

2.4.2 Quantification of the residual solvent after purification of the formulation

Organic volatile chemicals contained into pharmaceutical formulation for human use have to be restricted mainly due to toxicity issues. Besides, the volume of residual solvent contained within the formulation may contribute to the alteration of the physicochemical attributes of the product due to for example particle fusion. The restricted amount of residual solvent is dictated by the ICH Q3C guidelines. IPA, the solvent used for the preparation of CAF01 belongs to the class 3 solvents, which represent solvents with low toxic potential and therefore the agreed limit for this solvent is 0.5% (5000 ppm). The residual solvent in the formulations manufactured using microfluidics was quantified by GC. A calibration curve was established (Figure 2.9A) and from that, the concentration of residual solvent in the samples was calculated. The calibration curve obtained showed a good linearity ($R^2 = 0.998$) and the limit of detection (LOD) and quantification (LOQ) calculated were 0.1% and 0.2% respectively. Due to toxicity and stability issues, ensuring the removal of any trace of organic solvent is important. For this purpose, two dialysis methods with different dialysis durations were tested: 1 and 4 hours. CAF01 microfluidics formulations prepared at TFR 10 mL/min and different flow rate ratios were analysed. Regarding initial volume of organic solvent within the formulations before purification, samples produced at a flow rate ratio of 1:1 contain 50% organic solvent, whereas ratios of 3:1 and 5:1 contain 25% and 16.7% respectively. After purification of the microfluidic liposomal formulations, both dialysis methods showed a residual solvent content below 0.5% in all the formulations tested (Figure 2.9B)

The majority of the techniques involving liposomal preparation involve the use of organic solvents for the dissolution of the lipids. Most of the published papers do not quantify the volume of residual solvent within the formulation. As reported by Carugo et al. who reviewed the use of microfluidics for liposomal production, no data about the residual solvent content is provided in any of the articles evaluated [186]. However, chromatographic techniques are generally used for solvent quantification and several techniques exist for the purification of particles, the traditional methods such as centrifugation, dialysis and gel filtration, and the newer techniques such as diafiltration and tangential flow filtration (TFF) [187, 188]. For liposomal preparation, the use of centrifugation techniques may alter the final characteristics of the product. On the other hand, gel filtration and TFF risk the loss of lipids due to interaction with the column membrane due to the cationic nature of the liposomes and the commonly anionic nature of the membranes. Thus, the use of dialysis was the most appropriate method for the removal of solvent. Dialysis is a common method and it has been reported its use for liposomal purification [177, 178]. It usually requires buffer exchange in order to modify the solvent gradient, favouring removal from the formulation. Here, we present a rapid and validated dialysis

method with levels of solvent below the ICH limit although residual solvent should be always checked when changing the solvent used for the formulation, as solvent levels might be different.

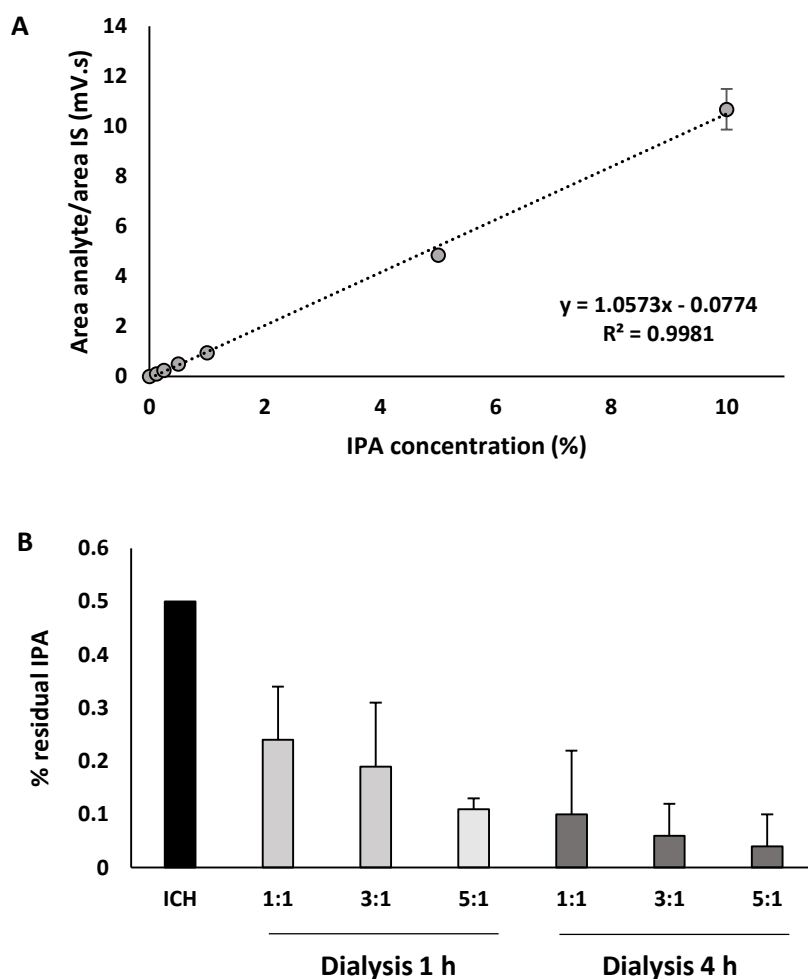


Figure 2.9 Gas chromatography: **(A)** 2-propanol calibration curve and **(B)** Concentrations (%) of solvent in the liposomal samples produced using microfluidics after the different 1 and 4 hours dialysis. Results represent the mean \pm SD from at least 3 independent experiments.

2.4.3 Evaluation of the impact of the manufacturing technique on the production of CAF01 and CAF01-based liposomes

In order to compare the differences between traditional methods for the manufacture of liposomal adjuvants such as LH and more recently developed techniques such as HSM and MF, selected liposomal adjuvant formulations were manufactured by using these three methods. Individual physicochemical characterisation of each sample was performed and the effect of the liposome composition and the manufacturing method were evaluated.

Therefore, liposomes were prepared by three different methods 1) the traditional LH method [57], 2) the LH method followed by HSM [165] and 3) MF using the protocols described in section 2.3.2. For

MF, lipids were dissolved and mixed in IPA at the selected concentration (3 mg/mL). Tris buffer (pH 7.4, 10 mM) and the lipid solutions were heated up before and during the process since the transition temperature of DDA is above room temperature ($T_m = 47^\circ\text{C}$) and thus, heating is needed for the liposome formation (Table 2.1). The microfluidics parameters selected for further evaluation were based on the reported results in section 2.4.1 for the optimisation of the CAF01 production. Therefore, the speed for liposome production was set at 10 mL/min, but the all three FRR (1:1, 3:1 and 5:1) were tested again for a broad overview of the impact of the lipid composition during manufacturing.

Using the above processes, four liposomal formulations were prepared (Table 2.6): DDA and TDB concentrations were fixed at 2.5 mg/mL and 0.5 mg/mL (CAF01) respectively and cholesterol was added to the CAF01 formulation at two different concentrations (low = 0.4 mg/mL and high = 0.8 mg/mL) in order to decrease the fluidity of the membrane bilayer and favour the formulation of liposomes at room temperature since it is known that cholesterol reduces and/or eliminates the transition temperature of the systems [189]. In the fourth formulation, DDA was completely replaced by DMPC and kept at the original concentration.

Table 2.6 Lipid concentrations (mg/mL) used for the formulation of the four liposomal formulations: DDA and TDB concentrations were fixed at 2.5 mg/mL and 0.5 mg/mL (CAF01) respectively and cholesterol was added to the CAF01 formulation at two different concentrations (low = 0.4 mg/mL and high = 0.8 mg/mL). In the fourth formulation, DDA was completely replaced by 1,2-dimyristoyl-sn-glycero-3-phosphocholine (DMPC) and kept at the original concentration.

LIPOSOMAL FORMULATIONS	DDA (mg/mL)	TDB (mg/mL)	Cholesterol (mg/mL)	DMPC (mg/mL)
CAF01	2.5	0.5		
CAF01 + low cholesterol	2.5	0.5	0.4	
CAF01 + high cholesterol	2.5	0.5	0.8	
DMPC-TDB		0.5		2.5

Characteristics of the liposomes manufactured using LH are displayed in Figure 2.10A and D. CAF01 formulation showed a size of around 600 nm with a PDI of 0.3 and a highly cationic surface charge of +80 mV in line with previously reported studies [75, 189, 190]. After addition of low concentrations of cholesterol into the formulation, the size of the liposomes increased up to 700 nm and showed a PDI

slightly higher than DDA:TDB liposomes. In terms of zeta potential, the inclusion of cholesterol in the CAF01 liposomal formulation did not significantly modify the positive surface charge. Increasing the cholesterol content to 0.8 mg/mL further increased the vesicle size into the micron range (~ 1700 nm with a PDI of 0.8; Figure 2.10A), while again higher cholesterol content did not impact upon the zeta potential (+72 mV; Figure 2.10A). In contrast, when the cationic DDA was replaced by the neutral lipid DMPC, the characteristics of these liposomes notably changed; the zeta potential was ~ 0 mV, representative of neutral liposome surface and the liposome size was ~ 2 μm , more than three times larger than CAF01 (Figure 2.10).

In order to produce SUVs, preparation of the lipid film using the LH method was followed by hydration of the lipid film by HSM. In general, significantly ($p < 0.01$) smaller liposomes and better polydispersity index could be seen in all the formulations (Figure 2.10B). By this method the size of the CAF01 liposomes went down to 200 nm whereas the PDI remained equal as for the LH method. Inclusion of low or high cholesterol content in the formulations resulted in a decrease in size compared to the LH method (230 nm and 270 nm respectively). The DMPC-TDB formulation also significantly ($p < 0.05$) reduced in size after HSM yet remained in the micrometre range (~ 1.5 μm). The measured zeta potentials remained intact for all the formulations tested after the size reduction method (Figure 2.10E).

Once LH and HSM were tested for the manufacturing of CAF01 liposomes, the next step was to prepare these formulations using MF. The influence of the different parameters adopted for the preparation of these formulation can be seen in Figure 2.10C. Sizes of the liposomes obtained by using this method ranged from micrometres to nanometres. In general, cationic liposomes produced at FRR 1:1 showed the largest size and highest PDI in all the cationic formulations tested, followed by FRR 3:1 and 5:1 irrespective of the cholesterol content. However, the addition of high cholesterol content within the formulation significantly ($p < 0.001$) decreased vesicle sizes compared to CAF01 (down to 65 nm when using FRR 5:1, compared to CAF01 at 190 nm) whilst incorporation of low concentration of cholesterol did not modify it. The zeta potential of all the DDA-containing liposomes remained highly cationic (Figure 2.10D). In contrast, with the neutral DMPC-TDB formulation all were in the micrometre range with high PDI values and no trend could be seen when altering the FRR.

Overall, these results demonstrate that cationic liposomes formulated by microfluidics can be formulated in sizes below 100 nm depending on the parameters adopted. In general, increasing FRR reduces the size of the particles. This is in contrast to vesicles subject to HSM, where the minimum size was ~ 200 nm. On the other hand, liposomes prepared by LH showed the largest particle size. However, liposomes produced using microfluidics tended to be more heterogeneous in nature.

Addition of cholesterol was shown to facilitate the production of liposomes by microfluidics with formulations containing high cholesterol content providing small, reproducible liposome suspensions. This might be due to the decrease of transition temperature in the formulation when cholesterol is incorporated [189].

When considering cholesterol-containing liposomes formulated by the traditional lipid film hydration method, these liposomes were larger in size compared to the CAF01 formulation. A slight increase in the liposome size has been previously seen in other studies where the influence of cholesterol incorporation into CAF01 liposomes was evaluated [189]. Published results correlate with the reported particle size obtained at low cholesterol concentrations [189]. When high concentrations of cholesterol were added, the resulted particle sizes were larger than those reported by Kaur et al. This might be explained for the higher cholesterol concentration used during these studies (0.8 mg/mL) compared to the published data. In this case, the DDA:TDB concentration was kept fixed whereas Kaur et al. adjusted the molar ratios when adding cholesterol. Therefore, it is believed that the addition of high cholesterol content (0.8 mg/mL), favoured the formation of larger liposomes. When these vesicles were reduced in size using HSM, DDA-containing liposomes showed similar size independent of the amount of cholesterol added suggesting that the shear forces are strong enough to reduce vesicle size irrespective of the cholesterol content. It has been previously reported in literature that liposome size increases upon incorporation of cholesterol and thus, increasing cholesterol content further increases the liposome size since more cholesterol molecules will be inserted into the lipid bilayer [191-193]. Besides, cholesterol is known to increase the rigidity of the lipid bilayer due to increasing the lipid packing density in the liposome bilayer which can consequently increases the liposomal particle size [194]. In contrast to this, inclusion of cholesterol reduces the size of the liposomes formulated using microfluidics. The higher the amount of cholesterol added, the smaller liposomes are obtained. Given that cholesterol helps the packing of the lipids in the bilayer [189] it is thus hypothesised this may support the rapid assembly of smaller vesicles within the microfluidic mixing process.

DMPC-TDB liposomes were larger than DDA-containing liposomes after any of the three manufacturing methods compared. MLVs based on neutral phospholipids tend to form larger vesicles due to increased liposome fusion [195]. When HSM method was applied to the DMPC-TDB formulation the size reduction was less effective. This may be a result of reduced homogenisation time, since the protocol followed for the preparation of all four formulations was based on the patented method for CAF01 [165]. Consequently, DMPC-TDB liposomes might require longer homogenisation HSM time in order to produce smaller liposome size, but for comparison studies, the manufacturing conditions remained the same. Regarding the manufacture of DMPC-TDB liposomes

using microfluidics, this did not result in a liposome size reduction as observed for the other formulations. This may be related to solubility or packing issues. Besides, fusion or lipid aggregation due to the neutral nature of the DMPC might contribute to the large particle size obtained [195]. Regarding zeta potential, no significant differences were noted between liposomes prepared by any of the three manufacturing methods applied. DDA-containing formulations remained highly positive due to the cationic charge attributed to the quaternary ammonium head group, whereas DMPC-containing formulations were neutral, which is related to the zwitterionic phosphate head group which confers the neutral charge to the liposomes.

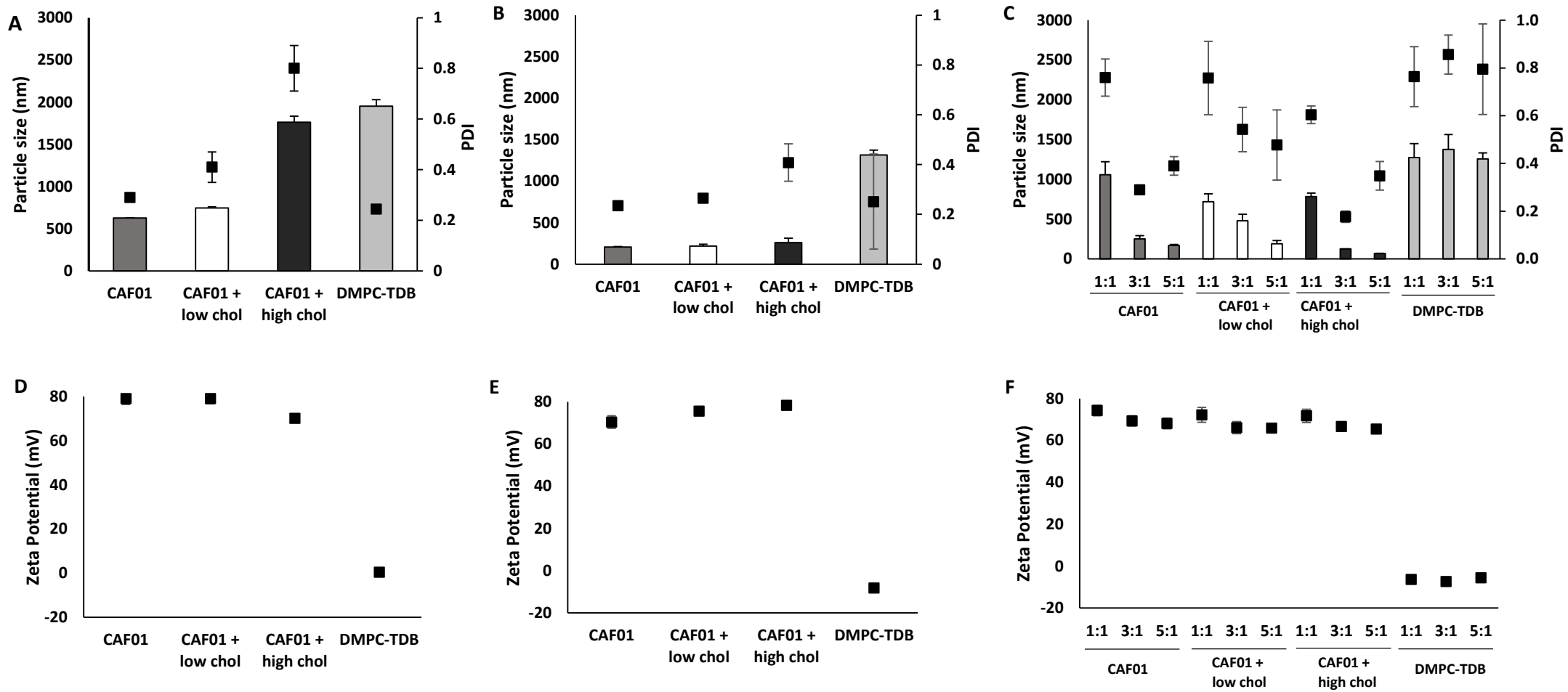


Figure 2.10 Physicochemical characteristics (size, PDI and ZP) of the empty CAF01 and CAF01-based liposomal formulations manufactured using (A, D) the traditional LH method, (B, E) HSM and (C, F) MF. Particle size (bars) and PDI (dots). Results represent the mean \pm SD of at least 3 independent batches.

2.4.4 Loading of ovalbumin (OVA) as a model antigen onto the preformed liposomal adjuvant formulations

Incorporation of ovalbumin (OVA), which is commonly used as a model antigen, was investigated with the CAF01-based formulations prepared via LH, HSM and microfluidics. As these adjuvant formulations are to be used for a TB vaccine, OVA was chosen due to its similarities in molecular weight with the H1 (Ag85b-ESAT-6) tuberculosis antigen developed by Statens Serum institute (SSI) (OVA ~45 kDa and H1 ~46 kDa). Besides, both antigens are negatively charged at physiological pH (OVA isoelectric point $pI= 4.5$, H1 $pI= 4.9$), favouring the electrostatic interaction with the liposomal surfaces. Hence, OVA was added on to the preformed liposomes at the usual H1 concentration which is $2 \mu\text{g} / \text{vaccine dose (50 } \mu\text{L)}$ which corresponds to a final antigen concentration of 0.04 mg/mL .

After incorporation of OVA onto the surface of the liposomes and removal of the non-loaded protein through either dialysis (microfluidics and HSM samples) or ultracentrifugation (LH samples), liposomes were characterised according to their size, PDI and zeta potential using DLS (Figure 2.11). Loading of protein did not significantly change the size of the liposomes manufactured by using either LH or HSM (Figure 2.11A-B). In contrast to the results obtained from the LH and HSM, loading of OVA onto the surface of the liposomes formulated through microfluidics significantly ($p<0.05$) changed the size of the particles; CAF01 formulations loading OVA increased up to 2600, 790 and 336 nm for FRRs 1:1, 3:1 and 5:1 respectively (Figure 2.11). As with the 'empty' liposomes, addition of cholesterol to the formulation reduced the liposomal size compared to CAF01 liposomes, but a significant ($p<0.05$) increase was observed when OVA was loaded onto these formulations. For the DMPC-TDB liposomes, all the particles were in the micrometre range and they increased from 1300 nm to 1700 nm when OVA was loaded. Zeta potential values did not significantly change after loading of OVA, DDA-containing liposomes were highly cationic in nature whereas the DMPC-TDB liposomes were neutral (Figure 2.11). In terms of polydispersity, DMPC-TDB liposomes showed a heterogeneous size population ($PDI\sim 0.6$) when produced by microfluidics. However, when manufactured by LH or HSM, a more homogeneous population of sizes were observed ($PDI\sim 0.25$). DDA-containing liposomes were heterogeneous in nature when prepared by any of the three manufacturing methods tested. Increasing the FRR produced more homogeneous particle size liposomes. Thus, liposomes formulated using microfluidics FRR 5:1 showed the lowest polydispersity index (~ 0.3).

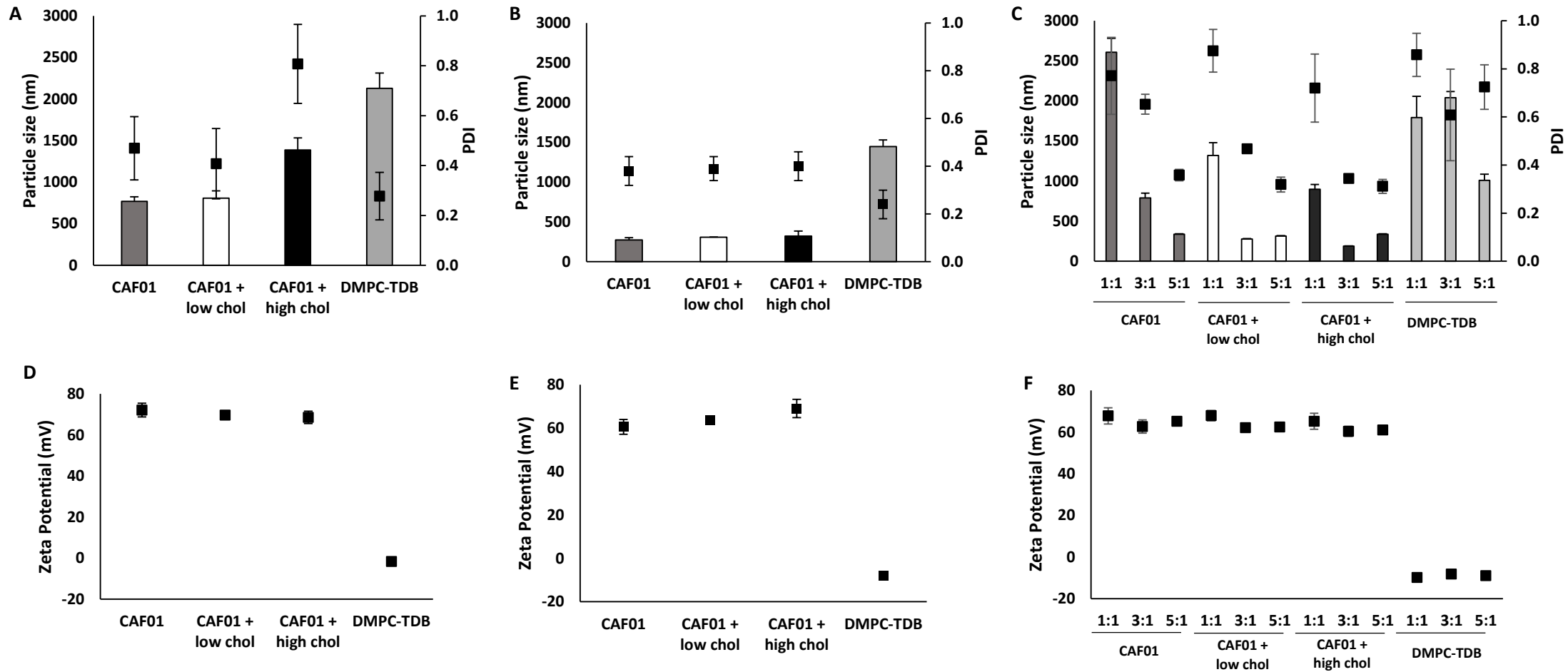


Figure 2.11 Physicochemical characteristics (size, PDI and ZP) of the OVA loaded CAF01 and CAF01-based liposomal formulations manufactured using (A, D) the traditional LH method, (B, E) HSM and (C, F) MF. Particle size (bars) and PDI (dots). Results represent the mean \pm SD of at least 3 independent batches.

Loading efficiency of DDA and DMPC containing adjuvant formulations was measured on an HPLC-ELSD detector. Results showed that OVA was able to bind electrostatically to the surface of the highly cationic liposomal surface of DDA containing liposomes irrespective of the method of manufacture used. The loading efficiency of the liposomes manufactured through LH, HSM and microfluidics method was above 90% (Figure 2.12). The inclusion of cholesterol in the formulations did not impact the loading efficiency. In contrast, when DDA was replaced for DMPC, OVA could not be attached to the liposomal surface showing approximately 10% loading when liposomes were manufactured through the LH and HSM. Values below the limit of detection of the HPLC-ELSD were obtained for the microfluidic formulations (loading (%) < 5%).

Gel electrophoresis was performed on the liposomal adjuvants after OVA loading (Figure 2.12D). OVA control of 0.04 µg/mL, which is the final concentration added to 1 mL of liposomal sample, was set on the first lane of the gel. Samples containing liposomes and protein were ultracentrifuged for 30 min at 125,000 x g. Supernatant was removed and pellet was resuspended in Tris buffer(10 mM, pH 7.4). Each fraction (pellet and supernatant) was loaded in the gel. Figure 2.12D shows the results of the liposomal formulations prepared by the LH method. DDA containing liposomes, due to its positive surface charge, electrostatically bind the negatively charge protein. Thus, protein appeared in the pellet, whereas for DMPC containing liposomes, due to its neutral surface charge, OVA do not electrostatically bind to their surface, and hence, the protein appears on the supernatant. These results confirm the loading data from the ELSD and also show no degradation of the protein resulting from the loading process.

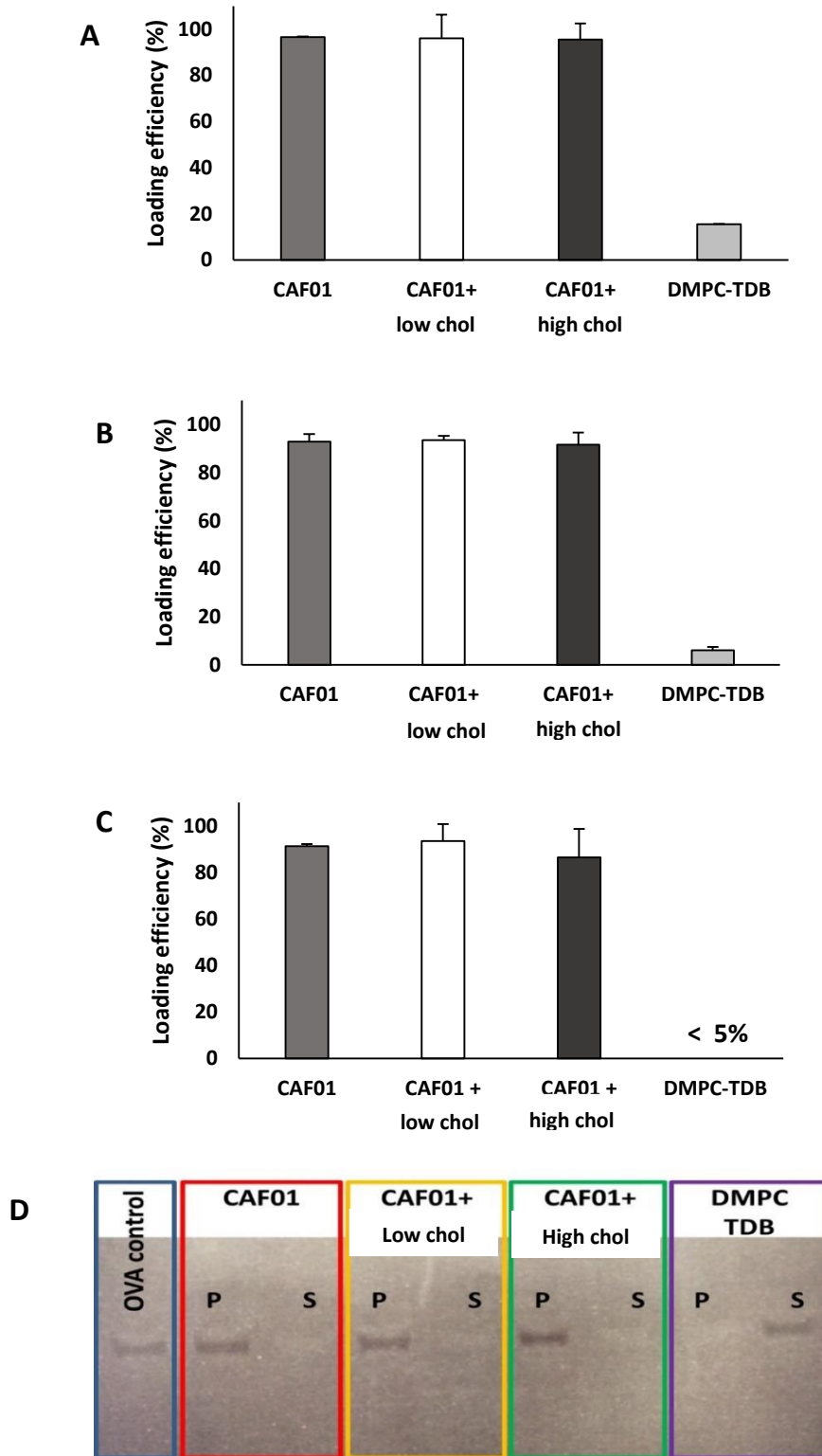


Figure 2.12 Percentage of antigen (OVA) loaded onto the liposomal adjuvants manufactured using (A) lipid film hydration methods (LH), (B) high shear mixing (HSM) and (C) microfluidics. Results represent the mean \pm SD of at least 3 independent batches. (D) SDS-Page gel of the liposomal formulations after preparation by LH method. Protein is attached to the cationic liposomes as we can see it is in the pellet (P) whereas in the neutral liposomes the protein is not attached to them and therefore it appears in the supernatant (S).

In general, all the cationic formulations studied increased particle size after incorporation of the model antigen OVA onto the surface of the preformed liposomes independent of the manufacturing method applied and the nature of the lipid formulation. Henriksen et al. studied the influence of the liposome charge on the absorption of the H1 TB antigen and other proteins into the CAF01 liposomes and the neutral DSPC-TDB liposomes manufactured using the LH method [70]. The reported results for DSPC-TDB liposomes are in agreement with the results obtained for DMPC-TDB liposomes. Liposomes were in the micrometre range (~ 1600 nm), heterodisperse and neutrally charged ($- 8$ mV) [70]. In terms of antigen loading, OVA adsorption is dependent on the attractive electrostatic interactions (Van der Waals forces) between the liposomal surface and the negatively charged protein at physiological pH. For this reason, OVA was efficiently loaded onto the positively charged membrane of the liposomes containing DDA whereas liposomes containing DMPC were not as effective due their neutral surface charge. These results are in line with reported results showing the high loading efficiency of CAF01 when loaded with TB antigens or negatively charged model proteins [70, 189, 190, 196]. Furthermore, Kaur et al. investigated the effect of the addition of cholesterol into the CAF01 formulation [189] and reported same loading efficiencies as CAF01 which correlates with the reported results, where the addition of cholesterol did not significantly modify the antigen loading on the liposomal membrane of CAF01. This is explained by the cationic nature of the liposomes formed independent of whether cholesterol is incorporated and the manufacturing method. Regarding the loading of OVA onto the neutral DMPC-TDB liposomes, it has been reported that loading of H1 TB antigen onto DSPC-TDB liposomes was approximately 20%, which can be compared to the values obtained for DMPC-TDB as both lipids contain a zwitterionic phosphate head group and a saturated alkyl chain which only differs on its length (C14 for DMPC and C18 for DSPC) [70]. Consequently, the increase in particle size might be explained by this low protein loading. Besides, the high polydispersity values obtained for DMPC-TDB which are representative of a very heterogeneous formulation might contribute to more variable particle sizes.

2.4.4.1 Quantification of the lipid concentration using HPLC-ELSD

Quantification of the lipid amount within the formulations is crucial for the efficacy and stability of the adjuvant formulations. A rapid and accurate HPLC-ELSD method for the quantification of all four lipids used for the preparation of liposomes was therefore developed and validated. The duration of the HPLC-ELSD method was 35 min and it was able to analyse DDA, DMPC, cholesterol and TDB at the same time. A chromatogram of the four lipids is shown in Figure 2.13. The elution peaks obtained were well separated, sharp and high, except for the TDB peak which was wide and short. Due to the

gradient elution method and the column selected for this purpose, lipids are eluted according to their hydrophobicity. The least hydrophobic lipid eluted first and the more hydrophobic eluted last. Therefore, the order of elution was as follows first the cationic lipid DDA at 7.1 min, followed by DMPC at 9.2 min, cholesterol at 10.9 min and TDB at 19.9 min. Despite the fact that all four lipids eluted within the first 20 min, in order to allow the column to re-equilibrate, analysis time was established at 35 min. Validation of the method was carried on cholesterol as a model example and linearity, sensitivity, accuracy, reproducibility and robustness were assessed in accordance to the ICH guidelines Q2 (R1) [30], and cholesterol was selected for this purpose.

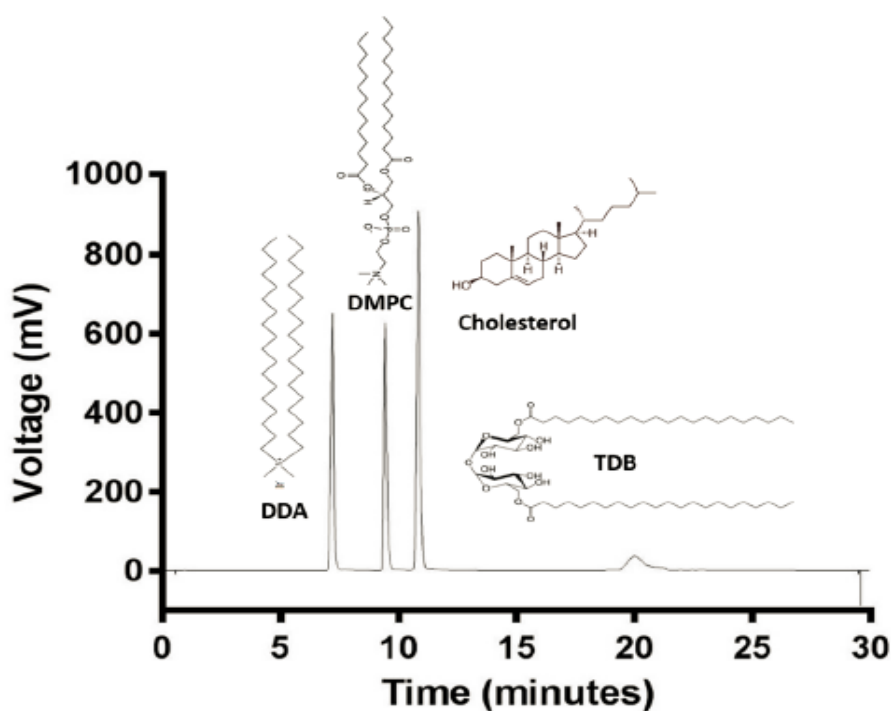


Figure 2.13 HPLC-ELSD chromatogram showing the four lipids used for the preparation of liposomal formulations: DDA (1.5 mg/mL), DMPC (1.5 mg/mL), cholesterol (2 mg/mL) and TDB (1 mg/mL). The ELSD gain was 3 for DDA, DMPC and cholesterol whereas TDB was quantified at gain 12.

Standard curves prepared in chloroform:methanol (9:1 v/v) were prepared for each lipid based on the lipid concentrations used for the preparation of the adjuvant formulations. Thus, concentrations ranged from 0.125–2.5 mg/mL for DDA; for DMPC, from 0.25–2.5 mg/mL; for TBD, from 0.2–1 mg/mL; and for cholesterol, 0.025–1 mg/mL. The calculated peak area average \pm standard deviation (SD) was plotted against the known concentrations of the lipids (Figure 2.14). Commonly, ELSDs are non-linear, and in order to get a linear fit, a log of the ELSD response against the log of the concentration of the standard is used to plot the calibration curves, however, SEDEX 90LT detector gives linear responses. All four calibration curves showed correlation coefficients (R^2) \geq 0.997, indicative of a good linearity.

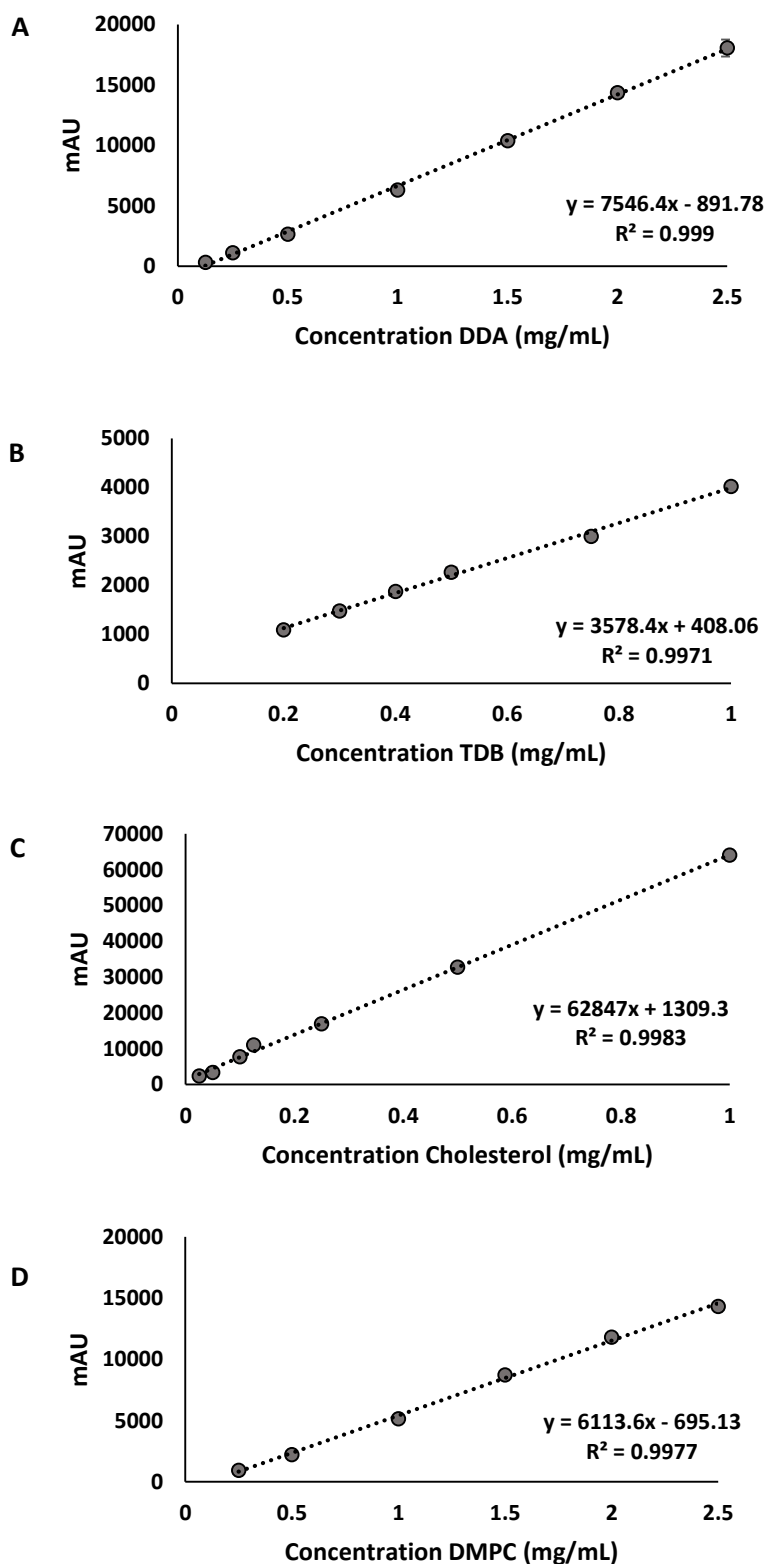


Figure 2.14 Calibrations curves of (A) DDA (from 0.125 – 2.5 mg/mL) (B) TDB (from 0.2 – 1 mg/mL) (C) Cholesterol (from 0.125 – 1 mg/mL) and (D) DMPC (0.25 to 2.5 mg/mL) obtained from the HPCL-ELSD using gain 3 for DDA, DMPC and cholesterol and gain 12 for TDB. Results represent the mean \pm SD of at least 3 independent batches.

For the study of the sensitivity of the method, the limit of detection (LOD) and limit of quantification (LOQ) of each lipid were determined (Table 2.7). LOD is the minimum concentration which the method is capable to detect whereas the LOQ is the minimum concentration which the method is able to quantify. Equations 1 to 3 were used for the calculation of these values, using the slope (S) and the SD obtained from the linearity assessment. In conformity to the ICH Q2 (R1) guidelines, a signal-to-noise ratio of 3 and 10 was set for the calculation of the LOD and LOQ respectively.

$$\sigma = \frac{\sqrt{\sum(Y - Y_i)^2}}{n - 2} \quad (\text{Equation 2.4})$$

$$LOD = \frac{3\sigma}{S} \quad (\text{Equation 2.5})$$

$$LOQ = \frac{10\sigma}{S} \quad (\text{Equation 2.6})$$

Table 2.7 Calculated LOQ and LOD values for each lipid. TDB was the most difficult compound to quantify due to the low concentrations used within the liposomal formulations which was depicted by the intensity peaks obtained from the chromatogram. The determined LOD and LOQ were 0.11–0.36 mg/mL, 0.02–0.08 mg/mL, 0.06–0.20 mg/mL, and 0.05–0.16 mg/mL for DDA, cholesterol, DMPC and TDB respectively.

Compound	LOD mg/mL	LOQ mg/mL
DMPC	0.11	0.36
Cholesterol	0.02	0.08
DDA	0.06	0.20
TDB	0.05	0.16

In order to determine the repeatability and reproducibility of the HPLC-ELSD method developed, calibration curves of cholesterol were carried out in triplicate within same day (intraday) and during different days (interday). Figure 2.15 shows the cholesterol calibration curves ranging from 0.025 to 1 mg/mL lipid concentration obtained during the intra- and interday linearity assessment. No significant differences were detected from the results obtained from any of the calibration curves carried out within the same day or on different days. The accuracy of the method was calculated as the relative standard deviation (%RSD) and the recovery of the three lowest cholesterol standards. Calculated

values were between 90 and 110% for the recovery and for the %RSD $\leq 5\%$, which fall within the acceptance limit.

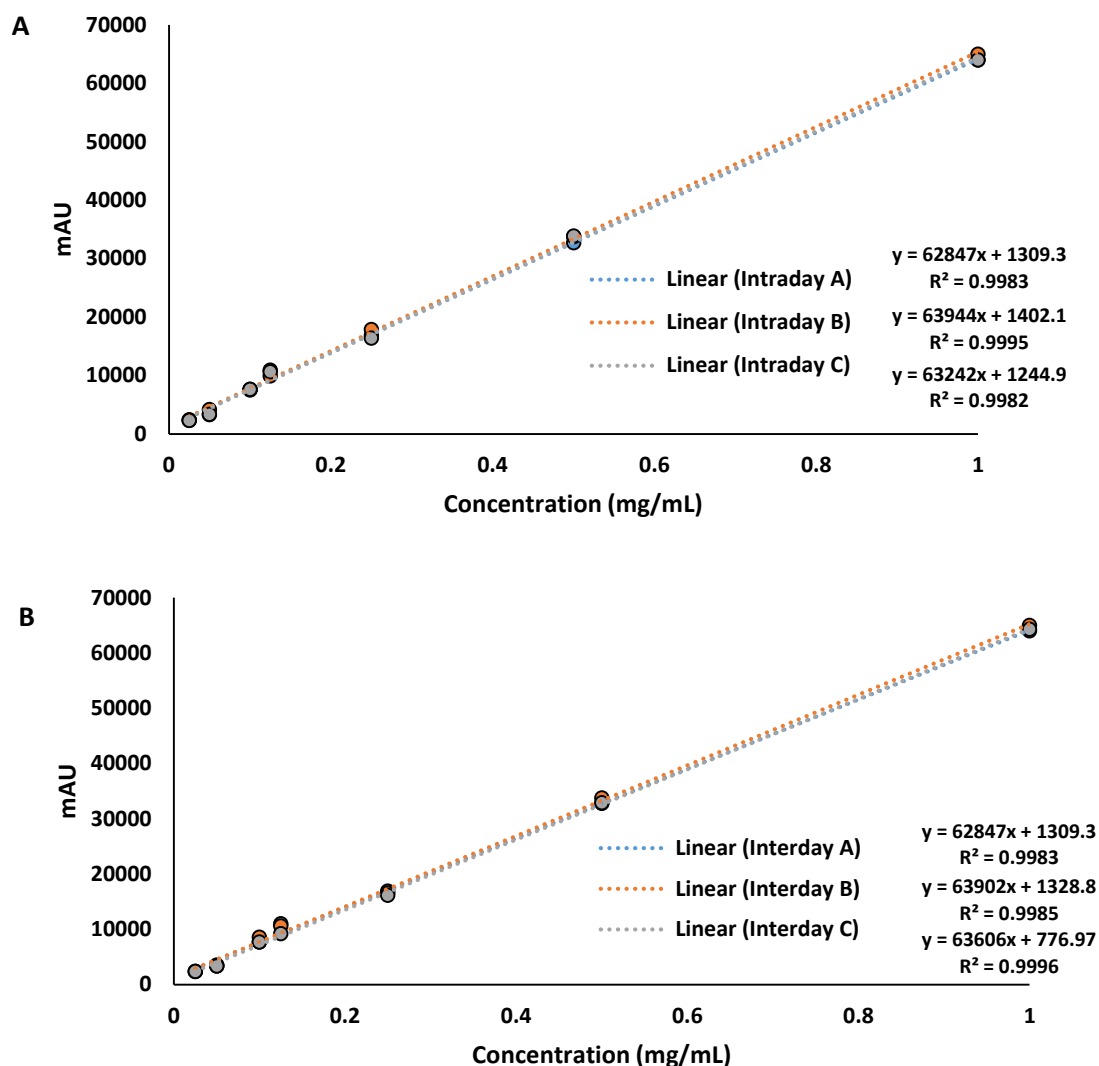


Figure 2.15 Method validation for cholesterol as a model compound (reproducibility and repeatability): **(A)** Intraday (same day) and **(B)** interday (different days) reproducibility. Cholesterol concentration range used from 0.25 to 1 mg/mL. Results represent the mean \pm SD of at least 3 independent batches.

The ability of the quantification method to generate reproducible results with little variation of the initial settings is represented as the robustness. For this purpose, variations in the initial column temperature ($35 \pm 0.5^\circ\text{C}$) and the flow rate (1.5 ± 0.2 mL/min) were carried out in order to evaluate the effect of this changes on the HPLC-responses. Therefore, flow rates (mL/min) of 1.3, 1.5 and 1.7 mL/min were compared as well as column temperatures of 30, 35 and 40°C . Figure 2.16 shows the elution peaks for the variation in temperature (A) and flow rate (B). Modification of the initial temperature did not affect significantly neither the retention times (between 9.7 and 10.9 min) nor

the height of the HPLC responses (~600 mV). Cholesterol eluted slightly faster when the column temperature was set at 40°C due to an increase in the particle diffusion. When the flow rate was varied, changes in retention times were observed. An increase in the speed at which the sample goes through the column caused a faster elution of the cholesterol peak (retention time 8.7 min). Opposite to that, when the flow rate was decreased down to 1.3 mL/min, cholesterol eluted after 10 min. All the data generated for the validation of the HPLC-ELSD method, fulfilled the criteria established by the ICH guidelines.

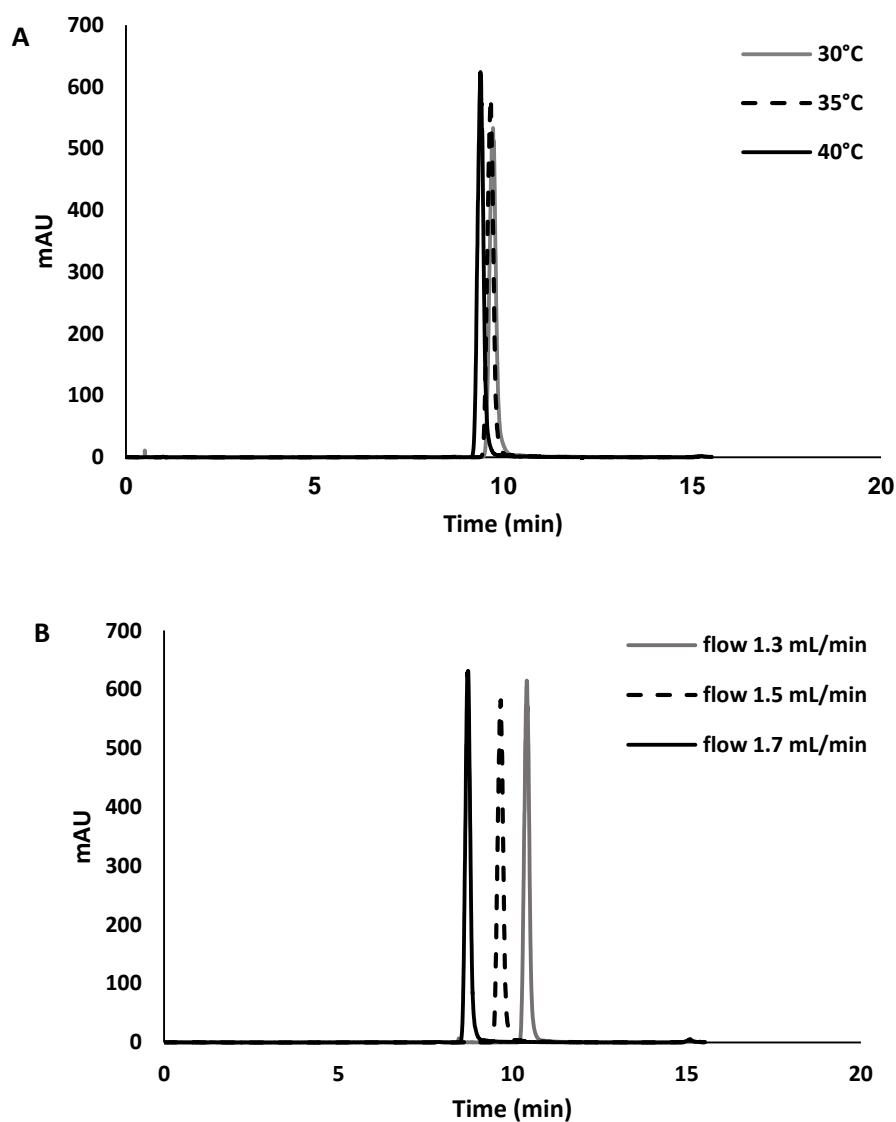


Figure 2.16 Method validation for cholesterol (robustness): (A) elution peaks at different column temperatures and (B) elution peaks at different flow rates.

2.4.4.2 Quantification of the individual lipid recovery after process manufacture

After method validation, quantification of the concentration of each lipid after three manufacturing techniques was performed. Briefly, four liposomal formulations were prepared using the lipid film hydration method, a combination of the LH method and high shear mixing, and microfluidics. Concentrations of DDA and TDB were fixed at 3.96 mM and 0.5 mM respectively, cholesterol was added to this formulation at a low and high concentration (0.4 and 0.8 mg/mL respectively). For the preparation of the fourth formulation DDA was replaced by the neutral lipid DMPC and kept at the same concentration. Since the aim of the development of the HPLC-ELSD method was to establish a procedure capable of quantifying lipids within liposomal adjuvant formulations in a rapid and easy way, samples were injected into the HPLC system without previous preparation. DDA, DMPC and cholesterol were quantified using HPLC gain 3 whereas TDB was quantified using gain 12. TDB was the most difficult lipid to quantify since the intensity of the peaks and the concentration used for the formulation was low. TDB concentrations below 0.2 mg/mL could not be quantified by using this method on the HPLC-ELSD. Therefore, for microfluidics samples prepared using FRR 3:1 and 5:1, samples had to be up-concentrated by freeze drying overnight and rehydration the day after by adding less volume of dH₂O. Results show that a recovery of between 90 and 100% of DDA, cholesterol and DMPC lipids independently of the technique used for the preparation (Figure 2.17). There are no significant differences in the recovery of the lipids between LH, HSM or microfluidics. TDB showed highly variable recovery values $\geq 80\%$ across all the formulations tested. The high gain (gain 12) needed for its quantification resulted in a noisy baseline, therefore, the standard deviation is larger than for the rest of the lipids.

Lipid content of liposomal adjuvant formulations was successfully quantified by using a HPLC-ELSD method. Lipid film hydration, HSM and microfluidics have shown to be suitable methods for manufacturing of liposomal adjuvants since the recovery of the lipids was not significantly different across the three manufacturing methods evaluated.

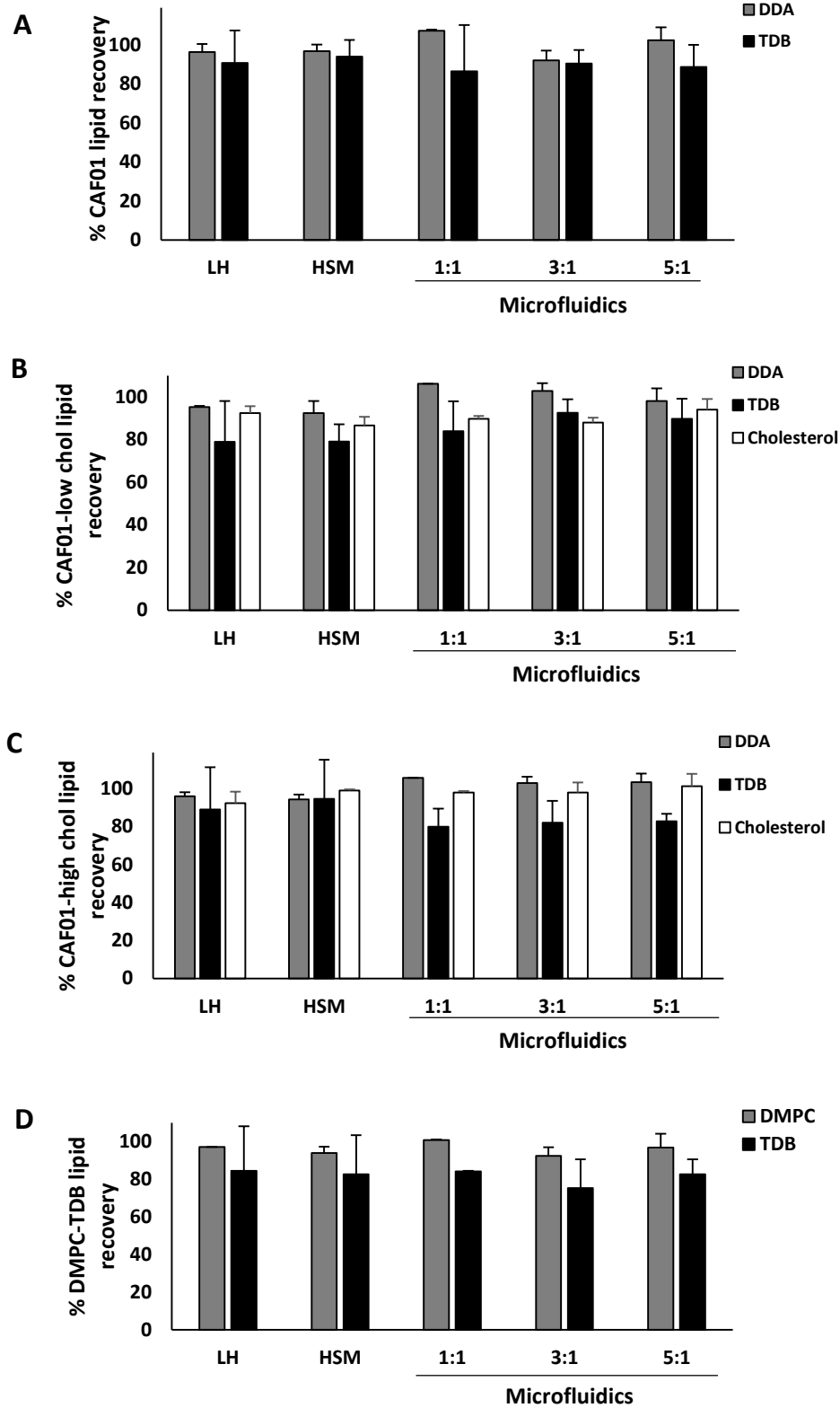


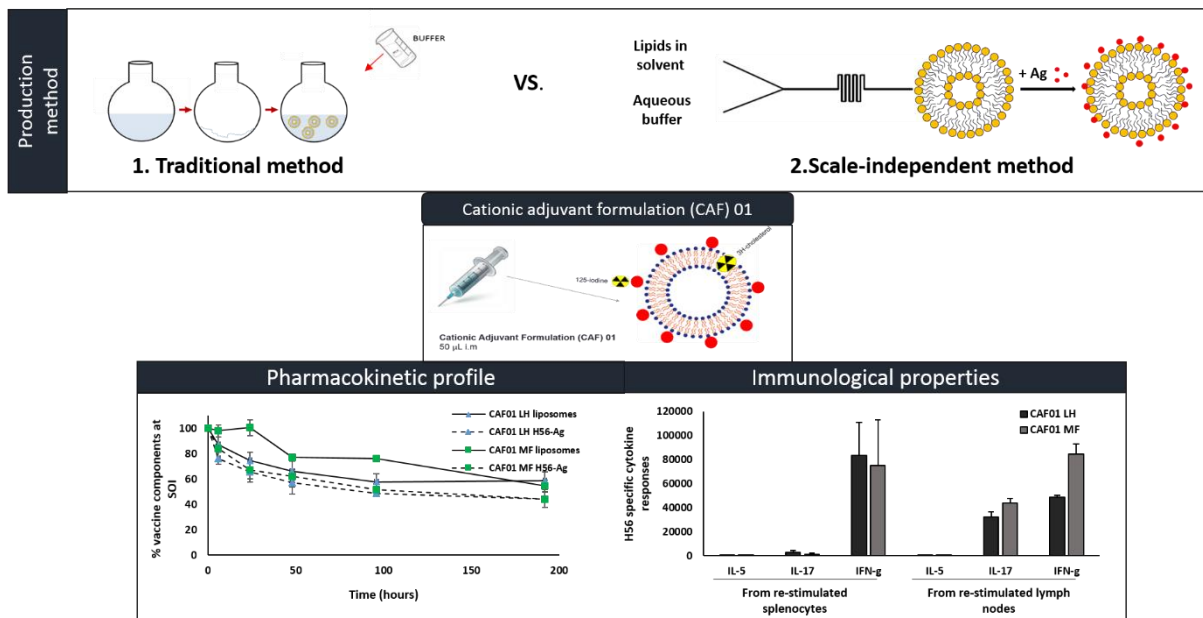
Figure 2.17 Lipid recovery quantification for the four liposomal formulations manufactured using the lipid film hydration (LH), high shear mixing (HSM) and microfluidics at FRR 1:1, 3:1 and 5:1 (A) CAF01 (DDA-TDB) (B) CAF01 + 18mol% cholesterol, (C) CAF01 + 31mol% cholesterol and (D) DMPC-TDB.

2.5 Conclusions

Traditionally, the liposomal adjuvant formulation CAF01 has been manufactured in a batch scale manner using either the lipid film hydration method or high shear mixing. Production of CAF01 using these techniques can be an inefficient time consuming process, especially with regards to high scale industrial manufacture. If large scale production of a TB vaccine is to be achieved for global immunisation, new manufacturing methods that can achieve this must be considered. Novel techniques to rapidly produce liposomal vesicles such as microfluidics could alleviate large scale production issues. Results demonstrated here indicate the ability of a microfluidic platform to produce CAF01 with highly similar physicochemical characteristics when compared to the traditional methods mentioned above. As well as particle size and PDI, all of the techniques evaluated showed high loading efficiencies with high lipid recovery values. Additionally, the use of microfluidics allows for the control of numerous production parameters yielding a range of particle sizes for CAF01. Therefore, the use of a microfluidic based manufacturing method shows potential for the production of vaccine adjuvants in a scalable process.

Chapter 3

In vivo biodistribution and immunogenicity of CAF01 liposomal formulations manufactured by different methods



Papers related to this chapter:

C. B. Roces, D. Christensen and Y. Perrie (2018) Scale-independent manufacture of the cationic adjuvant formulation (CAF) 01 retains the immunogenicity of the formulation *in vivo* (in preparation).

3.1 Introduction

A wide variety of subunit vaccines, including HIV, TB, chlamydia and influenza, have been studied alongside CAF01 in order to elucidate its adjuvant effect (e.g. [73, 87-90]). The cationic surface charged related to the quaternary ammonium of DDA has shown to be crucial for its immunological profile since by this means antigens are attached the liposomal surface and thus, allows the co-delivery of both antigen and adjuvant to the APCs. The biodistribution of CAF01 *in vivo* has been studied by dual radiolabelling of the individual vaccine components (¹²⁵I-antigen and ³H-adjuvant). Results have shown the formation of a depot at the injection site (SOI) after parenteral vaccination [90, 91]. The depot effect has been proved to be related to the cationic nature of the formulation and the rigidity of the liposomal membrane at body temperature (CAF01 $T_m \sim 42^\circ\text{C}$). Hereby, APCs are recruited to the SOI where they engulf the vaccine components and become activated. These activated immune cells move to the draining lymph nodes for antigen presentation to the T cells and subsequently, activating them [91]. The depot formation is of utmost importance for the Th1/Th17 stimulation. Moreover, the inclusion of the immunopotentiator TDB results in an improved activation of APCs through interaction with the C-Lectin type receptor (CLR) Mincle which has been reported to activate the Syk-Card9 signalling pathway in mice and human [92-97].

As outlined in the previous chapter, CAF01 liposomes are commonly prepared by the thin film method which has several drawbacks including scale-up and reproducibility. In contrast, controllable technologies such as microfluidics have advantages in material preparation such as uniform flow and mixing, high efficiency, continuous operation, easy control and low cost. Thus, within this chapter the use of both liposome manufacturing techniques was evaluated and compared *in vivo* in order to assess the suitability of microfluidics as a technique for liposome preparation since by this method it is possible to produce particles suitable for scale up.

3.2 Aim and objectives

In the previous chapter, alternative methods for the scale-independent production of CAF01 liposomes were investigated. However, given the differences in sizes of the vesicles produced it is important to assess their efficacy *in vivo*. To achieve this the objectives of the work presented in this chapter was the *in vivo* evaluation of microfluidics as a tool for DDA:TDB preparation.

3.3 Materials and methods

3.3.1 Material used for the preparation of liposomal formulations

Dimethyldioctadecylammonium (DDA) bromide and trehalose 6,6'-dibehenate (TDB) were purchased from Avanti Polar Lipids Inc. (Alabaster, USA). Tris-base was obtained from IDN Biomedical Inc. (Aurora, OH, USA) and used to make 10 mM Tris buffer and adjusted to pH 7.4 using HCl. H56 TB antigen was donated by Statens Serum Institut (Copenhagen, Denmark). Trehalose [D-Trehalose (99 %) anhydrous] was obtained from Acros Organics. All other reagents were of analytical grade and were purchased from commercial suppliers.

3.3.2 Material used for the radiolabelling of the vaccine components and biodistribution study

The radionucleotides Iodine ¹²⁵I (NaI in NaOH solution) and Tritium ³H-cholesterol (tritium-labelled cholesterol in ethanol), and Ultima Gold™ scintillation fluid were purchased from Perkin Elmer (Waltham, MA, USA). Chicago blue (Pontamine blue), sodium hydroxide (NaOH) and hydrogen peroxide (H₂O₂) were purchased from Sigma-Aldrich Company Ltd. (Poole, UK). Bicinchoninic acid protein assay (BCA) kit and Sephadex G-75 superfine were purchased from Fisher Scientific (Leicestershire, UK). IODO-GEN® pre-coated iodination tubes from Pierce Biotechnology (Rockford, IL) and scintillation vials from Sarsted Ltd (Leicester, UK).

3.3.3 Material used for the immunisation studies

Horseradish peroxidase (HRP) enzyme (HRP-streptavidin), purified rat anti mouse IFN- γ and IL-17, biotin conjugates IFN- γ and IL-17, IL-17 standard, and mouse IL-5 ELISA set were purchased from Becton Dickinson (BD biosciences, New Jersey, US). Mercaptoethanol, concanavalinA (conA), Tween 20, Bovine serum albumin (BSA), carbonate-bicarbonate buffer tablets, sulfuric acid, IFN- γ standard, skimmed milk powder, heparin, BSA, sodium chloride (NaCl), sodium azide (NaN₃), Triton X-100 and protease inhibitor cocktail were purchased from Sigma-Aldrich Company Ltd. (Poole, UK). Tetramethylbenzidine (TMB) substrate, isotype-specific immunoglobulins (Goat anti-mouse IgG1 and IgG2c), Penicillin-Streptomycine (10,000 U/mL), L-glutamine 200 mM, sodium pyruvate 100 mM, MEM non-essential amino acids solution (100x), Roswell Park Memorial Institute (RPMI) 1640 media, Fetal

Bovine Serum (FBS), HEPES (1 M), Phosphate Buffered Saline (PBS) (10x) were purchased from Fisher Scientific - UK Ltd (Loughborough, UK).

3.3.4 Biodistribution studies in mice of radiolabelled vaccine components

3.3.4.1 Radiolabelling of the tuberculosis antigen H56

In order to radiolabel the antigen H56 with ^{125}I , 500 μL from the antigen stock (1.1 mg/mL) was added into an IODO-GEN[®] tube and mixed with 6.5 MBq of the iodine isotope. IODO-GEN[®] tube contains an oxidizing reagent that converts Na^{125}I into a reactive iodine molecule that can be inserted into the tyrosol group of tyrosine amino acids [197] (Figure 3.1). The ^{125}I -H56 mixture was left for an hour with intermittent vortexing to allow this reaction to happen [198].

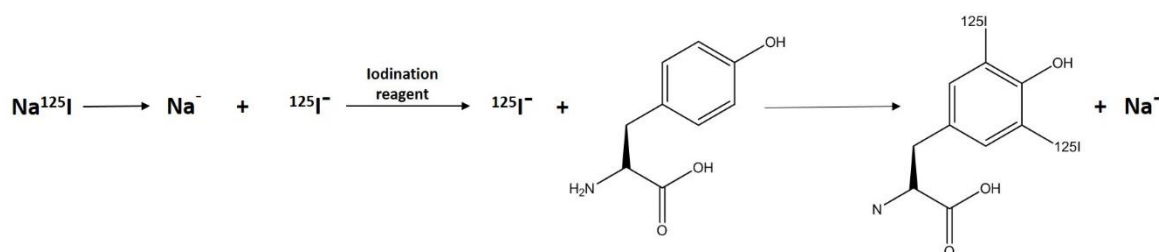


Figure 3.1 Diagram showing the incorporation of ^{125}I into amino acid residues of proteins during the radiolabelling procedure.

Once the iodination reaction took place, a gel filtration procedure to separate unbound ^{125}I from the ^{125}I -labelled H56 antigen was carried out. For the preparation of the column, 1 g of Sephadex G-75 superfine was rehydrated at 90°C for 2 hours with 20 mL Tris buffer (10 mM, pH 7.4). Hydrated Sephadex G-75 beads were then poured into the column and let cool down. The ^{125}I /H56 mixture (~500 μL) was then added to the column and eluted using a steady flow of Tris buffer. Aliquots were collected at 1 minute intervals for 40 minutes and then analysed for ^{125}I content. Aliquots (25 μL) were mixed with 10 mL scintillation cocktail (Gold Ultima[™]) and ^{125}I content measured using a Packard Tri-Carb Liquid Scintillation Counter (GMI company, Minneapolis, US). BCA assay analysis was carried out in parallel to confirm the presence of the H56 antigen measuring the absorbance at 562 nm using microplate reader model 680 (Bio-rad Laboratories. Inc., Hertfordshire, UK). The samples with the highest antigen and ^{125}I concentration were collected, pooled together and diluted in order to get desired dose of protein (0.1 mg/mL of H56) and radioactivity (~100 kBq of ^{125}I /dose) to load into the liposomal formulations for biodistribution studies. Figure 3.2 shows the overlay of the results obtained from the scintillation counter and the BCA assay. It is possible to see the existence of a second ^{125}I

peak starting on aliquot 31, which represents the unbound ^{125}I . Antigen was freshly labelled before each biodistribution study.

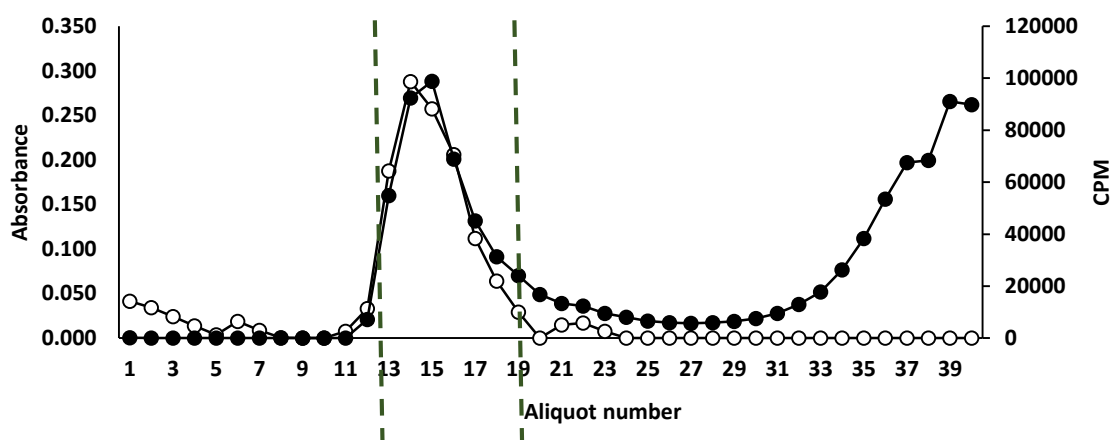


Figure 3.2 Overlay plots of the BCA assay (white) and beta counts (black) for the separation of the non-labelled H56 antigen for the biodistribution study. BCA assay was carried out in order to quantify where the H56 antigen was located within the aliquots whereas the beta counting was performed for the confirmation of radiolabelling of the antigen. Aliquots containing both antigen and iodine were pooled together and diluted for future use.

3.3.4.2 Radiolabelling of the liposomal formulations

Liposomal formulations were radiolabelled with ^3H -Cholesterol by incorporation of the isotope into the lipid bilayer [198]. For liposome formulations produced by lipid film hydration, tritium was added into the lipid mixture. Organic solvent (9:1 v/v chloroform: methanol) was evaporated for 20 min at 220 rpm using a rotary evaporator. Lipids with tritium were rehydrated above transition temperature with isotonic tris buffer. For isotonicity, 10% w/v of the sugar trehalose was added to the filtered buffer (0.22 μm filter). Radiolabelled H56 antigen was added to the hydrated formulation at the desired concentration (0.1 mg/mL) for surface loading onto the DDA:TDB formulation. This formulation was used as a control since its biodistribution has been reported previously [70, 157, 189, 196, 199, 200].

For the liposomal formulations manufactured by microfluidics (Nanoassemblr™, Precision Nanosystems, Vancouver, Canada), ^3H -Cholesterol was added to the lipid mixture prior to organic phase injection. The amount of ^3H -Cholesterol added was based on the radioactivity of ^3H and the concentration of cholesterol in the liposomes so that the physicochemical properties of the liposomes were not changed (200 kBq per dose). The selected liposome formulations for the biodistribution studies are shown in Table 3.1. Total flow rate was kept constant at 10 mL/min whereas the flow rate ratios were varied (1:1, 3:1 and 5:1). The transition temperature of DDA is approximately 47°C [75],

therefore, the microfluidics heating block was set at 60°C. Once the liposomes were prepared, ¹²⁵I-H56 antigen was added onto the surface of the liposomes at a final concentration of 0.1 mg/mL with intermittent vortexing. Liposomes were purified in terms of removal of organic solvent and unbound protein by dialysis (Spectra-Por® Dialysis tubing 300 kDa, Spectrum Labs, Germany) overnight against a total volume of 1 L tris buffer with buffer exchange at set intervals. In order to provide isotonicity within the formulation, trehalose was added to the purified formulation at a final concentration of 10 % w/v. All liposomal formulations contained a final concentration of 250 µg DDA/50 µg TDB/5 µg H56 per vaccine dose (50 µL). H56 antigen was added to the preformed liposomes for surface adsorption in all the formulations prepared unless otherwise stated.

Table 3.1 List of liposomal formulations selected for the biodistribution studies in mice. The lipid concentrations correspond to the initial concentration used in order to have equal final lipid composition in all the formulations.

Liposomal Formulations	DDA (mg/mL)	TDB (mg/mL)	Final H56 (mg/mL)	Manufacturing method
CAF01	5	1	0.1	Lipid film
CAF01 MF	10	2	0.1	TFR 10 FRR 1:1
CAF01 MF	20	4	0.1	TFR 10 FRR 3:1
CAF01 MF	30	6	0.1	TFR 10 FRR 5:1

3.3.4.3 Pontamine blue injection

Three to four days before injection of the radiolabelled formulations, a volume of 200 µL pontamine blue 0.5% (w/v) in isotonic (10% w/v trehalose) and filtered (0.22 µm) Tris buffer was subcutaneously injected into the neck scruff of the mice. Pontamine blue is a dye used as a marker which helps with the visualisation of lymph nodes and it also served as a marker for identification of infiltrating macrophages to the SOI [200, 201].

3.3.4.4 Organ and tissue processing for the quantification of the radioactive isotopes

All *in vivo* studies were conducted under the regulations of the Directive 2010/63/EU. All protocols have been subject to ethical review and were carried out in a designated establishment. Inbred female BALB/C mice (3 mice per time point) were obtained from the Biological Procedure Unit (BPU) at the

University of Strathclyde, Glasgow. Mice were housed under conventional conditions (22°C, 55% humidity, 12 hours day/night cycle) and were caged in their experimental groups (6 mice/cage) and given a standard diet ad libitum. All mice were used at 6-10 weeks of age at the start of the experiment.

Mice were injected intramuscularly with 50 µL of the radiolabelled formulation in the right quadriceps. Five time points were selected and therefore, mice were killed after 6, 24, 48, 96 and 192 hours. Specific organs/tissues were isolated: inguinal lymph node (ILN), mesenteric lymph node (MLN), popliteal lymph node (POP), spleen and site of injection (SOI). These organs/tissues were put in a scintillation vial and 2 mL NaOH 10 mM was added in order to dissolve them. Mice carcasses were kept in a bottle and dissolved with 60 mL of NaOH 10 mM for mass balance calculation. All vials containing NaOH were incubated in an oven at 60°C overnight. From the carcasses 2 mL were withdrawn and put into a scintillation vial. All scintillation vials containing 2 mL of either carcasses, organs or tissues were bleached with 200 µL of H₂O₂ and incubated for 2 hours in the oven at 60°C. Vials were let to cool down and 10 mL of scintillation cocktail (Ultima Gold) was added to them for the quantification of the radiation with a scintillation counter TriCarb 2810 Liquid Scintillation Counter.

The protocol followed for the quantification of radiation was set as follows: Region A was set from 0 to 18.6 KeV and region B was set from 18.6 to 80 KeV. ³H and ¹²⁵I have energy overlap from 0 - 18.6 keV since ³H emits radiation in that range and ¹²⁵I emits from 0 - 80 keV, leading to an over-spill of iodine in tritium region. To eliminate this over-spill, a calibration curve was prepared with different volumes of ¹²⁵I in 10 mL of scintillation cocktail. A linear regression of the CPM A (y-axis) and CPM B (x-axis) was obtained from the reading and the equation was used to eliminate the interference that the ¹²⁵I would have on the ³H values determined by scintillation counter (Figure 3.3) and therefore, by using this protocol, it is possible to quantify tritium and iodine simultaneously.

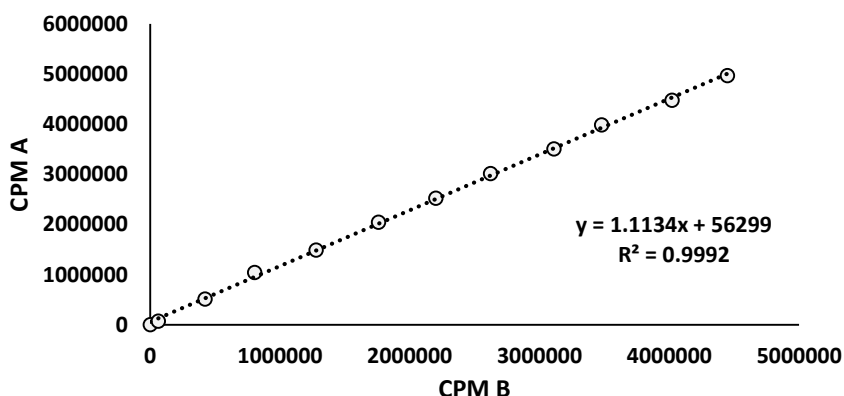


Figure 3.3 Calibration curve with different volumes of iodine to eliminate the iodine overspill in the tritium region. Counts per minute A (CPM) which correspond to the region A (0 – 18.6 KeV) was plotted on the y-axis against the CPM B (x-axis) which correspond to the region (0 – 80 keV).

Scintillation vials containing the original dose (50 µL radiolabelled formulation) were prepared and treated under the same conditions as the organs/tissues in order to compare the percentage of ^3H and ^{125}I present in the injected vaccine volume and therefore, calculate the percentage of liposomes (^3H) and antigen (^{125}I) detected within the isolated organs/tissues.

3.3.4.5 Stability of liposomes in simulated *in vivo* conditions

Stability of the liposomal formulations was assessed in terms of size, PDI and zeta potential under simulated *in vivo* conditions. Briefly, liposomes were placed in a water bath at 37°C with 50% Foetal Bovine Serum (FBS) and aliquots were taken at specific time points to match with the biodistribution time points (0.05, 1, 24, 48, 72, 96 and 192 hours).

3.3.5 Immunisation studies in mice

3.3.5.1 Preparation of the vaccine formulations

Preparation of the vaccine formulations for the immunisation studies was carried out as outlined in section 3.3.4.2 but without the addition of the radioactive isotope. Selected formulations from the biodistribution study were prepared in order to study the correlation of the distribution of the liposomes within the body and their immunological behaviour. Table 3.2 shows the formulations used for this study.

Table 3.2 Liposomal formulations selected for the immunisation study. Lipid concentrations correspond to the initial concentrations used for the preparation of the liposome adjuvants

Liposomal Formulations	DDA (mg/mL)	TDB (mg/mL)	Final H56 (mg/mL)	Manufacturing method
CAF01	5	1	0.1	Lipid film
CAF01 MF	30	6	0.1	TFR 10 FRR 5:1

3.3.5.2 Dynamic light scattering

The size of the liposomal formulations was determined by DLS using a Zetasizer nano ZS (Malvern PANalytical Ltd., Worcestershire, UK). Three measurements at 25°C were conducted on the samples, which were previously diluted in filtered Tris buffer (10 mM, pH 7.4) to achieve the optimal vesicle

concentration (10- fold dilution) and vortexed to provide a homogeneous solution. Square single-use cuvettes were filled in with 1 mL of diluted sample and placed into the instrument which uses a 4-mW He-Ne 633 nm laser. For determination of the zeta potential, a folded capillary zeta cell was used and filled with the same diluted sample as for the size. Data was collected and analysed by using Malvern Dispersion Technology Software (DTS) v.7.12 (Malvern Panalytical, Worcestershire, UK).

3.3.5.3 Quantification of H56 antigen loading by HPLC-UV

Quantification of the antigen loading of the liposomal formulations was performed by reverse phase HPLC (RP-HPLC) using a UV detector (Agilent Technologies, Edinburgh, UK). Jupiter 5 μ C18(2) column (Phenomenex, Cheshire, UK) pore size 300 Å was used as stationary phase. For the preparation of the standards and samples, antigen alone or liposomes loaded with H56, were diluted in 50% Tris/IPA (1:1 v/v) [202]. Figure 3.4 shows the HPLC method used for the H56 antigen quantification. A gradient elution method was followed where both mobile phases contain the same solvents in different proportions (Mobile phase A: 90% H₂O, 10% acetonitrile and 0.1% TFA; Mobile phase B: 70% acetonitrile, 30% H₂O and 0.1% TFA) in order to favour the mixing of both phases during the run. The instrument settings were set as follows: 50 μ L injection volume, flow rate 1 mL/min, UV wavelength 210 nm and column temperature either 60°C. Calibration curve shows a good linearity, being $R^2 > 0.99$ and the calculated LOQ and LOD were 0.019 and 0.006 mg/mL respectively.

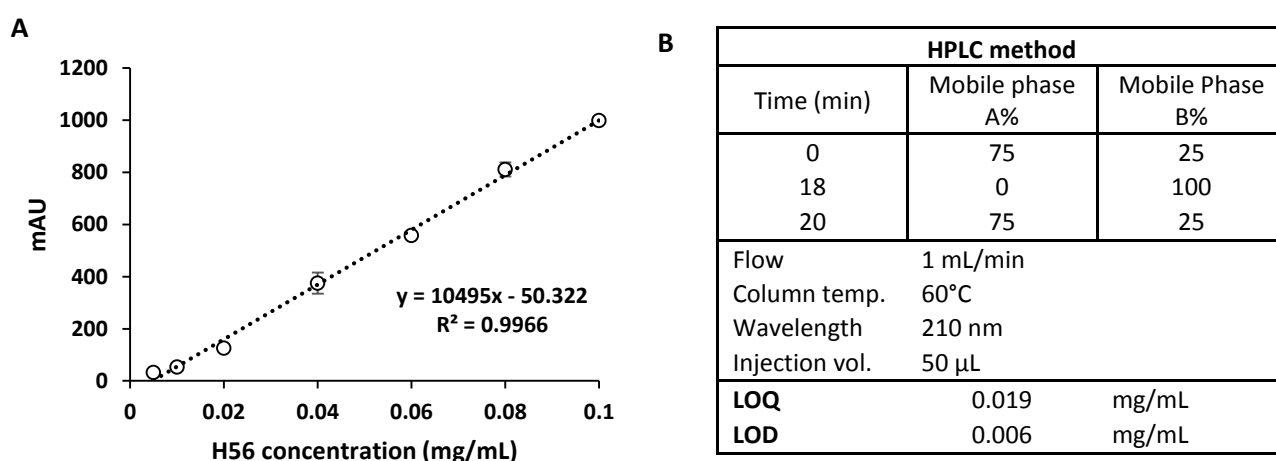


Figure 3.4. (A) Calibration curve for the H56 antigen in 50% IPA/Tris (1:1 v/v) and (B) HPLC-UV setting used for its quantification. Results represent the mean value of at least 3 independent experiments \pm SD.

3.3.5.4 Animal ethics and immunisation protocol

Female 6-10 week-old C57BL/6 mice were used to study immunisation of above formulations. 5 mice per group were injected i.m. (50 μ L) into the right quadricep with formulations freshly prepared on the day of injection as given in table 5.3. All *in vivo* studies were conducted under the regulations of the Directive 2010/63/EU. All protocols have been subject to ethical review and were carried out in a designated establishment. Mice received 3 immunisations at 2 week intervals (days 0, 14 and 28) and were terminated 3 weeks after the last immunisation (on day 49) (Figure 3.5).

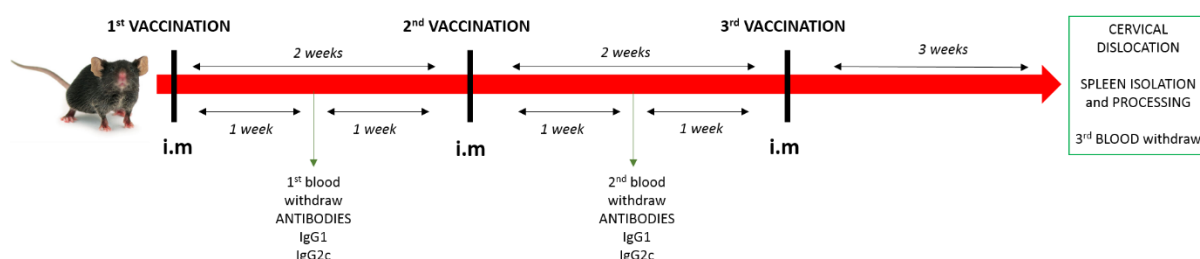


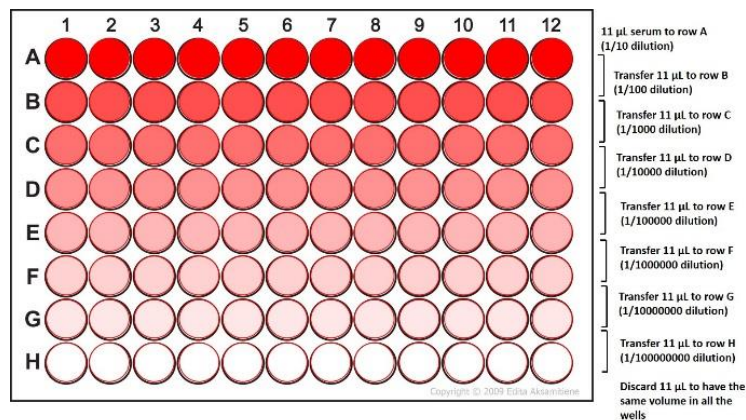
Figure 3.5 Scheme of the immunisation protocol followed in this study. Three intramuscular injections containing CAF01:H56 manufactured using either the lipid film hydration or microfluidics were administered with 2 week interval in between. Blood was collected at days 7, 21 and 49 whereas organs were isolated and processed at the end of the study on day 49.

3.3.5.5 Antibody analysis

For the quantification of serum immunoglobulins, 50 μ L of blood was collected via tail-bleed on days 7, 21 and 49. Blood was collected in a heparinised eppendorf (1% w/v heparin) and centrifuged for 10 minutes at 10,000 \times g (Mini centrifuge Mikro200, Hettich (Tuttlingen, Germany) in order to separate blood cells (pellet) from serum (supernatant). Serum was transferred to another eppendorf and stored in the freezer (-20°C) for further processing.

A standard direct enzyme-linked immunosorbent assay (ELISA) was carried out to detect immunoglobulins IgG1 and IgG2c in serum (Figure 3.6). Maxisorp 96-well plates flat bottom (Fisher scientific, Loughborough, UK) (high binding and affinity) were coated by passive absorption overnight at 4°C with 0.5 μ g/mL H56 antigen diluted in carbonate buffer 0.05 N pH 9.6 (100 μ L/well). The next day, plates were emptied, washed with washing buffer (PBS pH 7.2, 10 mM containing 0.2% Tween 20) and blocked for 1.5 – 2 hours at room temperature with 200 μ L/well of PBS (pH 7.2, 10 mM) containing 2% BSA to block any non-specific binding. Plates were emptied and washed 3 times with washing buffer and samples were added and serially diluted into the plates. Briefly, 11 μ L of the serum

was added into the first well containing 100 μL of 1% BSA in PBS and mixed up and down with the pipette. Serial dilutions (1/10) were done by transferring 11 μL from the first well to the next one and so on 7 – 12 times. In order to have the same volume/well, 11 μL were withdrawn from the last well of the column (Figure 3.6). Plates were incubated at room temperature for 2 hours and after that, plates were emptied and washed 3 times. HRP-conjugated antibody was diluted in 1% BSA in PBS (1:20000 and 1:5000 for IgG1 and IgG2c respectively) and added in a volume of 100 μL /well to the washed plates. Plates were incubated for an hour and washed 5 times. TMB substrate (room temperature), a chromogenic substrate which develops blue colour when it detects horseradish peroxidase (HRP), was added to the plates 100 μL /well. After approximately 20 minutes the reaction was stopped by adding 100 μL /well 0.2 M sulfuric acid. The reaction was stopped when the maximum blue colour reaction was obtained for the wells containing the first dilution, being careful to not exceed the optical density of 4 which would give inaccurate results. Addition of sulfuric acid changes the colour to yellow, enabling measuring the absorbance at 450 nm (with wavelength correction 570/620 nm). Results were plot as the Log₁₀ of the end point titre giving and optical density value (OD_{450}) of 0.1 or higher.



DIRECT ELISA

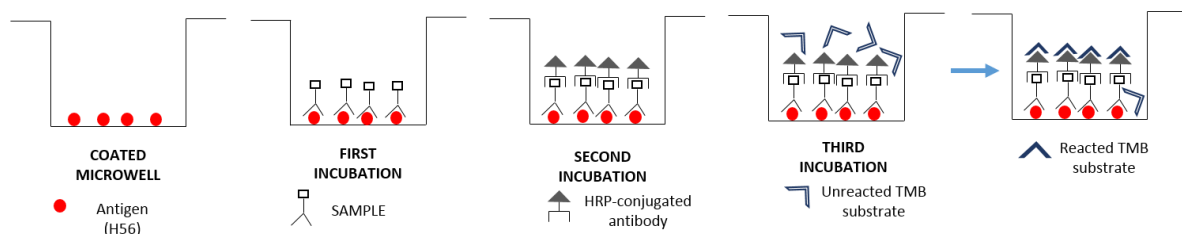


Figure 3.6 Outline of the ELISA plate set-up used for the antibody analysis study and schematic representation of direct ELISA protocol followed.

3.3.5.6 Re-stimulation of the splenocytes and lymph nodes

Spleens and popliteal lymph nodes from each mouse were isolated and processed on day 49. Individual spleens were placed in 15 mL falcon tubes containing 2 mL of PBS and kept ice-cold whereas the lymph nodes from each group were pooled together. Spleens and lymph nodes were forced through a metal mesh using the bottom part of a 3 mL plastic syringe and transferred back to a falcon tube filled with 12 mL of PBS. Samples were spun down at 600 x g for 5 min with break (break 9) and at 4°C. Supernatant was discarded and pellet was resuspended in 8 mL of RPMI and spun down at 600 x g for 5 minutes with break (9) at 4°C. Cells were resuspended in 1.8 mL or 0.5 mL of complete RPMI (RPMI supplemented with HEPES, penicillin-streptomycin, L-glutamine, sodium pyruvate, non-essential amino acids, mercaptoethanol and 10% heat inactivated FCS) for spleens and lymph nodes respectively. Cells were counted and diluted in complete RPMI to a final concentration of 2×10^6 cells/mL.

Cells were counted using the trypan blue exclusion assay. Briefly, cells were dyed with trypan blue in a 1:10 ratio (10 μ L cells: 90 μ L trypan blue). Subsequently, 100 μ L were placed on a haemocytometer and cells were counted (Figure 3.7). Trypan blue allows to check the viability of the cells, since the cells become blue when they are dead or damaged as the blue dye is allowed to permeate through the cell membrane in these situations. The calculation of the cells was carried out according to equation:

Calculation:

$$\text{Number of cells/mL} = \text{number of cells/square} * \text{DF} * 10,000$$

DF = dilution factor

Number cells/sq. = average cells from 4 corners

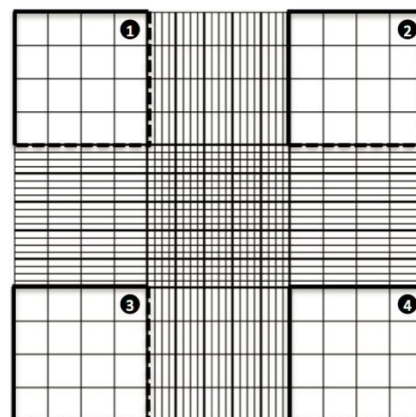


Figure 3.7 Schematic representation of the haemocytometer grid for the cell count and equation followed for calculation of the viable cells.

Once the cells were diluted to the same concentration, 100 μ L of this diluted cells were plated on a Nunclon 96-well round bottom (Fisher scientific, Loughborough, UK) (Figure 3.8). Cells were stimulated with either 100 μ L of ConA (5 μ g/mL) which serves as a positive control since it stimulates

the production of cytokines, RPMI media as a negative control, or H56 antigen (5 $\mu\text{g}/\text{mL}$) as the investigated antigen. Splenocytes and lymph nodes from immunised mice were incubated at 37°C, 5 % CO_2 and 95 % humidity for 72 hours. After 3 days of incubation, supernatants were harvested (approximately 160 μL) and stored at -20°C for further processing.

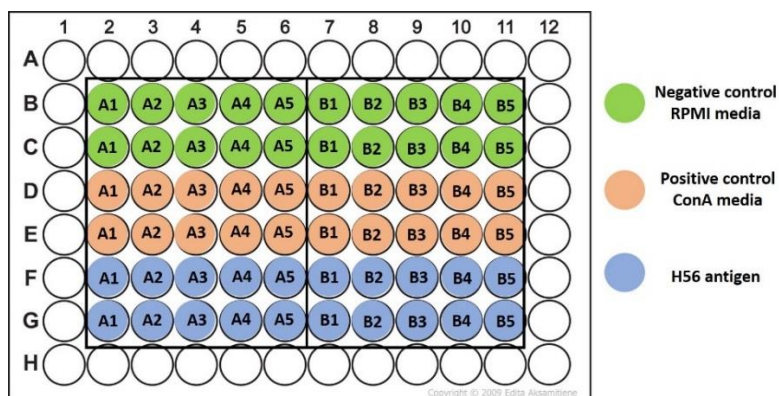


Figure 3.8 Outline of the ELISA plate set-up used for the cytokine analysis study. Samples were plated in duplicate. ConA was used at a concentration of 5 $\mu\text{g}/\text{mL}$ as a positive control RPMI media was used as a negative control and H56 antigen for the quantification of antigen-specific responses.

3.3.5.7 Cytokine analysis of restimulated splenocytes, lymphocytes and at the injection site

Supernatants from restimulated splenocytes and lymph nodes were analysed using a sandwich ELISA protocol for the production of cytokines IL-17 and IFN- γ (Figure 3.9). Plates were coated with the specific capture cytokine diluted in carbonate buffer, either purified anti mouse IL-17 (1:500 dilution) or IFN- γ (1:1000 dilution) overnight at 4°C. Next day plates were emptied and blocked for 1.5 – 2 hours at room temperature with 200 $\mu\text{L}/\text{well}$ PBS containing 2% milk powder. Plates were emptied and washed and samples and standards were diluted in 2% BSA in PBS and incubated at room temperature for 2 hours (total volume in all wells was 100 μL). Plates were washed 3 times and biotin conjugate was diluted in 1% BSA in PBS (IL-17 1:2000, IFN- γ 1:5000) and 100 μL were added on each well. Plates were incubated for an hour at room temperature followed by washing and 30 min incubation with 100 $\mu\text{L}/\text{well}$ of HRP-streptavidin in 1% BSA (1:5000). Plates were washed and TMB substrate (room temperature) was applied to the plates 100 $\mu\text{L}/\text{well}$. After approximately 15 minutes the reaction was stopped by adding 100 $\mu\text{L}/\text{well}$ 0.2 M sulfuric acid.

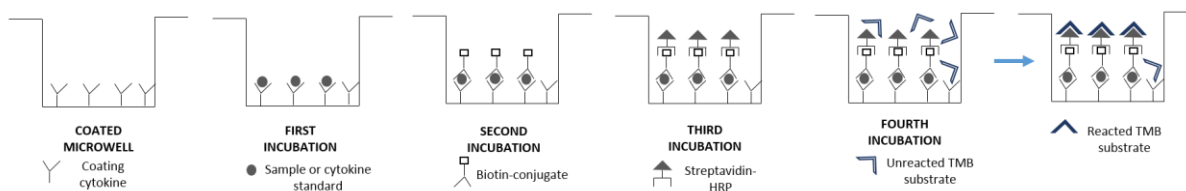
SANDWICH ELISA

Figure 3.9 Schematic representation of sandwich ELISA protocol followed for the quantification of cytokines in the spleen, popliteal lymph node and site of injection.

A modification of the above mentioned ELISA method was used for the quantification of the IL-15 cytokine production following manufacturer's instruction (ELISA IL-5 kit, BD Biosciences). In this case, ELISA washing buffer contained 0.05% Tween 20 and instead of BSA in PBS, the assay diluent was PBS supplemented with 10% heat inactivated FBS and both detection antibody and HRP-streptavidin were premixed and diluted in assay diluent (1:250 each). All experiments were carried out in duplicate and absorbance was measured at 450 nm with wavelength correction (570/620 nm).

3.3.5.8 Processing of the site of injection

The sites of injection (i.e. the right quadriceps) were excised 3 weeks after the last immunisation (on day 49) and the method from Sharp et al. for the analysis of cytokines at the SOI was followed [203]. Quadriceps muscles were removed from the bone and weighted out individually. Individual muscles were homogenised in 2.5 mL of homogenisation buffer 500 mM NaCl/50 mM HEPES, pH 7.4 containing 0.1% Triton X-100, 0.02% NaN_3 and 1% v/v protease inhibitor cocktail. Homogenates were sonicated twice for 15 seconds and centrifuged at $2390 \times g$ 20 minutes at 4°C . Supernatant were removed and stored at -20°C for further quantification of the cytokines by sandwich ELISA.

3.3.6 Statistical analysis

All experiments were carried out at least in triplicate unless otherwise stated. Means and standard deviations are plotted on the graphs. Statistical analysis of data was calculated by one-way analysis of variance (ANOVA). When significant differences were indicated, differences between means were determined by Tukey's post hoc test.

3.4 Results and discussion

3.4.1 Physicochemical characterisation of the CAF01:H56 adjuvant formulations prepared for biodistribution

The aim of the study was to evaluate the suitability of the microfluidics system for the preparation of CAF01 liposomes. Therefore, liposomal formulations containing DDA and TDB were manufactured by the traditional method of the lipid film hydration and by microfluidics. The *in vivo* dose for the CAF01:H56 formulation is 250 µg DDA/50 µg TDB/5 µg H56 per 50 µL dose [51, 204]. A total of 4 different formulations were selected for the comparison of the pharmacokinetic profile of CAF01:H56 using different manufacturing techniques. The lipid film hydration method was used as a control since this manufacturing technique has been broadly used and studied [189, 190, 199]. The other three formulations were produced by microfluidics by altering the processing parameters. Based on the results obtained in Chapter 2, the TFR was set at 10 mL/min whereas the FRR was varied from at 1:1, 3:1 or 5:1 since the FRR has a large impact on the physicochemical characteristics of the liposomes produced. Therefore, in order to match their final concentration, different initial DDA and TDB concentrations were used for the microfluidics manufacturing due to the unavoidable dilution factor characteristic of this method. For example, the FRR 1:1 produces a 2-fold dilution, whereas FRR 3:1 and 5:1 produce a 4- and 6-fold dilution respectively, thus initial lipid concentration was increased 2-, 4- and 6- fold. H56 antigen was added to the pre-formed liposomal formulations after removal of the organic solvent by dialysis. These formulations were non-radiolabelled and the same lipid stock was used for the biodistribution study of the individual vaccine components (antigen and liposomes).

Figure 3.10 shows the physicochemical characteristics of the CAF01 liposomal adjuvant formulations prepared for this study. CAF01 liposomes produced by lipid film hydration showed a size of approx. 700 nm and high PDI. Microfluidics formulations showed different sizes depending on the FRR applied. FRR 1:1 showed the largest particle size, being in the micrometre range, whereas FRR 3:1 and 5:1 were in the nanometre range (~900 and ~400 nm respectively). All CAF01 formulations were highly cationic and heterodisperse in nature (PDI > 0.2).

After purification of the unbound H56 antigen by dialysis overnight, liposomes were solubilised in 50% Tris/IPA (v/v) for the separation of the antigen from the liposomes and antigen loading was then quantified using HPLC-UV [202]. Figure 3.10B shows the antigen loading for the formulations used for the biodistribution study. The vaccine antigen candidate H56 has an pI of 4.9 and therefore, it is negatively charged at a pH 7.4 [205]. Hence, binding occurs through electrostatic interactions between the liposomal surface due to the cationic nature of the surfactant DDA and the negatively charged

antigen. No significant differences were found in all 4 CAF01 formulations in terms of H56 antigen loading, since they all showed highly cationic zeta potential.

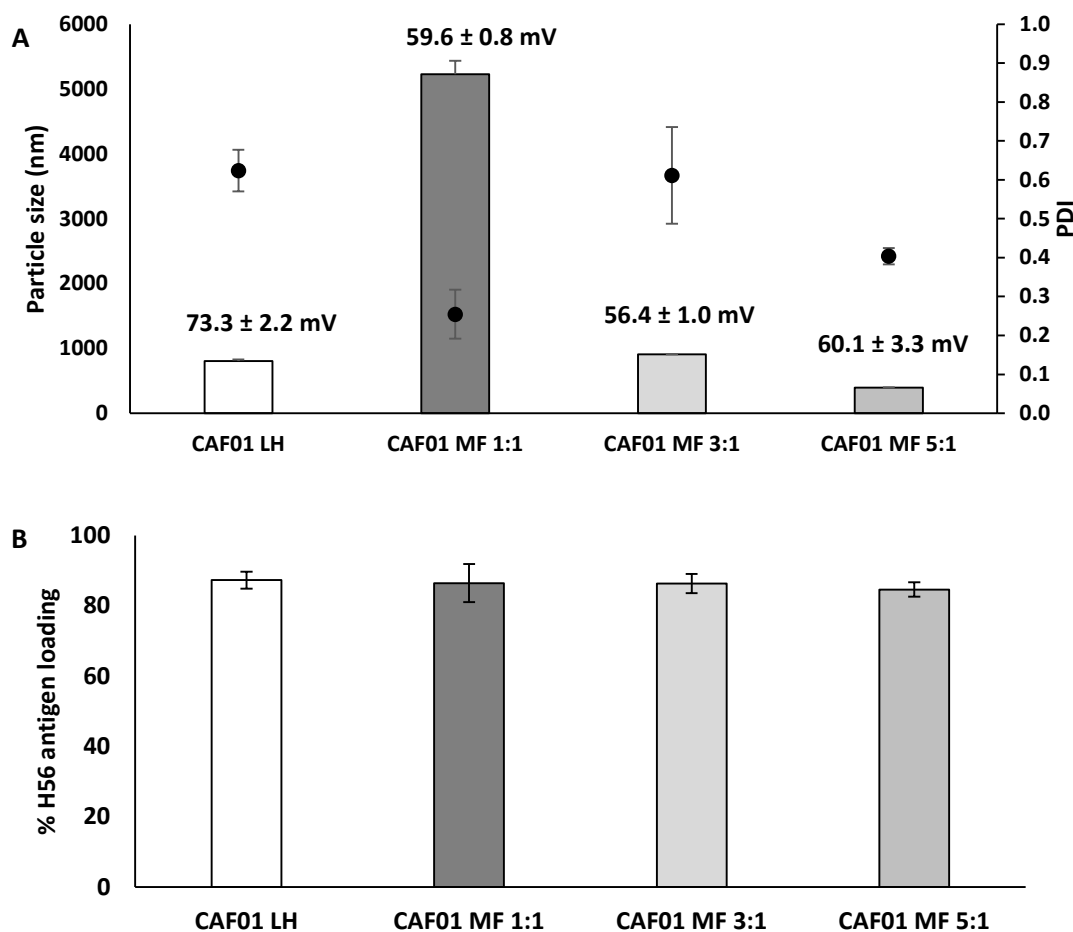


Figure 3.10 Physicochemical attributes (**A**) size (bars), PDI (dots), ZP (values) and (**B**) loading efficiency (as percentage) of the formulations selected for the biodistribution study. Non-radiolabelled formulations were prepared in triplicate using the same lipid stock as for the biodistribution study. Results represent the mean value of at least 3 independent experiments \pm SD.

3.4.2 Interaction of liposomes with serum proteins in simulated *in vivo* condition

Upon injection of the formulations, liposomes will encounter an environment with a high content of proteins. Thus, in an attempt to mimic the conditions these formulations will encounter upon injection into the body, CAF01:H56 liposomes were incubated at 37°C in 50% FBS and at chosen time points, were characterised in terms of size, polydispersity and zeta potential. Liposomes formulated using the traditional lipid film hydration were selected for this study in order to get an overview of their physicochemical modifications after injection.

Previous studies on CAF01 have shown that this formulation aggregates upon injection, increasing vesicle size, being this the reason of the depot effect [90]. Figure 3.11 shows the physicochemical

characteristics from CAF01 at the selected time points (0, 0.05, 1, 6, 24, 48, 96 and 192 hours). The highly cationic formulation CAF01:H56 aggregates with the negatively charged serum proteins, increasing in size and decreasing in zeta potential when it is administered. Particle size increased from ~800 nm to ~1800 nm after 3 minutes (Figure 3.11A). After one hour, the vesicle size goes up to ~3000 nm, reaching a steady state for 8 days were no significant differences in terms of size could be seen. The cationic ZP of the formulations gets shielded by the serum proteins going down to -20 mV upon injection (Figure 3.11B). No specific trend was observed regarding the PDI at any of the time points studied (Figure 3.11C).

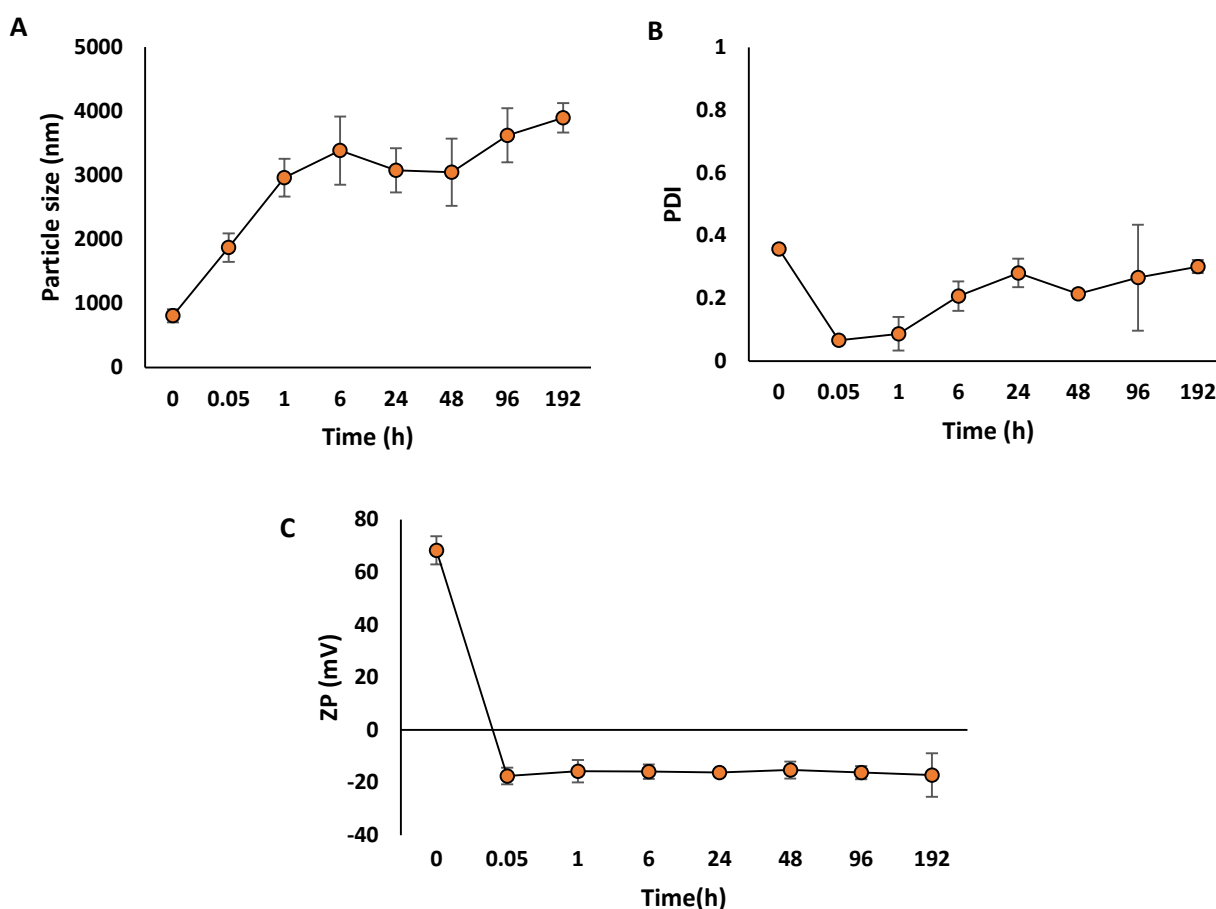


Figure 3.11 Stability study of the liposomal formulations under simulated *in vivo* conditions. Physicochemical characteristics of CAF01 LH under simulated *in vivo* conditions (50% FCS and 37°C). (A) Particles size (B) polydispersity and (C) zeta potential. Results represent the mean value of at least 3 independent experiments \pm SD.

3.4.3 The effect of the manufacturing method on the pharmacokinetic profile of the DDA:TDB formulation *in vivo*

Liposomal formulations containing CAF01 were labelled with ^3H -tritium cholesterol whereas the H56 antigen candidate was labelled with ^{125}I -NaOH. All vaccine formulations contained the same amount of DDA and TDB (250 μg / 50 μg per dose) and were loaded with the same concentration of antigen. Vaccine dose was 50 μL and it was administered intramuscularly on the right quadriceps. Groups of 3 mice per formulations were terminated at selected time points and tissues/organs processed for quantification of ^3H and ^{125}I .

3.4.3.1 Detection of the vaccine components at the site of injection (SOI)

The pharmacokinetic profile of the CAF01 liposomes manufactured using different technologies after intramuscular injection was studied by dual radiolabelling of the individual vaccine components (liposomes and antigen). Four groups formulated either using the lipid film hydration (LH) or microfluidics adopting different flow rate ratios (FRRs) were studied (see Table 3.1). As a control group, CAF01:H56 prepared using the traditional LH technique was used since its pharmacokinetic profile has been previously reported [70, 157, 189, 196, 199, 200, 206]. By this method, highly cationic (+73 mV) multilamellar vesicles of approximately 800 nm were produced. The other 3 groups consisted of the microfluidics CAF01 formulation prepared at FRR 1:1, FRR 3:1 and FRR 5:1 with characteristics as outlined in Figure 3.10. Figure 3.12 shows the percentage of liposomes at the site of injection (right quadriceps) at different time points. After 6 hours, liposomes remained at the SOI independent of either the technique used for their production and the vesicle size. No significant differences were found between the groups, with approximately 90% of the initial liposome dose remaining. Drainage from the injection site followed a similar trend for all 4 liposomes formulations, with between 90 and 100% of the dose remaining after 24 hours, dropping to approximately 50% after 8 days (Figure 3.12). These results are in line with previously published data, showing that 1 day post injection, CAF01 liposomes begin to drain steadily from the SOI and on day 8 between 40-60% of the initial dose is still detectable there [157]. In terms of H56 antigen retention at the SOI, again similar clearance trends were seen for antigen adsorbed to CAF01 prepared by LH and microfluidics at all three flow rate ratios. Whilst the CAF01 formulations prepared has different sizes, all had similar high cationic zeta potentials. The mechanism of action behind the adjuvant effect of DDA has been attributed to its cationic nature and its ability to associate antigens [207]. This was further investigated using ovalbumin (OVA) as a model antigen [208]. Stimulation of immature bone marrow-derived dendritic

cells with fluorescently labelled OVA showed that adsorption of OVA onto DDA enhanced the cellular acquisition of the antigen. Further, inhibition of active cellular processes by OVA stimulation at 4 °C or by the addition of cytochalasin D reduced the cellular uptake, suggesting that active actin-dependent endocytosis is the predominant uptake mechanism [208]. However, when considering the biodistribution of liposomes, size is often shown to have a significant impact. Yet, CAF01 liposomes prepared via LH and subsequent sonication to produce small (<200 nm), medium (500-600 nm), and large (~1500 nm) vesicles were shown to have no significant difference in the drainage of the liposomes or their adsorbed antigen from the site of injection [157]. This would suggest that due to their cationic nature, and independent of their size, the vesicles aggregate after administration, due to interaction with interstitial proteins which are generally anionic in nature, thus prohibiting their clearance from the site of injection and supports the findings in Figure 3.12.

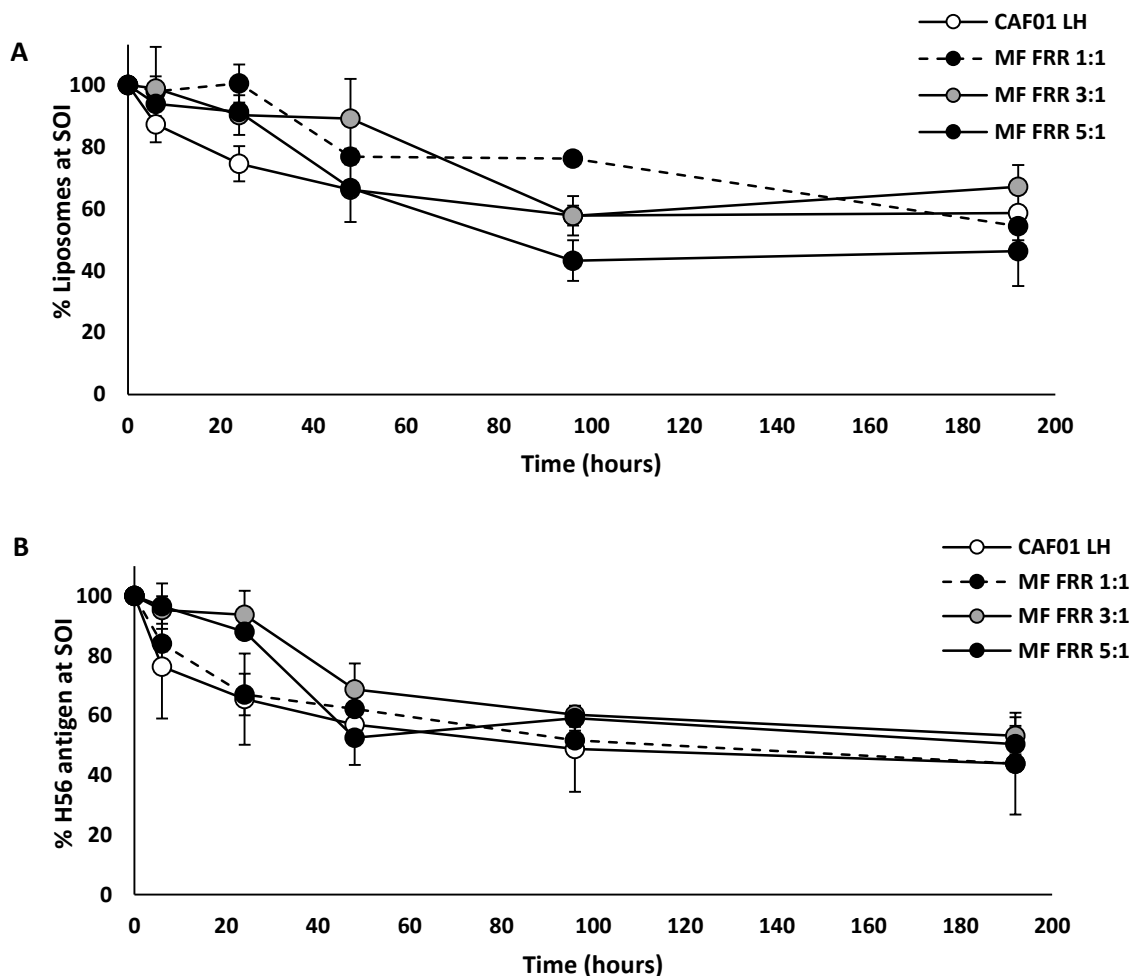


Figure 3.12 Biodistribution study: Percentage of (A) liposomes and (B) antigen retained at the site of injection (SOI). Dual labelling of liposomes and antigen by incorporating either ^3H or ^{125}I was used for the detection of the individual components of the vaccine at different time points. Results represent the mean of 3 mice \pm standard deviation.

Monocyte influx was also qualitative analysed at the site of injection as mice were injected before the start of the experiment with 200 μ L of pontamine blue, a blue dye which serves as a marker for monocyte infiltration [198, 199]. Figure 3.13 shows the site of injections from the mice immunised with the various formulations at the chosen time points. After 6 hours, minimal blue colour can be seen on the muscles since the monocytes have not have time to travel to the injection site, whereas from 1 day onwards, the blue colour becomes more noticeable for all formulations. No visual differences could be seen in the monocytes influx to the SOI independently of the manufacturing techniques or particle size.

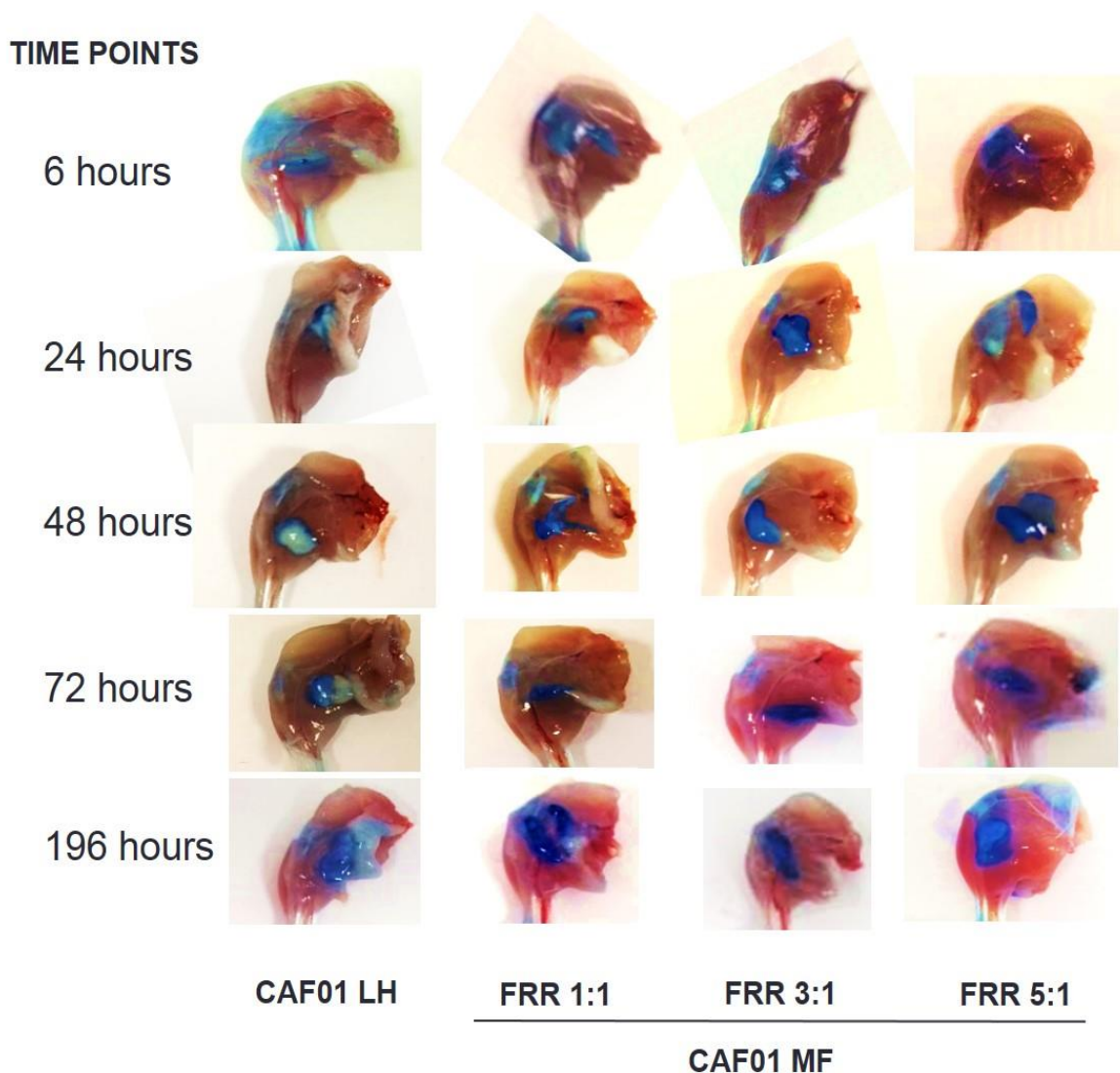


Figure 3.13 Pictures of the site of injection from all four groups at selected time points. Mice were injected with pontamine blue 3-4 days prior the start of the experiment as a marker to detect the monocytes influx and to visualise the lymph nodes by dyeing the macrophages.

3.4.3.2 Detection of the vaccine components at the lymph nodes (POP, ILN and MLN)

Besides the site of injection, the detection of liposomes and antigen in the lymph nodes was investigated as vaccine delivery of antigens to the lymphatics is believed to be important for the protection against most diseases, including TB [209]. The popliteal (POP) lymph node is the first draining lymph node where the formulations will move after intramuscular injection in the mouse quadriceps, so as mice were injected in the right quadriceps, popliteal and inguinal lymph node from the right side were isolated for quantification of ^3H and ^{125}I . These lymph nodes are representative of the local biodistribution of the formulations, whereas mesenteric lymph nodes were isolated as representation of their systemic biodistribution. CAF01 formulations carrying H56 were detected in small amounts in the POP. No significant differences were found from any of the groups tested, in the amount of liposomes nor on the amount of antigen, being less than 0.4% of the initial vaccine dose administered (Figure 3.14B and E). This is in contrast to results previously reported in literature showed that large CAF01 liposomes (1.5 μm) had higher draining to the POP compared to the medium (700 nm) and small size liposomes (200 nm) [157]. When quantification of the amount of liposomes and antigen in the ILN and MLN (Figure 3.14), again no significant differences were seen between the liposomes prepared by the different manufacturing methods.

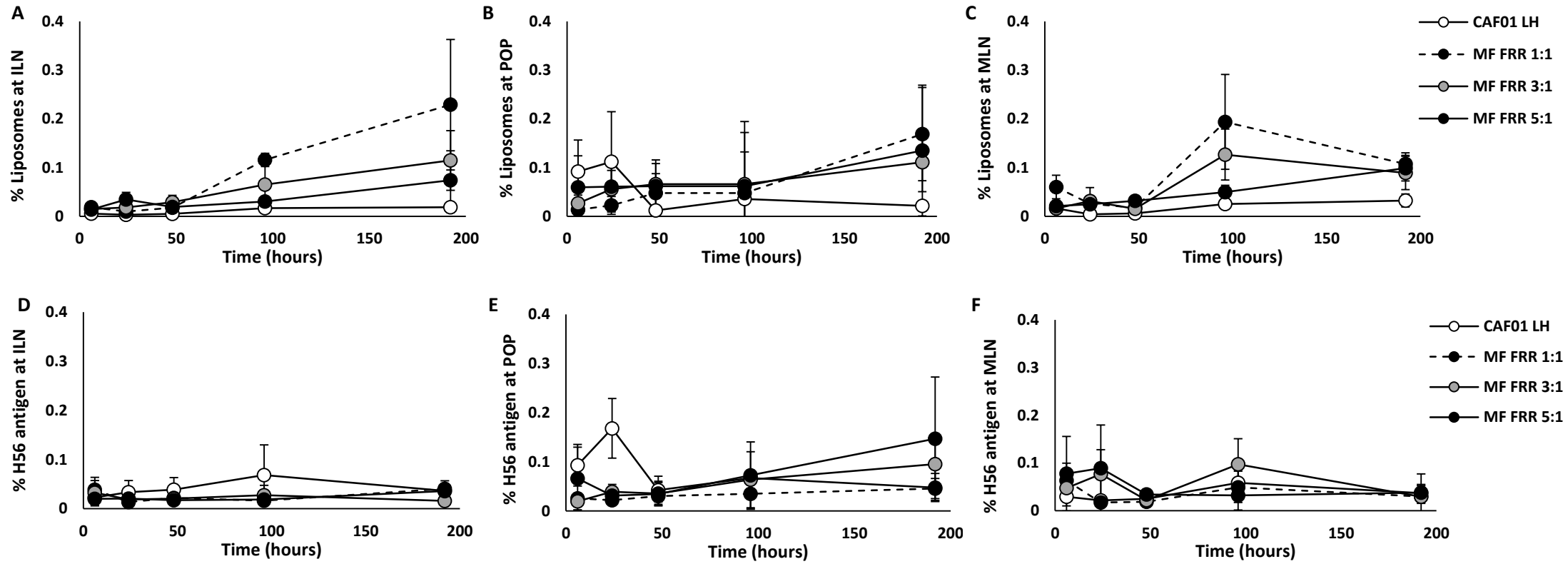


Figure 3.14 Biodistribution study: Percentage of liposomes and antigen detected in the (A, D) ILNs, (B, E) POP and (C, F) MLNs. Dual labelling of liposomes and antigen by incorporating either ^3H or ^{125}I was used for the detection of the individual components of the vaccine at different time points. Results represent the mean of 3 mice \pm standard deviation.

3.4.4 Effect of the manufacturing method on the immunogenicity of the formulation

3.4.4.1 Physicochemical characterisation of the liposomal formulations for immunisation

Given no significant differences were identified between the biodistribution of 3 microfluidics formulations, 1 microfluidics formulation proceeded into the immunisation study and was compared to the traditional LH vesicles. The selected microfluidics formulation was formulated at FRR 5:1 since CAF01 FRR 3:1 was slightly larger than produced by the LH method. Although the previous chapter showed potential better physicochemical characteristics for CAF01 FRR 3:1, it is necessary to take into account that the amount of antigen loaded onto the liposomal surface was lower than the concentration used for the *in vivo* study. Therefore, CAF01 FRR 5:1 became the selected vaccine for the immunisation study. Figure 3.15 summarises the physicochemical characteristics in terms of particle size, PDI and zeta potential of the vaccine adjuvants studied. In total 2 groups of 5 mice were immunised with the formulations CAF01 LH (control group, traditional method) and CAF01 MF (microfluidics) three times with a 2 week interval between immunisations. Formulations were freshly prepared within the 24 hours before injection due to unknown stability of the liposomes. Mice were weighed weekly to detect any significant change related to toxicity. The average weight of each group is also shown in Figure 3.15D. All mice had a healthy weight, characteristic of the strain and age, with no significant differences between groups.

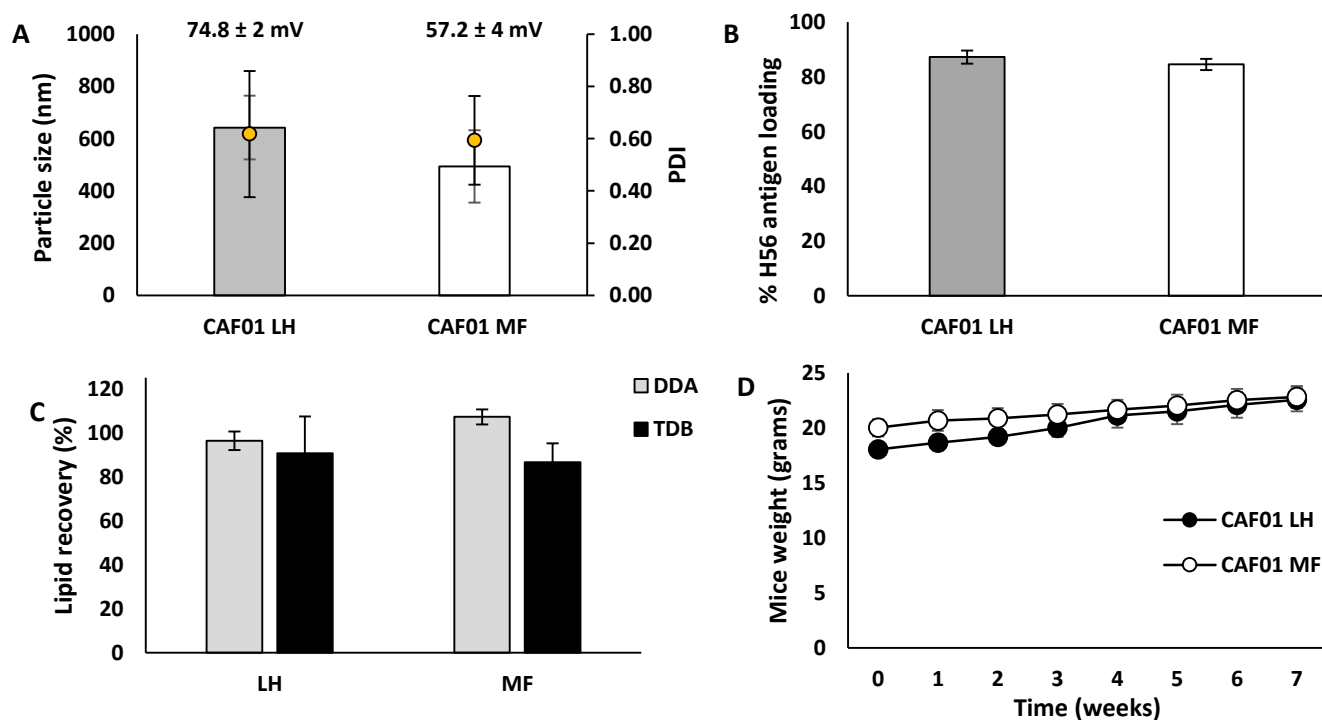


Figure 3.15 Physicochemical characteristics of the liposomal adjuvant formulations used for the immunisation study in mice (A) Particle size (bars), PDI (dots) and ZP (values), (B) antigen loading and (C) lipid recovery. (D) Average mice weight. Results represent the mean value of at least 3 independent experiments ± SD.

3.4.4.2 Antigen specific antibody secretion detected in serum

The amount of H56-specific IgG1 and IgG2c secretion was determined by ELISA in the serum collected from blood samples one week after the first and second immunisation (day 7 and 21) and three weeks after the last immunisation (day 49). Results were plotted as the log₁₀ of the end point titre showing an OD value ≥ 0.1 . Figure 3.16A shows the results from each group at the analysed time points for the IgG1. A week after priming, low production of H56 specific IgG1 subclass was detected with no significant differences between the 2 groups. After the second immunisation, IgG1 responses were higher for all the groups and again no significant differences could be seen. The analysis of the antibody response after the third immunisation also showed no significant difference in responses between the groups. A similar profile was seen with IgG2c responses with both formulations performing well, with no significant differences detected (Figure 3.16B). In general, these results correlate with published literature data using CAF01 produced by LH, where the CAF01 formulation have been shown to have a strong Th1 immunological profile [157, 190, 196]. However, these results also show that the new rapid scale-independent liposomes produces vesicles as effective as the standard small scale lipid hydration method.

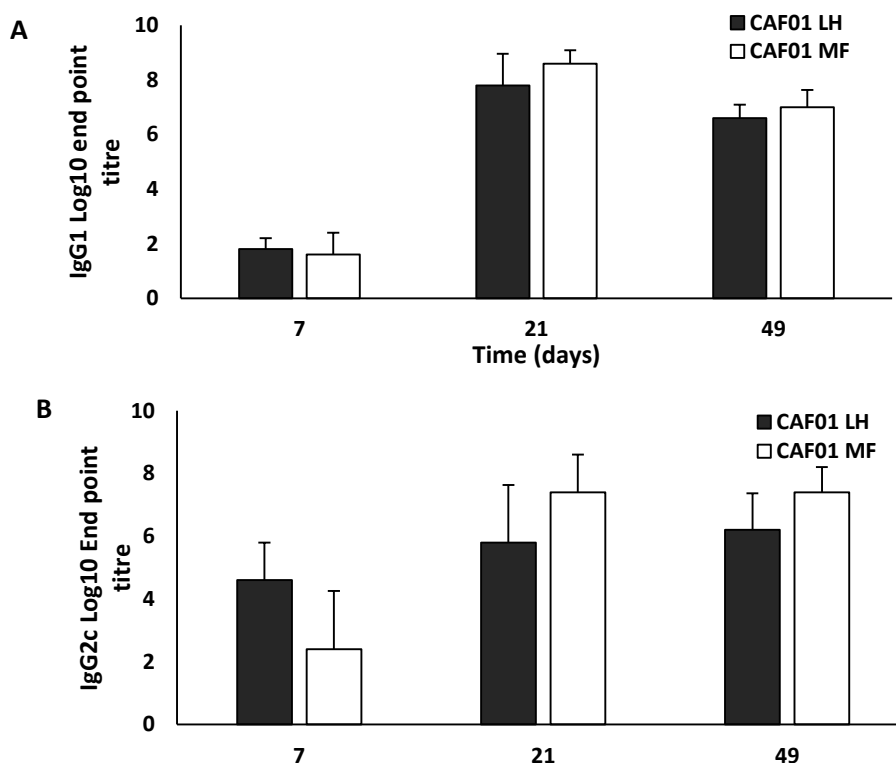


Figure 3.16 Antigen-specific (A) IgG1 and (B) IgG2c responses. C57BL/6 mice were intramuscularly immunised with H56 combined with different adjuvants and humoral response was analysed in blood. H56-specific IgG1 serum response detected by ELISA on sera collected (A) 7, (B) 21 and (C) 49 days after i.m. immunization. Antibody titres were expressed as the reciprocal of the highest dilution with an OD value ≥ 0.1 after background subtraction.

3.4.4.3 Cytokine secretion analysis from restimulated splenocytes and lymphocytes

Antigen specific T-cell responses producing IL-5, IL-17 and IFN- γ were analysed on the supernatant of restimulated splenocytes from immunised mice using ELISA assay. IFN- γ and IL-17 cytokines are frequently used as markers for the determination of the vaccine efficacy against TB [210, 211]. Furthermore, these three cytokines are characteristics of the immunological CAF01 profile. CAF01 immunological finger print is distinguished by the production of high levels of IFN- γ and IL-17 (Th1/Th17 stimulation) and low levels of IL-5 cytokine, which correlates with the results shown here (Figure 3.17). These results confirm that the liposomes produced by microfluidics were as effective adjuvants as those produced by microfluidics again confirming this method can be used for the rapid manufacture of these adjuvants.

Analysis of the cytokine secretion in the popliteal lymph nodes was also performed by ELISA. Interestingly, the CAF01 formulation manufactured using microfluidics showed larger levels of IFN- γ and IL-17 cytokines compared to the control CAF01 formulation prepared by LH. These differences correlate with published studies where CAF01 formulations of medium particle size (~500 nm), were more immunogenic in terms of Th1 cytokine responses compared to smaller (~200 nm) and larger (1.5 μ m) particle sizes [157]. It is hypothesised that CAF01 liposomes of medium size possess the adequate particle size to better interact with APCs and stimulate the production of cytokines in the draining lymph node. APCs are recruited to the site of injection where they engulf the liposomal-antigen system. Subsequently, these immune cells become activated and move to the draining lymph nodes where they present the antigen to T cells, activating them [91]. Thus, loading of the antigen onto the surface of the CAF01 adjuvant formulation produced by microfluidics, showed better presentation of the antigen to the APCs and therefore better stimulation of the Th1 cells.

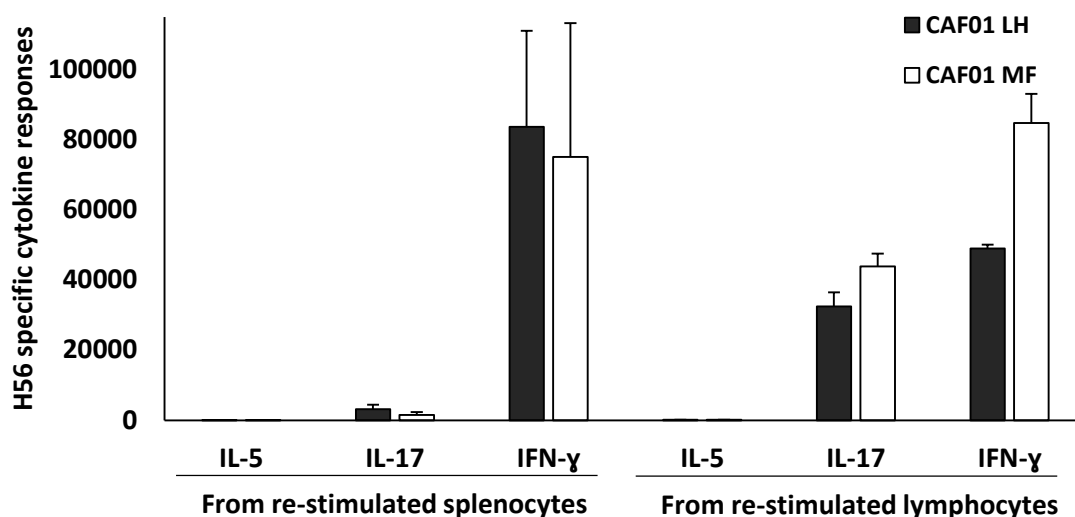


Figure 3.17 Cytokine production in splenocyte and lymph node (POP) culture supernatants (A) IL-5 (B) IL-17 and (C) IFN- γ . C57BL/6 mice were intramuscularly immunized with H56 combined with different and spleens were collected 3 weeks after the last immunization. Values, expressed as picograms per milliliter, are reported as the mean value \pm SD of H56-stimulated of five animals per group.

3.4.4.4 Cytokine detection at the injection site

The same cytokines analysed in the splenocytes and lymph nodes from immunised mice, were also analysed at the site of injection. Supernatant from the SOI were analysed by ELISA and results were normalised by individual mouse muscle weight. The formation of the depot at SOI has shown to be crucial for the Th1/Th17 adjuvanticity, therefore, quantification of IFN- γ , IL-17 and IL-5 cytokines at the SOI was performed as production these cytokines has shown to be essential for the protection against TB. No significant differences were detected for the secretion IL-17 and IL-5 cytokines. In general low levels of IL-5 and high production of IL-17 was observed in both adjuvant formulations tested (Figure 5.27). As mentioned, these high immune responses at the SOI are a result of the high retention of the vaccine components (liposomes and antigen) at the injection site due to the cationic nature of the formulations. These results correlate with the pontamine blue results, showing macrophage and monocyte infiltration at the SOI after intramuscular administration of the vaccine. These results again demonstrate the ability to manufacture a highly effective liposomal adjuvant formulation using a scale-independent production method.

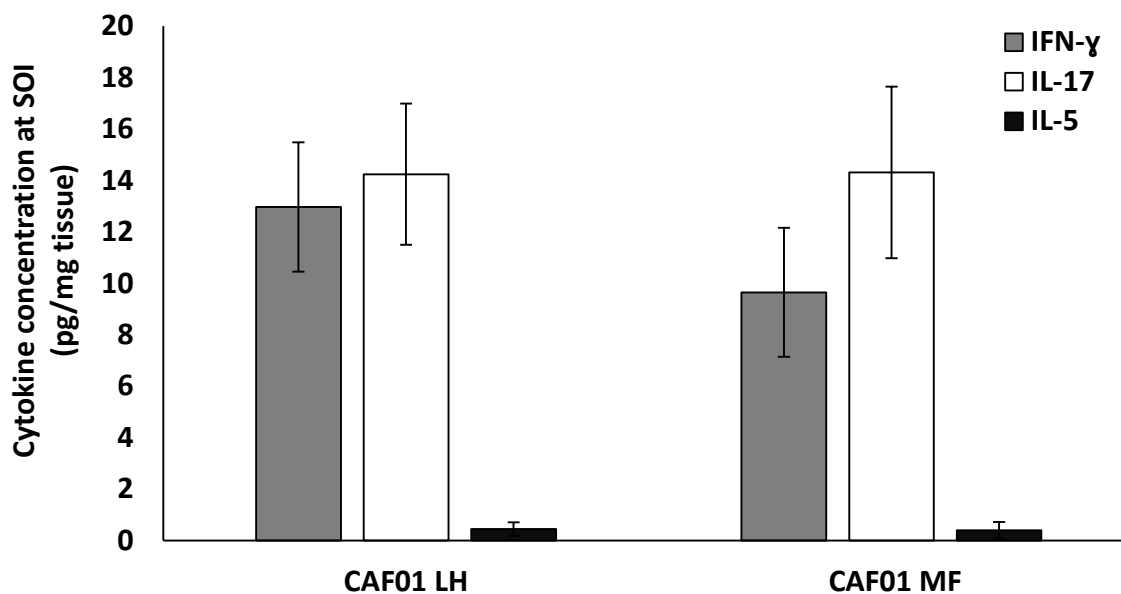


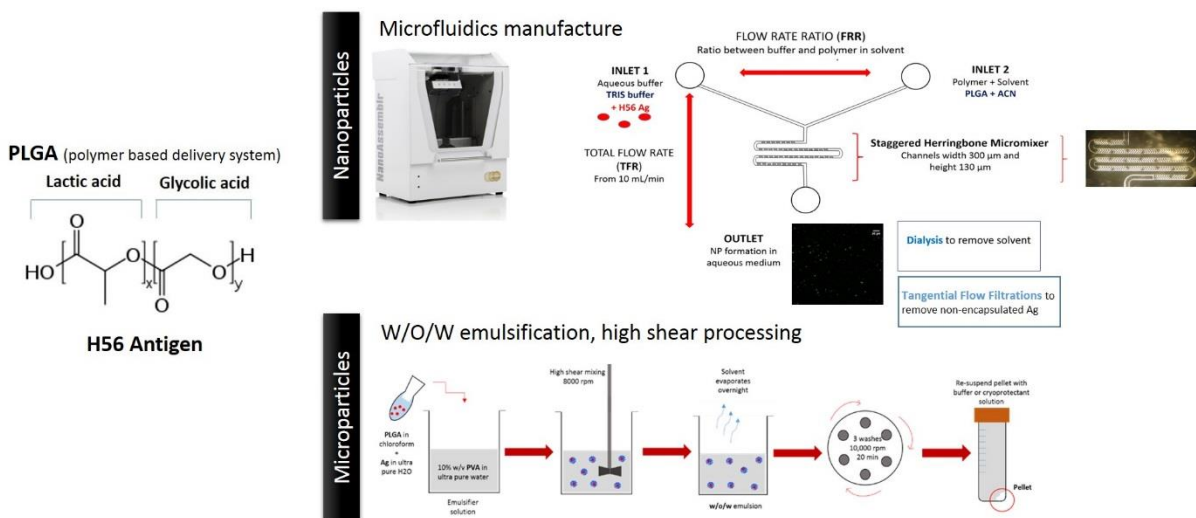
Figure 3.18 Cytokine production at the injection site (A) IFN- γ (B) IL-5 and (C) IL-17. C57BL/6 mice were intramuscularly immunized with H56 combined with different adjuvants and site of injections were excised 3 weeks after the last immunization. Values, expressed as picograms per milligram, are reported as the mean value \pm SD of H56-stimulated of five animals per group.

3.5 Conclusions

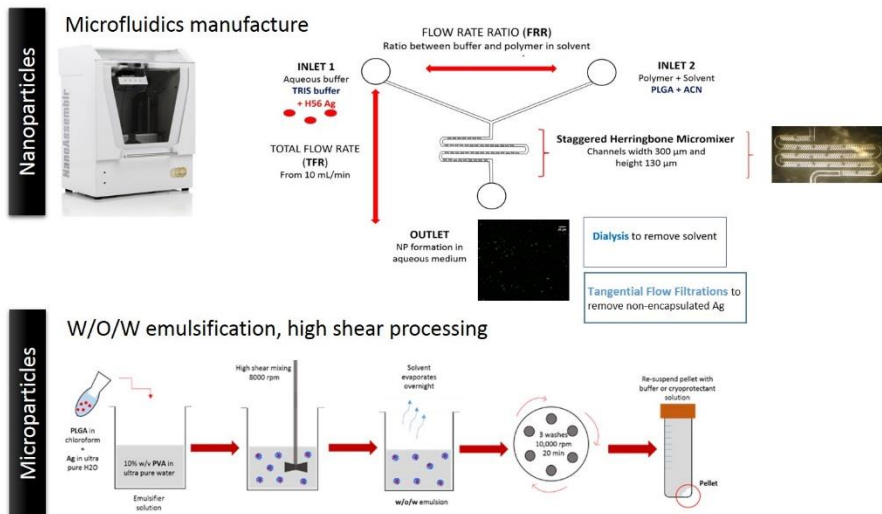
Vaccine production is a high-cost area involving large economic investments in both research and development and vaccine manufacture. In order to bring overall costs of new vaccines down, streamlining the manufacturing process is an essential task. Novel techniques such as microfluidics offer a scale-up alternative to batch production. Determining the amenability of novel techniques to produce vaccines that are similar in both physicochemical and immunological characteristics to traditional production methods is however required. The findings from this chapter indicate the pharmacokinetic and immunological profile of these formulations produced via microfluidics remained intact when compared with the common method used for the preparation of this adjuvant formulation. Both production methods showed high liposome and antigen concentrations at the site of injection - due to the highly cationic nature of these liposomes. This data demonstrated the applicability of this manufacturing method as part of the prime-pull strategy aimed for the development of a TB vaccine against pulmonary TB.

Chapter 4

Manufacture of poly(lactic-co-glycolic acid) (PLGA) particulate antigen delivery systems



H56 Antigen



Papers related to this chapter:

C. B. Roces and Y. Perrie (2018) Fabrication of poly(lactic-co-glycolic acid) (PLGA) particulate delivery systems (in preparation).

4.1 Introduction

As discussed in previous chapters, the inclusion of adjuvants in the subunit vaccine formulation is a prerequisite in order to induce the appropriate immune response since antigens are poorly immunogenic by themselves. Tuberculosis remains one of the major global health problems and the development of a vaccine effective against this infectious disease is yet to be elucidated. It is essential to study the physicochemical characteristics of the adjuvants and adjuvant-antigen systems to understand their mechanism of interaction within the body. Characteristics such as size, polydispersity, surface charge and shape are of utmost importance since these can determine the fate of the vaccines once administered in the body. During the past decades, polymeric particles such as poly(lactic-co-glycolic acid) (PLGA), polylactic acid (PLA) and polyglycolide (PGA) have attracted the interest of many researchers as delivery systems for drugs and peptides/proteins due to their high safety profile, biodegradable and biocompatible properties and their approval by the FDA for human use [102]. These particulate delivery systems can be manufactured through a wide range of methods and therefore their physicochemical properties (size, morphology, surface charge) can be easily manipulated in order to achieve the adequate characteristics for the right interaction with biological cells [101-103]. Commonly PLGA nanoparticles (NPs) and microparticles (MPs) are manufactured by using methods such as double emulsion, coacervation, nanoprecipitation, extrusion or solvent evaporation [104-111]. Antigens can be encapsulated within these PLGA NPs which provide antigen protection and controlled release profiles [102, 212]. All these methods, with the exception of nanoprecipitation, can be applied for the preparation of both NPs and MPs by adjusting the process parameters. However, these methods are time consuming, difficult to scale up, and use large amounts of solvents. In contrast, controllable technologies such as microfluidics has several advantages over traditional methods due to scalability, reproducibility, easy process control and reduced manufacturing time.

4.2 Aim and objectives

The aim of the work outlined within this chapter was to produce PLGA particulate systems as carriers for antigen delivery in the deep lungs (alveoli). In order to provide a wide range of particle sizes, PLGA particles were manufactured by using two different methods: the double emulsion method and microfluidics. Therefore, the main objectives for this study were:

1. To evaluate the ability of the microfluidics system (Nanoassemblr™ Benchtop) to produce poly(lactic-co-glycolic acid) (PLGA) nanoparticles.

2. To analyse the influence of the microfluidic process parameters during the production of nanoparticles as well as the PLGA intrinsic factors such as copolymer ratio in the physicochemical characteristics of the particles.
3. To study the physico-chemical attributes (including morphology, size, pdi, antigen loading and release) of the formulated PLGA nano- and microparticles.
4. To investigate the purification of nanoparticles using dialysis and tangential flow filtration (TFF).

4.3 Materials and methods

4.3.1 Materials

For the preparation of delivery systems, poly(lactic-co-glycolic acid) 85:15 (Mw: 50,000-75,000), 75:25 (Mw: 66,000-107,000), 50:50 (Mw: 30,000-60,000) from Sigma-Aldrich were used. Two model antigens (OVA and BSA), sodium hydroxide (NaOH), and the stabiliser polyvinyl alcohol (PVA Mw: 31,000) were purchased from Sigma-Aldrich Company Ltd., Poole, UK. The tuberculosis vaccine candidate H56 was donated by Statens Serum Institut (SSI), Copenhagen, Denmark. 2-amino-2-(hydroxymethyl)-1,3-propanediol (Tris) was obtained from ICN Biomedicals Inc. (Aurora, OH, US) and prepared at a 10 mM concentration and pH 7.4 unless otherwise stated. Acetonitrile (ACN), trifluoroacetic acid (TFA) and all other reagents were of analytical grade and purchased from commercial suppliers.

4.3.2 Methods for the manufacture of poly(lactic-co-glycolic acid) particles for antigen delivery:

PLGA particles were prepared in the nanometre and micrometre range by using two different manufacturing techniques: microfluidics and double emulsion method.

4.3.2.1 Manufacturing of poly(lactic-co-glycolic acid) nanoparticles by using microfluidics (Nanoassemblr™)

PLGA nanoparticles were manufactured by the microfluidics method using the Nanoassemblr™ Benchtop (Precision Nanosystems Inc., Vancouver, Canada). Briefly, polymer (either PLGA 85:15, 75:25 or 50:50) was dissolved in acetonitrile at a concentration of 10 mg/mL (1% w/v). For the production of empty nanoparticles, Tris buffer was used as aqueous phase whereas for antigen loaded

nanoparticles, antigen (OVA, BSA or H56) was loaded in the aqueous phase at the desired concentration (0.2, 0.5 or 1 mg/mL). In order to evaluate the impact of the different microfluidics parameters, different TFRs (5, 10 and 15 mL/min) and FRRs (1:1, 3:1 and 5:1) were selected and a fixed waste volume was discarded during the production in order to get the core sample (initial and final waste volume of 0.25 and 0.05 mL, respectively). Polymer in solvent and buffer phase were injected into the systems at the selected parameters and the produced PLGA nanoparticles were collected in the outlet (Figure 4.1).

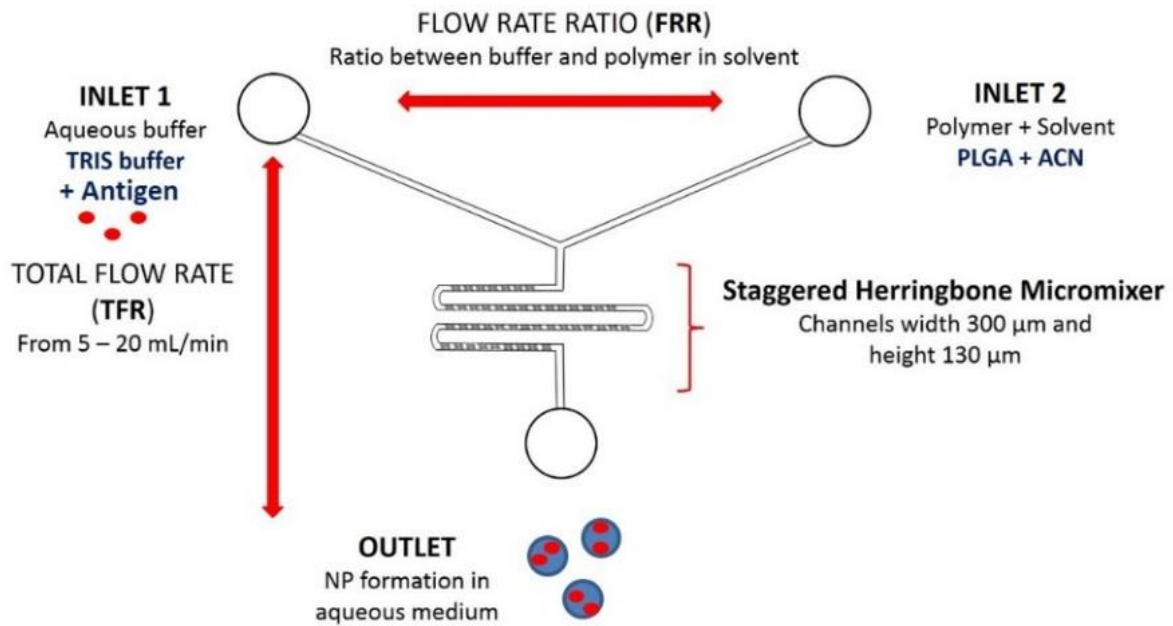


Figure 4.1 Schematic representation of microfluidics cartridge from Precision Nanosystems. There are two inlets where the aqueous (inlet 1) and organic phase (inlet 2) are injected in. Both fluids are mixed at the selected ratio (FRR) and speed (TFR) and by chaotic lamellar flow nanoparticles are formed and collected in the outlet.

4.3.2.2 Manufacturing of poly(lactic-co-glycolic acid) microparticles using the double emulsion (w/o/w) solvent evaporation method

The most common method for microparticle preparation is the double emulsion process ($w_1/o/w_2$), whereby an initial primary water in oil (w_1/o) emulsion is formed by dispersion of an aqueous solution with or without antigen (w_1) into an organic polymer solution. This primary emulsion is then mixed by high-speed homogenisation into a secondary water phase (w_2), often containing an emulsion stabiliser or surfactant such as PVA, in order to form a secondary $w_1/o/w_2$ emulsion. The organic solvent is then allowed to evaporate to facilitate the formation and hardening of the MPs. PVA is removed from the vaccine formulation by centrifugation [213]. Briefly, 20 μL of buffer or OVA (10 mg/mL stock) were mixed with 417 μL of 3% PLGA in chloroform and vortexed for 1.5 min in order to

form the initial primary emulsion. This primary emulsion was then mixed with 10 mL of PVA (10% w/v in dH₂O) using high speed homogenization (Homogenizer Ultraturrax T25, IKA laboratories) at 8000 rpm during 3 min. Samples were left stirring overnight to remove chloroform. The next day, samples were centrifuged (Hermle Z323K, Labnet International Inc., US.) and washed three times with 10 mL of dH₂O for 20 min at 5500 xg. After the final washing step, the MPs were reconstituted with 2 mL of Tris buffer (Figure 4.2)

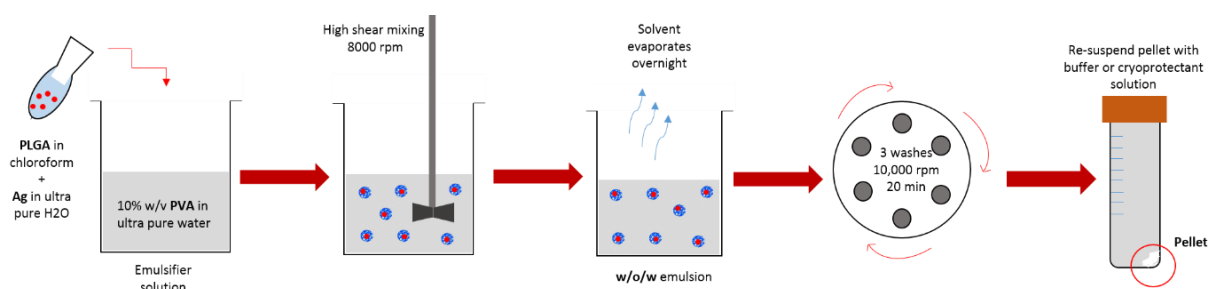


Figure 4.2 Schematic representation of double emulsion ($w_1/o/w_2$) solvent evaporation method. Initial primary water in oil (w_1/o) emulsion is formed by dispersion of an aqueous solution with or without antigen (w_1) into an organic polymer solution. This primary emulsion is then added into a secondary water phase solution containing 10% PVA and homogenised at high speed for 3 min. Solvent is evaporated overnight. Next day, samples are centrifuged and washed with ultrapure water 3 times to remove any non-incorporated trace of PVA. In the final centrifugation step, the pellet is reconstituted with the desired volume of buffer.

4.3.3 Characterisation of the PLGA particles by dynamic light scattering (DLS)

4.3.3.1 Malvern nano ZS

The particle size of the polymer nanoparticles was determined by dynamic light scattering (DLS) using a Malvern nano ZS (Malvern Instruments, Worcestershire, UK). Three measurements at 25°C were conducted on the samples, which were previously diluted in filtered Tris buffer (10 mM, pH 7.4) to achieve the optimal particle concentration (0.25 mg/mL) with the optimum attenuator number (att. 6 - 9). Therefore nanoparticles produced at FRR 1:1, 3:1 and 5:1 were 20-fold, 10-fold and 5-fold diluted. Square single-use plastic cuvettes were filled in with 1 mL of sample and were placed into the instrument which uses a 4-mW He-Ne 633 nm laser to analyse the samples [170]. For zeta potential, samples were diluted in the same fashion as for the size and a cell capillary electrophoresis cuvette was used. For collection and data analysis Malvern Dispersion Technology Software (DTS) v.7.12 (Malvern Instruments, Worcestershire, UK) was used (Table 4.1).

Table 4.1 DLS Instrument parameters for particle size measurements using dynamic light scattering (DLS).

Material	Parameters
Refractive Index	1.45
Absorption	0.00
Dispersant	Water
Temperature	25 °C
Viscosity	0.8872 cP
Refractive Index	1.330
General options	
Equilibrium time	120 s
Cell type	ZEN0040
Measurement	
Angle	173° Backscatter
Number of runs	Automatic
Number of measurements	3
Delay between measurements	10 s
Data Processing	General Purpose (Normal resolution)

4.3.3.2 Mastersizer 2000

The size of the MPs was determined by laser diffraction analysis using a Mastersizer 2000 (Malvern Instruments). Samples were dispersed into the sample dispersion cell unit until the right obscuration was obtained (above 10%) while stirring at 2000 rpm. Water was used as dispersant agent and PLGA refractive index was set at 1.43. Three measurements of each sample were recorded every 12 seconds. For zeta potential, Zetasizer nano ZS was used. Samples were diluted in Tris buffer in the same fashion as the nanoparticles (20-fold dilution).

4.3.3.3 Malvern AT-line

To prove the applicability of the microfluidics method for continuous manufacturing, an AT-line Malvern sizer was used to measure the PLGA nanoparticles. Thus, 5 mL of nanoparticles were prepared using microfluidics and run through the Malvern AT right after microfluidics (without solvent removal). Specific parameters were set on the system in order to compare the size measurements obtained with Malvern nano ZS. Therefore, the parameters set in this system were the following: 0.5 mL/min sample flow rate, 10 mL/min diluent flow rate and 90 s delay time between measurements.

4.3.4 Stability test: The effect of PVA content

Evaluation of the stability of the PLGA nanoparticles encapsulating H56 TB antigen was carried out for a period of one month. The stabiliser PVA was added at different concentrations (0, 0.5, 1 and 2% w/v) into the aqueous phase during the production of PLGA nanoparticles. Physicochemical characterisation of the loaded nanoparticles was carried out to evaluate the need of a stabiliser during the microfluidics production due to agglomeration of the particles.

4.3.5 Purification of the PLGA nanoparticles: solvent removal and non-encapsulated antigen

4.3.5.1 Dialysis for removal of organic solvent

Solvent is used for the dissolution of the polymer and preparation of nanoparticles. Therefore, in order to remove solvent, samples were dialysed against Tris buffer. Samples were loaded into a dialysis membrane (Mw= 12,000-14,000 Da, Sigma-Aldrich Company Ltd., Poole, UK) and dialysed against 250, 500 and 1000 mL Tris buffer to optimise the method for solvent removal.

4.3.5.2 Tangential Flow Filtration (TFF) for removal of non-encapsulated antigen

Tangential flow filtration (TFF), also known as crossflow filtration, is a rapid and efficient method for separation and purification of proteins. TFF can be used to concentrate and desalt sample solutions ranging in volume from 1 mL to 10 litres. The sample stream passes parallel to the membrane face as one portion passes through the membrane (permeate) while the remainder (retentate) is recirculated back to the feed reservoir [214].

PLGA nanoparticles were purified through this system (KR2i TFF System[®], SpectrumLabs, US) at 27 mL/min and were washed 12 times with buffer in order to remove unbound protein. Unfortunately, due to the incompatibility of the column with the acetonitrile used for the preparation of the nanoparticles, 1 hour dialysis was carried out prior passing the samples through the TFF for removal of the organic solvent. The membrane used had a MWCO of 12,000 to 14,000 Da, which is big enough to remove solvent but small enough to avoid protein removal. The TFF column used for this purpose was a 750 kDa modified polyethersulfone (mPES) column which is slightly negatively charged.

4.3.6 Quantification of the residual solvent by gas chromatography (GC)

Quantification of the residual acetonitrile within the PLGA formulations after purification of the samples by dialysis was performed by using GC. GC is a chromatography technique mainly used for quantitative analysis of the residual solvent within sample formulations. It can separate mixtures of volatile analytes. Standards were prepared with different volumes of the analyte of interest (acetonitrile from 0 to 0.1%) whereas the volume of internal standard remained the same (1% 1-butanol). For sample preparation, samples were diluted (1:5) in Tris buffer and the same percentage of the internal standard used for the calibration curve was included in the sample preparation. The internal standard, 1-butanol, was chosen because it is not contained in any of the samples and has a different boiling point (117°C, whereas ACN boiling point is 82°C) which allows the separation of the volatile analyte mixture in two well separated and defined peaks (there is no coelution). Calibration curves of ACN were made plotting the area ratio of the analyte/IS of triplicate results against the acetonitrile concentration.

4.3.7 High Performance Liquid Chromatography (HPLC)

4.3.7.1 HPLC-UV for antigen quantification

Quantification of the protein loading within the PLGA nanoparticles was performed by reverse phase HPLC (RP-HPLC) using a UV detector. Jupiter 5 μ C18(2) column (Phenomenex) pore size 300 Å was used as stationary phase. For the preparation of the calibration standards, proteins were dissolved in 0.1 M NaOH/Tris buffer (1:1 v/v) and heated up for approx. 1.5 - 2 hours in a waterbath at 35°C. Samples were prepared in the same fashion but in this case just adding NaOH as the samples are formulated in Tris buffer. Table 4.2 shows the HPLC method used for the protein quantification, which is a modification of a method found in literature [215, 216]. A gradient elution method was followed and both mobile phases contain the same solvents in different proportions (Mobile phase A: 90% H₂O, 10% acetonitrile and 0.1% TFA; Mobile phase B: 70% acetonitrile, 30% H₂O and 0.1% TFA) in order to favour the mixing of both phases during the run. The instrument settings were as follows: 50 μ L injection volume, flow rate 1 mL/min, UV wavelength 210 nm and column temperature either 25°C (OVA and BSA) or 60°C (H56).

Table 4.2 HPLC-UV method followed for the quantification of encapsulated antigen within the polymer nano- and micro-particles using 210 nm UV wavelength [215, 216].

Time (min)	% Eluent A (0.1% TFA, 90% dH ₂ O, 10% ACN)	% Eluent B (0.1% TFA, 30% dH ₂ O, 70% ACN)	Flow rate (mL/min)
0	75	25	1
18	0	100	1
20	75	25	1

4.3.7.2 HPLC-ELSD for quantification of polymer recovery

Quantification of the polymer recovery was performed by HPLC using an ELSD detector. Luna 5 μ C18(2) column (Phenomenex) pore size of 100Å was used. For the preparation of the standard curves, polymer was dissolved in ACN and samples containing the PLGA nanoparticles were injected without previous preparation. HPLC-ELSD settings were kept constant as follows: 30 μ L injection volume in a partial loopfill injection mode, 100 μ L loop volume and 15 μ L tubing volume. Column temperature was maintained at 35°C whereas the ELSD temperature was set at 52°C in all the runs. Analysis time, flow rate and mobile phases are outlined in Table 4.3. Nitrogen was used as a carrier gas at 3.5 bar inlet pressure. Clarity DataApex version 4.0.3.876 was used for data analysis.

Table 4.3 Gradient method used for the quantification of the polymer recovered after microfluidics using HPLC-ELSD [217].

Time (min)	% Eluent A (0.1% TFA, 95% dH ₂ O, 5% ACN)	% Eluent B (0.1% TFA, 5% dH ₂ O, 95% ACN)	Flow rate (mL/min)
0	50	50	2
3	0	100	2
7	0	100	2
7.1	100	0	2
9	100	0	2
10	50	50	2
12	50	50	2

Calculation of the recovery of the samples manufactured through microfluidics was performed according to Equation 4.1. Basically, the area of the peak given by the HPLC-ELSD was converted into concentration by using the adequate calibration curve previously carried out. This result was divided by the initial concentration in the stock solution and multiplied by the dilution factor (DF) related to the FRR used and by 100.

$$\frac{\text{concentration of the sample } \left(\frac{\text{mg}}{\text{mL}}\right)}{\text{concentration stock solution } \left(\frac{\text{mg}}{\text{mL}}\right)} \times DF \times 100 = \% \text{ recovery} \quad (\text{Equation 4.1})$$

4.3.8 Bicinchoninic acid assay (BCA) for the quantification of polymer recovered after purification of the nanoparticles using TFF

The bicinchoninic acid assay (BCA) (Pierce™ BCA Protein Assay Kit, Sigma Aldrich, Poole, UK) was used for the quantification of polymer recovery after TFF. Briefly, 25 µL of sample purified using TFF was pipetted into a 96-well plate and 200 µL of working reagent (reagent A + B at a ratio 50:1 v/v) was added on top. The plate was incubated for 30 mins at 37°C and the absorbance was read at 562 nm. A standard curve for the calculation of the concentration found was performed in triplicate. PLGA nanoparticles after solvent removal by dialysis were used for the preparation of the standard curves.

4.3.9 Release studies at different temperatures

Purified PLGA nanoparticles encapsulating OVA (1 mL) were transferred to a dialysis bag (300 kDa) and introduced to a beaker containing 40 mL of release media (PBS pH 7.4, 10 mM). This beaker was incubated at 37°C in a shaking bath under mild agitation (60 rpm) or at 4°C. Antigen release was measured by quantification of the remained antigen concentration inside the nanoparticles at 1, 4 and 6 hours. For the quantification of the antigen remaining inside the nanoparticles after each time point, PLGA was degraded by adding 0.1 M NaOH (final concentration) to the samples and incubation at 35°C during approximately 2 hours to accelerate the hydrolysis process. The amount of antigen released was calculated as percentage of the total antigen loaded into the NPs, which was considered as 100%.

4.3.10 Morphological characterisation of the nanoparticles

4.3.10.1 Scanning electron microscopy (SEM)

The principle behind this technique is based on a beam of electrons which scan around the particles without penetrate them. As a result, secondary electrons are emitted from the sample and detected

by a detector which gives a 3D image of the surface of the particles [218]. Polymer nano- and microparticles (sample) were fixed and air dried onto a metal stub and then coated with gold and observed under the microscope. This procedure was carried out by David McCarthy from DMmicroscopy.

4.3.10.2 Cryogenic transmission electron microscopy (CryoTEM)

CryoTEM is a type of transmission electron microscopy technique which operates under cryogenic conditions, showing the samples in their native environment and obtaining detailed 2D structures of the molecules. It is a valuable tool to obtain structural information of amphiphilic molecules in solutions within the nanometre size range [219, 220]. It gives information about the morphology of the vesicles, bilayer thickness and their size distribution. CryoTEM also allows visualizing the coexistence of different populations of nanostructures [220].

400 mesh holey Carbon grids (Lacey Formvar/Carbon) neutrally charged were used for this procedure. First grids were glow discharged to remove any residual hydrocarbon and make them hydrophilic. Subsequently, 8 μ l of sample were deposited onto the grid and the excess of sample was blotted off the grid and the sample was plunged into the liquid nitrogen. The liquid nitrogen was cooled down with a mixture of 30% propane/ethane to approximately -172°C . After vitrification, the grid was immediately transferred to Cryo-transport system and mounted in the Gatan Cryo-holder (Gatan, Pleasanton, CA, USA). Subsequently, the sample on the grid was inserted in the Jeol 2010F TEM with the Cryo-holder. Observations were made at an acceleration voltage of 200 kV and images were obtained with GATAN camera and different magnifications.

4.3.11 Statistical analysis

One-way ANOVA and two-way ANOVA followed by Tukey's multiple comparison test were used for the data analysis. All the experiments were carried out at least in triplicate unless otherwise stated. Results are the mean of at least 3 measurements \pm standard deviation (SD) which is plotted as error bars.

4.4 Results and discussion

The particle size, surface charge and morphology of the adjuvants, among other characteristics, are important in order to obtain a good immunoresponse as these characteristics will influence the interaction with the biological cells [103, 221]. There are several studies based on the importance of the adjuvant size [221]. The size distribution or uniformity of the particles, i.e. polydispersity index (PDI), is also an essential characteristic of the delivery systems. Low PDIs are difficult to obtain in some formulations depending on the nature of the compounds used and the manufacturing techniques applied. However, it is necessary to have a narrow range of particle sizes within the samples since a broad range of sizes may have different adjuvant activities [221]. Another useful factor of the adjuvant systems is the electrical charge on the surface of the particles which can be indirectly measured by measuring the zeta potential. Neutral or slightly negative/positive ZP values may lead to aggregation or instability whereas highly anionic/positive ZP values can improve stability due to the repulsion between charged particles [222].

4.4.1 Microfluidics manufacturing of PLGA nanoparticles: the effect of process parameters

PLGA is a synthetic copolymer of lactic and glycolic acid which can be produced at different monomer ratios which are available in the market. For example, PLGA 75:25 means that the composition of the copolymer is based on 75% of lactic acid and 25% of glycolic acid. Therefore, PLGA polymers with ratios 50:50, 75:25 and 85:15 were selected for the nanoparticle formulation using microfluidics in order to study the effect of the copolymer composition in the produced particles.

To get an overview of the influence that different microfluidics parameters have on the mean particle size, PDI and zeta potential of the PLGA nanoparticles, the TFR and the FRR were altered during preparation. TFR was set at 3 different speeds: 5, 10 and 15 mL/min and for each speed, three aqueous:organic phase ratios (FRR) were used: 1:1, 3:1 and 5:1. Regarding solvent choice, PLGA polymers can be dissolved in a wide range of solvents such as chlorinated solvents. Yet, these solvents are not compatible with the microfluidics cartridge, which is made of thermoplastics Cyclic Olefin Polymer (COP) and Cyclic Olefin Copolymer (COC). Therefore, due to compatibility issues, acetonitrile was chosen as organic phase for the dissolution of PLGA. The initial PLGA concentration in ACN was 10 mg/mL (1% w/v) for all the formulations prepared. Higher (12.5 mg/mL) and lower (7.5 mg/mL) concentrations were also tested (data not shown) but the results did not differ significantly from each other, and thus, the concentration was fixed at 10 mg/mL for all the experiments carried out.

Particle size and size distribution of the polymer NPs in suspension was determined by DLS. Figure 4.3 depicts the physicochemical characteristics of the purified PLGA nanoparticles (after 4 h dialysis against 200 mL of Tris buffer). PLGA NPs produced using the copolymer 50:50 showed the smallest particle sizes among the three PLGA copolymers studied, ranging from 94 to 150 nm (Figure 4.3). With increasing production speed (from 5 to 15 mL/min (total flow rate)) there was no notable change in particle size for copolymers 75:25 and 85:15. In contrast, PLGA 50:50 nanoparticles decreased in size when increasing the flow rate (Figure 4.3A, B and C). However, varying the flow rate ratio was shown to have a significant impact on vesicle size with particles significantly ($p < 0.05$) decreased in size for all three copolymers. For example, with PLGA 50:50, NP particle size decreased from 150 to 120 nm for FRR 1:1; from 145 to 94 nm for FRR 3:1 and from 136 to 94 nm for FRR 5:1 (Figure 4.3). This trend was seen with all three polymer ratios tested and became more notable with increasing polymer ratio (Figure 4.3). In general, across the formulations the polydispersity values were ≤ 0.2 , and no obvious relationship between the microfluidic parameters and sample homogeneity was observed. These PDI values are representative of a homogeneous particle size distribution within the samples.

Regarding surface charge, all three copolymers produced highly anionic (Figure 4.3D). No significant differences were observed between the different microfluidics parameters applied. In general, PLGA 50:50 produced particles with ~ -40 mV at all FRRs and TFRs tested. Particles prepared using PLGA 85:15 produced particles with ~ -50 mV and PLGA 75:25 produced the more anionic particles, with a ZP of approximately ~ -60 mV.

Based on these studies, it can be seen that the size of PLGA NPs prepared using microfluidics can be controlled by the FRR selected whereas the TFR had little impact (the exception being PLGA 50:50). This is in line with previous studies based on microfluidics [167, 181]. It has been proposed that FRR impact on the NP formation is due to the increase in the polarity within the microfluidics cartridge and therefore the different solvent phase concentration. Chiesa et al. showed the same trend regarding FRR on PLGA NPs produced using the micromixer system [223]. On the other hand, TFR has shown to moderately influence the characteristics of the particles produced since the physicochemical properties of the PLGA NPs produced were not highly influenced by this parameter. This represents an advantage for the manufacturing process as it allows the system to work at high volumetric flows and thus, high production outputs [167].

The intrinsic factors of the PLGA copolymer dictate the physicochemical characteristics of the resulting nanoparticles. PLGA NPs with 85:15 ratio of lactide and glycolide monomers have shown the largest sizes, followed by PLGA 75:25 and PLGA 50:50. This can be explained by their monomer ratio composition. PLA has a methyl side group whereas PGA lacks one. Therefore, the methyl group is the

reason for the increased size of this polymeric NPs. PLGA 85:15 has 85% of PLA and 15% of PGA which correlates with the abovementioned explanation of the different sizes. PLGA 75:25 consist of 75% PLA and 25% of PGA, therefore, second largest sizes are obtained with this polymer. The smallest sizes were obtained with PLGA 50:50 since the amount of PLA is decreased. The highly negative zeta potential denotes a negative surface charge of the nanoparticles. The presence of carboxyl groups on the surface of the nanoparticles might be attributed to their anionic nature [224].

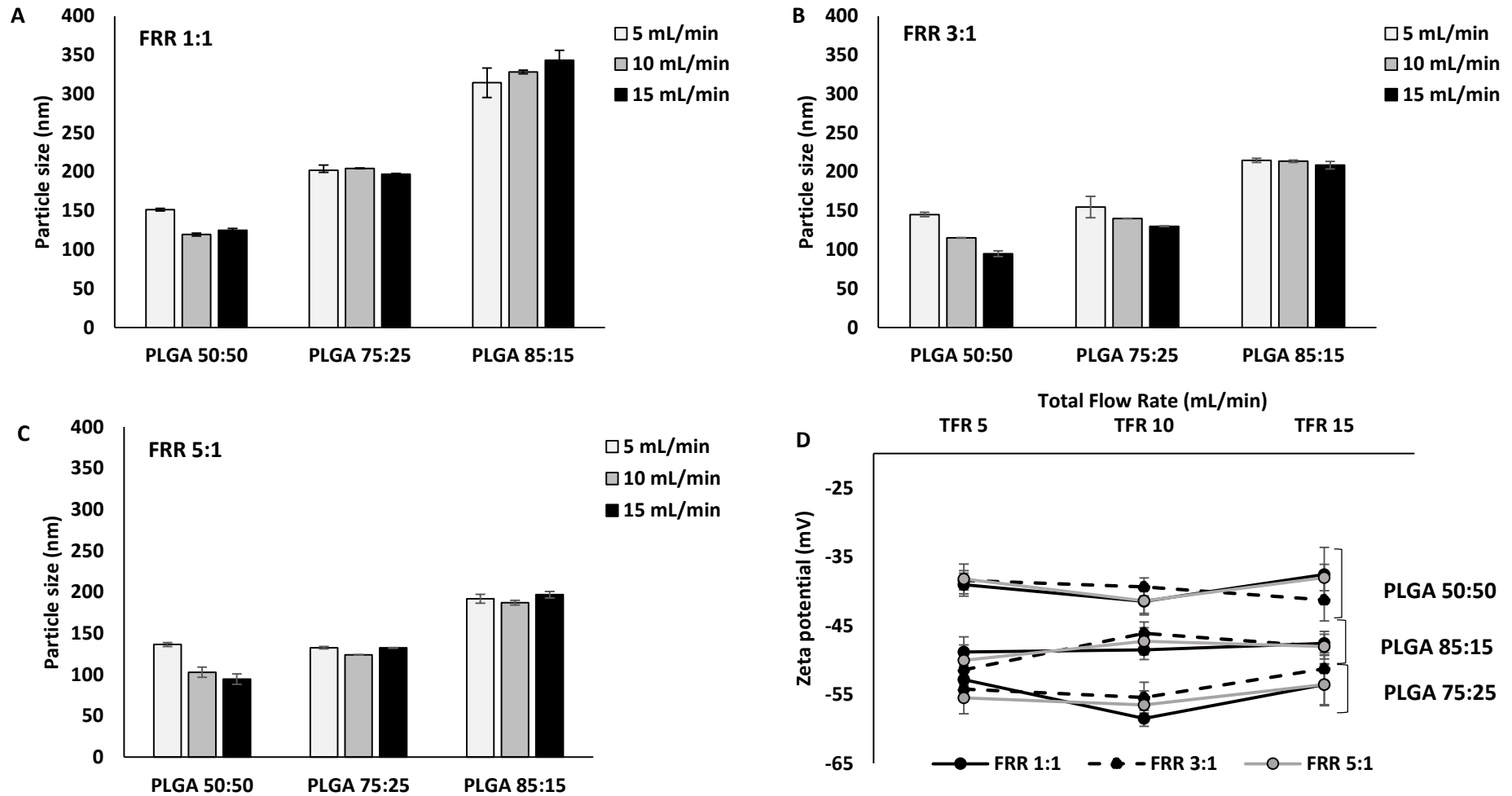


Figure 4.3 Effect of the process parameters from the microfluidics system in the physicochemical characteristics of the PLGA nanoparticles (A) FRR 1:1, (B) FRR 3:1 and (C) FRR 5:1 and (D) zeta potential. Results represent the mean \pm SD of at least three independent batches.

4.4.2 Continuous processing of nanoparticles: AT-line particle size analysis

Formulation of delivery systems should be scalable in order to succeed as a product for commercial use. Continuous processing offers several advantages over batch processing. For example, microfluidics, which is considered as a continuous method for processing of nanoparticles, can produce scalable volumes as determined by the run time. In contrast, batch processing is restricted by the size of the instrument used for the manufacture. The main disadvantage of the microfluidics system is the removal of the solvent from the formulation but this can be overcome with the addition of a tangential flow filtration system. The development of analytical methods which provide better information and control of the manufacturing process are required for the production of monodisperse and size controlled delivery systems. The size of the particulate delivery systems can be measured by a wide range of techniques such as dynamic light scattering, microscopy and particle tracking. Many of these techniques are only available for off-line measurements and cannot be applied for continuous processing. Real time particle size analysis can be performed during continuous processing thus any problem arising during production can be detected and corrected. Moreover, if the nanoparticle size measurement obtained is out of specification, particles can be discarded without endangering the whole batch. In contrast, batch measurements can only take place once the nanoparticles are produced and therefore, if the particle size measurements obtained do not fall within the product key specifications this would lead to disposal of the entire batch.

The results in Figure 4.4 demonstrate PLGA nanoparticles with 85:15, 75:25 and 50:50 copolymer composition formulated using microfluidics at a selected TFR 10 mL/min and FRR 1:1. Particle size measurements were performed with an off-line system and with an at-line system (real time measurement), both from Malvern Zetasizer. Figure 4.4 shows the mean particle size values obtained from both particle sizer systems. Particle size measurements obtained from the off-line and AT-line systems were compared. Size results were similar for both measurements whereas PDIs resulted larger in the AT-line system.

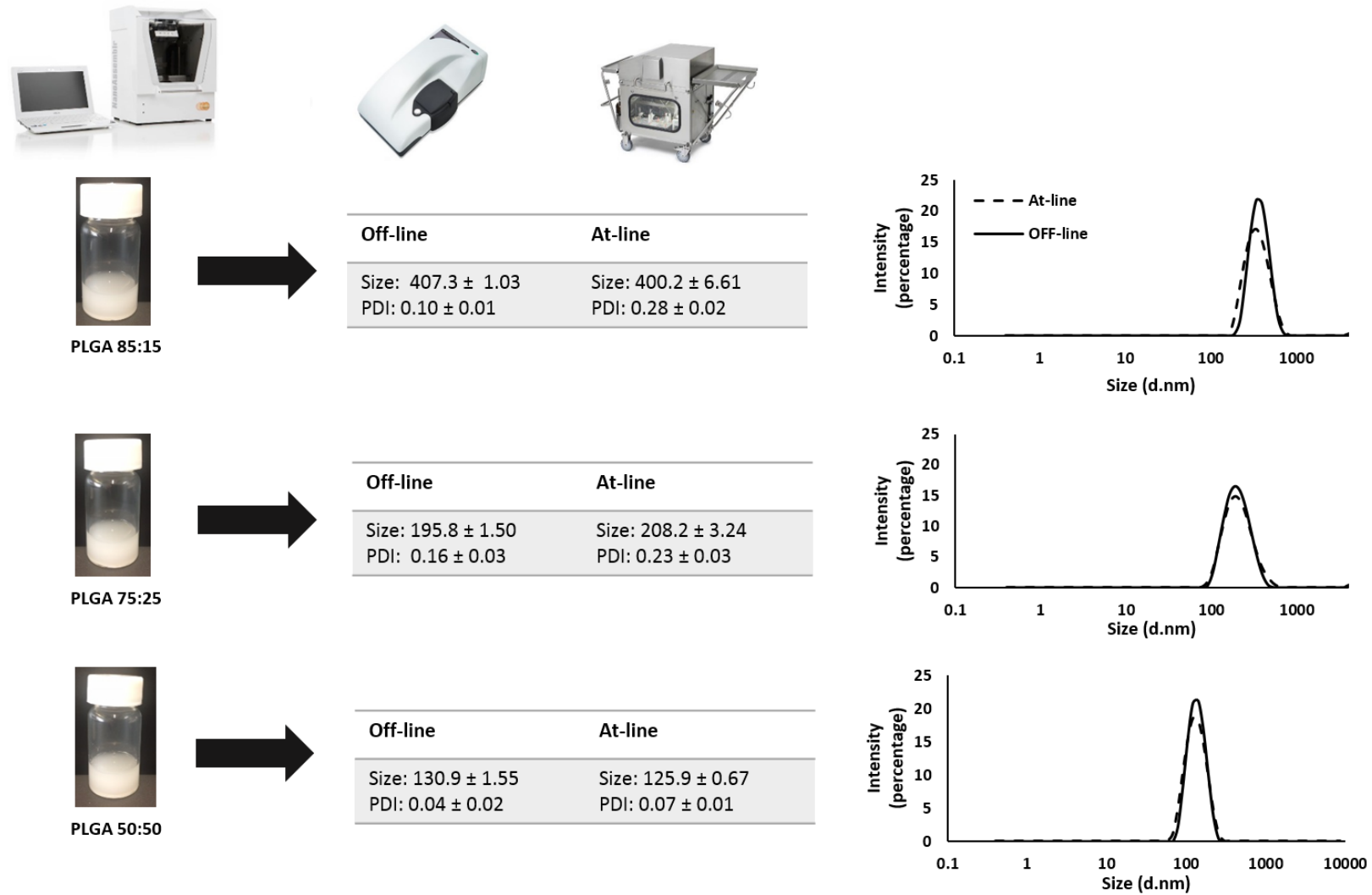


Figure 4.4 Comparative study of the size measurements obtained with Malvern OFF-line and AT-line in order to demonstrate the capability of the microfluidics method for continuous manufacturing of PLGA nanoparticles. Particle sizes and intensity graphs of the PLGA 85:15, 75:25 and 50:50 nanoparticles manufactured by using microfluidics at TFR 10 mL/min and FRR 1:1.

4.4.3 Quantification of the residual solvent within the formulation after purification of the nanoparticles by dialysis and effect of the purification method on the physicochemical characteristics of the PLGA-NPs.

Depending on the method applied, impurities such as organic solvents might be present in the final product. The presence of residual solvent might not only cause toxicity issues, it might also modify the physicochemical characteristics of the nanoparticle formulations. Thus, selection of the adequate manufacturing and purification method for the preparation of nanoparticles is of extreme importance to assure the quality and control of the product [225]. With the current microfluidics process developed, the formulations prepared by microfluidics contain a specific amount of solvent depending on the FRR applied; for example, a formulation prepared at FRR 1:1 contains 50% of solvent, at FRR 3:1 contains 25% whereas at FRR 5:1 contains 16.67%. The International Conference on Harmonization (ICH) of Technical Requirements for Registration of Pharmaceuticals for Human Use, classifies acetonitrile as a class II solvent due to its toxicity and establishes that the limit of residual acetonitrile should be no more than 400 ppm (0.04%) [169]. Consequently, quantification of the residual acetonitrile in the formulations manufactured by microfluidics was carried out by gas chromatography (GC).

Several methods can be used for the purification nanoparticles. Ultracentrifugation, gel filtration and dialysis are the conventional methods for removal of solvent [226-228]. Gel filtration and ultracentrifugation techniques were performed but resulted in low polymer recovery yield (results not shown). Dialysis was therefore the selected method for purification of PLGA nanoparticles. To calculate the dialysis volume and dialysis time needed for removal of the solvent below the levels stated by the ICH guideline Q3C, formulations containing the highest solvent concentration were used (FRR 1:1). Figure 4.5A shows the calibration curve made with different concentrations of acetonitrile and fixed volume of butanol (internal standard). The calibration curve shows a good linearity $R^2=0.980$ and low LOD and LOQ being 0.01% and 0.02% respectively.

For the purification of the samples, PLGA NP formulations were dialysed either against 200 mL and 500 mL of Tris buffer for 1 hour. Figure 4.5B shows the calculated percentage volume of residual acetonitrile after both methods. The residual solvent was between 0.1 and 0.4%, being lower for the formulations dialysed against 500 mL buffer. These results are good enough for working in the laboratory as the residual solvent in the samples will have minimum impact on the physicochemical properties of the NPs, but as they do not fall within the ICH guidelines for residual solvent in the formulations for human use, these formulations would not be accepted for *in vivo* studies. In order to fulfil with the regulations, the dialysis time and the buffer volume were optimised. Samples were

dialysed against a total of 1 L of Tris buffer for two hours, with buffer exchange after 1 hour (i.e. 500 mL 1 hour and another 500 mL for another hour). By using this method complete removal of the solvent was achieved.

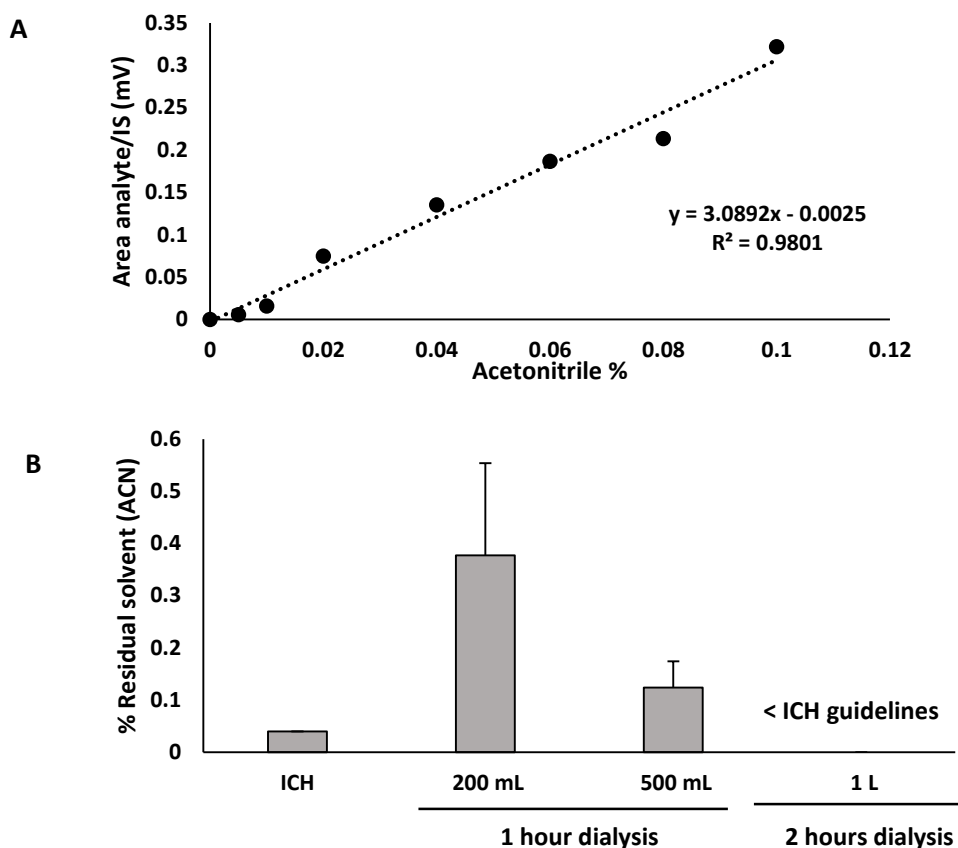


Figure 4.5 Gas chromatography results: (A) Calibration curve of the analyte of interest (acetonitrile) and (B) percentage of residual solvent after dialysis. Results represent mean \pm SD of triplicate measurements.

Dialysis is a time consuming method and it is also difficult to scale up. Thus, an alternative method, using cross flow filtration or TFF was used for the purification of the nanoparticles. Unfortunately, acetonitrile is not compatible with the TFF column material (mPES) therefore, one hour dialysis was carried prior TFF in order to remove the solvent from the formulations. TFF can also be used for removal of free antigen, which generally takes long time by dialysis, consequently, TFF was tested to assess its future application for further antigen removal. The purified samples were characterised in order to evaluate the effect of the purification method on the physicochemical characteristics of the PLGA nanoparticles. Measurement of the particle size, size distribution and zeta potential was carried out on the nanoparticles after either MF, dialysis or TFF (Figure 4.6). The size of the particles, nor the PDI significantly changed after any of the purification methods tested (Figure 4.6A, B). On the other

hand, the zeta potential of the nanoparticles after microfluidics was significantly ($p < 0.05$) lower compared to the purified nanoparticles (Figure 4.6C). This might be due to the presence of acetonitrile within the microfluidic formulation, since they contain 50% of organic solvent.

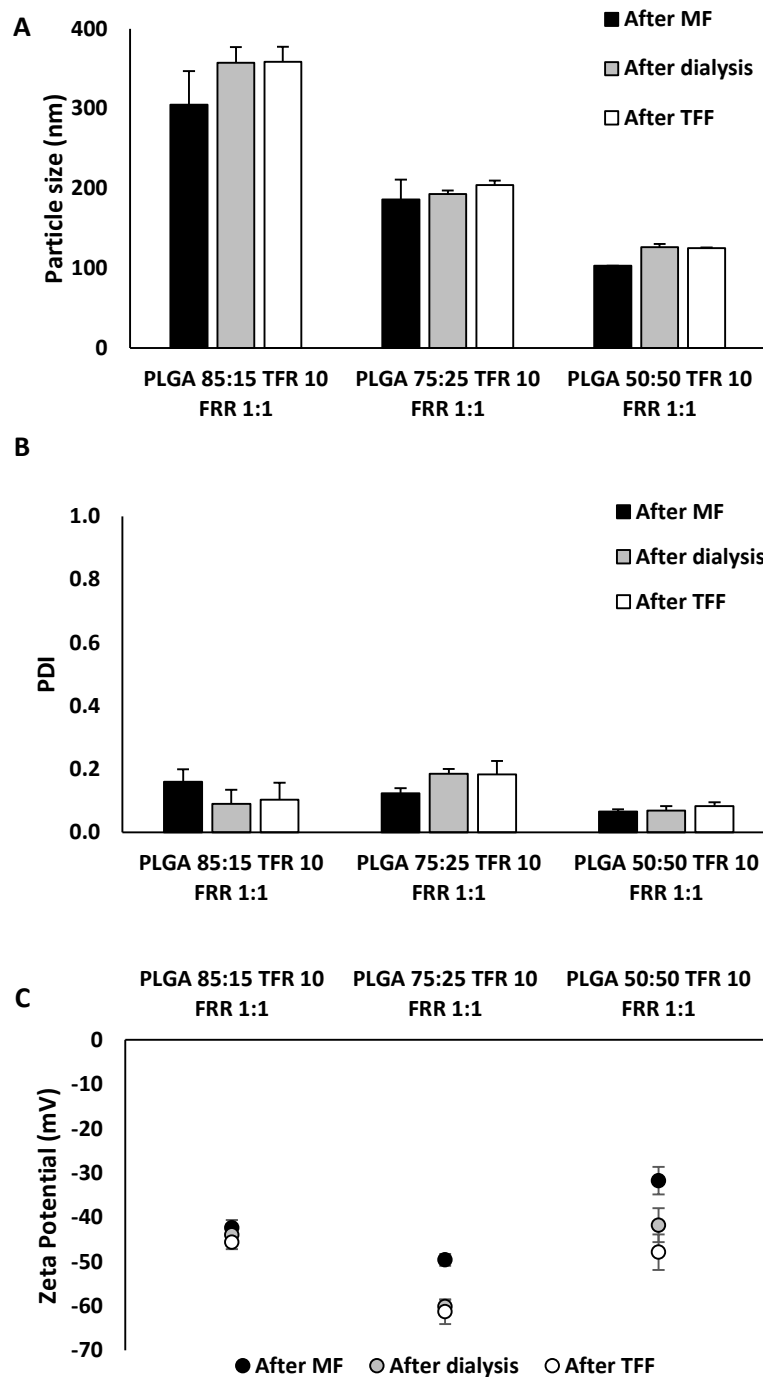


Figure 4.6 Physicochemical characteristics of the PLGA nanoparticles after microfluidics, dialysis and tangential flow filtration: (A) Particle size, (B) Particle size distribution and (C) Zeta potential. Results represent mean \pm SD of triplicate measurements.

4.4.4 Quantification of the polymer recovered after manufacturing of PLGA nanoparticles

Quantification of the polymer content in the PLGA nanoparticles is important for quality control, efficacy and stability. Polymer content was quantified using a HPLC with an ELSD connected to the system. A method developed by Marcus Rhiel et al., 2015 was followed [217]. Known amounts of PLGA copolymer (50:50, 75:25 and 85:15) were dissolved in ACN for the preparation of the standard curves. Solutions were injected into the system in order to determine the amount of polymer contained within the formulation. The peak area values obtained from the HPLC were plot against the polymer concentration (mg/mL). These calibration curves (Figure 4.7) showed an excellent fit ($R^2 = 0.996, 0.997$ and 0.999). LODs and LOQs were calculated for each copolymer and are depicted in Figure 4.7B. Sample analysis had a duration of 12 min since the retention time of PLGA 50:50, 75:25 and 85:15 were 4.4 min, 4.9 min and 5.3 min respectively (Figure 4.7). Analysis time could have been shortened since all three PLGA copolymers elute within the first 6 min, when the gradient is at 100% eluent B (0.1% TFA, 95% ACN and 5% dH₂O), but in order to give time to the column to equilibrate analysis time was kept constant at 12 min. Polymers eluted from lower to higher hydrophobicity, thus, PLGA 50:50 eluted first due to its lower hydrophobicity, followed by PLGA 75:25 and PLGA 85:15 (Figure 4.7). The absence of any methyl side group makes PGA more hydrophilic than PLA which contains one methyl side group. Hence, PLGA copolymers with higher ratio of PLA are more hydrophobic and elute after.

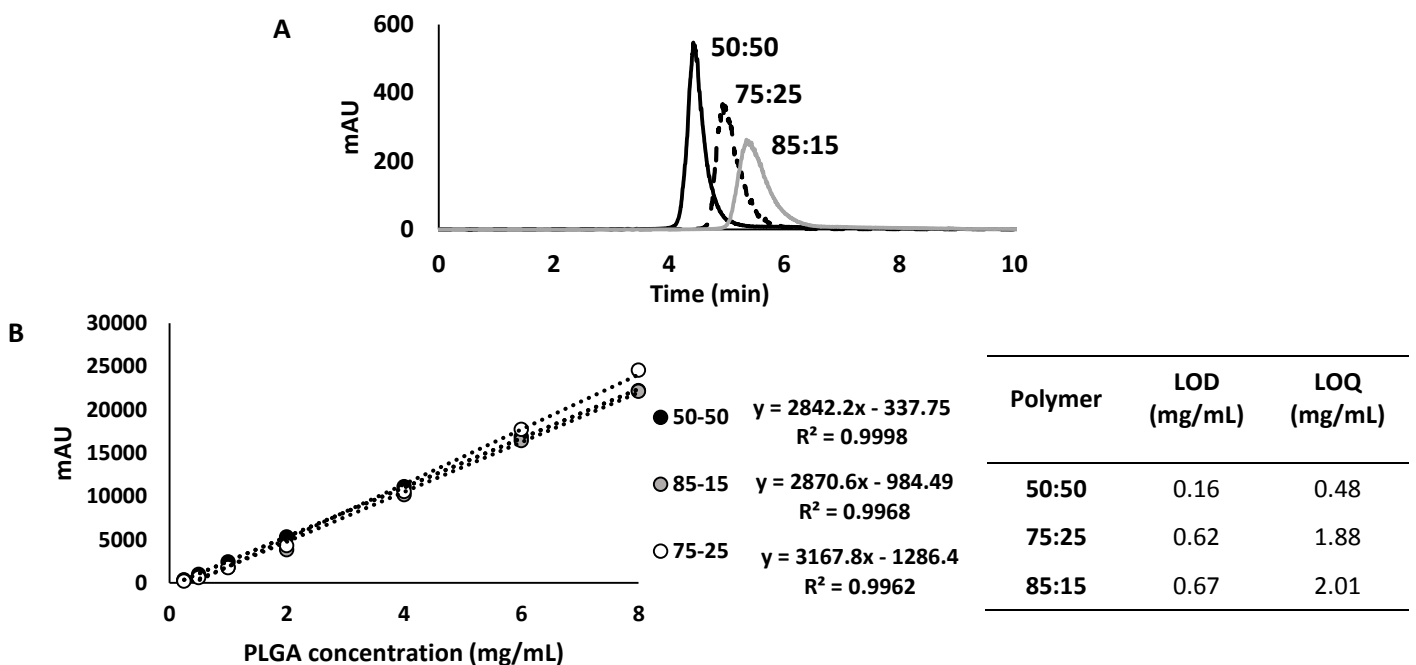


Figure 4.7 (A) HPLC-ELSD chromatogram showing the elution peaks for the copolymers 85:15, 75:25 and 50:50 and (B) their calibration curve with the calculated LOD and LOQ values for each polymer. Results represent mean \pm SD of triplicate measurements.

After establishment of the calibration curves, polymer NPs were prepared and polymer content quantified. Polymer NPs were manufactured at TFR 10 mL/min and FRR 1:1, 3:1 and 5:1 and injected into the HPLC-ELSD system in order to quantify the polymer recovery after microfluidics (Figure 4.8). With all three polymers, recovery was less than 80 % (Figure 4.8). Furthermore, the recovery of the NPs of 85:15 ratio was significantly ($p < 0.05$) lower compared to the other PLGA ratios; the polymer content for 85:15 PLGA NPs prepared at FRR 1:1 was $55.6 \pm 3.5\%$ whereas for FRR 3:1 and 5:1 the polymer content was $41 \pm 3.7\%$ and $49.2 \pm 0.6\%$ respectively (Figure 4.8). PLGA NPs of 75:25 monomer ratio showed $78.6 \pm 5.0\%$, $71.2 \pm 5.6\%$ and $63.5 \pm 1.1\%$ recovery for samples prepared at FRR 1:1, 3:1 and 5:1 respectively. Regarding PLGA 50:50 formulations, the recovery was up to $63.9 \pm 1.0\%$, $71.7 \pm 5.3\%$ and $72.4 \pm 3.6\%$ at FRR 1:1, 3:1 and 5:1. This suggests that polymer recovery is dependent on the FRR adopted since FRR 1:1 showed the highest recovery for PLGA 85:15 and 75:25, and highly dependent on the PLA:PGA ratio. The high PLA ratio is related to higher hydrophobicity [102], thus, the more hydrophobic the PLGA the more the polymer was noted to precipitate within the microfluidics chip.

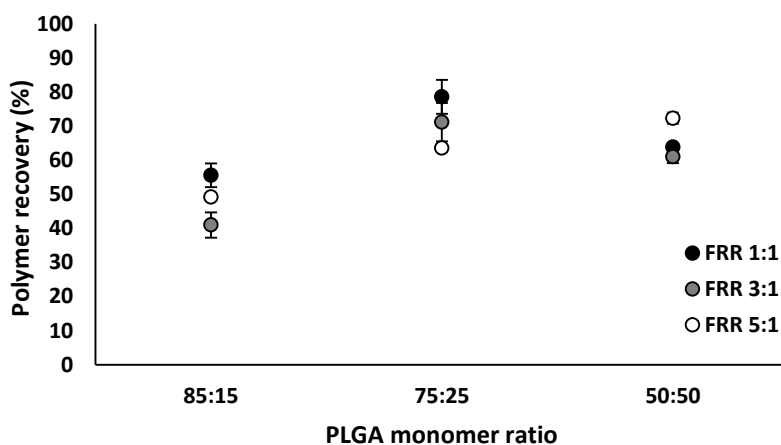


Figure 4.8 Polymer recovery of PLGA 85:15, 75:25 and 50:50 NPs manufactured through the microfluidics method: TFR 10 mL/min and FRR 1:1, 3:1, 5:1. Results represent mean \pm SD of triplicate measurements.

For the purification of PLGA NPs regarding the removal of non-encapsulated/unbound antigen TFF will be investigated as it is faster than dialysis and is more applicable for the continuous manufacturing of nanoparticles. Thus, determination of the polymer recovery after TFF was also carried out. The BCA assay was used for the PLGA quantification, and dialysed PLGA NPs were used for the establishment of a standard curve (Figure 4.9A). Figure 4.9A showed a good linearity ($R^2 = 0.991, 0.991$ and 0.996) and post TFF all three copolymers showed a recovery over 90%.

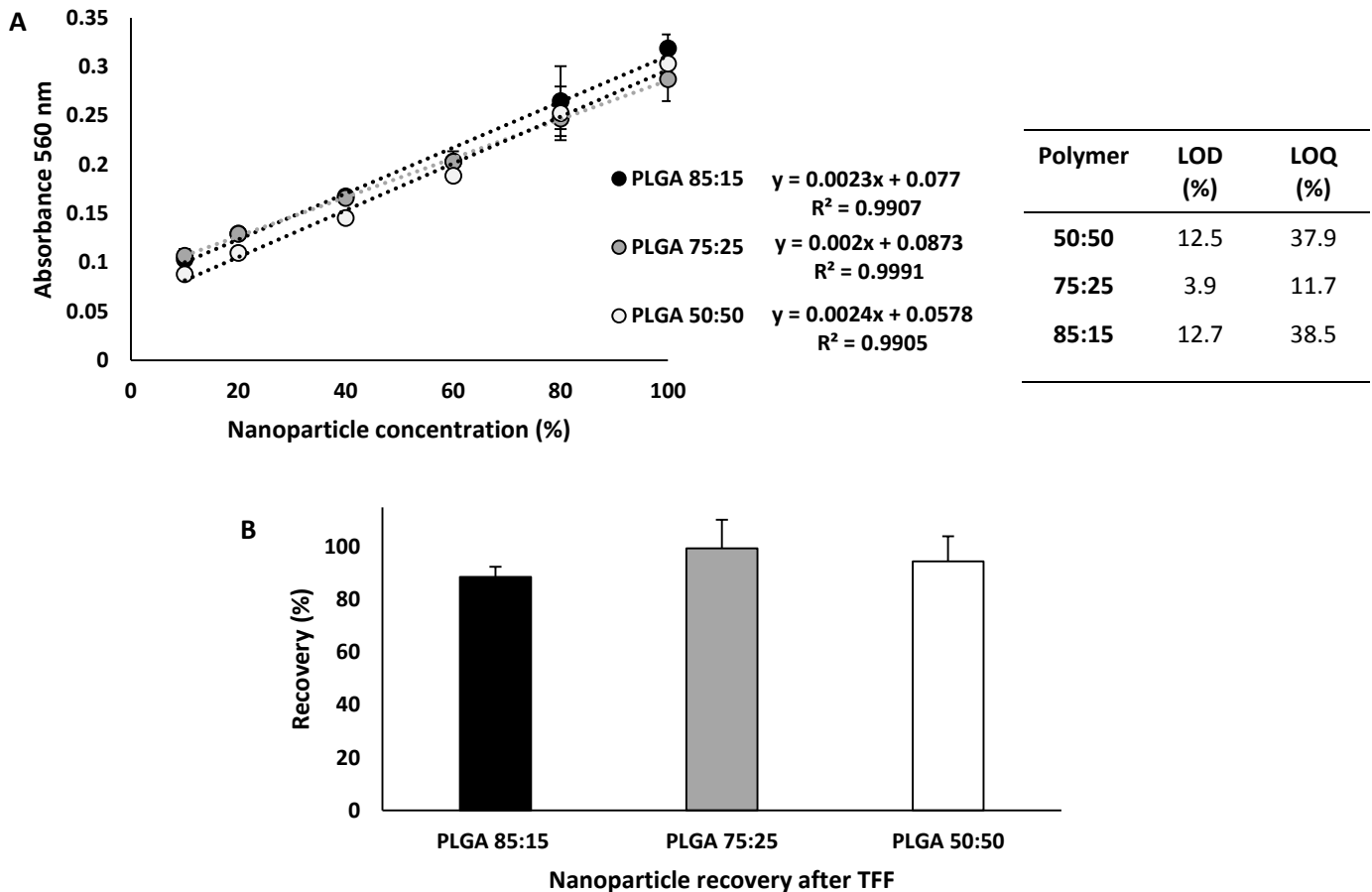


Figure 4.9 BCA assay for the quantification of PLGA within the nanoparticles after TFF: **(A)** Calibration curves obtained from the BCA assay using dialysed samples as standards and the LOQ and LOD values calculated for each polymer; **(B)** calculated recovery after TFF. Results represent mean \pm SD of triplicate measurements.

4.4.5 The effect of microfluidic process parameters on the physicochemical characteristics and loading efficiencies of the PLGA-NPs.

Quality control and characterisation of the interactions between adjuvants and antigen are important for the development of subunit vaccines in order to provide high efficacy and good safety. Manufacturing of PLGA nanoparticles encapsulating a model antigen (OVA) was carried out using microfluidics. OVA is a well characterise and established protein with a molecular weight of 45 kDa which is similar to the tuberculosis vaccine candidate H56 (48.3 kDa). Therefore, for the optimisation of the microfluidics parameters and the study of their influence in the antigen loading, OVA was loaded in-line in a single step process by adding it in the aqueous phase. PLGA NPs were prepared by altering the process parameters of the microfluidics system. After manufacturing using microfluidics, samples were dialysed for an hour against Tris buffer in order to remove the organic solvent and then passed

through TFF to remove non-encapsulated protein. TFF was selected instead of dialysis since the latter method is time consuming requiring over 24 hours and several buffer exchanges to remove non-encapsulated antigen.

4.4.5.1 Effect of the Flow Rate Ratio (FRR) in the physicochemical characteristics and encapsulation efficiency of the PLGA nanoparticles

In previous sections (section 4.4.1) the effect of the microfluidic parameters on the empty PLGA particles was evaluated. Now, the effect of the FRR was examined for the encapsulation of antigens by adding the antigen into the aqueous phase. Thus, the effect of FRRs (1:1, 3:1 and 5:1) was evaluated on the PLGA 85:15, 75:25 and 50:50 loaded with a fixed initial amount of OVA and prepared at a fixed TFR of 10 mL/min. The physicochemical characteristics of the antigen loaded PLGA NPs are shown in Figure 4.10A-B. Figure 4.10A shows the particle size and PDI of the NPs, which follows the same trend observed for the empty NPs. Increasing FRR resulted in a decrease particle size whereas this parameter did not affect the PDI. The copolymer 50:50 showed smallest sizes (below 115 nm) followed by copolymers 75:25 and 85:15. In general, PLGA 50:50 NPs loading antigen were more homogeneous in particle size distribution than the other 2 copolymers tested. All the PDIs were below 0.3 in all the cases. The addition of 0.2 mg/mL antigen slightly increased the size of the PLGA NPs when compared to the 'empty' NPs. In terms of ZP, all three copolymers resulted in highly anionic NPs as expected from PLGA-based systems with zeta potential values from -34 mV to -55 mV (Figure 4.10B) and no significant differences were observed between loaded and empty NPs.

Figure 4.10C-D show the impact of the FRR on the encapsulation efficiency of PLGA NPs at two different initial OVA concentrations (0.2 and 0.5 mg/mL respectively). In general the FRR 5:1 showed the lowest antigen loading with approximately 20% encapsulation of the initial amount loaded. In contrast, FRR 3:1 and 1:1 showed significantly ($p < 0.01$) higher loading efficiency for PLGA 85:15 and 75:25. In contrast, no significant differences were seen in the encapsulation efficiency of PLGA 50:50 at any of the FRR tested when loading 0.5 mg/mL whereas for lower antigen concentrations (0.2 mg/mL), FRR 3:1 showed significantly higher loading (~33%) when compared to the other FRRs (FRR 1:1 was ~17%; FRR 5:1 was 21%). It is hypothesised that PLGA 50:50 FRR 5:1 did not show lower encapsulation efficiency compared to the other FRRs due to the higher polymer recovery calculated from the HPLC-ELSD. Besides, the physicochemical characteristics of the copolymer 50:50 at all three FRRs was similar; in general, increasing the aqueous phase during the production of the nanoparticles reduces the encapsulation efficiency. This might be explained by the lower polymer concentration within the formulation as the initial polymer concentration was fixed at 10 mg/mL, therefore, when

PLGA nanoparticles are produced at FRR 1:1, 50% of the initial amount will be in the final formulation. In the case of FRR 3:1 and FRR 5:1, the polymer content is reduced down to 25% and 12.5% respectively.

Published studies have shown the correlation between polymer content and encapsulation efficiencies, demonstrating that increasing polymer concentration improves the loading within the PLGA particles [229-231]. Furthermore, the intrinsic properties of the PLGA have been shown to influence the loading as well. Results here, showed higher EE% for copolymers 75:25 and 85:15 than PLGA 50:50. However, most of the published data is based on the use of PLGA 50:50, whereas less information about the other copolymer ratios is available. The influence of the copolymer ratio has been reported by Cao et al. [232] when comparing PLGA 50:50 microparticles (MPs) and PLGA 85:15 MPs encapsulating OVA. PLGA 85:15 encapsulated approximately 24% whereas the copolymer 50:50 only encapsulated ~15% [232]. Mukherjee et al. also worked with PLGA 85:15 encapsulating protein (BSA) [233]. His results showed that the higher hydrophobicity of PLGA 85:15 resulted in approximately 38% EE compared to PLGA 50:50 (~10%). The authors also reported the enhanced protein encapsulation when polymer concentration was increased, which relates to our higher concentration at high FRRs [233]. De Rosa et al. produced PLGA MPs using copolymers 50:50 and 75:25. Here again, the higher hydrophobicity and viscosity of the PLGA 75:25 resulted in higher EE% compared to PLGA 50:50 MPs [234]. Moreover, Feng et al. showed that PLGA 75:25 MPs encapsulating a hepatitis B antigen had higher EE% compared to PLGA 50:50 MPs [235]. Witschi et al. demonstrated the influence of the PLGA hydrophilicity on drug loading, using tetracosactide [236]. In this case, EE% as well as particle size decreased with decreasing the lactic acid ratio [236]. On the other hand. Bilati et al. demonstrated that EE% decreased with hydrophobicity when producing PLGA NPs using w/o/w method and loading BSA [237]. However, this difference in trend may be a result of the different production method. Overall, the body of literature confirms that the use of PGLA of higher hydrophobic content promotes higher protein loading which might be the result of the hydrophobic polymers rapidly aggregating to form nanoparticles and thus capturing higher amounts of proteins.

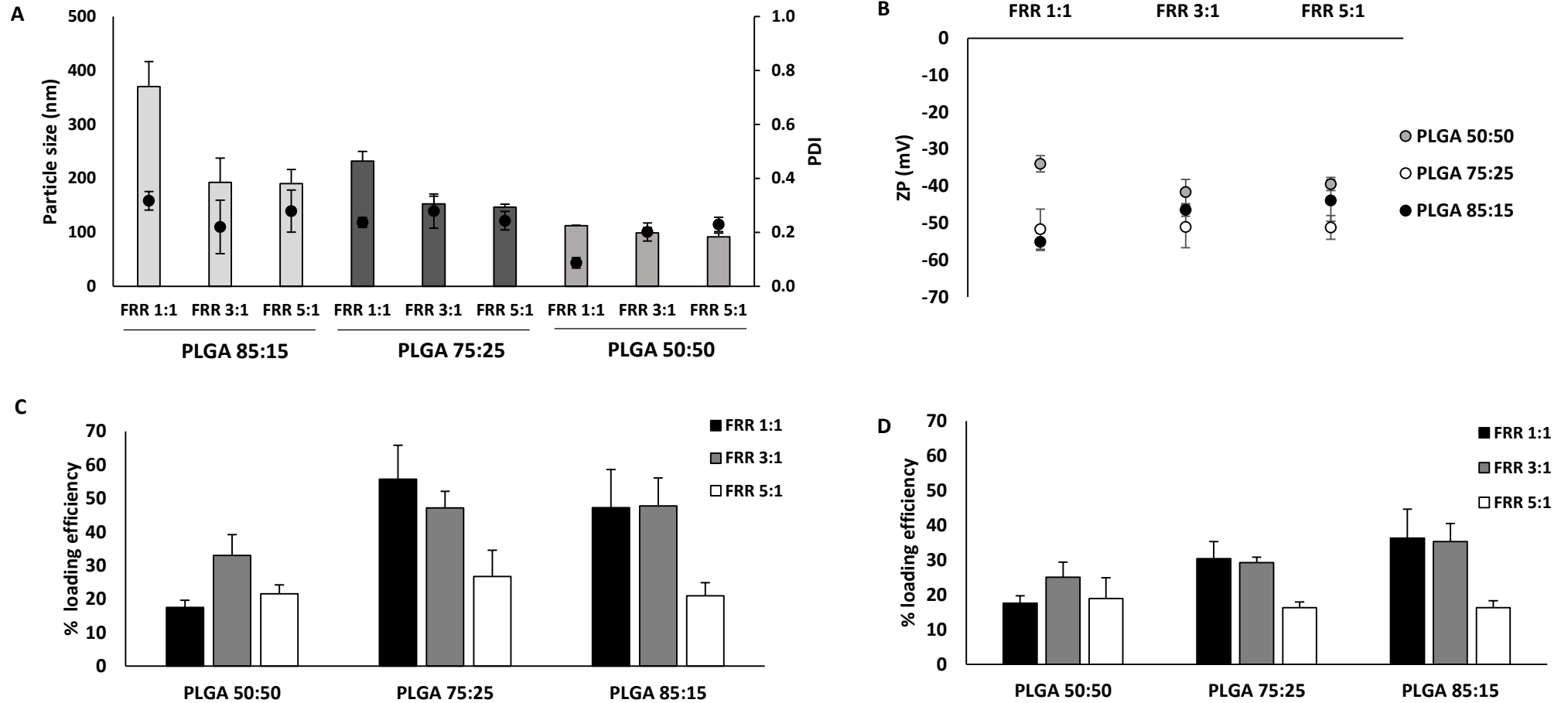


Figure 4.10 Effect of the flow rate ratio (FRR) on the physicochemical characteristics of the PLGA NPs produced using microfluidics at TFR 10 mL/min and encapsulating OVA as a model antigen: (A) Particle size and particles size distribution, (B) zeta potential and (C-D) encapsulation efficiency as percentage of PLGA NPs encapsulating 0.2 and 0.5 mg/mL OVA respectively. Results represent mean \pm SD of at least triplicate measurements.

4.4.5.2 Effect of the Total Flow Rate (TFR) on the physicochemical characteristics and encapsulation efficiency of the PLGA nanoparticles

After testing the FRR, the next step was to test the effect of the TFR in the formulation of these antigen loaded PLGA nanoparticles. In this case, the FRR was fixed at 1:1 whereas the TFR varied from 5 to 15 mL/min. Figure 4.11 shows the size, PDI, ZP and EE% of the different PLGA copolymers. In terms of size, PDI and ZP, values were similar to those of 'empty' nanoparticles (Figure 4.3), demonstrating that the loading of antigen had no notable effect. As shown previously, PLGA 85:15 produces the largest particle sizes, followed by PLGA 75:25 and PLGA 50:50 produced the smallest particle sizes. In terms of zeta potential, PLGA 75:25 nanoparticles were slightly more negative, than PLGA 85:15 and 50:50.

Regarding antigen loading (Figure 4.11C), there are no differences in the encapsulation efficiency when changing the TFR which is the speed at which both fluids (aqueous and organic) go through the microchannels within the microfluidics chip. As seen for the FRR, increasing hydrophobicity within the PLGA copolymer results in higher protein loading [232, 233]. PLGA 85:15 is the most hydrophobic of the three PLGA copolymers tested due to larger percentage of lactic acid (85%). EE% were approximately 12 - 22%, 25 - 30% and 36 - 40% for PLGA 50:50, 75:25 and 85:15 respectively. These results demonstrate that the manufacturing process of these nanoparticles can be run at various processing speeds without changing the encapsulation efficiency of the antigen. Furthermore, these results correlate with the size results obtained where no differences in size were seen when altering the TFR for the production of nanoparticles.

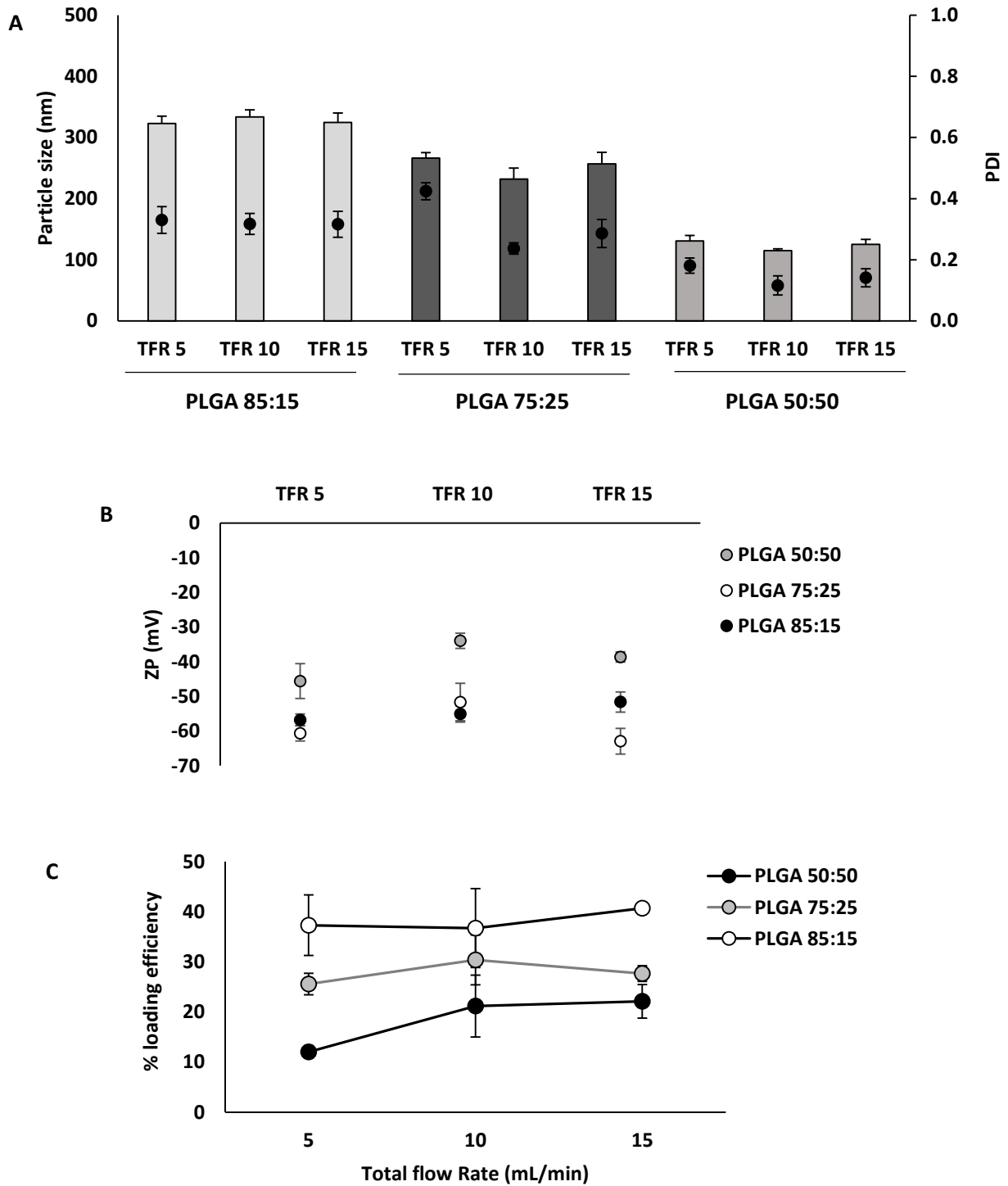


Figure 4.11 Effect of the total flow rate (TFR) on the physicochemical characteristics of the PLGA NPs produced using microfluidics at FRR 1:1 and encapsulating OVA as a model antigen: **(A)** Particle size and particles size distribution, **(B)** zeta potential and **(C)** encapsulation efficiency. Results represent mean \pm SD of at least triplicate measurements.

4.4.6 Effect of the initial antigen concentration loaded in the physicochemical characteristics and encapsulation efficiency of the PLGA nanoparticles

To consider the impact of varying OVA dose, different OVA concentrations (0.2, 0.5 and 1 mg/mL) were loaded in-line with the microfluidics system at a selected TFR of 10 mL/min and FRR 1:1. Physicochemical characteristics of the formulations are shown in Figure 4.12. The size of the particles notably increased for PLGA 85:15 nanoparticles from 300 nm to 800 nm (Figure 4.12A). In contrast, PLGA 75:25 nanoparticles showed only small changes in size (from 240 nm to 300 nm), and PLGA 50:50 nanoparticles remained approximately the same (112 to 130 nm). All the nanoparticles were highly anionic and no significant differences were found in terms of zeta potential as well as for the PDI values (Figure 4.12A-B).

In terms of varying the initial antigen concentration, no clear trend could be observed on loading efficiency (Figure 4.12C, D and E); antigen loading in PLGA 50:50 nanoparticles was approximately 20% irrespective of the initial antigen concentration tested. On the other hand, PLGA 85:15 and 75:25 showed a decrease in EE% when increasing the initial antigen concentration. PLGA 85:15 and 75:25 encapsulated ~55% OVA when 0.2 mg/mL were loaded and the EE% went down to 30% when OVA concentration was increased up to 0.5 mg/mL or 1 mg/mL (Figure 4.12D). The same trend was observed for PLGA 85:15 NPs which encapsulated ~47% at the lowest OVA concentration and down to 36% when increasing the initial OVA concentration (Figure 4.12E). Although the EE% was decreased upon increasing OVA concentration, the amount of protein loaded increased.

Studies published in literature have shown the change in the physicochemical characteristics of adjuvants systems upon incorporation of antigen [238]. In general, encapsulation of antigens within the nanoparticles provokes an increase in particle size. For example, Kissel et al investigated the loading of BSA onto block polymers at different concentrations and showed that increasing BSA concentration produced an increased in the polymer MPs size [239]. Yet, other studies have shown that incorporation of antigen does not affect the physicochemical characteristics of the nanoparticles. For example, Azizi et al. produced BSA loaded PLGA 50:50 NPs using different BSA concentrations (from 0.01 to 1% w/v) and the particle size of the NPs did not change upon increasing the protein concentration [240]. Furthermore, it is to be expected that increasing the initial antigen concentration can increase the total antigen incorporated until the system is saturated, however this translates into a decreased encapsulation efficiency as seen for other adjuvant systems [241]. Therefore the antigen/polymer ratio can be an important parameter to consider.

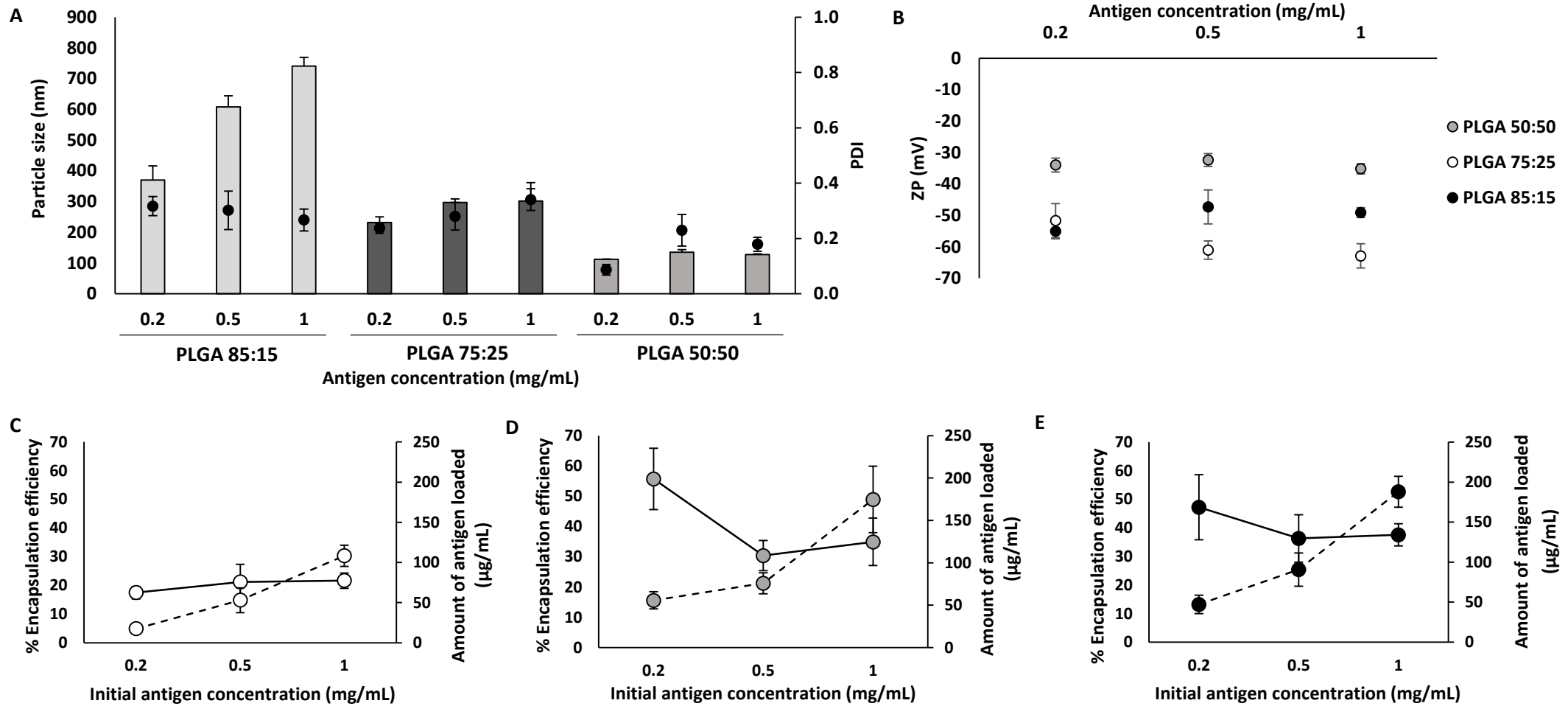


Figure 4.12 Effect of the initial antigen concentration loaded on the physicochemical characteristics of the PLGA NPs produced using microfluidics at FRR 1:1 and TFR 10 mL/min: **(A)** Particle size and particles size distribution and **(B)** zeta potential. The encapsulation efficiency (solid line) vs amount of antigen loaded (dotted line) for **(C)** PLGA 50:50, **(D)** PLGA 75:25 and **(E)** PLGA 85:15. Results represent mean \pm SD of triplicate measurements.

4.4.7 Varying the antigen incorporated within the nanoparticles

Further investigation into the effect of the type of antigen loaded was carried out at TFR of 10 mL/min and FRR 1:1. This flow rate ratio produces the largest particle sizes for all three PLGA copolymers studied and therefore, was chosen as large particle sizes are needed for pulmonary delivery. The selected antigens were: BSA due to its larger molecular weight (Mw 66.5 kDa), and TB vaccine candidate H56 (Mw 48.3 kDa), which will be the antigen used for the pulmonary delivery of a tuberculosis vaccine. Antigen loading was measured via ESLD and the calibration curves are shown in Figure 4.13. Calibration curves for the different proteins used during this project are depicted in Figure 4.13A, B and C. The R^2 shows a good linearity for all three calibration curves, being $R^2 > 0.998$ and the calculated LOQ and LOD were 0.03 and 0.01 mg/mL respectively for OVA and H56, whereas for BSA LOQ was 0.05 mg/mL and LOD 0.01 mg/mL Figure 4.13D.

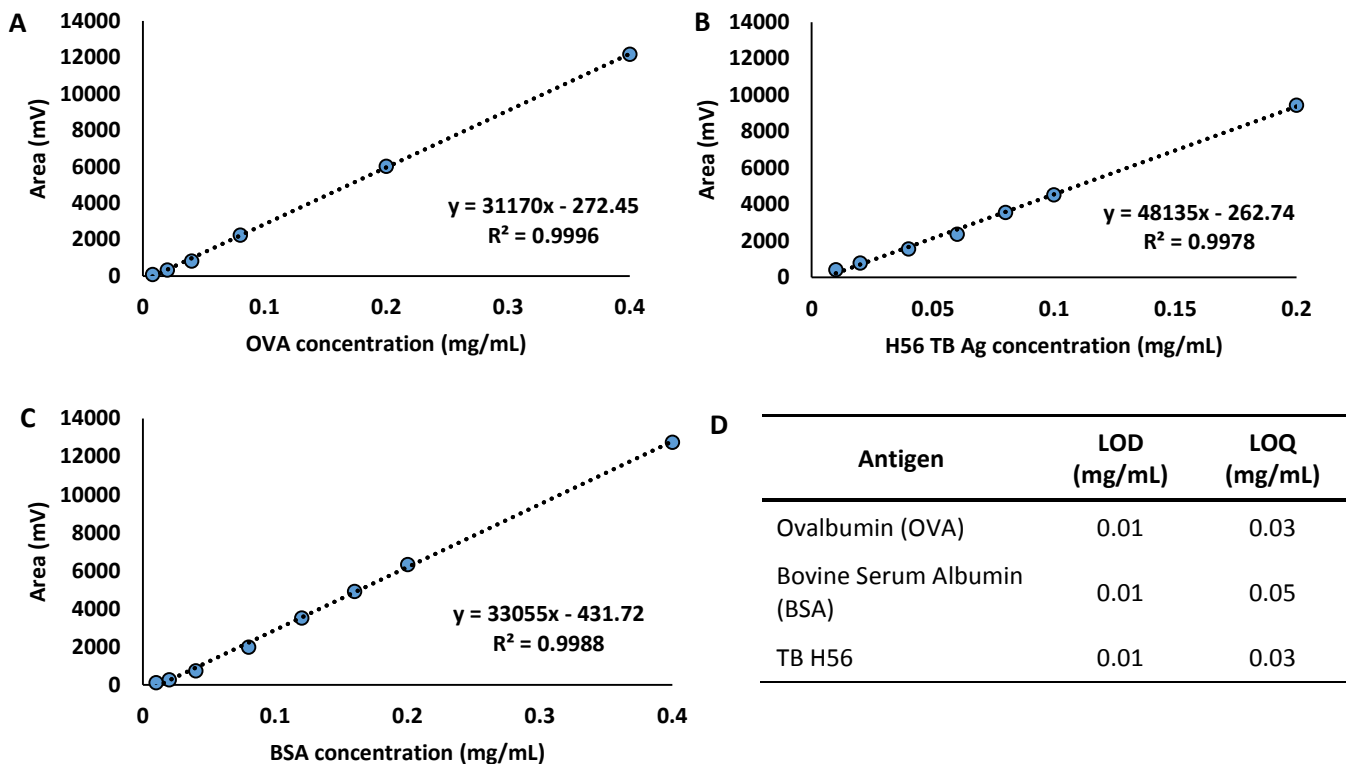


Figure 4.13 Calibration curves calculated from the HPLC-UV responses: (A) Ovalbumin standards, (B) H56 TB antigen standards, (C) Bovine Serum Albumin standards and (D) calculated limit of detection and limit of quantification for each antigen. Results represent mean \pm SD of triplicate measurements.

Table 4.4 shows the physicochemical characteristics of the PLGA copolymers encapsulating these proteins at an initial antigen concentration of 0.5 mg/mL. No differences could be seen in terms of size for PLGA 50:50. Particle sizes were \sim 138, 150 and 135 nm for BSA, H56 and OVA respectively. The largest sizes of PLGA 75:25 were obtained when OVA was loaded into the delivery system, followed

by BSA-loaded PLGA NPs and H56-PLGA NPs as shown in figure 4.14. The same trend was observed by PLGA 85:15 which produced large particles of approximately 600 nm when loaded with BSA and OVA, but in contrast, loading of H56 produced smaller particles of 270 nm. This differences in size when using H56 antigen for the loading of the copolymers might be due to the buffer in which this antigen is produced, as it contains glycine and might alter the formation of the particles. All particles were highly anionic and homogeneous in nature with PDIs below 0.3.

Regarding antigen loading, no significant differences were observed for the PLGA 75:25 NPs which were able to encapsulate 30-35% of the initial amount loaded into the system. On the other hand, PLGA 85:15 NPs showed lower encapsulation values for BSA (approx. 26%) and similar encapsulation for the other two antigen tested. This might be explained by the bigger molecular weight of BSA which results in a reduced encapsulation efficiency. Indeed similar results have been shown by Koppolu et al. when loading different size molecular weight proteins (insulin, OVA, BSA and Concanavalin A) into chitosan based delivery systems [242]. The smallest molecular weight (insulin 6 KDa) resulted in near 100% EE whereas 66.5 KDa BSA resulted in 56 %EE. OVA and H56 have similar molecular weights and therefore no significant differences were observed in their loading.

Table 4.4 Effect of the initial antigen concentration loaded on the physicochemical characteristics and antigen loaded of the PLGA NPs produced using microfluidics at FRR 1:1 and TFR 10 mL/min. Results represent mean \pm SD of triplicate measurements.

Ovalbumin (OVA)				
	Particle size (nm) \pm SD	PDI \pm SD	ZP (mV) \pm SD	EE (%) \pm SD
PLGA 50:50	135.2 \pm 8.8	0.23 \pm 0.06	-32.4 \pm 5.4	21.2 \pm 6.2
PLGA 75:25	297.2 \pm 12.0	0.28 \pm 0.05	-51.1 \pm 2.9	35.0 \pm 1.1
PLGA 85:15	608.2 \pm 36.0	0.3 \pm 0.07	-47.31 \pm 2.1	36.3 \pm 5.9
Bovine Serum Albumin				
	Particle size (nm) \pm SD	PDI \pm SD	ZP (mV) \pm SD	EE (%) \pm SD
PLGA 50:50	137.81 \pm 6.2	0.11 \pm 0.02	-37.8 \pm 2.4	24.8 \pm 3.6
PLGA 75:25	238.9 \pm 8.8	0.26 \pm 0.02	-53.5 \pm 1.7	31.0 \pm 6.7
PLGA 85:15	613.2 \pm 72.2	0.35 \pm 0.06	-46.4 \pm 2.0	22.6 \pm 2.4
Hybrid 56 (H56 TB Ag)				
	Particle size (nm) \pm SD	PDI \pm SD	ZP (mV) \pm SD	EE (%) \pm SD
PLGA 50:50	151 \pm 5.7	0.24 \pm 0.02	-32.8 \pm 1.6	8.6 \pm 0.3
PLGA 75:25	177.6 \pm 3.1	0.13 \pm 0.02	-47.6 \pm 2.3	34.8 \pm 45
PLGA 85:15	270.2 \pm 11.3	0.16 \pm 0.01	-43.6 \pm 1.8	38.0 \pm 1.7

4.4.8 The effect of the addition of a stabiliser into the PLGA nanoparticles

The effect of the incorporation of surfactants/stabilisers into the PLGA NPs formulated using microfluidics was studied. Polyvinyl alcohol (PVA) is a non-anionic surfactant which is one of the most common stabilisers used during the emulsification method for the preparation of PLGA particles. PVA favours the emulsification process and avoids the aggregation of PLGA droplets [243]. For this reason, different amounts of PVA were incorporated into the formulations to consider if this enhanced particle stability [244-247]. Due to the high hydrophilicity of this polymer, PVA was added into the aqueous phase (Tris buffer pH 7.4, 10 mM). Size measurements of the different PLGA nanoparticles encapsulating H56 antigen (0.2 mg/mL) with or without PVA and a stability study over a period of one month are shown in Figure 4.14. Incorporation of PVA produced larger particle sizes, increasing the particle size from 200 nm to 300 nm with the addition of 2% PVA (Figure 4.14A). Although addition of PVA resulted in a decreased PDI (Figure 4.14A), all four formulations showed PDIs below 0.2, which are representative of a homogeneous particle size population within the samples. The zeta potential of the PLGA nanoparticles changed from highly anionic to neutral upon addition of PVA in the formulations (Figure 4.14B). This results from the incorporation of PVA on the surface of the NPs which results in a shield of the charge as PVA forms an interconnected network with the PLGA polymer at the interface [243]. Overall, all four formulations (no PVA, 0.5% PVA, 1% PVA and 2% PVA) were stable over the period of time studied, demonstrating that there is no need for the incorporation of a stabilizer in these formulations (Figure 4.14C-D).

Chiesa et al. added the same concentrations of PVA into PLGA 75:25 NPs manufactured through microfluidics and showed that increasing PVA concentration resulted in increased NP size from approximately 200 to 500 nm and lower PDIs. The measured zeta potential was also reduced upon incorporation of PVA [223]. Kumar et al investigated the loading of insulin in PLGA50:50 and 75:25 NPs and demonstrated that addition of stabilisers into the formulation increased the particle size [248]. In contrast, other reported work using the w/o/w for the production of NPs showed that increasing surfactant concentration produces smaller particle sizes and the lack of stabiliser increases the particle size [249]. This may be due to the stabiliser being added to stabilise the emulsion during the formation of the NPs. However, in the case of microfluidics, the nanoparticles are formed rapidly due to nanoprecipitation thereby circumventing the need for additional stabilisers such as PVA. Indeed, such stabilisers may undermine the nanoprecipitation process. Chiesa et al. hypothesised that the increase in viscosity due to incorporation of PVA into the microfluidics systems might decrease the mixing speed and therefore, favour the formation of larger particles [223].

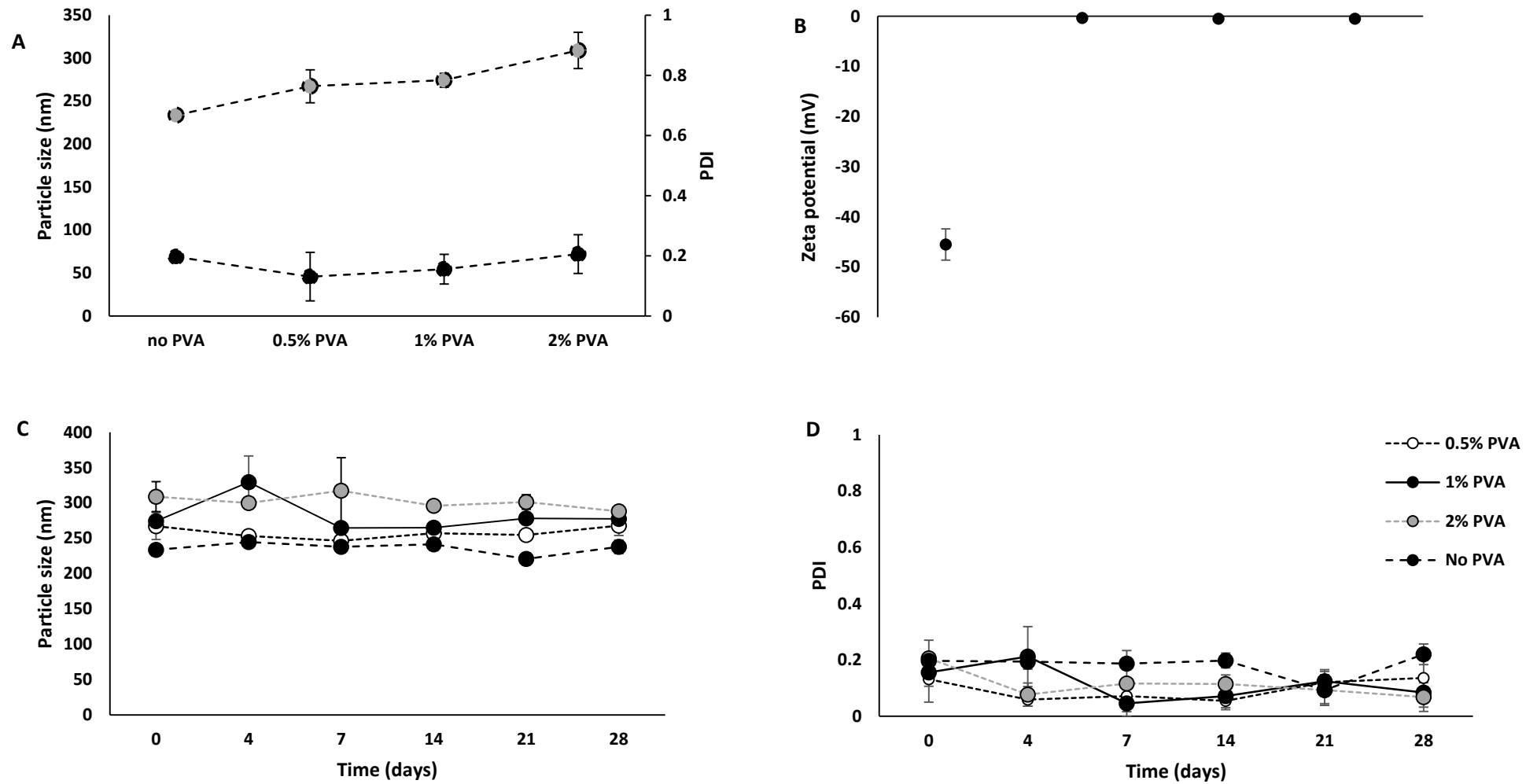


Figure 4.14 Effect of the incorporation of different concentrations of PVA as stabiliser in the PLGA 75:25 nanoparticles formulated using microfluidics TFR 10 mL/min and FRR 1:1: (A) particle size (grey dots) and PDI (black dots) and (B) Zeta potential. A stability study of the particles was carried out for a month: (C) particle size and (D) size distribution of H56 loaded PLGA 75:25. Different amounts of PVA (0.5%, 1% and 2%) were added into the aqueous phase in order to compare the stability of the nanoparticles over the period of one month. Results represent mean \pm SD of triplicate measurements.

4.4.9 Morphological characterisation of the PLGA nanoparticles

The morphology of the polymeric NPs was analysed by microscopic techniques such as SEM and CryoTEM. CryoTEM images of the nanoparticles of PLGA 75:25 reported spherical and regular shaped particles with a smooth outer surface (Figure 4.15). The importance of surface examination of these NPs is related to the antigen release profile. Any change or asymmetry will provoke a faster release due to the increase of surface area [250].

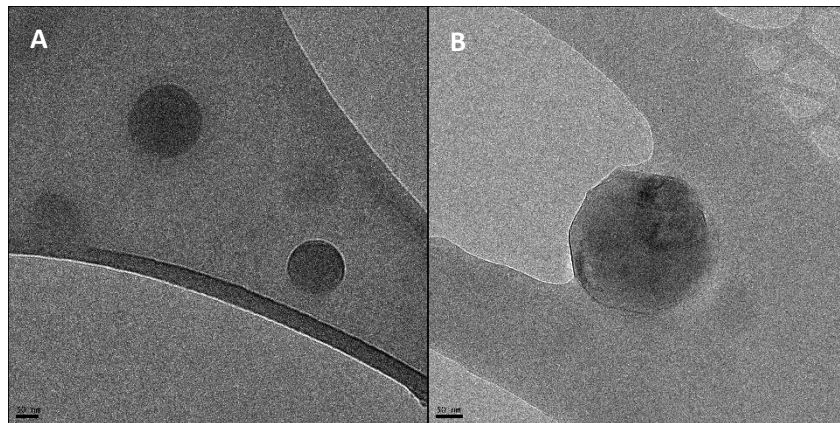


Figure 4.15 (A-B) CryoTEM micrographs of PLGA 75:25 nanoparticles manufactured using microfluidics at TFR 10 mL/min and FRR 5:1. Particles are in the nanometre range and show a regular and spherical shape.

SEM produces 3D images with high resolution which allow for particle surface examination. Images of empty PLGA 75:25 NPs manufactured at different FRR show spherical, regular-shaped nanoparticles with a smooth surface (Figure 4.16). Size and size distribution correlated with the results obtained from the DLS. Images revealed samples with a satisfactory polydispersity index, with small size. The agglomeration/clumping displayed by the PLGA nanoparticles prepared at FRR 3:1 and 5:1 (Figure 4.16) might be due to the smaller size compared to PLGA NPs manufactured at FRR 1:1 and it might be due to the sample melting under the electron beam.

The morphology of the antigen loaded polymeric nano- and microparticles was analysed by scanning electron microscopy (SEM). SEM produces 3D images with high resolution which allow for particle surface examination. Images of PLGA 85:15, 75:25 and 50:50 NPs manufactured by using microfluidics at TFR 10 mL/min and FRR 1:1 are shown in Figure 4.16. Two different methods to purify these particles were used: dialysis and tangential flow filtration. SEM micrographs showed spherical, regular-shaped nanoparticles with a rough surface. Size and size distribution correlated with the

results obtained from the DLS. Images revealed samples with a satisfactory polydispersity index and with small size except for the PLGA 85:15 nanoparticles.

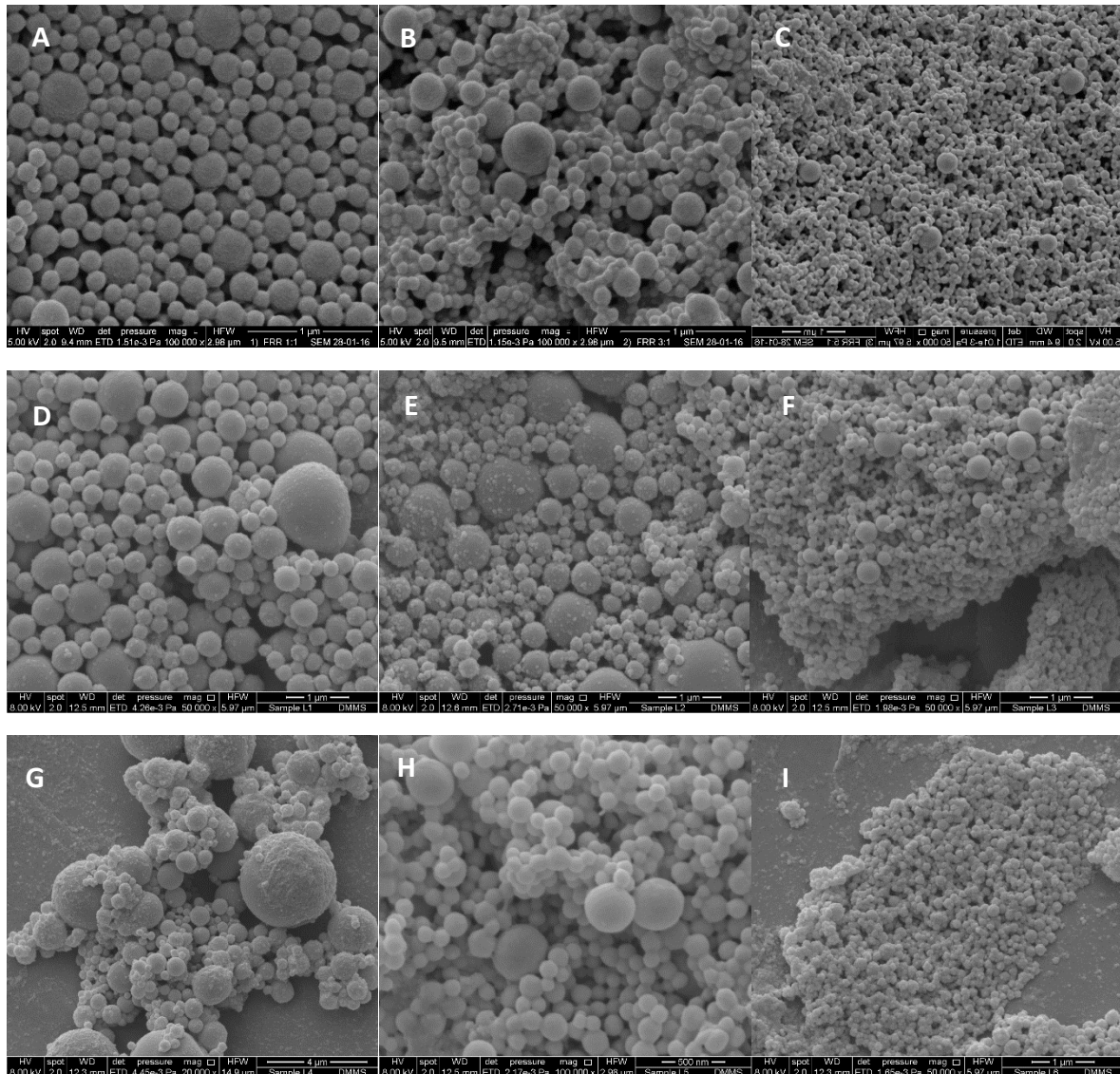


Figure 4.16 SEM micrographs (A) empty PLGA 75:25 NPs FRR 1:1 (B) empty PLGA 75:25 NPs FRR 3:1, (C) empty PLGA 75:25 NPs FRR 5:1, (D) antigen loaded PLGA 85:15, (E) antigen loaded PLGA 75:25 FRR 1:1 after dialysis, (F) antigen loaded PLGA 50:50 FRR 1:1 after dialysis, (G) antigen loaded PLGA 85:15 FRR 1:1 after TFF, (H) antigen loaded PLGA 75:25 FRR 1:1 after TFF and (I) antigen loaded PLGA 50:50 FRR 1:1 after TFF.

4.4.10 PLGA nanoparticles: Antigen release studies

Various factors can affect the antigen release from PLGA nanoparticles. Particle size, the lactide:glycolide ratio, molecular weight and morphology have shown to influence the degradation rates of the PLGA particles [251-254]. Antigen release studies were carried out for all three PLGA copolymers in order to evaluate the influence of the monomer ratio. Besides PLGA NPs produced at

TFR 10 mL/min and FRR 1:1 and 5:1 were selected as these microfluidic process parameters produced the largest and smallest particle sizes respectively. The effect of the temperature on the release of the model antigen OVA was also studied, thus, release studies at 37°C and at 4°C were carried out. As these particles are meant to be delivered into the deep lungs, they will be cleared by the macrophages in rapidly, therefore, the antigen released was studied for a period of 6 hours.

Figure 4.17 shows the physicochemical characteristics of the OVA loaded PLGA NPs manufactured using FRR 1:1 as well as the amount of OVA remained inside these PLGA NPs during the release study at 37°C for 6 hours. The size of the nanoparticles has been reported previously in this chapter, with PLGA 50:50 showing the smallest particle size, followed by PLGA 75:25 and PLGA 85:15. The particle size of the PLGA NPs did not significantly change during the release for PLGA 85:15 and 75:25 NPs whereas for PLGA 50:50 NPs it decreased by 20 nm at the end of the study (Figure 4.17A-F). Regarding ZP, no significant differences were observed during the period studied (Figure 4.17G). The total amount of antigen released from the PLGA NPs was approximately 38%, 44% and 55% for PLGA 75:25, 85:15 and 50:50 respectively (Figure 4.17H). PLGA 75:25 NPs showed the slowest antigen release for the three copolymer studied. It has been reported in literature that the intrinsic properties related to the PLGA monomer ratio dictate the release profile of the particles. In general, the highest content of PLA releases in a slower manner, therefore PLGA 85:15 should release the slowest, although these results demonstrate that PLGA 75:25 releases antigen faster than the other two copolymer tested [102]. When the release studies for the FRR 5:1 were carried out a different trend was seen (Figure 4.18). The size of the PLGA 75:25 and 85:15 NPs decreased during the study from approximately 165 to 140 nm and from 197 to 147 nm respectively, whereas PLGA 50:50 NPs did not change in size during the period studied (Figure 4.18A-F). Again the ZP of the PLGA NPs remained invariable as shown in Figure 4.18G. In this case, PLGA 75:25 and 50:50 released protein the fastest, 50% of the initial amount loaded was released within the 6 hours. In contrast, PLGA 85:15 released the antigen the slowest in correlation with literature (~40%). The final study was performed on OVA loaded PLGA NPs produced at FRR 1:1 but this time the release study was studied at 4°C. Decreasing the temperature of the release study did not alter either the particle size nor the ZP of any of the three PLGA copolymers studied (Figure 4.19A-G). PLGA NPs released in a slower manner compared to the NPs released at 37°C (Figure 4.19H). PLGA 85:15 and 75:25 both released approximately 30% of the initial payload whereas PLGA 50:50 released the fastest (~45%). The reason behind the influence of the temperature during the release of the antigen is due to the reduced degradation time. PLGA degrades by hydrolysis and temperature acts as a catalyser accelerating this process. Thus, increasing temperature resulted in an increase of antigen release.

Many studies have reported the influence of the copolymer ratio in the degradation rate of the particles and therefore its influence in the protein/drug release profile [102]. Commonly PLGA NPs and MPs show a biphasic release profile characterised by an initial burst release of the payload located near the surface, followed by a sustained release due to polymer degradation. Results reported here, show the biphasic profile typical of these copolymers. It is hypothesised that the period of time studied for the antigen release (i.e. 6 hours) represents the initial burst. For example, Swed et al. loaded lysozyme inside PLGA 75:25 NPs (400 nm, 70% EE and -30 mV) and showed that 20% of the payload was released during the first hours, followed by 45% release after 24 hours and a sustained release of 60% up to 30 days [255]. Here, all three studies showed that PLGA 50:50 NPs release faster than the other two copolymers tested. This has been widely observed in literature. PLGA 50:50 has the fastest degradation time of all the PLGA copolymers available. PLGA 50:50 MPs encapsulating Hepatitis B antigen released faster than the PLGA 75:25 MPs [235]. These could be explained by the smaller particle size of the MPs and the higher hydrophilicity of the copolymer 50:50 [235]. PLGA 85:15 and 75:25 showed a slower release of OVA as expected due to their higher hydrophobicity and thus, slower degradation rate. A decrease in the temperature reduced the antigen release in all three copolymers compared to the release at 37°C which it is suggested to be a result of the increased degradation of the polymer at higher temperature (37°C). Keles et al. studied the effect of temperature (50°C and 70°C) on the degradation rates of PLGA 50:50, PLGA 75:25 and PLA, and showed that the higher the glycolic ratio the faster the polymer degrades [256]. On the other hand, when PLGA NPs at FRR 5:1 were studied, both PLGA 75:25 and 50:50 showed a similar release pattern. This might be explained by the decrease in particle size and protein loading observed by the PLGA 75:25 NPs at that FRR (~160 nm and ~16% loading) compared to the particles produced at FRR 1:1 (~210 nm and ~30% loading). Besides, the polymer recovery of this formulation, as described in section 4.4.4, was the lowest of all three FRRs tested (FRR 1:1 was ~80%; FRR 5:1 was ~63%). Therefore it is hypothesised that a combination of intrinsic factors of this formulation resulted in a faster protein release profile. For example, Panyam et al. studied the influence of particle size on BSA-loaded PLGA 50:50 particles of 0.1, 1 and 10 µm and showed that the smaller particles released faster than the larger ones (BSA loading was ~90% at any of the particle sizes produced) [257].

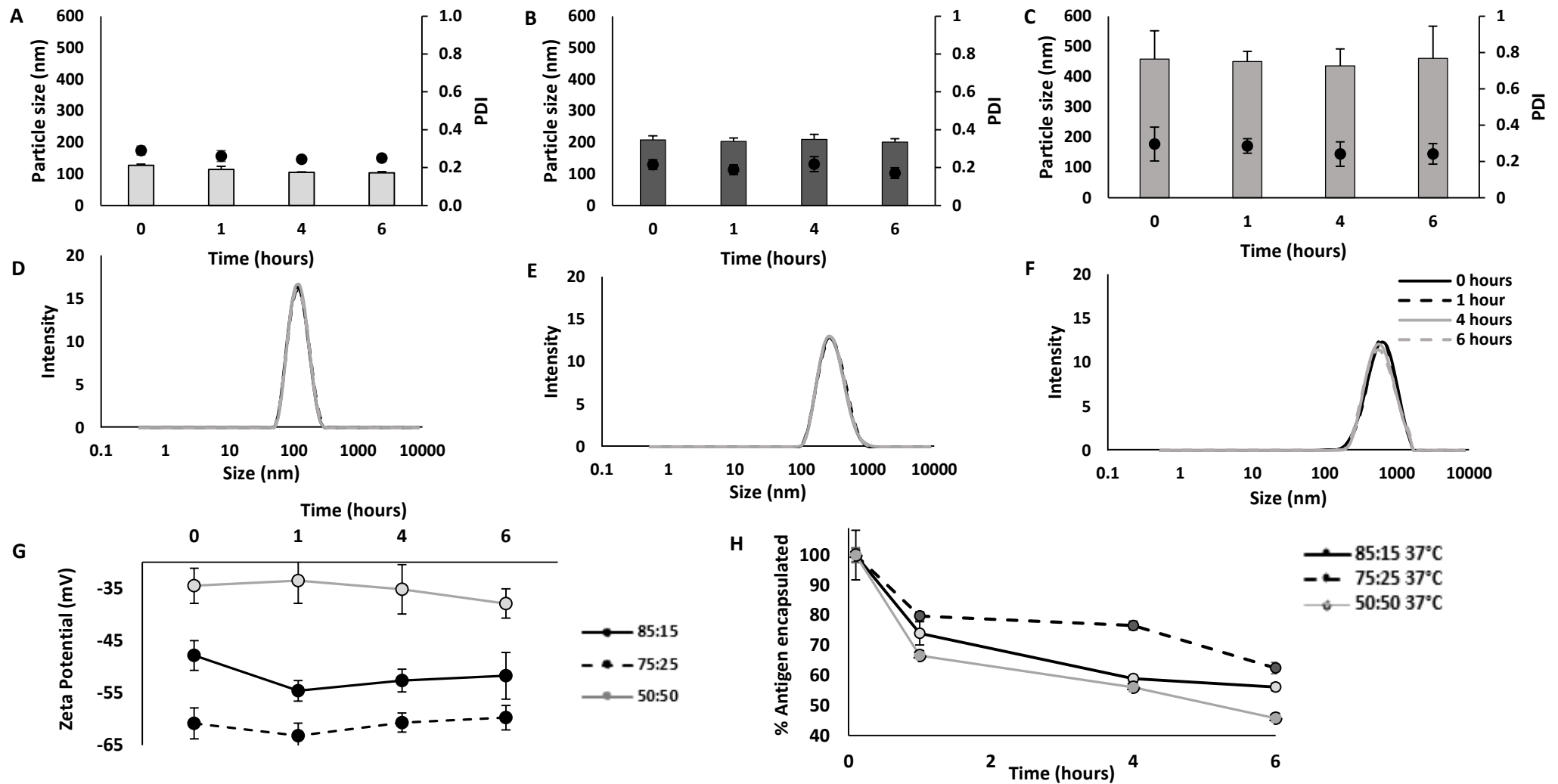


Figure 4.17 Particle size and PDI of the PLGA (A) 50:50, (B) 75: 25 and (C) 85:15, (D-F) overlay intensity plots and (G) ZP values at the selected time points measured for the release study. (H) Release study at 37°C of the PLGA 85:15, 75:25 and 50:50 nanoparticles manufactured by using microfluidics at a TFR of 10 mL/min and FRR 1:1. Results represent mean \pm SD of at least triplicate measurements.

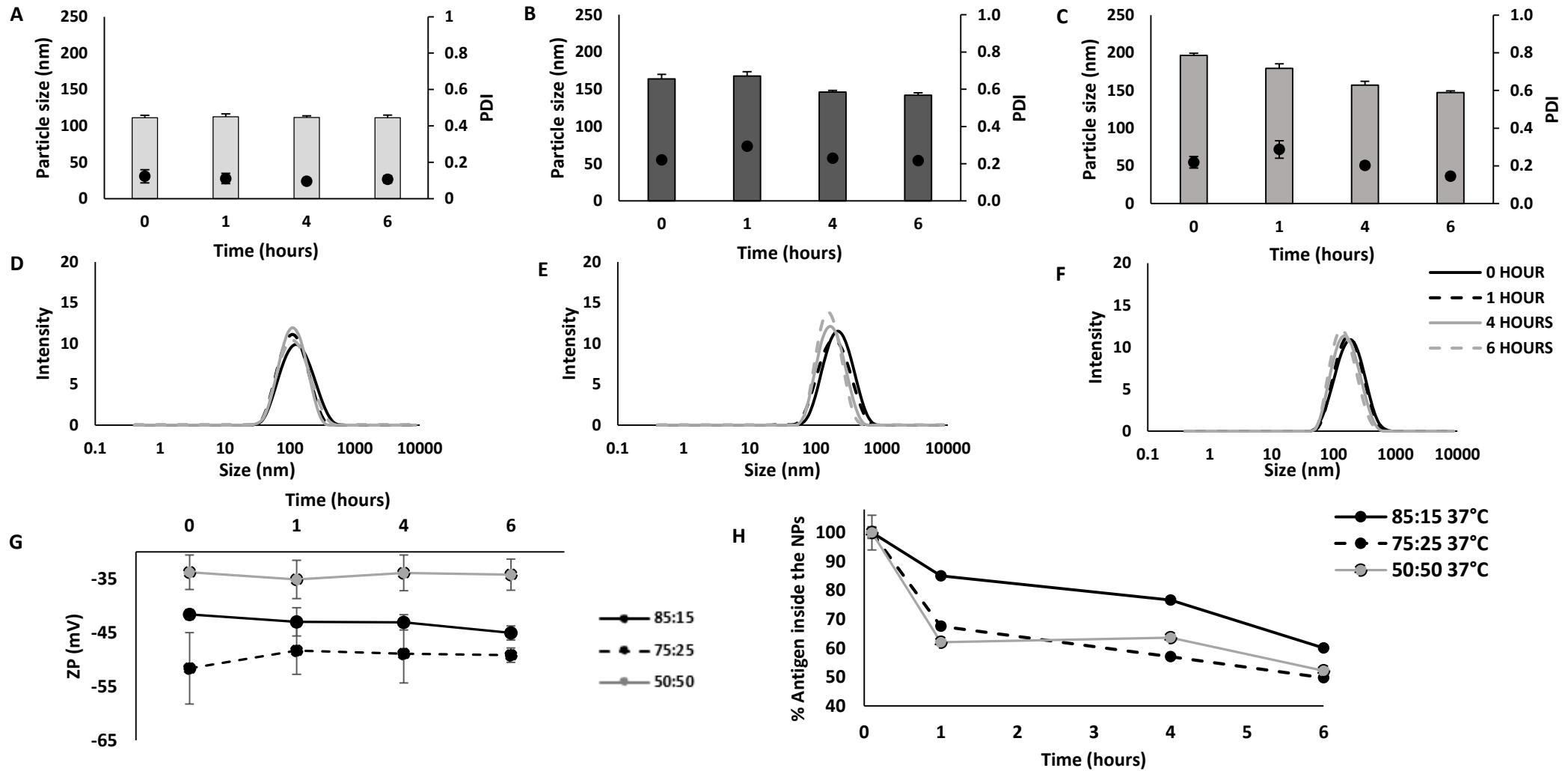


Figure 4.18 Particle size and PDI of the PLGA (A) 50:50, (B) 75:25 and (C) 85:15, (D-F) overlay intensity plots and (G) ZP values at the selected time points measured for the release study. (H) Release study at 37°C of the PLGA 85:15, 75:25 and 50:50 nanoparticles manufactured by using microfluidics at a TFR of 10 mL/min and FRR 5:1. Results represent mean ± SD of at least triplicate measurements.

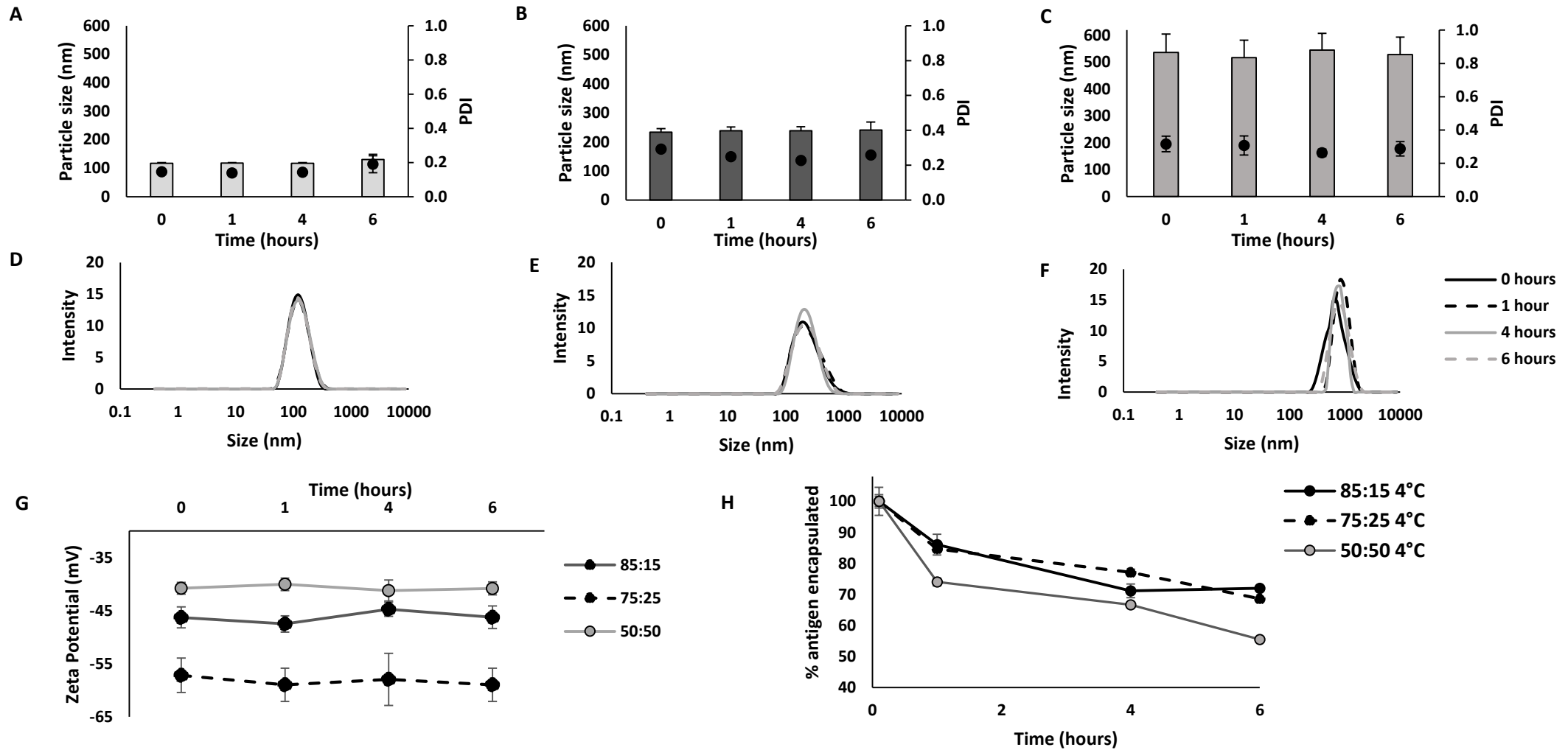


Figure 4.19 Particle size and PDI of the PLGA (A) 50:50, (B) 75:25 and (C) 85:15, (D-F) overlay intensity plots and (G) ZP values at the selected time points measured for the release study. (H) Release study at 4°C of the PLGA 85:15, 75:25 and 50:50 nanoparticles manufactured by using microfluidics at a TFR of 10 mL/min and FRR 1:1. Results represent mean ± SD of at least triplicate measurements.

4.4.11 Manufacture of microspheres

Once the method for preparation of PLGA NPs was studied in detail and optimised, microspheres were manufactured in order to get a wide range of PLGA particles to be used for further testing alongside nanoparticles in order to examine the relationship of particle size and deposition within the lungs. PLGA MPs were formulated using the well-known w/o/w method. PLGA particles formulated by this method were all in the micrometre range. Given the large volume of work already reported for these systems, only key characteristics (size, heterogeneity, ZP, morphology and antigen loading) were considered. Figure 4.20A depicts the sizes of the empty MPs obtained according to the different percentiles for each PLGA copolymer and the size distribution of the particles is represented by the SPAN number in Figure 4.20B. PLGA 85:15 microspheres produced the largest sizes, followed by PLGA 75:25 microspheres and PLGA 50:50. Due to the addition of PVA during the preparation of these microparticles, the zeta potential values measured were near neutral (Figure 4.20C). This reflects the presence of residual PVA in the surface of the microparticles, which was not completely removed after the three centrifugation washing steps performed during the MP production. When OVA was incorporated into the formulation, microspheres sizes did not change (Figure 4.20D). No significant differences were observed on the mean particle size measured for all three copolymers. In general, 10% of the particles within the samples were around 500 nm, 50% of the particles were in the range between 1 - 1.3 μm and 90% of the particle size population were below 2 μm . Zeta potential values remained neutral after encapsulation of antigen (Figure 4.20E). Encapsulation efficiency was lower compared to the nanoparticles produced using microfluidics. The highest loading was shown by the PLGA 85:15 copolymer which also showed the highest antigen encapsulation during nanoparticle production. In contrast, PLGA 50:50 showed the lowest encapsulation, being approximately 12% (Figure 4.20F).

As mentioned previously in this chapter (section 4.4.5.1), the methyl side group present on the lactic acid moiety of the copolymer might influence the size of the particles produced. Thus, the copolymer with higher lactic acid ratio resulted in the largest particle sizes when 'empty' MPs were produced. Moreover, PLGA 85:15 MPs showed the highest EE correlating to published data [232].

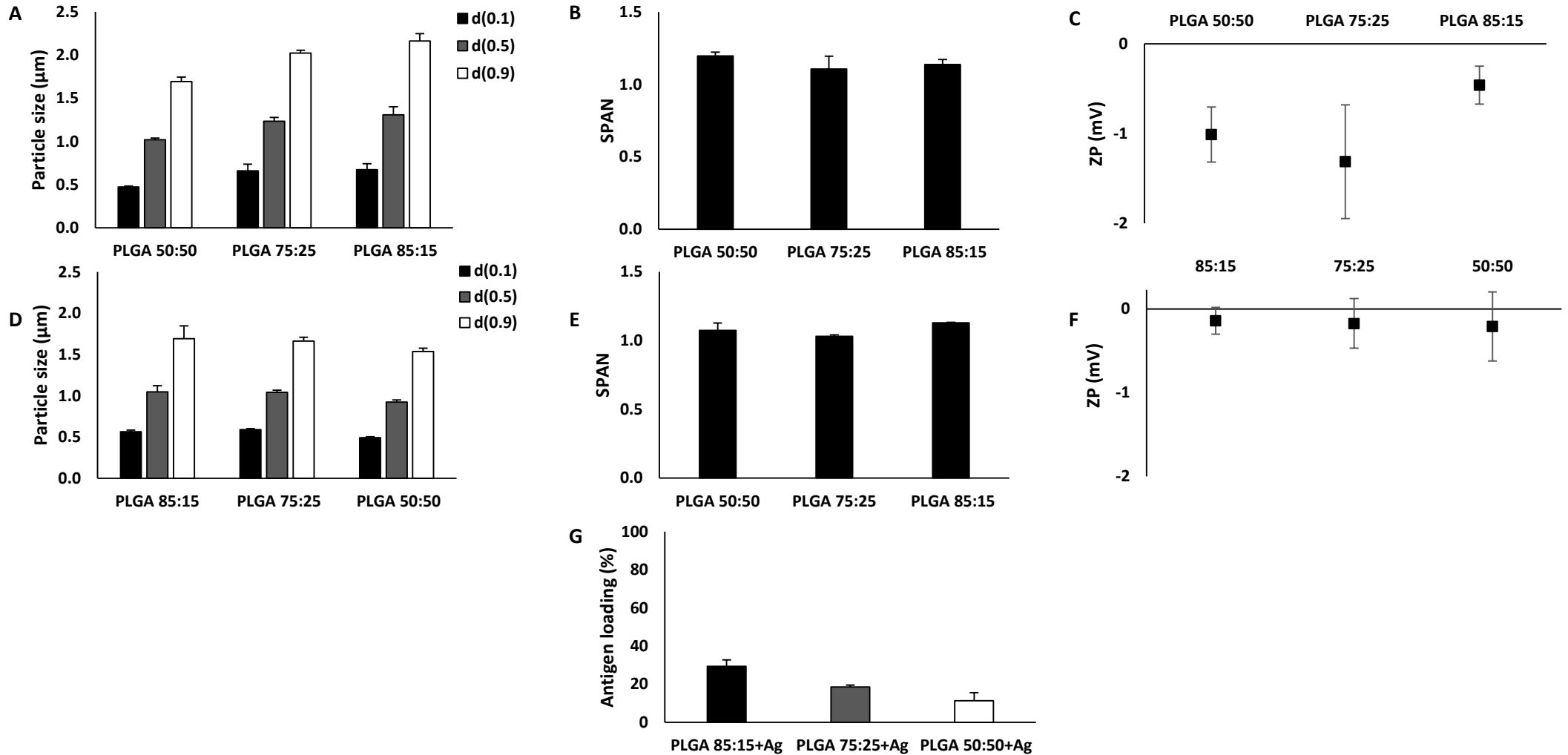


Figure 4.20 Physicochemical characteristics (A, D) Particle size, (B, E) SPAN, (C, F) Zeta potential and (G) encapsulation efficiency (EE %) of the (A-C) empty and (D-G) antigen loaded microspheres produced using the double emulsion method. Results represent mean \pm SD of at least triplicate measurements.

The morphological analysis of the PLGA microparticles by SEM showed uniform, spherical microparticles with rough surface and in the micrometre range (Figure 4.21). The particle size from the SEM micrographs correlates to the particle size values obtained by DLS.

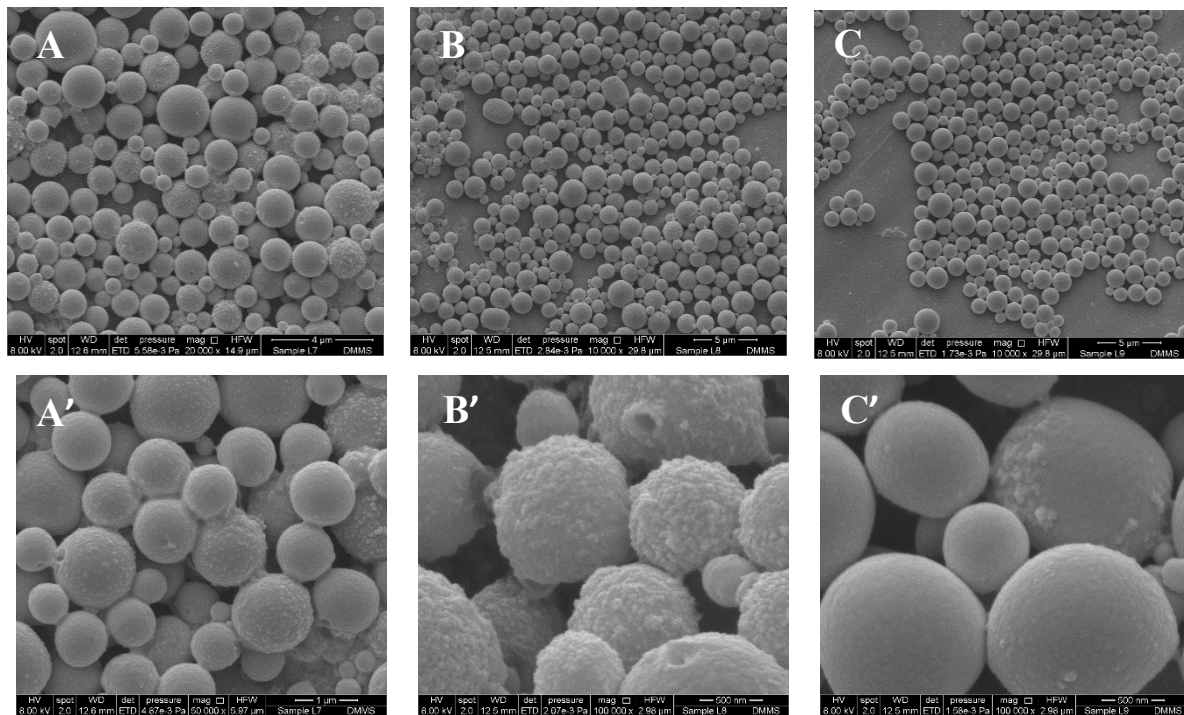


Figure 4.21 SEM micrographs PLGA microparticles encapsulating ovalbumin as a model antigen: (**A-A'**) PLGA 85:15, (**B-B'**) PLGA 75:25 and (**C-C'**) PLGA 50:50 at two different magnifications for better examination of the MP surface.

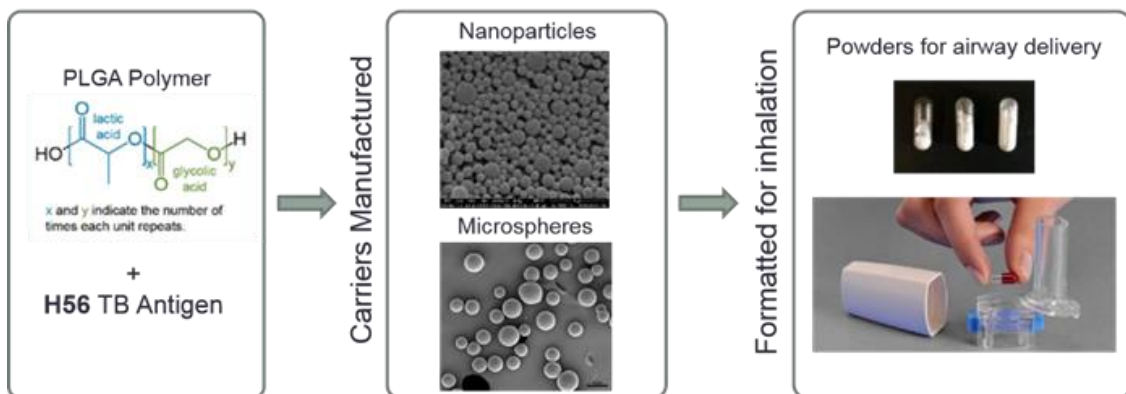
4.5 Conclusions

Altering the control parameters (FRR) of the microfluidics system has shown to control the size of the PLGA nanoparticles obtained as well as the PLGA ratio used with sizes between 95 to 340 nm being prepared depending on the parameters and polymer ratio selected. Furthermore the TFR and therefore the output capability of the system did not impact on these parameters demonstrating the suitable scalability of this system. The formed PLGA nanoparticles were spherical and regular shaped particles with a smooth outer surface suitable for pulmonary delivery. Encapsulation of the H56 tuberculosis antigen was achieved via a one-step in-line microfluidics process showing medium antigen loading (from 20 to 40%). Microfluidics has shown to be a fast, reproducible and easy method for the production of PLGA nanoparticles. However, the microfluidics system was limited to particles below 500 nm which may require further modification for appropriate cell uptake/lung deposition.

PLGA MPs were also formulated in order to have a wide range of particle sizes for further lung uptake and deposition studies.

Chapter 5

Aerodynamic engineering of a PLGA antigen delivery system for pulmonary delivery



5.1 Introduction

Mycobacterium tuberculosis bacilli can spread through the air from one person to another resulting in infection within the lungs. Commonly, alveolar macrophages (AM) are the first line of defence for the clearance of inhaled pathogens. However in the case of TB, AMs are the host site for the infection and this undermines the ability of these macrophages to promote protection. Therefore, formulation of an inhalable delivery system containing TB antigens to target the site of infection could be an interesting approach for the development of a subunit vaccine against this disease. Nano- and microparticles formulated using materials approved by the FDA and EMA for human use (e.g. PLGA) have been extensively investigated for pulmonary delivery due to their high safety profile. PLGA particles suffer hydrolytic degradation when stored in liquid environment for prolonged periods of time. Therefore, techniques such as freeze drying are used to overcome this problem. Preparation of PLGA delivery systems as dry powders can increase the stability of these particles and allow for the engineering of particles with suitable aerodynamic parameters to achieve deposition in the appropriate lung region. In this regard, particle size is one of the main factors dictating the aerosol deposition in the airways. There are three possible mechanisms for particle deposition (impaction, sedimentation and diffusion) and the mechanism is influenced by the size of the formulated particles. Particles larger than 5 μm will be most likely deposited in the upper airways due to impaction whereas particles from 0.5 μm and 5 μm will be deposited due to sedimentation in the lower airways. Particles smaller than 0.5 μm , due to random Brownian motion will be most likely deposited in the alveoli by diffusion, the main drawback is that due to the small particle size, these particles might be exhaled. Thus, an optimum particle size for pulmonary delivery with deposition in the lower airways would be between 0.5 and 5 μm .

5.2 Aim and objectives

This study aimed to develop dry powders for inhalation containing PLGA as delivery system for the delivery of the H56 tuberculosis antigen into the deep lungs (alveoli). To achieve this, the main objectives studied were:

1. Particle engineering of the PLGA nanoparticles: selection of cryoprotectant and freeze drying method for the preparation of dry powders.
2. Aerodynamic diameter and particle deposition within the lungs using a Pharmacopoeia approved airway simulator.
3. Thermal and morphological microscopy for the characterisation of the dry powders.

4. *In vitro* viability, uptake and processing of the PLGA nano- and microparticles in three macrophages cell lines.

5.3 Materials and methods

5.3.1 Materials

For the preparation of delivery systems, poly(lactic-co-glycolic acid) 85:15 (Mw: 50,000-75,000), 75:25 (Mw: 66,000-107,000), 50:50 (Mw: 30,000-60,000), the model antigen ovalbumin (OVA), sodium hydroxide (NaOH), sucrose, L-leucine and the stabiliser polyvinyl alcohol (PVA Mw: 31,000) were purchased from Sigma-Aldrich Company Ltd., Poole, UK. DQ-ovalbumin™ and Dil Stain (1,1'-Dioctadecyl-3,3,3',3'-Tetramethylindocarbocyanine Perchlorate (DiIC) were purchased from ThermoFisher Scientific (Loughborough, UK). The tuberculosis vaccine candidate H56 was donated by Statens Serum Institut (SSI), Copenhagen, Denmark. 2-amino-2-(hydroxymethyl)-1,3-propanediol (Tris) was obtained from ICN Biomedicals Inc. (Aurora, OH, US) and prepared at a 10 mM concentration and pH 7.4 unless otherwise stated. Acetonitrile (ACN), trifluoroacetic acid (TFA) and all other reagents were of analytical grade and purchased from commercial suppliers.

5.3.2 Preparation of PLGA nanoparticles

PLGA nanoparticles were manufactured by the microfluidics method using the Nanoassemblr™ Benchtop (Precision Nanosystems Inc., Vancouver, Canada). Briefly, polymer (either PLGA 85:15, 75:25 or 50:50) was dissolved in acetonitrile at a concentration of 10 mg/mL (1% w/v). For the production of empty nanoparticles, Tris buffer was used as aqueous phase whereas for antigen loaded nanoparticles, antigen (OVA or H56) was loaded in the aqueous phase. The process parameters TFR 10 mL/min and FRR 1:1 were selected and a fixed waste volume was discarded during the production in order to get the core sample (initial and final waste volume of 0.25 and 0.05 mL, respectively). Polymer in solvent and buffer phase were injected into the systems at the selected parameters and the produced PLGA nanoparticles were collected in the outlet. To remove solvent, samples were loaded into a dialysis membrane (Mw= 12,000-14,000 Da, Sigma-Aldrich Company Ltd., Poole, UK) and dialysed for one hour against 250 mL of Tris buffer.

5.3.3 Purification of the PLGA nanoparticles: removal of non-encapsulated antigen

PLGA nanoparticles were purified through this system (KR2i TFF System®, SpectrumLabs, US) at 27 mL/min and they were washed 12 times with buffer (12 washes per 1 mL sample) in order to remove non encapsulated antigen. Due to the incompatibility of the column with the acetonitrile used for the preparation of the nanoparticles, 1 hour dialysis was carried out prior passing the samples through the TFF for removal of the organic solvent. The column used for these purpose was a 750 kDa mPES column which is slightly negatively charged.

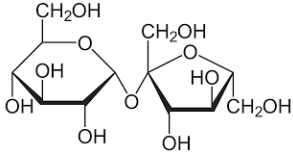
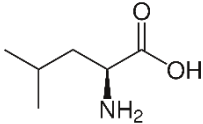
5.3.4 Preparation of PLGA microparticles by the double emulsion method

Briefly, 20 µL of buffer or OVA (10 mg/mL stock) were mixed with 417 µL of 3% PLGA in chloroform and vortexed for 1.5 min in order to form the initial primary emulsion. This primary emulsion was then mixed with 10 mL of PVA (10% w/v in dH₂O) using high speed homogenization (Homogenizer Ultraturrax T25, IKA laboratories) at 8000 rpm during 3 min. Samples were left stirring overnight to remove chloroform. The next day, samples were centrifuged (Hermle Z323K, Labnet International Inc., US.) and washed three times with 10 mL of dH₂O for 20 min at 5500 x g. After the final washing step, the microparticles were reconstituted with Tris buffer.

5.3.5 Freeze drying of nano- and microparticles

The process involves freezing a liquid product, and then removing the water by sublimation under reduced pressure. Under such conditions, a liquid-to-solid-to-vapour transition occurs at low temperatures and reduced pressures, resulting in a dry product. The inclusion of cryoprotectants such as sugars and/or amino acids is generally a prerequisite in order to preserve the initial physicochemical characteristics of the manufactured particles. Table 5.1 shows the cryoprotectants used during the development of the method.

Table 5.1 Type and concentration of cryoprotectant used for the formulation of PLGA nanoparticles in powder format.

Cryoprotectant	Concentration (w/v) (%)
Sucrose 	3%, 5%, 7%, 10%
Leucine 	0.5%, 0.7%, 1%
Sucrose + Leucine	3 + 0.7%, 3 + 1%, 10 + 0.7%, 10 + 1%

For the preparation of the polymer particles for freeze drying, samples were manufactured using microfluidics and the double emulsion solvent evaporation method. For microfluidics, 1 mL of cryoprotectant was added into 1 mL nanoparticle formulation. For microsphere formulation, the cryoprotectant was used to reconstitute the microspheres after the third washing step. Both, nano- and microparticles were frozen for minimum 2 hours at -80°C and then introduced into the freeze drying machine with the following settings: main drying was set at -50°C for 18 hours and final drying was set at -20°C for 6 hours. These setting were based on a modification of the method developed by Mohammed et al. [258, 259].

5.3.6 Antigen release study of PLGA reconstituted nanoparticles

Purified PLGA nanoparticles encapsulating OVA (1 mL) were transferred to dialysis tubing (300 kDa) and introduced into a beaker containing 40 mL of release media (PBS pH 7.4 10 mM). This beaker was incubated at 37°C in a shaking bath at 60 rpm. Antigen release was measured by quantification of the remaining antigen concentration inside the nanoparticles at 1, 4 and 6 hours.

5.3.7 HPLC-UV for antigen quantification

Quantification of the protein loading within the PLGA nanoparticles was performed by reverse phase HPLC (RP-HPLC) using a UV detector. Jupiter 5 μ C18(2) column (Phenomenex) pore size 300 Å was

used as stationary phase. For the preparation of the calibration standards, proteins were dissolved in 0.1 M NaOH/Tris buffer (1:1 v/v) and heated up for approx. 1.5 - 2 hours in a waterbath at 35°C. Samples were prepared in the same fashion but in this case just adding NaOH as the samples are formulated in Tris buffer. A gradient elution method was followed and both mobile phases contained the same solvents in different proportions (Mobile phase A: 90% H₂O, 10% acetonitrile and 0.1% TFA; Mobile phase B: 70% acetonitrile, 30% H₂O and 0.1% TFA) in order to favour the mixing of both phases during the run. The instrument settings were as follows: 50 µL injection volume, flow rate 1 mL/min, UV wavelength 210 nm and column temperature either 25°C (OVA) or 60°C (H56).

5.3.8 HOT-stage microscopy

Hot stage microscopy was used to study the melting temperatures of the PLGA powders and the starting materials. A hot stage (MettlerToledo FP90HT, Switzerland) with a Mettler Toledo central processor was attached to the microscope. The powder sample was mounted on a microscope glass slide with a coverslip and heated from 30°C to 300°C at a rate of 6°C/min. Images were recorded using a Leica camera attached to the microscope.

5.3.9 Dynamic Light Scattering

5.3.9.1 Malvern nano ZS

The particle size of the polymer nanoparticles was determined by dynamic light scattering (DLS) using a Malvern nano ZS (Malvern Instruments, Worcestershire, UK). Three measurements at 25°C were conducted on the samples, which were previously diluted in filtered Tris buffer (10 mM, pH 7.4). For zeta potential samples were diluted in the same fashion as for the size and a cell capillary electrophoresis cuvette was used. For collection and data analysis Malvern Dispersion Technology Software (DTS) v.7.12 (Malvern Instruments, Worcestershire, UK) was used.

5.3.9.2 Mastersizer 2000

The size of the microparticles was determined by laser diffraction analysis using a Mastersizer 2000 (Malvern Instruments). Samples were dispersed into the sample dispersion cell unit until the right obscuration was obtained (above 10%) while stirring at 2000 rpm. Water was used as dispersant agent and PLGA refractive index was set at 1.43. Three measurements of each sample were recorded every

12 seconds. For zeta potential, Zetasizer nano ZS was used. Samples were diluted in Tris buffer in the same fashion as the nanoparticles (20-fold dilution).

5.3.10 Scanning electron microscopy

Antigen loaded PLGA micro- and nanoparticles (sample) were fixed and air dried onto a metal stub and then coated with gold and observed under the microscope. This procedure was carried out by David McCarthy from DMmicroscopy.

5.3.11 Pharmacopoeia airway simulator: Next Generation Impactor (NGI)

The *in vitro* aerosol dispersion performance of the PLGA-loaded dry powders was determined using a Next Generation Impactor (NGI™; Copley Scientific Ltd., Nottingham, UK) equipped with vacuum pump (Model HCP5) and a critical flow controller (TPK 2000). In brief, approximately 20 mg of powder sample was manually filled into a size 3 hydroxypropyl methyl cellulose (HPMC) capsule and inserted into the aeroliser (Plastiaple Monodose Dry Powder Inhaler, Plastiaple S.p.a, Milan, Italy). By pushing the side buttons of the aeroliser, the end of the capsules were punctured prior to aerosolisation. The air flow rate was verified and adjusted to $60 \pm 5\%$ L/min using an electronic digital flow meter. The aeroliser with the punctured capsule was attached to the induction port through a silicone mouthpiece adaptor. Each capsule was aerosolized at flow rate 60 L/min for 4 s (temperature = 23°C; Pa = 101.6 kPa; Relative Humidity = 41.7%). After each shot, the powders deposited in the induction port and in all the stages were collected by rinsing with ultrapure water and analysed as percentage deposition of the powders using BCA assay. The NGI effective cut-off diameters at $60 \pm 5\%$ L/min for each impaction stage according to the manufacturer are displayed in Table 5.2. *In vitro* aerosolisation studies were performed in triplicate for each sample and the following equations were used for the calculation and analysis of the aerosol performance of the dry powders:

Fine particle dose (FPD) = mass of particles on Stages 2 through 7

$$\text{Fine particle fraction (FPF)} = \frac{\text{Fine particle dose}}{\text{Initial particle mass loaded into the capsules}} * 100\%$$

$$\text{Respirable fraction (RF)} = \frac{\text{Mass of particles on stages 2 to 7}}{\text{Total particle mass on all stages}} * 100\%$$

$$\text{Emitted dose (ED)} = \frac{\text{Initial mass in capsules} - \text{final mass remaining in capsules}}{\text{Initial mass in capsules}} * 100\%$$

The mass median aerodynamic diameter (MMAD) was calculated from plotting the logarithm of the cut-off diameters against the cumulative mass percentage calculated from each stage. From that graph, the MMAD was determined as the point where 50% of particle deposition crossed the x-axis.

Table 5.2 Cut-off diameters of the Next Generation Impactor stages at flow rate $60 \pm 5\%$ L/min.

NGI stages	Cut-off diameters
Stage 1	8.06 μm
Stage 2	4.46 μm
Stage 3	2.82 μm
Stage 4	1.66 μm
Stage 5	0.94 μm
Stage 6	0.55 μm
Stage 7	0.34 μm
MOC	< 0.34 μm

5.3.12 Bicinchoninic acid assay (BCA) for the quantification of polymer recovered after NGI

The bicinchoninic acid (BCA) assay (Pierce™ BCA Protein Assay Kit, Sigma Aldrich, Poole, UK) was used for the quantification of polymer recovered from each stage of the NGI. Briefly, 25 μL of sample was pipetted into a 96-well plate and 200 μL of working reagent (reagent A + B at a ratio 50:1 v/v) was added on top. The plate was incubated for 30 mins at 37°C and the absorbance was read at 562 nm. A standard curve for the calculation of the concentration found was performed in triplicate. PLGA loaded nano- or microparticles after freeze drying were used for the preparation of the standard curves.

5.3.13 *In vitro* studies

In vitro studies for the PLGA nano- and microparticles were carried out in collaboration with Maryam Hussain, a fellow Ph.D. student from our group. Cell viability, nanoparticle uptake and antigen processing studies were carried out in both loaded PLGA nanoparticles and microparticles. These antigen loaded PLGA NPs and MPs formulated by either microfluidics or the double emulsion method were tested *in vitro* in a variety of macrophages cell lines: THP-1, MH-S and RAW264.7.

- **THP-1 cells – human monocytes**

THP-1 cells were obtained from ECACC (European Collection of Authorized Cell Cultures). They are a continuous cell line derived from human blood monocytes. In order to use the cells as macrophages, the human monocytes need to be stimulated to undergo differentiation. To induce differentiation, Vitamin D3 (VD3) is added to the cells at 100 nM (1:1000 dilution). The cells are then poured into a petri dish and left for 48 hours to undergo differentiation. The marker CD14 is used to confirm the cells have undergone differentiation into macrophages using flow cytometry.

- **RAW 264.7 cells – mouse macrophages**

RAW264.7 cells were a gift from Dr. Andy Paul (University of Strathclyde, SIPBS). They are a continuous cell line derived from macrophages of mouse origin. The cells are adherent and are grown in Dulbecco's modification of Eagle medium (DMEM) supplemented with 10% FBS and Penicillin-Streptomycine allowed to grow till 60 - 70% confluency before being passaged.

- **MH-S cell line – mouse alveolar macrophages**

MH-S cells are mouse derived alveolar macrophages. They are adherent in nature and are circular in shape. These cells were obtained from ECACC. The cell line was derived by SV40 transformation of adherent alveolar macrophages from a seven week old male. The cells retain many of the properties of alveolar macrophages including morphology, phagocytic nature, esterase positive and peroxidase negative. Treatment with lipopolysaccharide (LPS) encourages the production of IL-1. The cells are grown using complete RPMI with 0.05 M 2-mercaptoethanol and 10% FBS.

5.3.13.1 Cell viability

For the determination of the cell viability or toxicity after incorporation of the PLGA particles, an *in vitro* colorimetric assay was used. The selected method was the Cell Titre blue (CTB) assay which is based on the ability of active cells to convert resazurin into the fluorescent product resorufin. This metabolic conversion will cause a visual colour change from blue to pink if cells are alive. The amount of live cells can be quantified using a spectrophotometer at 590 nm wavelength.

Confluent cells (THP-1, MH-S or RAW264.7) were plated on a 96 well plate at a density of $1-2 \times 10^6$ /mL, which was calculated by cell counting using a light microscope. Cells were allowed to settle for 24 hours before addition of the particles and subsequently, PLGA nano- and microparticles were added at a concentration of 0.006 - 0.2 mg/mL for 24 hours. CBT was added to these wells at a volume of 20 μ l per 100 μ l of media, and left until a colour change occurred (approximately 1 to 5 h). Based on the

viable cell difference between the positive control, which was represented by cells without exposure to the PLGA particles, and the sample test, cell viability was calculated. Three controls were used during the experiments: a negative control containing cells exposed to PLGA particles and lysed, PLGA particles in absence of cells and a positive control containing untreated cells.

5.3.13.2 Particle uptake

For the quantification of the PLGA particles uptake by the three cell lines used, particles were fluorescently labelled with the fluorophore 1,1'-Diiodo-3,3',3'-Tetramethylindocarbocyanine Perchlorate (DiIC). A small volume of DiIC (0.5 μL per mL of sample) was added into the polymer stock before formulation of the nano- and microparticles, as larger volumes of DiIC increased the size of the polymer particles. Fluorescently labelled PLGA NPs and MPs were diluted to a concentration of 20 $\mu\text{g}/\text{ml}$ in serum free RPMI 1640 medium and added at 1:1 v/v ratio to the cells which were plated at a density of 1×10^5 cells/mL in 24 well plates. This mixture was incubated at 37°C 5% CO₂ and at specific intervals (0.5, 1, 2 and 3 h) 200 μl of co-culture was mixed with 200 μl of ice cold cRPMI before analysis. Interaction of fluorescent PLGA NPs and MPs with the cells was analysed via flow cytometry (BD FACSCanto) using a minimum of 5000 events per sample. A parallel experiment was carried out with the cells kept at 4°C to stop endocytosis as a negative control experiment.

5.3.13.3 DQ-OVA processing

The DQ™ovalbumin is a self-quenched conjugate used for the quantification of the amount of OVA processed by cells. The DQ-OVA is conjugated to the dye BODIPY FL and only fluoresces once the OVA undergoes enzymatic degradation by the cells. If degradation occurs the DQ-OVA exhibits bright green fluorescence.

PLGA NPs and MPs encapsulating a mixture (1:1 w/w) of OVA and DQ-OVA were produced by either microfluidics or the double emulsion method and diluted to a concentration of 20 $\mu\text{g}/\text{ml}$ in serum free RPMI 1640 medium and added at 1:1 v/v ratio to the plated cells (cell density 1×10^5 cells/mL in 24 well plates). This mixture was incubated at 37°C 5% CO₂ and at selected time points 200 μL of co-culture was mixed with 200 μl of ice cold cRPMI before analysis. The cells were then added to flow cytometer tubes and measured using the BD FACSCanto at 505/515 nm of excitation/emission wavelengths.

5.3.14 Statistical analysis

One-way ANOVA and two-way ANOVA followed by Tukey's multiple comparison test were used for the data analysis. All the experiments were carried out in triplicate unless otherwise stated. Results are the mean of at least 3 measurements \pm SD. Standard deviation is plotted as error bars. Results $p < 0.05$ were considered statistically significant.

5.4 Results and discussion

In chapter 4, the production of antigen loaded PLGA nanoparticles manufactured using the microfluidics was optimised. Therefore, formulations prepared at selected process parameters were used for the production of dry powders for inhalation in further experiments. According to the obtained results, the TFR did not significantly alter neither the particle size nor the loading of the nanoparticles, thus, TFR of 10 mL/min was chosen (since it is medium speed at which nanoparticles can be formulated). These particles are aimed to be delivered to the deep lungs, specifically the AM which, as reported in literature, should have particle sizes from 500 nm to 5 μ m for a better deep lung deposition and interaction with AMs [148, 149]. The FRR was the main parameter dictating the particle size; therefore, FRR 1:1 was selected as this ratio produced the largest particle sizes. As the loaded PLGA nanoparticles produced used microfluidics ranged from 100 nm to 500 nm, further aerodynamic modification of the particles is needed. Besides, direct inhalation of the PLGA nanoparticles is not possible due to its particle size (sub-micron), as they would be exhaled [260]. Consequently, these PLGA NPs were formulated as dry powders using freeze drying with prior addition of cryoprotectants to prevent these particles from agglomeration/fusion [134, 261, 262].

5.4.1 Selection of the adequate cryoprotectant

One of the main problems limiting the use of PLGA for the development as a delivery system is its physical and chemical instability in aqueous suspensions. After a prolonged period of time, PLGA particles tend to fuse/aggregate and the payload leaks from the particle due to hydrolytic degradation/erosion [263-265]. An optimal method to enhance the nanoparticles stability is freeze drying (also known as lyophilisation). Freeze drying generally consists of three steps: freezing (solidification), primary drying (sublimation) and secondary drying (desorption) [264]. However, this method also promotes fusion or aggregation of the particles, which can occur during the freezing step due to the formation of ice crystals and/or during the drying step due to the removal of the water content from the formulation [264, 266]. For this reason, cryoprotectants are added prior to freezing

to protect and to stabilise the NPs, preserving their physical and chemical characteristics and helping with the redispersion of the powder in aqueous media [266-268]. The most common cryoprotectants are sugars which exert their stabilising effect through the formation of hydrogen bonds with the polar groups at the NPs surface. This hypothesis is known as the water replacement theory which is named due to their mechanism of action (sugars act as water substitutes). These sugars create a glassy matrix around the nanoparticles, immobilising the nanoparticles and thus avoiding aggregation due to the mechanical stress produced during the formation of ice crystals [269]. This protection depends on the cryoprotectant ability to form this glassy matrix around the particles which is proportional to the cryoprotectant concentration [264, 265]. Another hypothesis of the mechanism of action of sugars is the particle isolation theory, which takes place during the freezing step (above T_g) and whereby sugars avoid aggregation of the NPs by isolating particles in the unfrozen part [270]. Amino acids such as alanine, leucine and glycine are also used in the formulations of dry powders working as dispersibility enhancers and improving aerosolisation performance of the powders for inhalation [271-273].

Therefore, in order to screen the effect of the addition of cryoprotectants in the PLGA nanoparticles, different concentrations of the nonreducing sugar sucrose and the amino acid L-leucine were externally added into the samples. Sucrose was added at concentrations of 3%, 5%, 7% and 10% (w/v) whereas L-leucine was added at a concentration of 0.5%, 0.7% and 1% (w/v). Samples were freeze-dried for 24 hours and then reconstituted with ultrapure water prior to measure their physicochemical characteristics including size, PDI and zeta potential.

5.4.1.1 Effect of sucrose

The PLGA-NP produced using microfluidics at a total flow rate of 10 mL/min and a flow rate ratio of 1:1 (aqueous:organic phase ratio) were freeze-dried with and without cryoprotectants present. Figure 5.1 shows the effect of the addition of sucrose on 'empty' PLGA NPs for the copolymers 50:50, 75:25 and 85:15. PLGA NPs without the addition of cryoprotectant were agglomerated and difficult to redisperse giving all three copolymers particles in the micrometre range and highly heterodisperse (results not shown). The size of the PLGA 50:50 nanoparticles particles was ~110 nm with a low polydispersity index (below 0.2) (Figure 5.1A). When only 3% of sucrose was added into the formulation, the size of the particles significantly ($p < 0.05$) increased, up to approximately 300 nm and the samples were more heterogeneous in nature, with a PDI from 0.3 to 0.4 (Figure 5.1A). However, PLGA 50:50 nanoparticles with 5%, 7% and 10% sucrose did not significantly change in size nor the polydispersity after freeze-drying and resuspension.

The particle size of the PLGA 75:25 nanoparticles after microfluidics and prior to freeze drying was ~170 nm, with a PDI below 0.2. After addition of 3% of sucrose the size and PDI of the particles increased up to 300 nm and 0.4 respectively (Figure 5.1B). As seen for PLGA 50:50, after addition of higher sucrose concentrations, PLGA 75:25 nanoparticles were stable in terms of size and PDI, no significant differences were found. In contrast the size and PDI of the PLGA 85:15 nanoparticles (Figure 5.1C) was preserved independent to the amount of sucrose added (3 to 10%; Figure 5.1C).

It has been reported elsewhere the need for cryoprotectants for the preparation of PLGA particles to prevent aggregation and assist in the reconstitution of the dry powders [274]. The level of cryoprotection is related to the concentration and type of cryoprotectant added to the formulation [264]. Thus, the ratio between the sugar and the polymer has to be optimised, and in this case it has been demonstrated that the necessary concentration of sucrose to protect the polymer from aggregation is above 3% (w/v) for a PLGA formulation of 5 mg/mL. For example, Saez et al. showed that PLGA NPs could be freeze dried with satisfactory results when sucrose was added at a concentration of 20% [275]. Chacon et al. demonstrated that at least 5% of cryoprotectant is fundamental to preserve the initial particle characteristics [276]. In general, higher concentrations of sugar produce better protection and redispersion of the formulation [277]. However, care should be taken when increasing the concentration of sugar as it can reach a point where the stabilisation limit is reached and consequently, the formulation destabilises and aggregates [259, 278]. In this case, it is suggested that 3% w/v sucrose is not enough to stabilise the NPs and resulted in slight aggregation of the polymer due to lack of sugar to form H-bonds with the polymer during the drying process (water replacement theory).

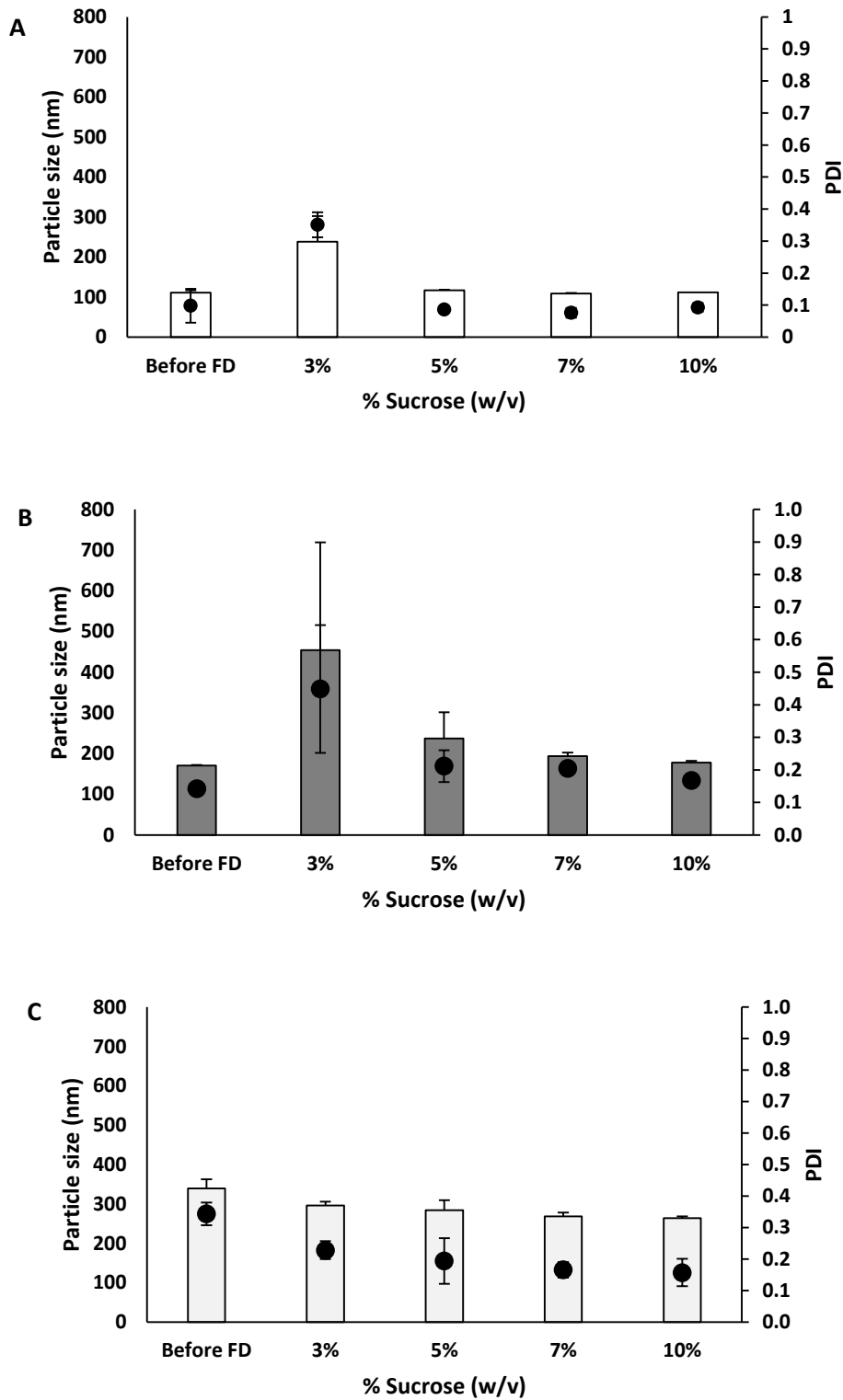


Figure 5.1 Particle size and particle size distribution of the empty PLGA (A) 50:50, (B) 75:25 and (C) 85:15 nanoparticles after addition of 3, 5, 7 and 10% w/v sucrose into the formulation prior freeze drying and reconstitution with ultrapure water. Results represent the mean \pm SD of at least three independent batches.

The zeta potential of the formulations was also measured and no significant difference was measured between them. All the formulations remained highly anionic after the addition of sucrose as cryoprotectant as it is characteristic of PLGA [279, 280]. (Figure 5.2). Zeta potential is an important characteristic as the nanoparticles will interact with cells, so the charge plays a role in the interaction. It has been reported that the anionic surface of PLGA particles favour their internalisation by phagocytic cells (e.g. macrophages) [281].

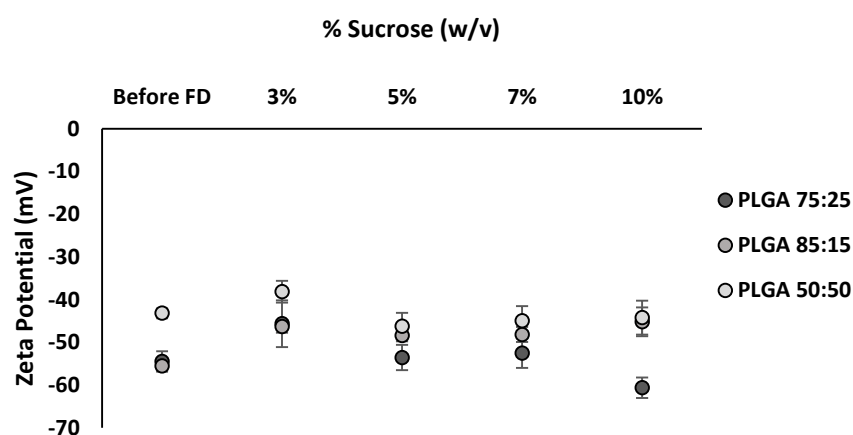


Figure 5.2 ZP of all three copolymers after addition of 3, 5, 7 and 10% w/v sucrose into the formulation prior freeze drying and reconstitution with ultrapure water. Results represent the mean \pm SD of at least three independent batches.

5.4.1.2 Effect of leucine

Leucine was added into the formulations at three different concentrations due to its performance as a dispersibility enhancer and improvement of the aerosolisation behaviour of the powders [271]. The addition of the amino acid resulted in a significant increase of the particle size and polydispersity of the samples (Figure 5.3A-C). In general, results were very variable for all three PLGA copolymers with the particle size increasing after the incorporation of leucine into the formulation independently of the concentration of cryoprotectant added. No obvious trend related to the amount of leucine added was observed. Zeta potential values did not significantly change for PLGA 50:50 being \sim -40 mV, whereas for PLGA 75:25 and 85:15 the ZP significantly increased ($p < 0.01$) after freeze drying. Nevertheless, all the particles retained the negative zeta potential after FD (Figure 5.4).

Seville et al. investigated the use of amino acids as dispersibility enhancer for the delivery of salbutamol as a powder for inhalation using spray drying [271]. Among all the amino acids investigated, leucine showed to be the best for improving the aerosolisation properties. The mechanism of action whereby leucine enhances the aerosolisation performance of the dried powders

is due to the surfactant like behaviour of this amino acid, which alters the surface of the particles [272, 273]. The hydrophobicity related to leucine might be the explanation for the increase in particle size upon its incorporation onto the PLGA formulations.

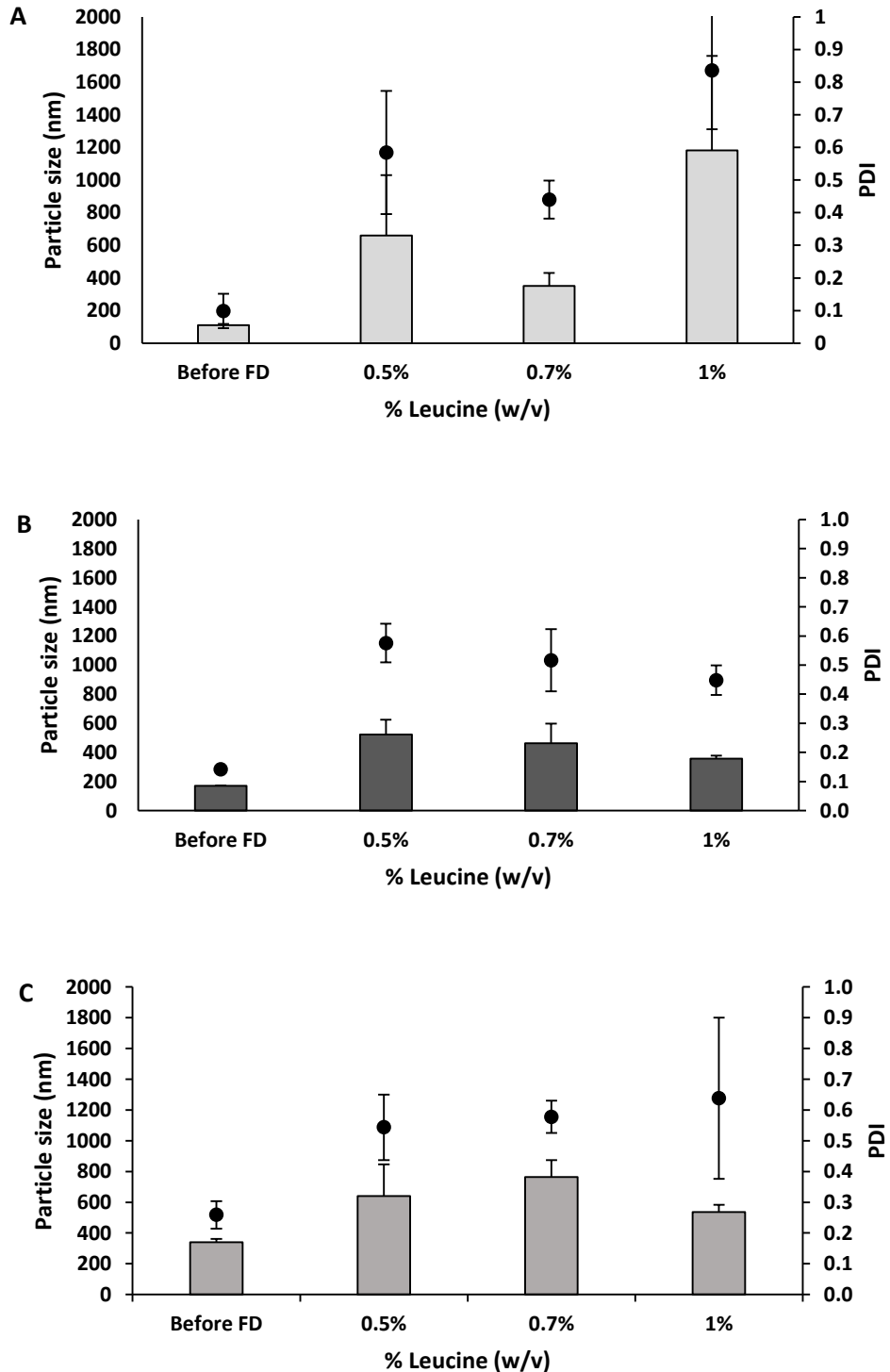


Figure 5.3 Particle size and particle size distribution of the empty PLGA (A) 50:50, (B) 75:25, (C) 85:15 nanoparticles after addition of 0.5, 0.7 and 1% w/v leucine into the formulation prior freeze drying and reconstitution with ultrapure water.

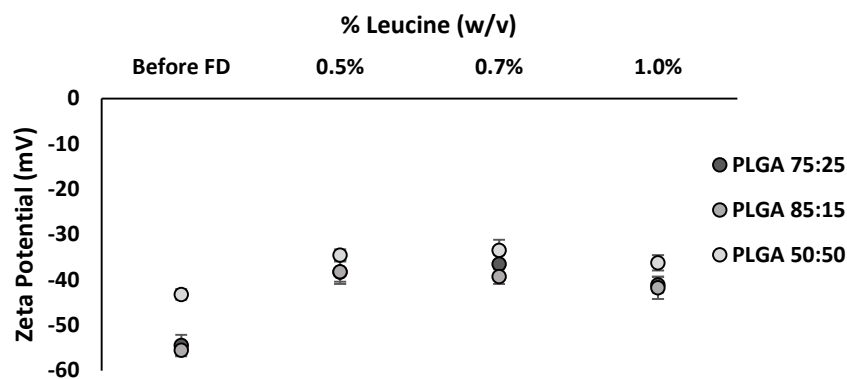


Figure 5.4 ZP of all three copolymers after addition of 0.5, 0.7 and 1% w/v leucine into the formulation prior freeze drying and reconstitution with ultrapure water.

5.4.1.3 The effect of combining both sucrose and leucine within a dried nanoparticle product

To further develop a freeze-dried nanoparticle formulation for inhalation, the combination of sucrose (as a cryoprotectant) and leucine (for improved aerosolisation) was considered. The selected formulations were 10% or 3% (w/v) sucrose in combination with 0.7% and 1% (w/v) leucine. Two options with four combinations were evaluated. Initially, the possibility of reducing the amount of sucrose in the formulation by incorporating leucine was considered. For this reason 3% (w/v) sucrose was selected. Therefore, 0.7 and 1% (w/v) leucine was added into the formulations. Next, to make sure that the PLGA nanoparticles were protected after FD, 10% (w/v) sucrose in combination with 0.7 and 1% w/v leucine was selected. Addition of the cryoprotectant combinations to all three PLGA nanoparticles resulted in an increased particle size and PDI (Figure 5.5). The formulations containing 10 % sucrose tended to show smaller particle sizes and PDI after reconstitution compared to the 3 % sucrose, irrespective of the leucine content or the PLGA copolymer blend. In terms of leucine content, there was no significant difference in particles freeze-dried with 0.7 and 1 % w/v. Figure 5.6 shows the zeta potential values for the formulations, which were all highly anionic with no notable difference.

The addition of leucine onto the formulations is desirable in order to improve the deposition into the deeper lungs and enhance the aerosolisation behaviour since it decreases the cohesivity of the particles and is also approved by the FDA as an excipient for inhalation delivery [134]. Eedara et al. used leucine in combination with 1,2-dipalmitoylphosphatidylcholine (DPPC) to deliver two anti-TB drugs into the deep lungs for the treatment of pulmonary TB [153, 154].

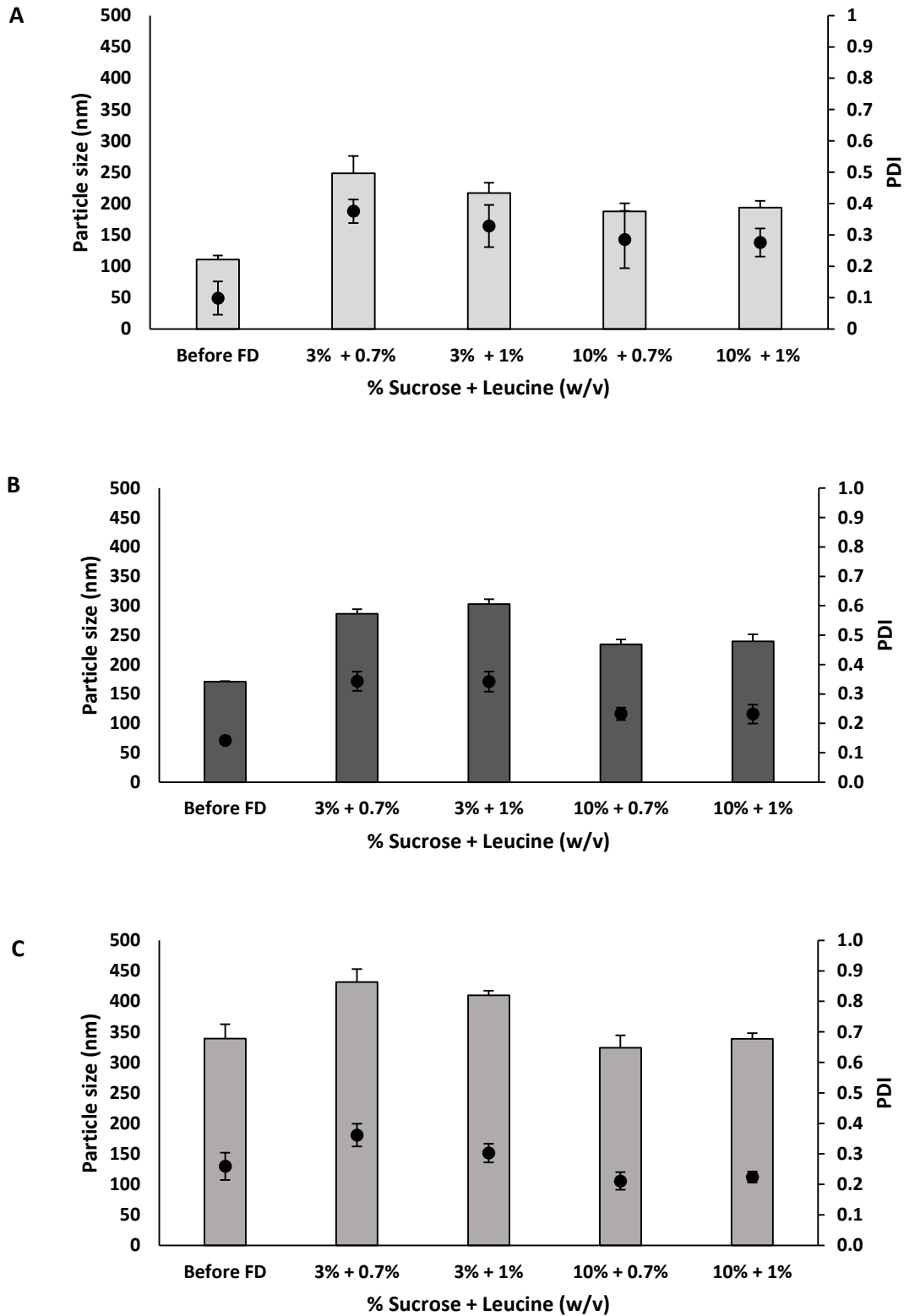


Figure 5.5 Particle size and particle distribution of the empty PLGA (A) 50:50, (B) 75:25 (C) 85:15 nanoparticles and (D) ZP of all three copolymers after addition of: 3% sucrose in combination with 0.5% or 1% (w/v) leucine; 10% sucrose in combination with 0.5% or 1% leucine into the formulation prior freeze drying and reconstitution with ultrapure water.

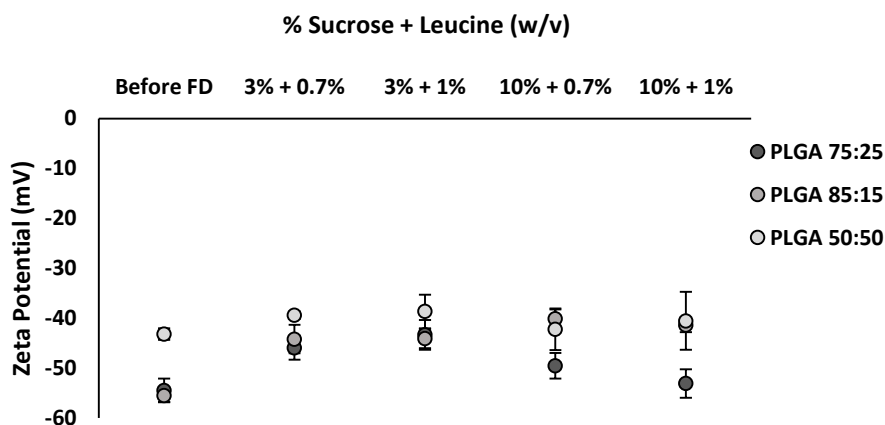


Figure 5.6 ZP of all three copolymers after addition of: 3% sucrose in combination with 0.5% or 1% (w/v) leucine; 10% sucrose in combination with 0.5% or 1% leucine into the formulation prior freeze drying and reconstitution with ultrapure water.

5.4.2 Characterisation of the PLGA particulate delivery systems (nano- and microparticles) after Freeze-drying

From the results in Figure 5.5 and 5.6, the combination of 10% (w/v) sucrose and 1% (w/v) leucine was chosen for further experiments. Therefore, these concentrations were added onto the PLGA MPs produced by the w/o/w method described in the previous chapter (Chapter 4). These selected PLGA NPs and MPs were formulated in a dry powder format with or without the addition of antigen (Table 5.3 and 5.4).

PLGA particles formulated using microfluidics were produced at TFR 10 mL/min and FRR 1:1. The largest sizes were seen with PLGA 85:15 followed by PLGA 75:25 and 50:50 with mean particle sizes approximately 300 nm, 200 nm and 100 nm respectively (Table 5.3). After freeze drying of the nanoparticles with the combination of 10% sucrose and 1% leucine incorporated within, the mean particle size of the PLGA 50:50 and 75:25 NPs increased after reconstitution with ultrapure water. In contrast, PLGA 85:15 NPs did not change in terms of particle size (Table 5.3). All PLGA NPs were homogenous in nature with PDIs below 0.25. All empty nanoparticles preserved the highly anionic zeta potential after FD (Table 5.3).

Incorporation of the antigen into the formulations did not increase the particle size when compared to the empty nanoparticles, therefore the physicochemical characteristics remained unaffected (Table 5.3). On the other hand, when antigen loaded NPs were freeze dried, all three copolymer NPs increased in size yet the polydispersity and zeta potential values were preserved after FD suggesting that a small degree of fusion/aggregation may be occurring during the FD process.

For the preparation of larger PLGA particles the double emulsion method was used. Table 5.4 shows D50 values (also known as mass median diameter) for the particle sizes obtained before freeze drying and after reconstitution of the dry powder for each PLGA copolymer. PLGA 85:15 microspheres showed the largest sizes (around 1.5 μm), followed by PLGA 75:25 microspheres and PLGA 50:50 with particle sizes of approximately 1.3 and 1 μm respectively. None of the particles showed a significant increase in size after freeze drying being all the particles in the range from 1 to 1.5 μm .

When antigen was incorporated into the formulation, microspheres sizes did not increase in particle size. In general, the particle size population D50 was between 1 – 1.3 μm . It has been reported in the literature that PVA remains on the surface of the microparticles even after washing. The presence of PVA associated to the MPs surface might further improve the lyophilisation of the microparticles by stabilising them [282]. SPAN values, which are representative of the width of the particle size distribution, were all in the range of 0.9 to 1.1 independent of the copolymer used, the addition of cryoprotectant and the incorporation of antigen. Besides, all the microparticles displayed neutral zeta potential values. This is due to the presence of PVA on the surface of the PLGA MPs, although PLGA MPs were centrifuged and washed to eliminate the PVA from the formulations, it has been reported the existence of residual PVA on the surface of the particles, and thus, this PVA increases the zeta potential to neutral values [264].

Table 5.3 Physicochemical characteristics of the empty and antigen loaded PLGA nanoparticles manufactured using microfluidics TFR 10 mL/min, FRR 1:1 containing 10% (w/v) sucrose and 1% LEU (w/v) before freeze drying and after reconstitution of the dried powders. All results represent the mean \pm SD of at least 3 different batches.

PLGA copolymer	EMPTY NANOPARTICLES						ANTIGEN LOADED NANOPARTICLES							
	<u>Before FD</u>			<u>After FD</u>			<u>Before FD</u>				<u>After FD</u>			
	Size (nm)	PDI	ZP (mV)	Size (nm)	PDI	ZP (mV)	Size (nm)	PDI	ZP (mV)	Antigen loading (%)	Size (nm)	PDI	ZP (mV)	Antigen loading (%)
PLGA 50:50	112.3 \pm 0.9	0.09 \pm 0.01	-41.8 \pm 3.8	153.3 \pm 2.12	0.15 \pm 0.01	-36.8 \pm 4.3	114.9 \pm 1.2	0.12 \pm 0.03	-43.7 \pm 0.04	17.6 \pm 3.0	152.3 \pm 22.9	0.11 \pm 0.05	-45.4 \pm 1.6	12.0 \pm 3.0
PLGA 75:25	199.0 \pm 6.6	0.13 \pm 0.02	-55.1 \pm 1.7	239.0 \pm 18.6	0.17 \pm 0.01	-56.6 \pm 1.9	231.0 \pm 7.3	0.24 \pm 0.04	-54.4 \pm 2.7	25.9 \pm 4.1	248.0 \pm 36.6	0.23 \pm 0.06	-54.6 \pm 2.6	19.9 \pm 3.4
PLGA 85:15	331.2 \pm 4.7	0.16 \pm 0.02	-44.0 \pm 1.5	338.2 \pm 14.2	0.21 \pm 0.05	-37.4 \pm 3.1	333.2 \pm 8.7	0.32 \pm 0.07	-44.4 \pm 2.9	36.7 \pm 9.3	375.6 \pm 48.0	0.19 \pm 0.1	-43.8 \pm 1.0	29.4 \pm 6.3

Table 5.4 Physicochemical characteristics of the empty and antigen loaded PLGA microparticles manufactured using microfluidics TFR 10 mL/min, FRR 1:1 containing 10% (w/v) sucrose and 1% LEU (w/v) before freeze drying in and after reconstitution of the dried powders. All results represent the mean \pm SD of at least 3 different batches.

PLGA copolymer	EMPTY MICROPARTICLES						ANTIGEN LOADED MICROPARTICLES							
	<u>Before FD</u>			<u>After FD</u>			<u>Before FD</u>				<u>After FD</u>			
	Size (μm) D50	SPAN	ZP (mV)	Size (μm) D50	SPAN	ZP (mV)	Size (μm) D50	SPAN	ZP (mV)	Antigen loading (%)	Size (μm) D50	SPAN	ZP (mV)	Antigen loading (%)
PLGA 50:50	1.03 \pm 0.02	1.2 \pm 0.01	-1.0 \pm 0.3	1.13 \pm 0.06	1.1 \pm 0.02	-2.7 \pm 0.1	1.15 \pm 0.03	1.07 \pm 0.05	-0.2 \pm 0.4	11.3 \pm 1.0	1.18 \pm 0.08	1.04 \pm 0.07	-0.6 \pm 0.3	8.44 \pm 0.01
PLGA 75:25	1.32 \pm 0.08	1.1 \pm 0.10	-1.3 \pm 0.6	1.27 \pm 0.04	0.9 \pm 0.05	-1.6 \pm 0.7	1.14 \pm 0.05	1.03 \pm 0.01	-0.2 \pm 0.3	18.5 \pm 4.3	1.20 \pm 0.02	1.10 \pm 0.07	-0.6 \pm 0.2	10.3 \pm 0.01
PLGA 85:15	1.56 \pm 0.07	0.9 \pm 0.12	-0.5 \pm 0.2	1.47 \pm 0.06	1.0 \pm 0.12	-3.7 \pm 1.0	1.31 \pm 0.05	1.13 \pm 0.01	-0.1 \pm 0.2	29.4 \pm 3.3	1.18 \pm 0.08	1.07 \pm 0.11	-0.6 \pm 0.3	21.7 \pm 0.01

Visual inspection of the samples demonstrated that all three copolymers, independent of the manufacturing method, had a cloudy appearance before freeze drying and after reconstitution with ultrapure water. The powder cakes formed during freeze drying were completely reconstituted after addition of ultrapure water and no visual aggregation could be seen. PLGA MPs were faster and easier to reconstitute compared to PLGA NPs. Both, nano and microparticles retained the same appearance before FD and after reconstitution. It has been reported in literature that the PVA (stabiliser) used during the production of PLGA particles by the w/o/w method remains in the nano- or microparticle surface despite of the many washing steps [243, 283]. The residual PVA contributes to the stabilisation of the polymer particles as well as improving protection during the freezing step. Therefore, it is hypothesised that this residual PVA assist with the reconstitution of the dry powders.

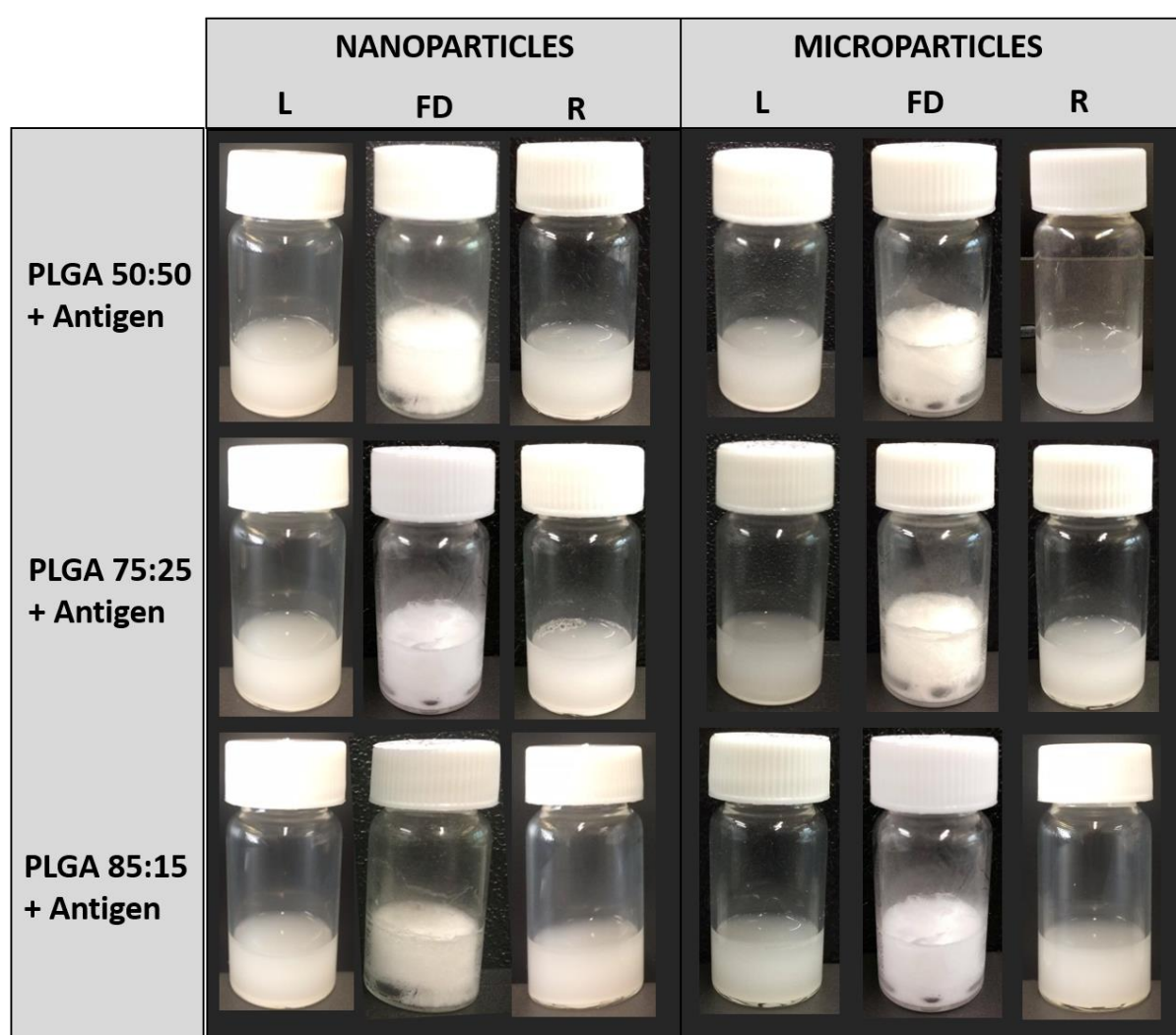


Figure 5.7 Visual inspection of the antigen loaded PLGA nanoparticles and microparticles before freeze drying, after freeze drying (dry powder) and after reconstitution to the original volume with ultrapure water.

5.4.3 Antigen release profiles from PLGA nanoparticles

The release profile of the PLGA nanoparticles after freeze drying was studied. Samples were freeze dried for 24 hours and reconstituted with ultrapure water back to the initial volume. PLGA NPs were dialysed (300 KDa) against PBS pH 7.4 10 mM at 37°C in a shaking bath (60 rpm). Overall, from the results shown in Figure 5.8 an initial burst release of antigen can be observed for all three copolymers NPs (20-40 % of loaded antigen). This is more marked for PLGA 50:50 NPs as they degrade the fastest [102]. PLGA 50:50 NPs approximately released 35% of the initial antigen loaded during the first hour, releasing up to 50% after 6 hours. PLGA 85:15 and 75:25 NPs released 40% and 30% of the initial payload respectively. The release of the freeze dried antigen loaded PLGA NPs was reduced when compared to the non-freeze dried PLGA NPs without cryoprotectant investigated in Chapter 4 (Table 5.5).

Table 5.5 Results from the release study carried out on PLGA NPs loading OVA before freeze drying and described in Chapter 4.

Time points (hours)	% Antigen inside the PLGA NPs (mean \pm SD)		
	PLGA 85:15 FRR 1:1	PLGA 75:25 FRR 1:1	PLGA 50:50 FRR 1:1
0	100 \pm 8.3	100 \pm 2.5	100 \pm 2.1
1	74 \pm 3.9	80 \pm 1.5	67 \pm 0.9
4	59 \pm 1.1	77 \pm 1.5	56 \pm 1.3
6	56 \pm 1.2	62 \pm 1.9	46 \pm 1.1

As seen in literature PLGA particles commonly show a characteristic biphasic or triphasic behaviour which consist on a burst release during the first hours, which according to literature corresponds to the amount of antigen loaded on the surface or in the matrix followed by a sustained released due to hydrolytic degradation of the polymer and in some cases a final burst release [102, 279, 284]. Due to the short duration of the release study, only the burst release could be detected, but it is hypothesised that a sustained release of the antigen would follow if the time of the study was extended but this was irrelevant for our purpose since the PLGA NPs will be cleared by the alveolar macrophages in a short period of time. The physicochemical characteristics of the PLGA NPs during the release study at the selected time points is reported in Figure 5.8. The mean particle size did not significantly change for any of the copolymer used, as well as the surface charge of the NPs, which remained highly negative. This might be explained by the burst release, since there is not degradation of the polymer and therefore, no size reduction can be detected. Release patterns of for PLGA NPs have been reported in

literature previously [285, 286] but there are few studies published showing the release profile of PLGA NPs after freeze drying [266, 274, 284]. Studies by Fonte et al. encapsulating insulin within PLGA NPs showed a burst release in the first 2 hours of 35% when sucrose was used as cryoprotectant, which was increased when no cryoprotectant was added (~60%). After 48 hours approximately 70% of the initial amount of insulin loaded was released [284]. A suggested explanation for the decreased release from the PLGA nanoparticles after freeze drying with the incorporation of cryoprotectants is due to the increased osmotic pressure in the buffer medium due to the existence of sugars in the formulation, which has been previously reported in literature [284, 287]. Therefore, the volume of water entering the dialysis tubing, where the sample is located, is reduced due to the osmotic difference between the medium and the sample. This reduction will result in a decrease in the water channel formation in the PLGA nanoparticles and thus, a decreased burst release [284, 288]. Release studies of the PLGA MPs were not performed due to the low antigen loading which resulted in antigen release concentrations below the limit of detection and quantification of the method.

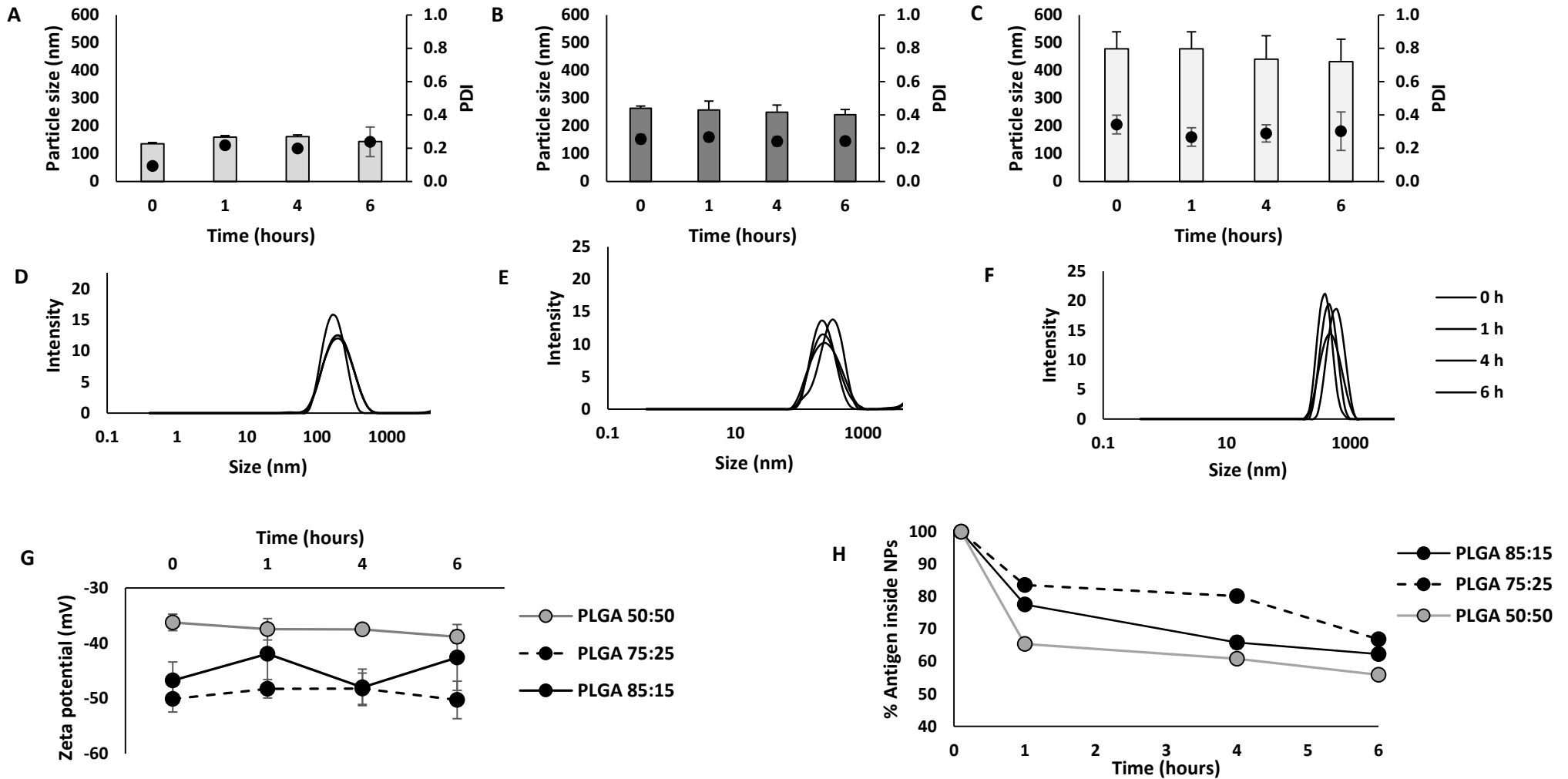


Figure 5.8 Particle size and PDI of the PLGA (A) 50:50, (B) 75:25 and (C) 85:15, (D-F) overlay intensity plots and (G) ZP values at the selected time points measured for the release study. (H) Release study at 37°C of the PLGA 85:15, 75:25 and 50:50 nanoparticles manufactured by using microfluidics at a TFR of 10 mL/min and FRR 1:1 after FD and reconstitution with ultrapure water. Results represent mean ± SD of triplicate measurements.

5.4.4 Thermal analysis of the dry powder PLGA formulations using HOT-Stage microscopy

In the formulation of delivery systems, thermal analysis plays an important role for the investigation of the phase transitions of the materials in use and their changes in heat capacity. Hot stage microscopy is the method of choice for the study of the thermodynamic properties of powders since it is relatively fast, cheap, straight forward and highly sensitive. Therefore, hot stage microscopy studies were carried out to study the thermo-microscopic changes of the antigen loaded PLGA nano- and microparticle powders as well as for the starting material used for the preparation of these particulate delivery systems. Representative micrographs at various temperature points are shown from Figure 5.9 to Figure 5.14. Citric acid powder was used as a control since its melting point is well known (156°C as shown in Figure 5.9).

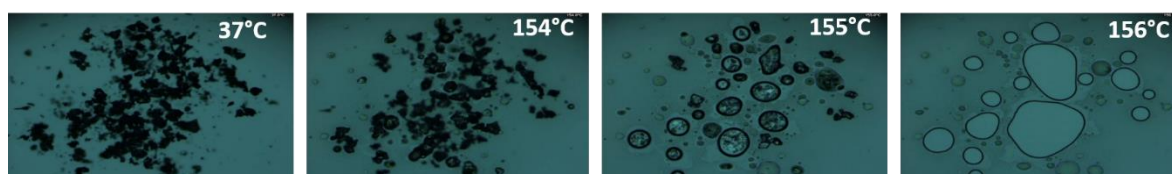


Figure 5.9 Representative HSM micrographs of citric acid powder used as a control (magnification 10x).

In order to characterise the PLGA micro- and nanoparticles formulations and understand their thermal behaviour, the starting material used during the manufacturing process of these particles was characterised individually. According to literature, the melting points for sucrose and leucine are 186°C and 293°C respectively. Figure 5.10 shows the representative micrographs of the sucrose and leucine powders used as cryoprotectants for the PLGA nano- and microspheres. Sucrose showed a melting temperature of 190°C, similar to the temperature found in other publications [289]. In contrast, leucine showed a lower melting temperature compared to literature (~293°C) [290], since the micrographs showed its melting at 260°C.

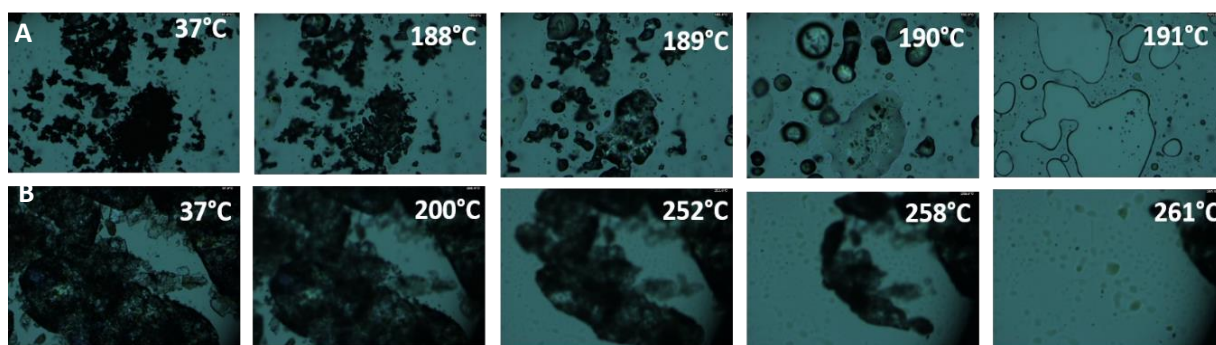


Figure 5.10 Representative HSM micrographs of the cryoprotectants used for the production of dry powders using freeze drying: (A) sucrose and (B) leucine (magnification 10x).

Polyvinyl alcohol is used during the manufacturing process of microspheres to avoid their agglomeration. Although the microspheres are washed by centrifugation several times to remove the PVA, traces usually remain in the formulation [243, 283]. Therefore, PVA was also characterised by HSM. Figure 5.11 shows the representative micrographs for PVA. Our results correlate to the results reported in literature, with a melting point of 200°C [291].

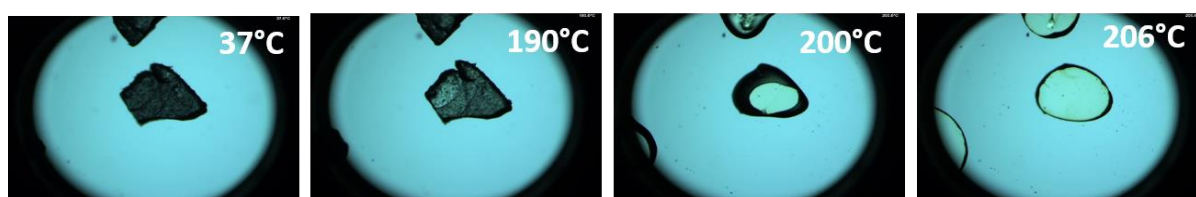


Figure 5.11 Representative HSM micrographs of PVA used during the preparation of PLGA microspheres by the double emulsion method (magnification 4x).

PLGA copolymers have different melting temperatures depending on the percent composition (commonly between 176°C to 220°C). Thus, PLGA 85:15, 75:25 and 50:50 crystals were examined by HSM as well as the different PLGA copolymer micro- and nanoparticles with and without the addition of cryoprotectant. Figures 5.12-14 show the micrographs for PLGA 85:15, 75:25 and 50:50 based particles respectively. The starting material was obtained after crushing the PLGA crystals to obtain smaller crystals (Figures 5.12-14A). PLGA 85:15 crystals showed a melting temperature of approximately 160°C, whereas PLGA 75:25 and 50:50 crystals showed lower melting temperatures (130°C and 100°C respectively). In general, PLGA NP and MP powders produced without the addition of cryoprotectants had similar melting temperature as their respective PLGA crystals. In contrast, when cryoprotectants were added to the formulation, all three copolymers showed higher melting

temperature (up to 180°C). The increase in melting temperature in the PLGA formulation containing cryoprotectant can be explained by the higher melting temperature of the sucrose and leucine as is shown in Figure 5.10A-B.

The differences in hydrophobicity of the three PLGA copolymers, attributed to the lactic acid ratio, contributes to the different melting points. Thus, the copolymer 85:15 which contains higher lactic acid ratio resulted in higher a melting point, followed by the copolymer 75:25 and 50:50 [102]. The mixture of the polymer, the protein, the sugar and the amino acid resulted in a different temperature compared to the individual components. The component with the lowest melting temperature melts first, and provokes an accelerated dissolution of the other compounds. Therefore, the compounds start to melt until the eutectic point(s) of the mixture is reached. In this case, PLGA nano- and microparticles, independently of the copolymer used, lowered the melting temperature of the cryoprotectants, enhancing the melting of the mixture [292]. There are many studies in the literature focused on the dissolution enhancement of delivery systems and drugs. For example, Stott et al. showed that mixing propranolol with fatty acids reduced the melting point of the drug improving its transdermal delivery [293]. Other studies have demonstrated the improved delivery of ibuprofen due to the formation of eutectic systems with terpenes [294]. Brostow et al. demonstrated that upon addition of different ratios of melamine resin with low density polyethylene, produced a depression on its melting point [295].

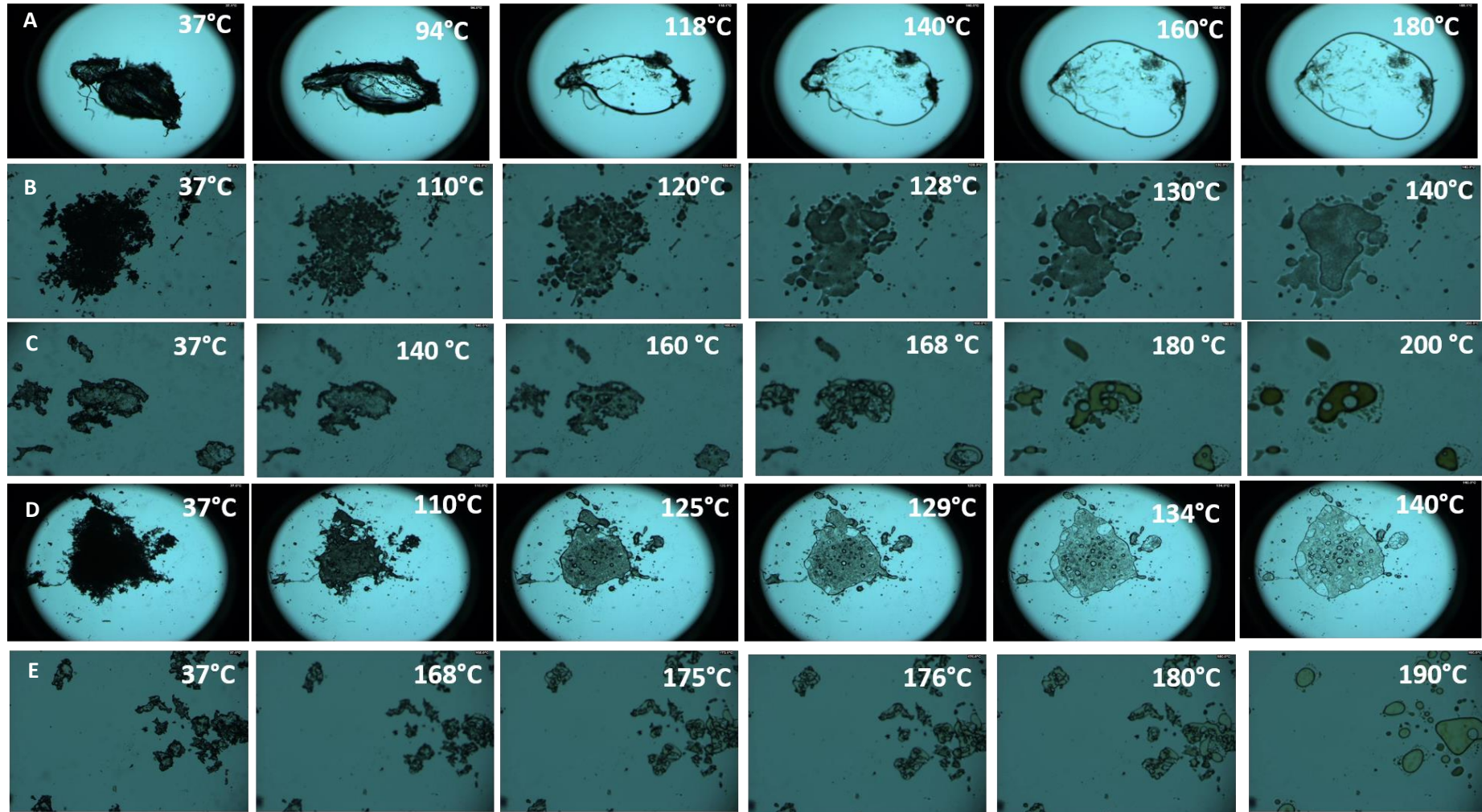


Figure 5.12 Hot-stage micrographs of the (A) PLGA 85:15 (starting material) (magnification 4x), (B) antigen loaded PLGA 85:15 microparticles after freeze drying with no cryoprotectant (magnification 10x), (C) antigen loaded PLGA 85:15 microparticles after freeze drying with a combination of sucrose (10% w/v) and leucine (1% w/v) (magnification 10x), (D) antigen loaded PLGA 85:15 nanoparticles after freeze drying with no cryoprotectant (magnification 4x) and (E) antigen loaded PLGA 85:15 nanoparticles after freeze drying with a combination of sucrose (10% w/v) and leucine (1% w/v) (magnification 10x).

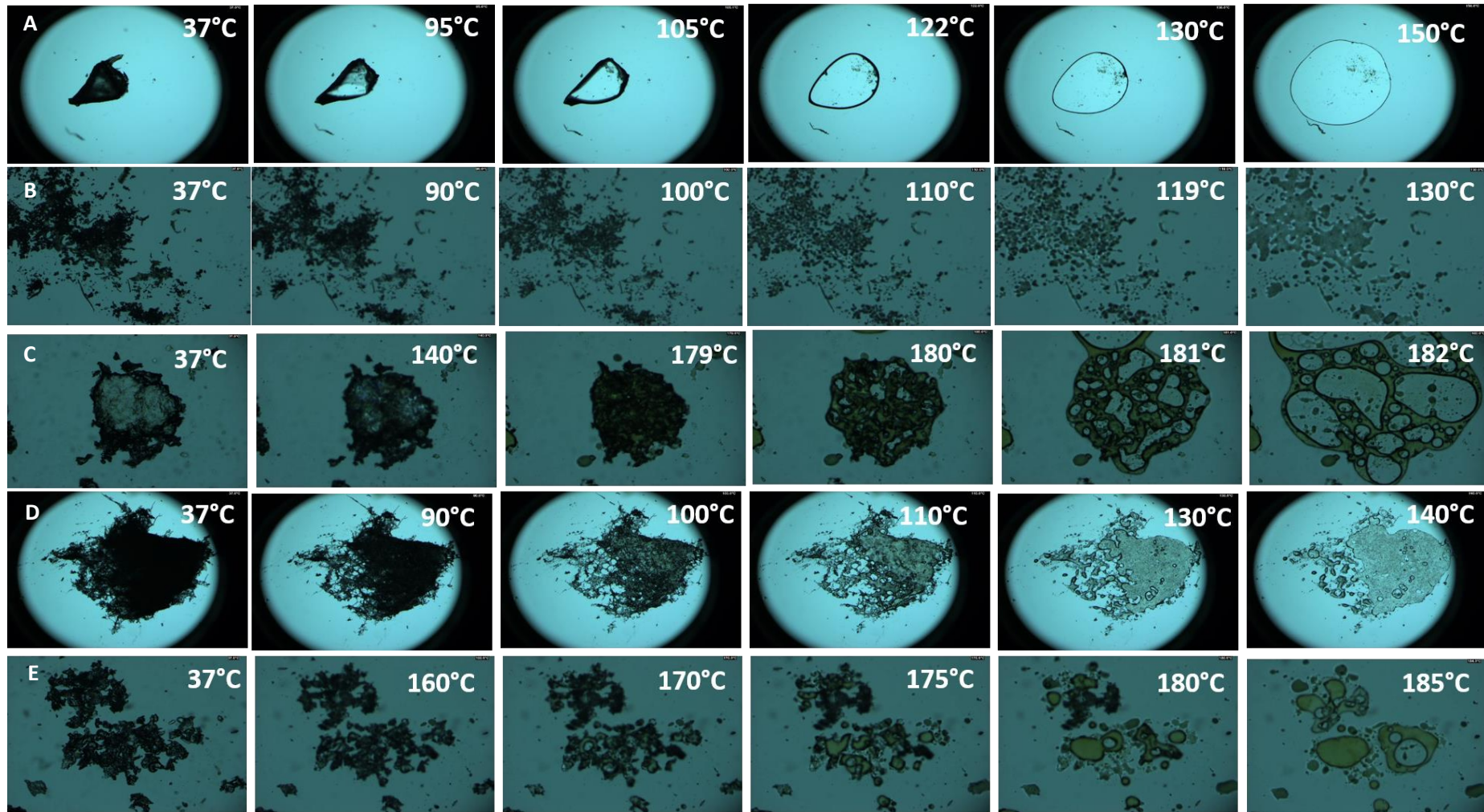


Figure 5.13 Hot-stage micrographs of the (A) PLGA 75:25 (starting material) (magnification 4x), (B) antigen loaded PLGA 75:25 microparticles after freeze drying with no cryoprotectant (magnification 10x), (C) antigen loaded PLGA 75:25 microparticles after freeze drying with a combination of sucrose (10% w/v) and leucine (1% w/v) (magnification 10x), (D) antigen loaded PLGA 75:25 nanoparticles after freeze drying with no cryoprotectant (magnification 4x) and (E) antigen loaded PLGA 75:25 nanoparticles after freeze drying with a combination of sucrose (10% w/v) and leucine (1% w/v) (magnification 4x).

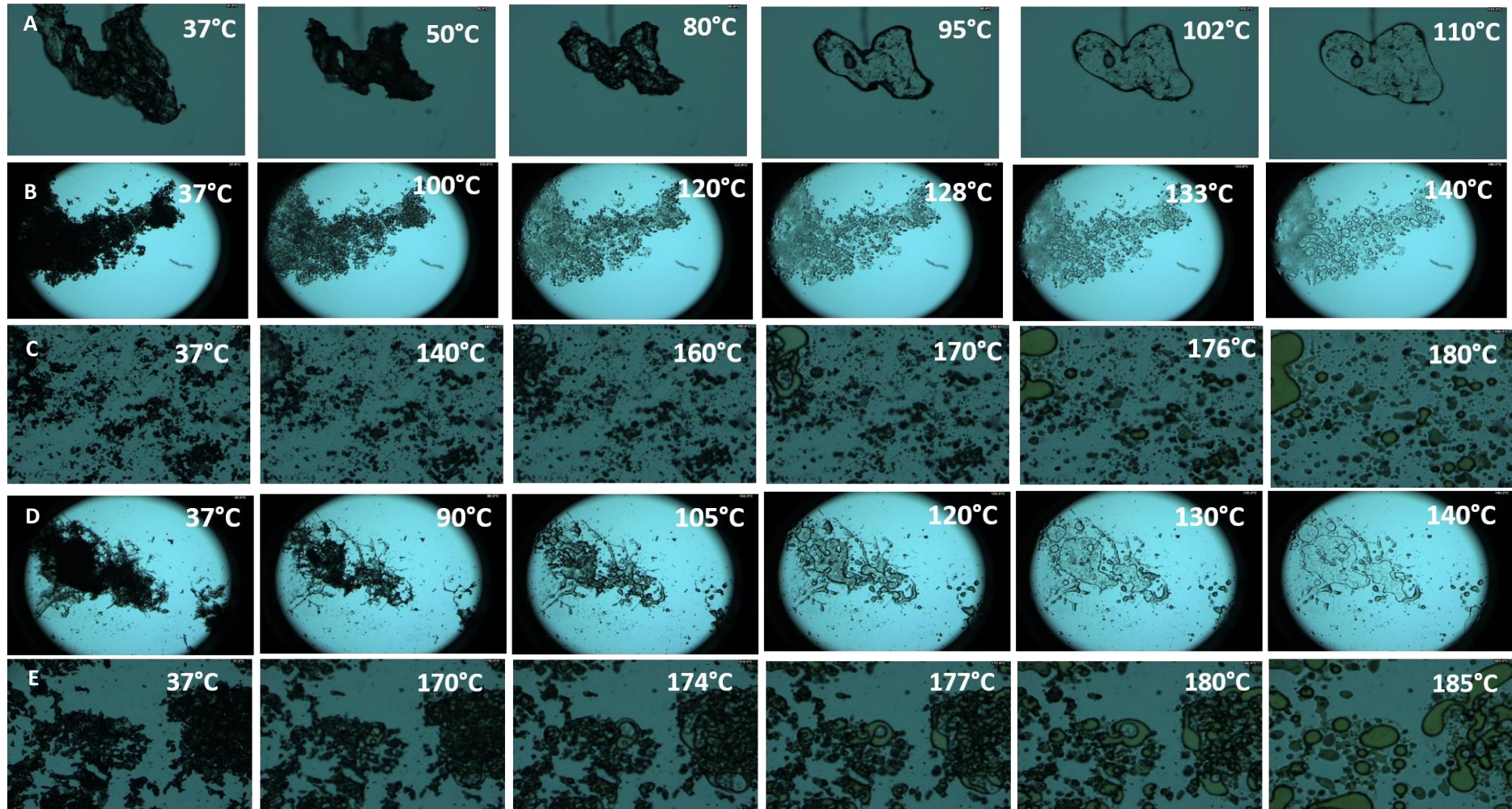


Figure 5.14 Hot-stage micrographs of the (A) PLGA 50:50 (starting material) (magnification 10x), (B) antigen loaded PLGA 50:50 microparticles after freeze drying with no cryoprotectant (magnification 4x), (C) antigen loaded PLGA 50:50 microparticles after freeze drying with a combination of sucrose (10% w/v) and leucine (1% w/v) (magnification 10x), (D) antigen loaded PLGA 50:50 nanoparticles after freeze drying with no cryoprotectant (magnification 10x) and (E) antigen loaded PLGA 50:50 nanoparticles after freeze drying with a combination of sucrose (10% w/v) and leucine (1% w/v) (magnification 10x)

5.4.5 Morphological characterisation of the antigen loaded PLGA nano- and micro-particles

Characterisation of the morphology of the PLGA nanoparticles and microparticles was done using SEM. Figure 5.15 shows the micrographs of the PLGA 85:15, 75:25 and 50:50 nanoparticles whereas Figure 5.16 shows the micrographs of the microparticles after freeze drying (powder state) and after reconstitution of the dry powder using ultrapure water.

In the powder samples, nano- and microparticles can be seen embedded in the cryoprotectant matrix, whereas the reconstituted powders showed spherical particles in the nanometre range (for the particles produced using microfluidics) and in the micrometre range (for the particles produced using the double emulsion method). The inclusion of cryoprotectant in the PLGA formulation creates a continuous glassy matrix embedding the NPs which has been previously reported in literature by other groups [264, 266, 284]. All three copolymers showed good redispersibility of the powders since the particle size was maintained after FD. Particle sizes from the SEM micrographs were in agreement with the values obtained from the DLS measurements.

Figure 5.17 shows the comparison between the PLGA microparticles produced with different monomer ratios. The morphology of the PLGA particles before freeze drying and after reconstitution was preserved. Interestingly, the surface of the particles produced with different monomer ratios was different. Overall, all three copolymers showed a rough surface but this was more markedly for PLGA 75:25. This rough surface, also reported as wrinkle surface in literature, has been related to hydrophobicity and surfactant-like properties of leucine which alter the surface viscosity of the particles [271, 296, 297]. Another theory to explain the increased roughness in the particle surface after FD might be due to the removal of water during the freeze drying process. This change has been seen by Fonte et al. (2015) when investigating the co-encapsulation of cryoprotectants for increasing the stability of insulin-loaded PLGA nanoparticles after FD [284]. This can affect the release of the protein, increasing the burst effect [284]. However, PLGA 50:50 microparticles did not display this wrinkle surface. PLGA 75:25 without the addition of leucine did also exhibit this rough surface, therefore, this change in surface morphology cannot be attributed to the inclusion of leucine into the formulation nor the freeze drying method.

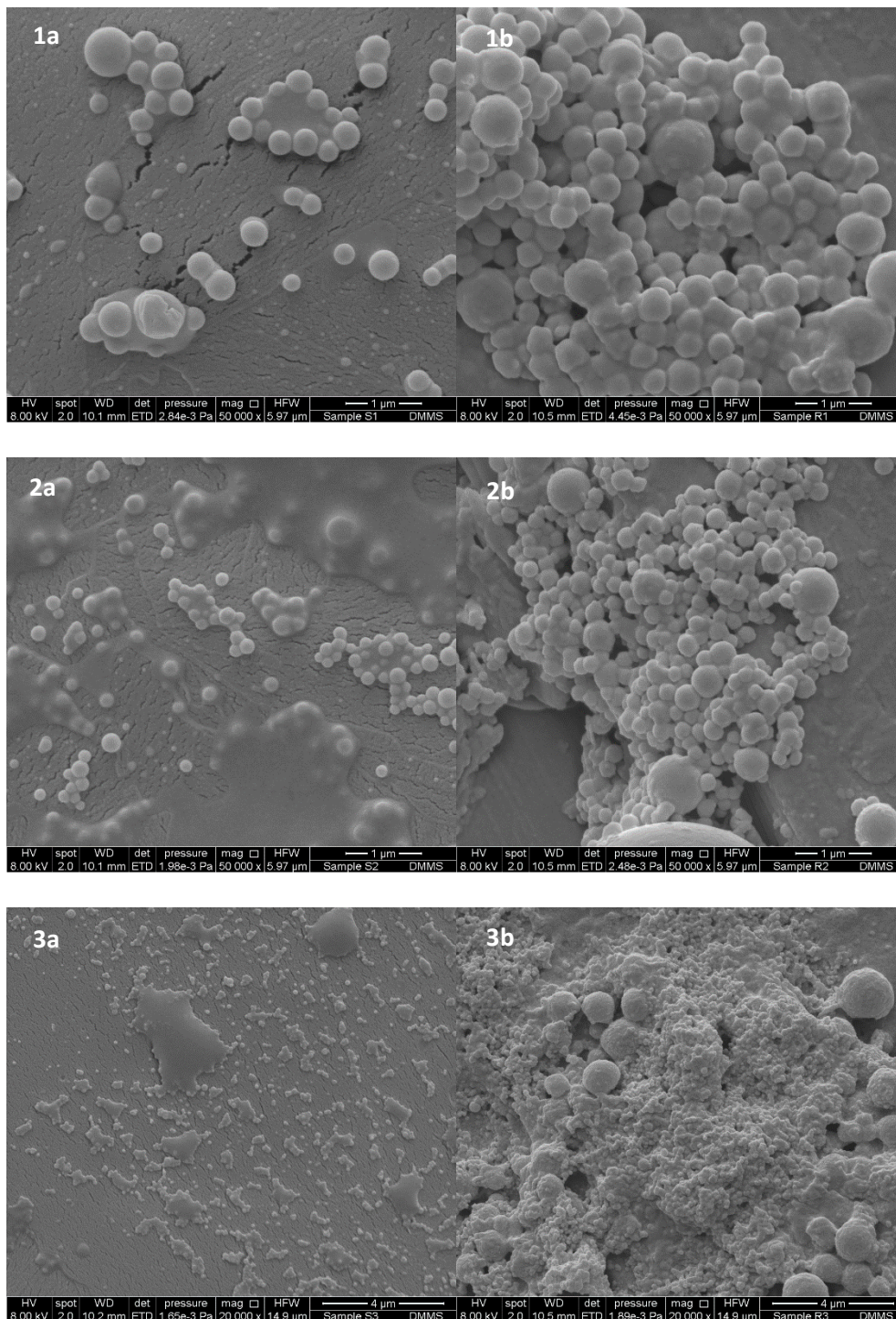


Figure 5.15 SEM micrographs of the OVA loaded PLGA nanoparticles (1) 85:15, (2) 75:25 and (3) 50:50 (a) powder state after freeze drying and after (b) reconstitution with ultrapure water.

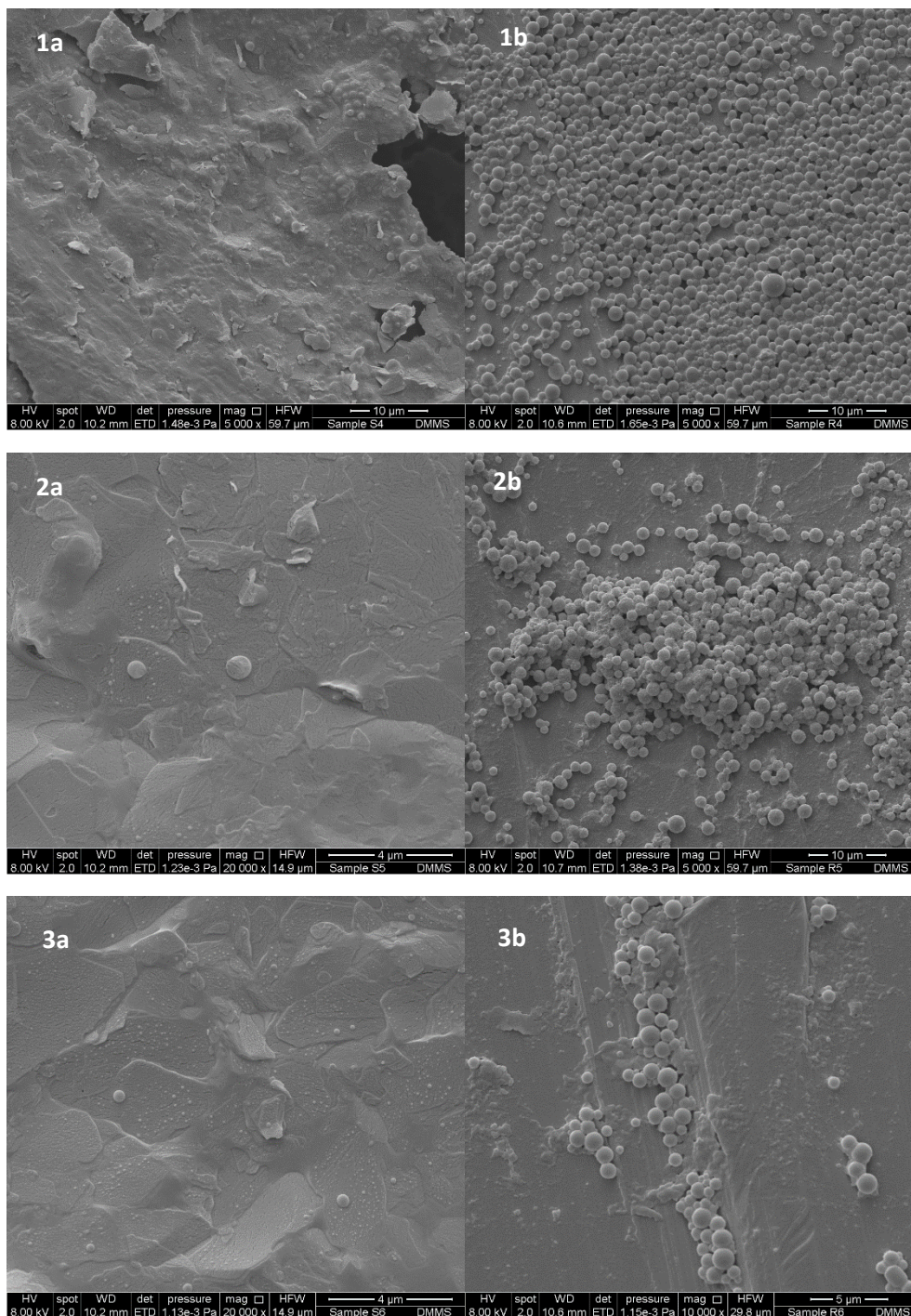


Figure 5.16 SEM micrographs of the OVA loaded PLGA microspheres **(1)** 85:15, **(2)** 75:25 and **(3)** 50:50 **(a)** powder state after freeze drying and after **(b)** reconstitution with ultrapure water.

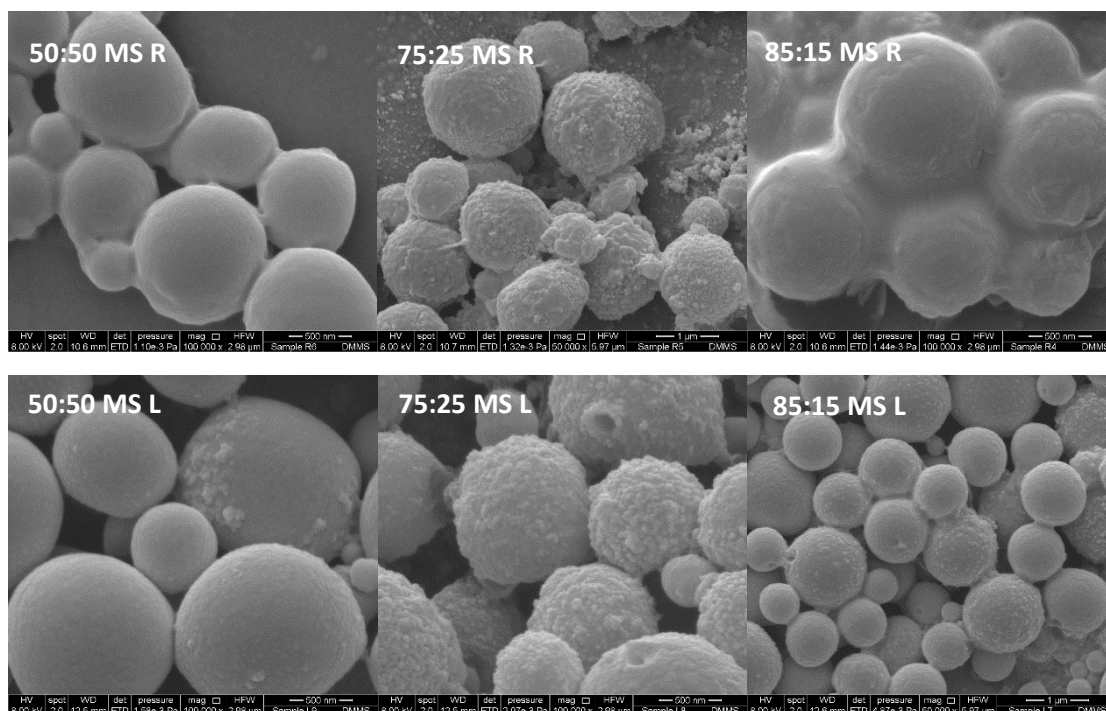


Figure 5.17 SEM micrographs of the OVA loaded PLGA microspheres (**L**) before freeze drying and (**R**) after reconstitution of the dry powder with ultrapure water.

5.4.6 Aerosol performance of the dried powder PLGA particles

The powder aerosolisation characteristics of the antigen-loaded PLGA formulations, was assessed *in vitro* using a dry-powder inhaler device with the aid of a NGI at an air flow rate of $60 \pm 5\%$ L/min. Powder aliquots of 20 mg were manually filled into a size 3 HPMC capsule and inserted into a monodose inhaler and the formulation was actuated once for 4 seconds. Simulated inhalation lifts the capsule located inside the inhaler up and down vigorously for the selected time (in this case 4 seconds). This movement favours the disaggregation of the powder inside the capsule and favours its exit from the pierced holes. The capsule is retained within the inhaler due to a grid located at the bottom of the mouthpiece. The particle deposition (%) on each stage of the NGI was estimated and plotted in Figure 5.18.

According to some reports, to achieve good deposition in the deep lungs, particles should have an aerodynamic diameter from 1-2 μm [298]. The calculated mass median aerodynamic diameter (MMAD) was between 1 - 1.8 μm for the PLGA NPs and whereas for PLGA MPs the calculated MMAD was between 1.3 - 2.5 μm . All PLGA particles tested showed a good dispersibility of the powders and good aerodynamic behaviour.

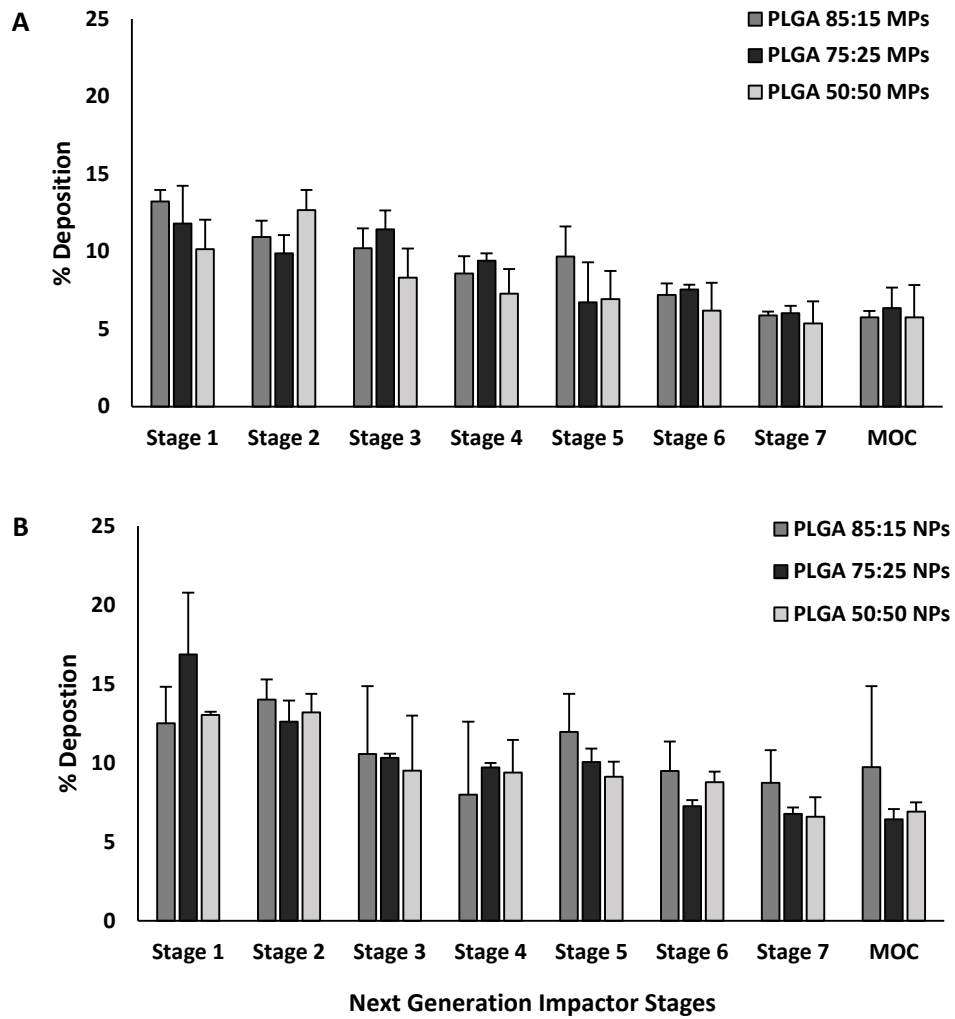


Figure 5.18 Aerosol dispersion performance of the loaded freeze dried (A) PLGA nanoparticles particles and (B) PLGA microparticles with different copolymer ratios 85:15, 75:25 and 50:50, as percentage deposition on each stage of the Next Generation Impactor (NGI). Results represent mean \pm SD, n =3 of independent batches.

It is not recommended to give more than 10 - 20 mg of powder in one actuation shot. To do so would trigger a cough reaction in the patient, resulting in the loss of the inhaled antigen into the air. In order to optimise the amount of powder filled within the capsules for the dry powder inhaler, different amounts of powder (10, 30 and 50 mg) were weighed and filled into the capsules. Figure 5.17 shows the particle deposition at the different stages of the NGI when different amounts were added into the capsules. As could be expected, the higher the amount loaded into the capsule, the higher the deposition of the powder in the throat whereas no significant differences were observed in the deposition of these particles in the deep lungs (stages 5-7).

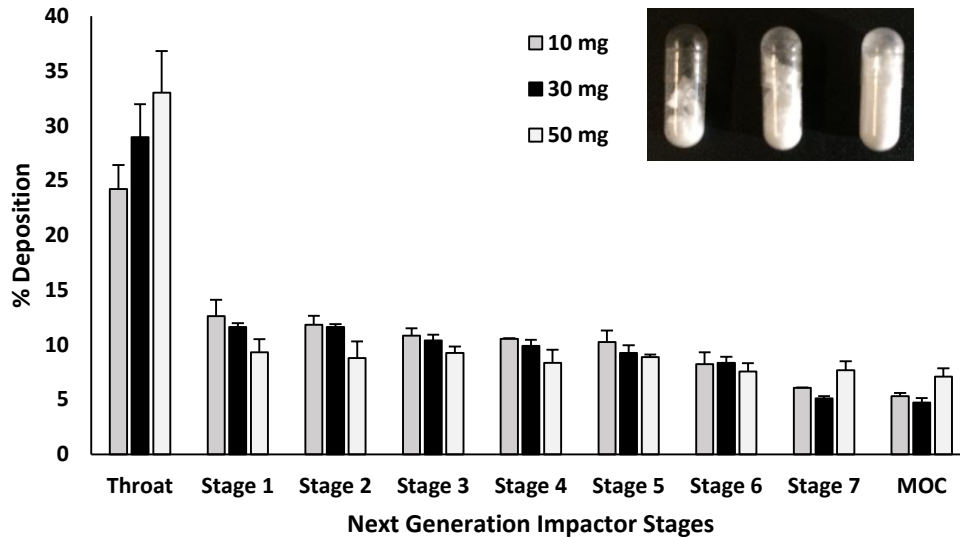


Figure 5.19 Aerosol dispersion performance of the freeze dried PLGA-loaded 85:15 TFR 10 FRR 1:1 nanoparticles as percentage deposition on each stage of the Next Generation Impactor (NGI). Results represent mean \pm SD, $n = 3$ of independent batches. Different amounts of dry powder were filled into the size 3 capsule: 10 mg, 30 mg and 50 mg.

Aerodynamic parameters representing the individual behaviour of the antigen loaded PLGA powders are displayed in Table 5.6. The emitted dose (%), which is defined as the amount of powder exiting the capsule compared to the initial amount loaded, was determined by weight after inhalation. The average emitted dose, ED% of the antigen loaded PLGA powders was determined to be 100% independent of either the copolymer used, the initial amount of powder added into the capsule or the particle production method used. The complete release of the powder during aerosolisation is representative of an adequate dose uniformity. Therefore, no static interaction of the dried powder with the capsule material occurred. The fine particle fraction, which is the mass of polymer/antigen reaching stages below $5 \mu\text{m}$ was approximately 60% for the antigen loaded PLGA NPs and significantly lower ($\sim 50\%$) for the loaded PLGA MPs. Studies by Seville et al. also showed high ED% with approx. 95% ED with powders formulated using spray drying and containing leucine [271]. The calculated respirable fraction as a percentage was above 80% in all the formulations tested. The studies by Seville et al. also showed high ED% with approx. 95% ED with powders formulated using spray drying containing leucine [271]. These powders also showed high FPD and high FPD (from 50 to 85% depending on the concentration of leucine added into the formulation). The use of leucine for the enhancement of the aerosolisation properties of the powders (mainly using spray drying) has been studied by several groups. For example, Najafabadi et al. [299] demonstrated addition of 9% w/w leucine into a formulation containing 91% sodium cromoglycate increased the dispersibility of the formulation when produced using spray drying. Chew et al. [300] investigated the use of amino acids

(5% w/w) in combination with sodium cromoglycate for the preparation of SD powders. Their studies showed that the accumulation of leucine on the surface of the particles produced better dispersibility when compared to any of the other amino acids studied. Chow et al [301] showed the improved aerosolisation of naked siRNA using Leucine as a dispersibility enhancer with high ED (80%) and modest FPF (45%). Other groups reported that the combination of the sugar mannitol and leucine produced the highest ED and FPF>80% compared to other combinations of sugars and amino acids [302]. Eadara et al. used leucine for the development of spray dried powder containing drugs for the treatment of tuberculosis and the obtained results showed that the addition of LEU increased the FPF up to 70% [154]. Some researchers have hypothesised that the improvement in the aerosolisation of powders containing leucine is due to its molecular structure, specifically to the hydrophobic alkyl side chain [271, 303].

Table 5.6 The table shows the calculated aerolisation parameters of the PLGA powders prepared using freeze drying: fine particle dose (FPD), fine particle fraction (FPF), emitted dose (ED) and respirable fraction (RF), after Next Generation Impactor (NGI).

Formulation NANOPARTICLES	Fine particle dose (FPD) mg	Fine particle fraction FPF (%)	Emitted dose ED (%)	Respirable fraction RF (%)
85:15	12.6 ± 0.1	62.8 ± 4.9	99.7 ± 0.4	83.4 ± 2.0
75:25	11.3 ± 0.1	56.7 ± 0.4	99.8 ± 0.2	77.1 ± 3.2
50:50	11.3 ± 1.2	56.6 ± 6.2	99.8 ± 0.2	81.3 ± 2.2

Formulation MICROPARTICLES	Fine particle dose (FPD) mg	Fine particle fraction FPF (%)	Emitted dose ED (%)	Respirable fraction RF (%)
85:15	10.5 ± 0.8	52.5 ± 3.8	99.05 ± 1.04	79.9 ± 2.3
75:25	10.2 ± 0.6	51.0 ± 3.1	98.15 ± 1.48	81.2 ± 2.1
50:50	9.4 ± 1.5	46.8 ± 7.4	99.68 ± 0.22	82.2 ± 2.3

Formulation	Fine particle dose (FPD)	Fine particle fraction FPF (%)	Emitted dose ED (%)	Respirable fraction RF (%)
10 mg	5.8 ± 0.2	57.8 ± 1.9	98.7 ± 0.47	82.1 ± 2.1
30 mg	16.4 ± 0.8	54.7 ± 2.7	99.6 ± 0.15	82.5 ± 2.1
50 mg	25.3 ± 1.7	50.6 ± 3.4	99.5 ± 0.34	84.4 ± 0.7

5.4.7 *In vitro* studies in different cell lines

Three macrophage cell lines were screened for viability, uptake and processing ability when exposed to PLGA nanoparticles and microspheres containing antigen. Two of the cell lines were of mouse origin, RAW264.7 cells (mouse derived monocytes) and MH-S (alveolar macrophages). The other, THP-1 monocytes was of human origin and was used only after stimulation into macrophages.

5.4.7.1 Cell viability studies

In vitro cytotoxicity studies carried out in both nanoparticles and microparticles (Figure 5.20) showed no toxic effects on either MH-S, THP-1 or RAW264.7 cells at all concentrations evaluated (6, 12, 25, 50, 100 and 200 $\mu\text{g}/\text{mL}$). In both cases >85% of cells were viable even at the highest concentration of 0.2 mg/mL tested. These results correlate with the results reported in literature (e.g. [304, 305]) as it has been extensively reported the high safety profile of PLGA, which upon hydrolysis in the body, degrades into its nontoxic metabolites lactic and glycolic acid and thus is approved for human use by the FDA and EMA.

5.4.7.2 *In vitro* uptake studies in macrophages cell lines

PLGA NPs and MPs were produced incorporating a fluorophore (DiIc) in order to quantify the macrophages uptake using fluorescence. Fluorescence intensity was measured after 30 min and 1, 2 and 3 h. Uptake studies were carried out at 37°C and 4°C to determine whether the particles were efficiently taken up by endocytosis or attached to the cell surface since, due to the inhibition of endocytosis at low temperatures (energy dependent process). We observed that NP uptake was significantly decreased at 4°C (Figure 5.21), suggesting that indeed NP uptake is mediated by endocytosis. Results from the PLGA NPs and MPs uptake study using three different macrophages cell lines are displayed in Figure 5.21 and 5.22 respectively. In general, results showed the ability of all three cell lines to take up PLGA particles independently of the copolymer used or the particle size. In all three cell lines, uptake was observed within 30 minutes for all PLGA formulations. Continuous uptake increase was seen within the first 3 h for all formulations used except for the particles studied on the RAW264.7 cell line which showed a sustained uptake from 30 min to 3 h. No major differences were observed in uptake between NPs and MPS, suggesting that in these studies the particle size is not making any difference.

Lorenz et al. tested the uptake of polymeric NPs in three different cell lines: HeLa cells, Jurkat cells (T cell model) and KG1a cells (for CD34+ hematopoietic stem cells) and observed no difference in particle uptake after 24 h [306]. Opposite to that, chitosan NPs loading α -hederin showed different uptake when incubated in HepG2 and HSC cell line [307]. Cartiera et al. investigated the uptake of PLGA particles in epithelial cells from the renal tubule, gut epithelium and respiratory airway (OK cells, Caco-e-cells and HBE cells respectively) and demonstrated that PLGA NPs were faster and more efficiently taken up in OK cells compared to the other two cell lines, which showed lower or negligible particle uptake [308]

Regarding the influence of the particle size on the particle uptake, Akagi et al demonstrated that PLGA NPs of 200 nm size encapsulating OVA were taken up faster by RAW264.7 cells than PLGA:OVA NPs of 40 nm [309]. Qaddoumi et al. investigated the uptake of PLGA nano- (100 nm and 800 nm) and microparticles (10 μ m) in primary cultured rabbit conjunctival epithelial cells, demonstrating highest uptake for the smallest PLGA NPs (100 nm) compared to larger PLGA particles [310]. Nicolette et al. compared the uptake of PLGA NPs (~400 nm and -35 mV) and MPs (6.5 μ m and -17 mV) in J774 cell line (macrophages, mice origin) and the results showed that PLGA NPs were efficiently taken up by the macrophages whereas PLGA MPs were attached to the cell surface [311].

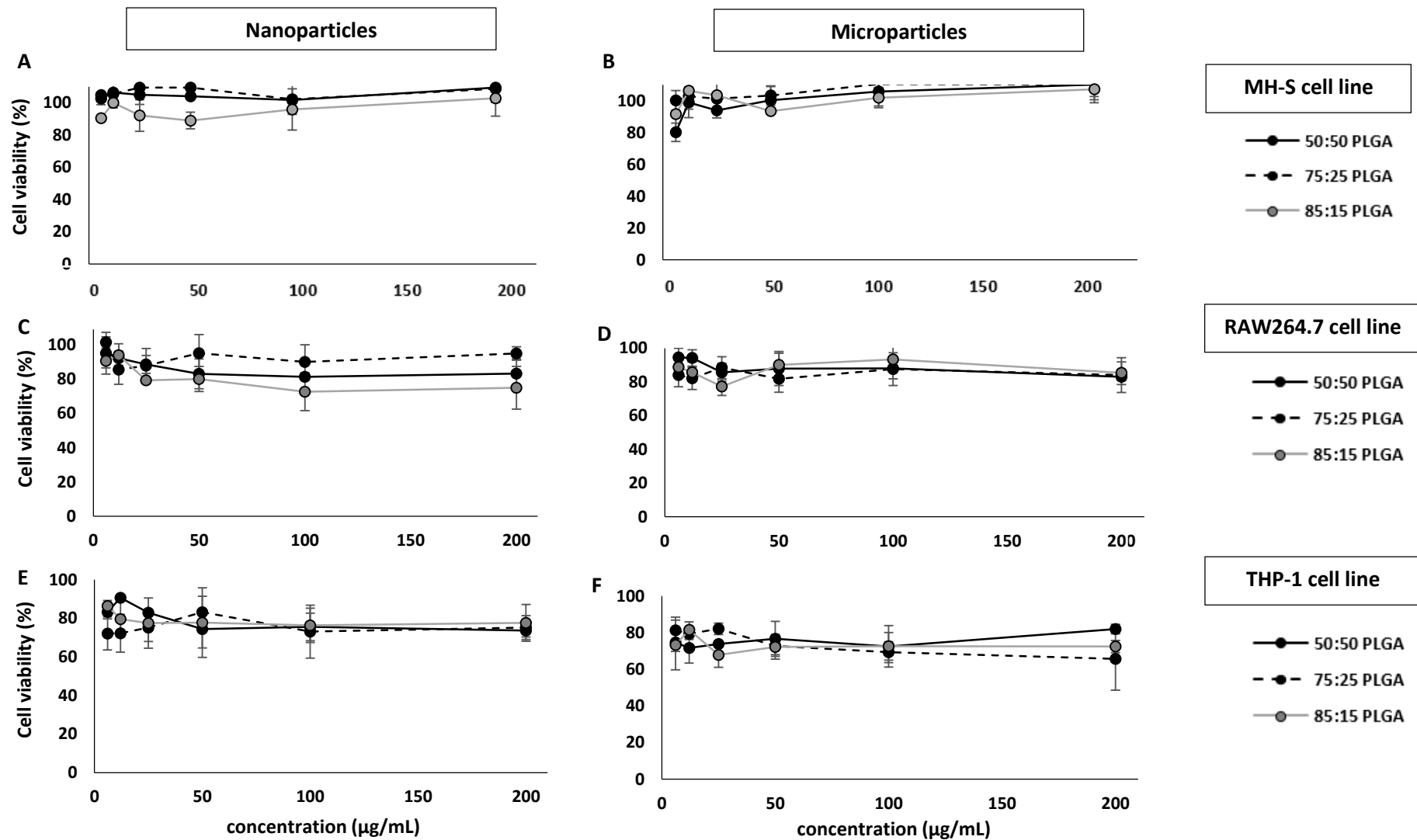


Figure 5.20 CTB assay for the quantification of nanoparticle and microparticle cell viability in three different cell lines: MH-S, RAW264.7 and THP-1. Results in collaboration with Maryam Hussain (Strathclyde Institute of Pharmacy and Biomedical Sciences).

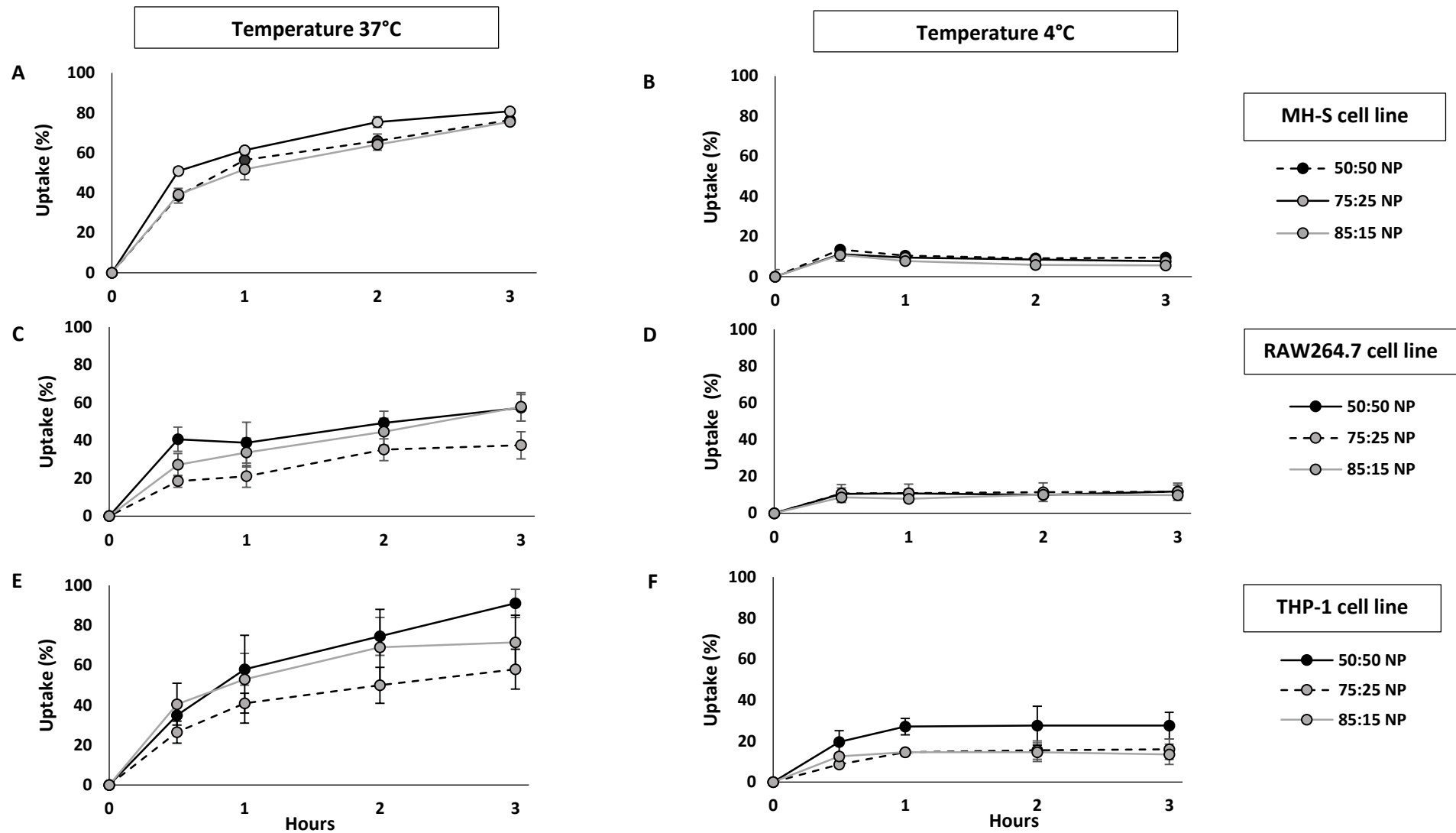


Figure 5.21 Nanoparticle uptake in three different cell lines MH-S, RAW264.7 and THP-1 at 37°C (A, C and E) and 4°C (B, D and F). Results in collaboration with Maryam Hussain (Strathclyde Institute of Pharmacy and Biomedical Sciences).

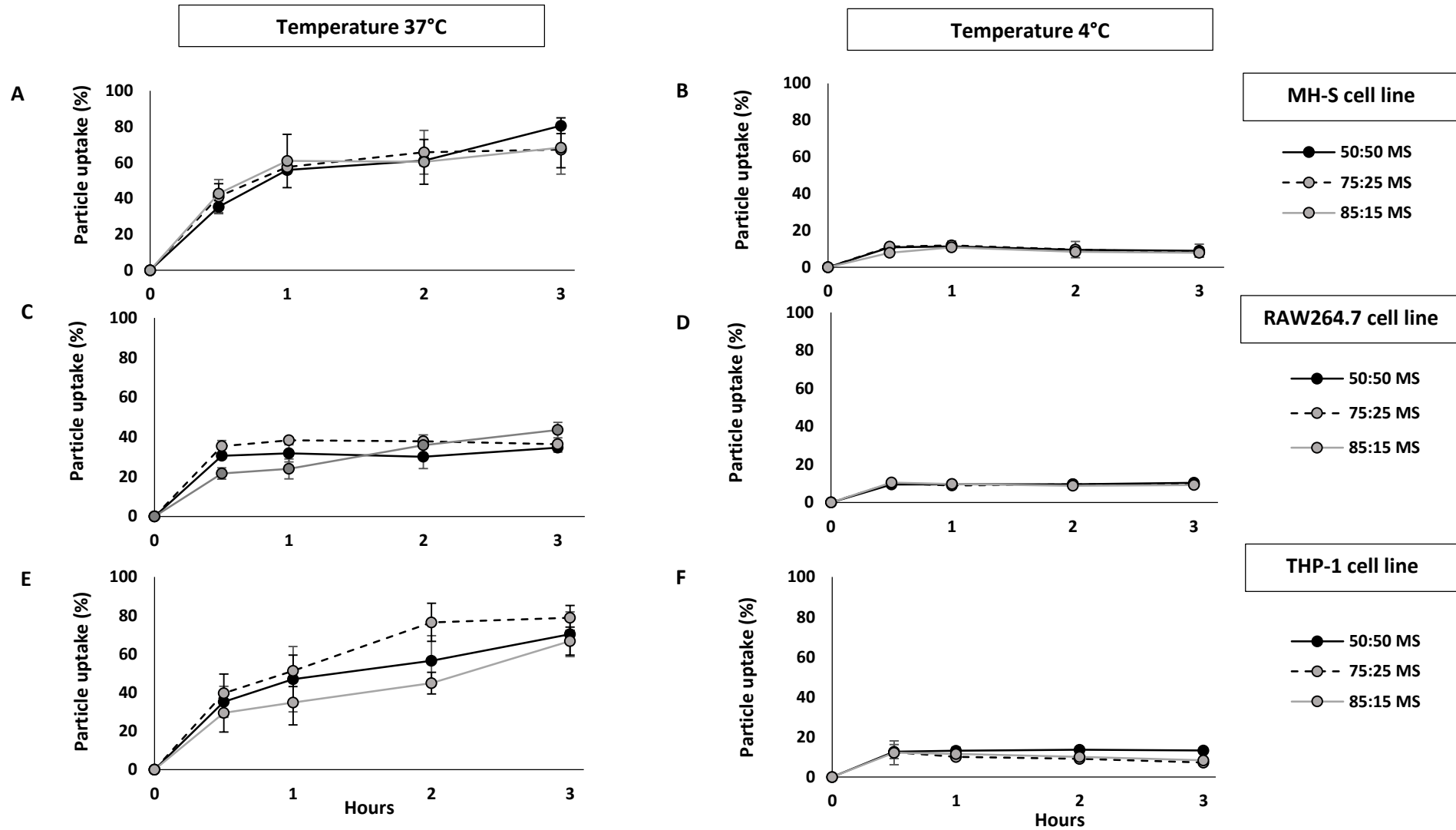


Figure 5.22 Microparticle uptake in three different cell lines: MH-S, RAW264.7 and THP-1 at 37°C (A, C and E) and 4°C (B, D and F). Results in collaboration with Maryam Hussain (Strathclyde Institute of Pharmacy and Biomedical Sciences).

5.4.7.3 DQ-OVA processing of PLGA particulate delivery systems

The functional ability of OVA being taken into the cells was tested using DQ-OVA. The conjugated OVA has a fluorescent tag attached to it which becomes fluorescent (bright green) when undergoing intracellular proteolytic degradation. Thus, DQ-OVA was encapsulated into the PLGA NPs and MPs in order to evaluate the ability of the formulated PLGA particles to deliver functional OVA to the cells (Figure 5.23). The results showed that 49 - 65% of the DQ-OVA delivered from the nanoparticles is degraded by RAW264.7 cells whilst THP-1 cells showed higher degradation, showing that 72- 83% of the DQ-OVA undergoes proteolytic degradation within three hours. The MH-S cells performed similarly to THP-1 cells with 51- 74% DQ-OVA undergoing proteolytic degradation after three hours. In contrast, there were no significant differences between the amounts of DQ-OVA processed by RAW264.7 and THP-1 cells when DQ-OVA was entrapped inside PLGA microparticles, showing low antigen degradation in both cell lines. In contrast, PLGA MPs showed higher OVA processing when exposed to MH-S cells (up to 16%).

In addition, degradation of OVA as a function of time was studied using PLGA 75:25 NPs and MPs incubated in the presence of RAW264.7, MH-S and THP-1 cells for up to 48 hours (Figure 5.24). Results showed that 100% DQ-OVA encapsulated within the PLGA NPs undergoes proteolytic degradation in all three cell lines after 24 h. In contrast, PLGA MPs did not show complete antigen presentation in any of the three investigated cell lines. The maximum DQ-OVA degraded by RAW264.7 cells was 23%, while THP-1 cells showed 28% whereas MH-S cells resulted in 57%. Overall, MH-S cells (alveolar macrophages) showed the best and most rapid uptake for both NPs and MPs and represent the target place for the delivery of the tuberculosis subunit vaccine.

As the three cell lines tested showed a similar trend, the differences observed were attributed to the particle size of the PLGA particles since PLGA NPs showed much higher antigen degradation compared to the MPs. This has been previously shown in literature. For example, Akagi et al. showed that PLGA NPs of 40 nm loading DQ-OVA showed less degradation of the protein compared to PLGA NPs of 200 nm in RAW264.7 cells, demonstrating the importance of the particle size for the antigen processing within polymer NPs. Besides, increased degradation was observed with increased incubation time [309]. The larger size of the MPs might contribute to a reduced antigen release due to slower polymer degradation in comparison to NPs, which has been shown in Chapter 4, to release up to 40 – 50% of the loaded content within the first 6 hours.

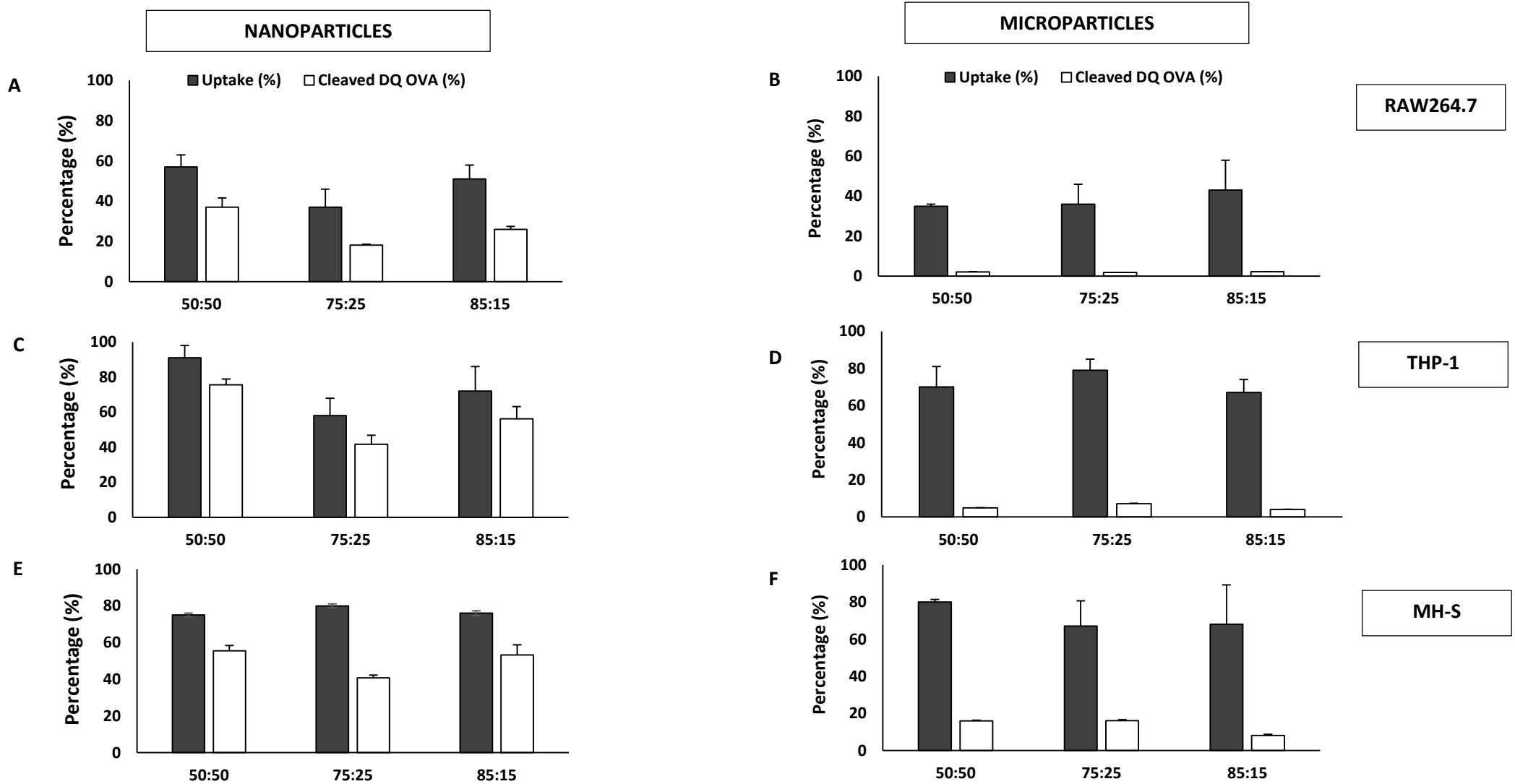


Figure 5.23 DQ-OVA encapsulated in PLGA NPs (A, C and E) and MPs (B, D and F) as a percentage of amount cleavage after 3 hours exposure to MH-S cells, RAW264.7 and THP-1 cell for PLGA nanoparticles and microparticles. Results in collaboration with Maryam Hussain (Strathclyde Institute of Pharmacy and Biomedical Sciences).

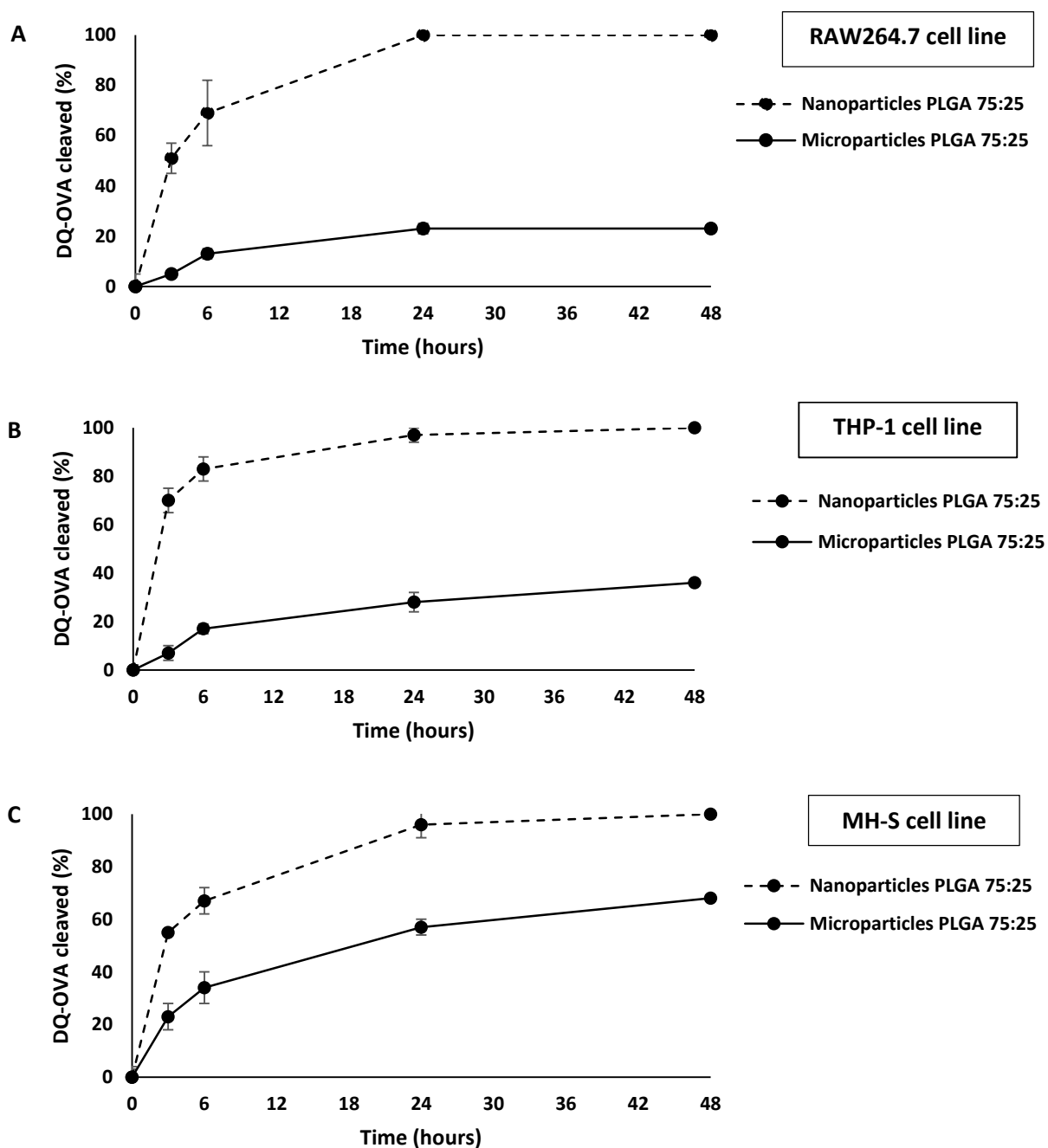


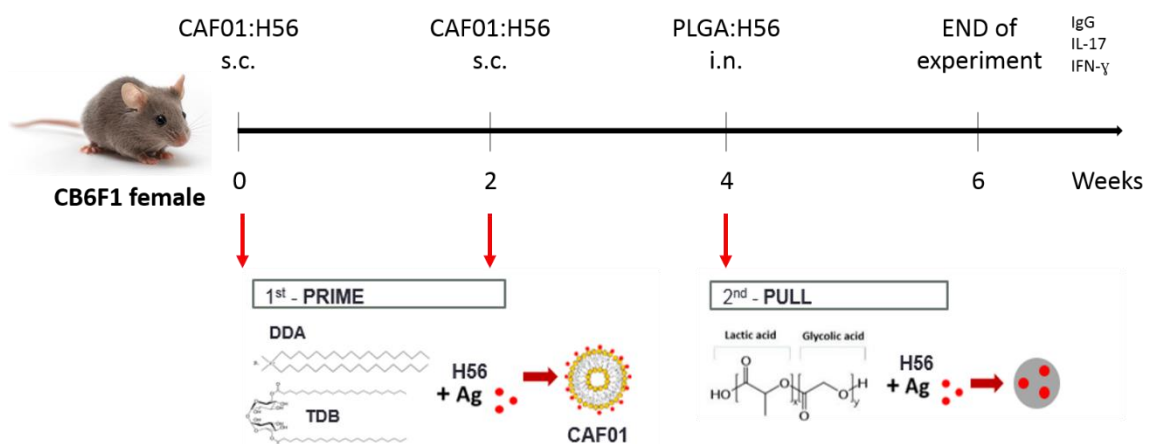
Figure 5.24 DQ-OVA encapsulated in PLGA NPs and MPs as a percentage of amount cleavage after 48 hours exposure to RAW264.7 (A), THP-1 (B) and MH-S cells (C). Results in collaboration with Maryam Hussain (Strathclyde Institute of Pharmacy and Biomedical Sciences).

5.5 Conclusions

Formulation development for the design of delivery systems for subunit vaccines is crucial to effectively deliver the antigen to the right place within the body. In this study, freeze dried powders composed of PLGA copolymers 85:15, 75:25 and 50:50, sucrose and leucine were produced using a freeze drying technique. All powders composed of different PLGA copolymers showed adequate particle size appropriate for deep lung delivery. Besides, *in vitro* studies in three different macrophages cell lines showed the ability of these cell to take up the formulated PLGA particles and their ability to deliver the antigen to the cells for processing. Based on these studies it has been shown that particles can be delivered to the lung and these particles can be taken up and antigen presentation can occur within 24 h. NPs gave consistently higher uptake and antigen presentation across the 3 cell lines tested. To see if this translates into *in vivo* performance, these formulations will move on to the immunisation studies where CAF01:H56 formulation will be administered as a priming vaccine, followed by PLGA encapsulating H56 antigen for its delivery to the lungs aiming to develop a prime-pull TB vaccine against pulmonary tuberculosis.

Chapter 6

An *in vivo* model: prime-pull vaccination by priming with CAF01:H56 and boosting with PLGA:H56



6.1 Introduction

Tuberculosis (TB) remains a major health problem, affecting approximately a quarter of the world population. The current TB vaccine, the BCG vaccine, was discovered 1921 and it is intradermally administered in children at the time of birth. However, BCG is only partially effective in protecting children against disseminate TB, showing severely variable protection versus primary infection in children and it does not protect against pulmonary TB which is the most common form of TB [312, 313]. Therefore, there is an unmet need for a new vaccine which can provide protective and durable immune responses, while also controlling among other forms, pulmonary TB. Despite the unsuccessful clinical trials carried out, all the efforts in research have given us some knowledge about how to defeat this disease. It is believed that the ineffectiveness of BCG protecting against pulmonary TB is due to the absence of antigen-specific T cells in the lungs [314]. Although the mechanism underlying TB protection is not well understood the majority of the studies agree on the critical protective role that T cell mediated immunity plays against TB [34, 139, 140, 315]. Recruitment of T cells to the infection site (lungs) takes approximately 10 days after natural infection, as Mtb infection lessens the T cell migration to the lungs. Overcoming this delay is a vital element for the design and development of a successful TB vaccine since this delay allows Mtb bacilli to proliferate in the alveolar macrophages. Thus, respiratory mucosal vaccines promoting the recruitment of T cell in the lungs in order to control Mtb growth might be a promising strategy against pulmonary TB, as it has been shown to be critical for early infection control [145].

6.2 Aim and objectives

In this chapter the development of a prime-pull vaccine approach for protection against pulmonary TB has been investigated. An immunisation protocol consisting of parenteral priming with the TB vaccine candidate (H56) alongside the cationic liposome adjuvant 01 (CAF01) followed by respiratory mucosal boosting of the H56 tuberculosis antigen within an inert delivery system (PLGA) was carried out in order to elucidate if intranasal administration of the H56 antigen produces the desired immunological responses for the protection against pulmonary TB. Therefore, the following analysis was conducted:

- Antibody analysis (total IgG) in serum from blood and lung supernatants.
- Cytokine analysis (IL-17 and IFN- γ) from re-stimulated splenocytes and lung lymphocytes.
- Intracellular staining to differentiate between the localisation of the CD4 T-cells producing IL-17 and IFN- γ in the lungs, spleen and lymph nodes.

6.3 Materials and methods

6.3.1 Materials

For the preparation of delivery systems, poly(lactic-co-glycolic acid) 85:15 (Mw: 50,000-75,000), 75:25 (Mw: 66,000-107,000), 50:50 (Mw: 30,000-60,000) from Sigma-Aldrich were used. Sucrose, leucine and the stabiliser polyvinyl alcohol (PVA Mw: 31,000) were purchased from Sigma-Aldrich Company Ltd., Poole, UK. The tuberculosis vaccine candidate H56 was donated by Statens Serum Institut (SSI), Copenhagen, Denmark. 2-amino-2-(hydroxymethyl)-1,3-propanediol (Tris) was obtained from ICN Biomedicals Inc. (Aurora, OH, US) and prepared at a 10 mM concentration and pH 7.4 unless otherwise stated. All other reagents were of analytical grade and purchased from commercial suppliers.

6.3.2 Preparation of PLGA nanoparticles for nasal delivery

PLGA nanoparticles were manufactured by the microfluidics method using the Nanoassemblr™ Benchtop (Precision Nanosystems Inc., Vancouver, Canada) as described in Chapter 4. Briefly, polymer (either PLGA 85:15, 75:25 or 50:50) was dissolved in acetonitrile at a concentration of 10 mg/mL (1% w/v). For the production of empty nanoparticles, Tris buffer was used as aqueous phase whereas for antigen loaded nanoparticles, antigen (H56) was loaded in the aqueous phase. The process parameters TFR 10 mL/min and FRR 1:1 were selected for PLGA NPs with copolymer ratios 85:15 and 75:25 and 1 mL core sample produced. For the production of PLGA 50:50 a TFR 15 mL/min and FRR 3:1 was used and 2 mL core sample produced. Polymer in solvent and buffer phase were injected into the systems at the selected parameters and the produced PLGA nanoparticles were collected in the outlet. To remove solvent, samples were loaded into a dialysis membrane (Mw= 12,000 - 14,000 Da, Sigma-Aldrich Company Ltd., Poole, UK) and dialysed for one hour against 250 mL of Tris buffer. A combination of 10% sucrose and 1% leucine was added to the purified particles prior freeze drying for 24 hours using the method described previously in Chapter 5.

6.3.3 Preparation of PLGA microparticles for nasal delivery

Polymer microparticles were produced as described previously (Chapter 5). H56 antigen was concentrated up to 10 mg/mL using Vivacon 2 (Sartorius, Goettingen, Germany) with a MWCO 50,000 Da. For this purpose, three different membrane treatments (Table 6.1) were investigated in order to increase the antigen recovered after centrifugation. Once the method was selected, the antigen was concentrated and the concentration verified using the standard BCA method. Briefly, 20 µL of H56 (10 mg/mL stock) were mixed with 417 µL of 3% PLGA in chloroform and vortexed for 1.5 min in order to form the initial primary emulsion. This primary emulsion was then mixed with 10 mL of PVA (10% w/v

in dH₂O) using high speed homogenization (Homogenizer Ultraturrax T25, IKA laboratories) at 8000 rpm during 3 min. Samples were left stirring overnight to remove chloroform. The next day, samples were centrifuged (Hermle Z323K, Labnet International Inc., US.) and washed three times with 10 mL of dH₂O for 20 min at 5500 x g. After the final washing step, the microparticles were reconstituted with 10% (w/v) sucrose and 1% (w/v) leucine. PLGA 85:15 MPs were chosen due to the higher EE% compared to the other two copolymer ratios.

Table 6.1 Methods used for increase the recovery of the antigen after concentration using Vivacon 2 (MWCO 50,000)

Methods	Membrane treatment	Centrifugation time and speed
Method 1	Membrane wetted with ultrapure water	10 minutes 5,000 xg
Method 2	Passivation method: 1% Tween in ultrapure water	10 minutes 5,000 xg
Method 3	No previous treatment	10 minutes 5,000 xg

6.3.4 Immunisation protocol

All animal experiments were conducted at Statens Serum Institut and conducted in accordance with regulations of the Danish Ministry of Justice and animal protection committees by Danish Animal Experiments Inspectorate Permit 2009/561-1655, 2012- 15-2934-00272, 2014-15-2934-01065 and in compliance with EU Directive 2010/63. Six groups of 6 – 8 weeks of age female Balb/c x C57BL/6 crossed (CB6F1 mice) (6 mice per group) were immunised three times with 2 week intervals between each immunisation. Mice were primed twice (2 week interval between each injection) with CAF01:H56 subcutaneously (DDA:TDB:56 250/50/5 µg dose) in a total volume of 200 µL and two weeks after the second injection they were boosted intranasally with 40 µL dose (10 µg H56 per dose) PLGA:H56 NPs and MPs (20 µL per nare). Two weeks after the final immunization they were terminated and blood and organs isolated (Figure 6.1). CAF01:H56 subunit vaccines were prepared at Statens Serum Institut whereas the PLGA boosters were prepared at the University of Strathclyde. Table 6.2 shows the vaccines administered per group.

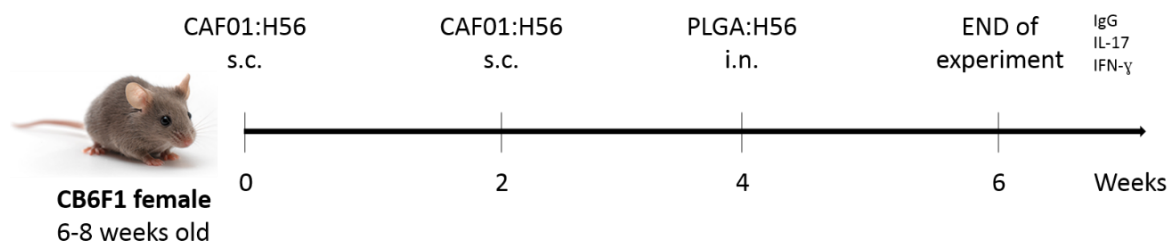


Figure 6.1 Immunisation protocol followed for the prime-pull immunisation of CB6F1 mice to investigate the production of antigen specific antibodies and cytokines for the development of a vaccine effective against pulmonary TB. Mice were immunised three times (2 x s.c. with CAF01:H56 and 1 x i.n. with PLGA:H56) with 2 weeks interval between immunisations and 2 weeks after the intranasal boosting they were terminated and data analysed.

Table 6.2 Vaccines administered to the CB6F1 female mice for the immunisation study following a prime-pull protocol. All mice were parenterally primed twice with CAF01:H56 except for the unvaccinated group. Each group was boosted with the same H56 antigen dose encapsulated in either PLGA NPs (50:50, 75:25 and 85:15) or PLGA 85:15 MPs.

Groups	1 st vaccination	2 nd vaccination	3 rd vaccination
G1- naïve or unvaccinated	N/A	N/A	N/A
G2- PLGA 50:50 NPs	CAF01:H56 s.c.	CAF01:H56 s.c.	H56:PLGA 50:50 NPs i.n boost
G3- PLGA 75:25 NPs	CAF01:H56 s.c.	CAF01:H56 s.c.	H56:PLGA 75:25 NPs i.n. boost
G4- PLGA 85:15 NPs	CAF01:H56 s.c.	CAF01:H56 s.c.	H56:PLGA 85:15 NPs i.n boost
G5- PLGA 85:15 MPs	CAF01:H56 s.c.	CAF01:H56 s.c.	H56:PLGA 50:50 MPs i.n boost
G6- Antigen alone	CAF01:H56 s.c.	CAF01:H56 s.c.	H56 alone i.n boost

6.3.5 Organ processing

Mice were intravenously injected with 250 µL anti-CD45.2- Fluorescein isothiocyanate (FITC) labeled antibodies (2.5 µg in 250 µl PBS) and terminated 3 minutes after injection under CO₂ atmosphere and individual organs isolated. This procedure was carried out with one mouse at a time. Individual spleen and lungs were isolated and were kept ice-cold until further processing. Lymph nodes (mediastinal and tracheobronchial) were isolated and pooled together. Blood samples were withdrawn for antibody analysis.

6.3.5.1 Lungs

Lungs were minced in small fragments and digested for 1 hour at 37°C in a solution containing collagenase and RPMI complemented with 10% FCS. Lungs were disrupted by passaging through a cell strainer and centrifuged at 600 x g for 7 min. Supernatant was harvested for further antibody studies and the pellet was washed and resuspended with 0.5 mL cRPMI. Cells were counted and re-stimulated with either 100 µL ConA (5 µg/mL), RPMI media or H56 (5 µg/mL) and incubated at 37°C, 5 % CO₂ and 95 % humidity for 72 hours. After 3 days of incubation, supernatants were harvested (approximately 160 µL) and stored at -20°C for further processing.

6.3.5.2 Spleens

Spleens from each mouse were isolated and processed as described in Chapter 3. Cells were counted and splenocytes were re-stimulated with either 100 µL ConA (5 µg/mL), RPMI media or H56 (5 µg/mL) and incubated at 37°C, 5 % CO₂ and 95 % humidity for 72 hours. After 3 days of incubation, supernatants were harvested and stored at -20°C for further processing.

6.3.6 Antibodies ELISA

Total IgG antibody measurements were performed as described previously (Chapter 3) in the serum and the supernatants from the lungs. Briefly, Maxisorp microtiter plates were coated with 0.5 µg H56 tuberculosis subunit vaccine per well and incubated overnight at 4°C. The next day, plates were blocked with a 2% BSA in PBS. Serial dilutions of serum samples in 2% BSA in PBS were added to the wells and incubated for 1.5-2 h. Attached H56-specific IgG, antibodies were detected with a horseradish peroxidase-conjugated goat anti-mouse IgG-isotype antibody. All incubations were performed at room temperature. TMB substrate (room temperature), a chromogenic substrate which develops blue colour when it detects horseradish peroxidase (HRP), was added to the plates 100 µL/well. After approximately 20 minutes the reaction was stopped by adding 100 µL/well 0.2 M sulfuric acid and the absorbance measure at 450 nm with a correction at 570/620 nm. Results were plot as the Log₁₀ of the dilution against the measured optical density value (OD₄₅₀).

6.3.7 Cytokines ELISA

Supernatants from restimulated splenocytes and lymph nodes were analysed using a sandwich ELISA protocol for the production of cytokines IL-17 and IFN-γ as described previously (Chapter 3).

6.3.8 Intracellular FACs staining (icFACS)

Antigen specific T cell production of both cytokines, IFN- γ and IL-17, was measured by intracellular flow cytometry. Mice were intravenously administered with fluorescein isothiocyanate (FITC)- labeled anti-CD45 monoclonal antibody (iv.CD45) CD45.2-FITC prior to euthanization which results in staining lymphocytes in the blood and therefore differentiating between blood cells (vasculature) from cells in the lung parenchyma [316]. Spleens, LNs (mediastinal and tracheobronchial) and lungs were *in vitro* stimulated with H56 antigen, and icFACS was run. The panel used for icFACS was surface stained for CD4 (CD4-APC-eFluor780), CD44 (CD44-PE) and CCR-6 (CCR6-AF647) and intracellular stained for IL-17 and IFN- γ (IFN γ -PE-Cy7 and IL-17-PerCp-Cy5.5). Compensation beads were used instead of cells. Results are expressed as percentage of activated (CD44+) cytokine producing (IFN γ +, IL17+) cells of the total CD4+ T-cell population. The chemokine receptor CCR6 was determined as the mean fluorescence intensity (MFI).

6.3.9 Statistical analysis

Data presentation, analysis and interpretation was performed at USTRATH using GraphPad Prism 7 software (GraphPad Soft-ware, La Jolla, CA) and Microsoft Excel. Means and standard deviations are plotted on the graphs. Statistical analysis of data was calculated by one- way analysis of variance (ANOVA) and when significant differences were indicated, differences between means were determined by Tukey's post hoc test. Statistical differences with $p < 0.05$ were considered significant.

6.4 Results and discussion

Within this chapter, the immunogenicity of a prime-pull approach by parenteral priming with CAF01:H56 followed by intranasal administration of H56 antigen encapsulated in an inert delivery systems (PLGA) was investigated as a new vaccine protocol for pulmonary TB. Lack of understanding of how TB immunology works in humans has delayed the development of an efficacious and protective vaccine against this infectious disease [317]. The H56 vaccine candidate is a fusion protein from *Mycobacterium tuberculosis* which is based on early secreted TB antigens Ag85B and ESAT-6 (ESAT-6 remains expressed during chronic infection) and the latency phase secreted antigen Rv2660; therefore, it is considered a multistage subunit vaccine, as it can be employed as a prophylactic and post exposure vaccine [51]. This multistage TB vaccine antigen has demonstrated to be protective in animal models and it is currently in clinical trials (phase 2a). It has been previously reported that the administration of the adjuvant formulation CAF01 in combination with H56 antigen by parenteral

route produces early CD4 T cell responses in the lungs after TB infection [140]. Recent studies by Woodworth et al. have also shown that parenteral administration of CAF01:H56 vaccine followed by respiratory mucosal boost with the same subunit vaccine further increases the recruitment of memory T cells to the lung, enhancing protection against TB [318].

6.4.1 Preparation of PLGA nano- and microparticles for the nasal delivery of H56 vaccine candidate: rational design

We have previously determined the critical process parameters for the development of dry powder PLGA NPs and MPs suitable for the delivery of the H56 vaccine candidate to the deep lungs (as determined through a wide range of *in vitro* techniques). PLGA nanoparticles were prepared using microfluidics at a TFR 10 mL/min and FRR 1:1. The amount of H56 antigen was fixed at 0.25 mg/mL (10 µg per dose). The mean particle size of the PLGA NPs encapsulating H56 before FD was approximately 110, 150 and 260 nm for the copolymers 50:50, 75:25 and 85:15 respectively (data not shown), in accordance with the data presented in Chapter 4. All the nanoparticles were homogeneous in nature showing PDI values below 0.15 (data not shown). The zeta potential values were highly anionic as it is characteristic from PLGA particles (values between -35 and -50 mV; data not shown). The initial antigen concentration injected into the microfluidics system was calculated according to the encapsulation efficiencies previously quantified by HPLC in order to get a final encapsulation of 10 µg per dose.

For the preparation of PLGA microparticles, H56 antigen was concentrated up to 10 mg/mL using a Vivacon 2 (Sartorius, Goettingen, Germany) with a MWCO 50,000 Da. The protocol was optimised and the antigen concentration was quantified using BCA in order to calculate the recovery during the centrifugation step. H56 antigen comes in a stock of 1.1 mg/mL (20 mM glycine, pH 8.8) therefore in order to get a final antigen concentration of 10 µg per 40 µL within the microparticles, a concentration step is needed. The results from the recovery study are shown in Figure 6.2. Wetting the membrane with ultrapure water (method 1) prior to the addition of the antigen into the column produced a recovery >90%, whereas the passivation method (method 2) or no previous treatment (method 3) produced recoveries of ~75% and ~50% respectively. The mean particle size (D50) of the PLGA 85:15 MPs was ~1.2 µm with neutral zeta potential (~ -0.7 mV). To achieve higher protein loading, modification (increase) of the internal aqueous volume, or the polymer concentration during the double emulsion method resulted in a large increase of the mean particle size for the MPs. Therefore, MPs were formulated as usual but reconstituted with lower volume of cryoprotectant solution to reach the desired final antigen loading of 0.25 mg/mL.

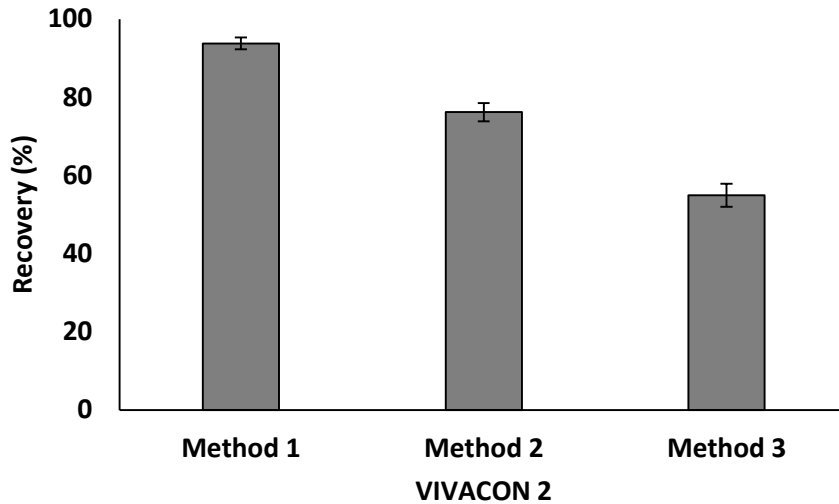


Figure 6.2 Percentage recovery of H56 antigen after using three different membrane treatments prior concentration of the antigen up to 10 mg/mL. Method 1 consisted in wetting the membrane with ultrapure water prior addition of the antigen. Method 2 consisted in addition of a surfactant to decrease binding affinity of the Ag to the membrane (passivation method) and Method 3 no treatment.

6.4.2 Prime-pull vaccination: immunological responses

CB6F1 mice were subcutaneously primed with H56 (Ag85B-ESAT6-Rv2660) in combination with the CAF01 adjuvant (which promotes Th1/Th17 responses) and boosted with different PLGA copolymers encapsulating H56 as outlined in Figure 6.1. Humoral and cellular mediated immune responses were measured in serum and supernatants from stimulated lungs, spleens and LNs to evaluate the efficacy of this approach as a prophylactic vaccine to replace BCG.

6.4.2.1 Humoral immune responses: IgG quantification

Systemic and mucosal antigen specific IgG responses were measured in blood serum and lung lymphocytes, respectively, 14 days after the last immunisation by direct ELISA. Results are represented as the mean OD₄₅₀ value obtained from each dilution \pm the standard deviation (SD) against the log₁₀ of the dilution.

From the results in Figure 6.3, it can be seen that no significant differences were observed between the vaccinated groups. All the PLGA formulations as well as the mice that received the antigen alone gave significant ($p < 0.001$) higher H56 specific IgG immune responses when compared to the naïve (unvaccinated) group (Figure 6.3A). H56-specific IgG responses in the supernatants from lung

lymphocytes showed similar results (Figure 6.3B). In general, mice boosted with PLGA NPs and MPs gave comparable results to those boosted with H56 antigen alone thus demonstrating that incorporation of the antigen within the NPs and MPs was not detrimental to the antigen efficacy, and that incorporation of the antigen within these systems allows for them to be delivered in a stable dry-powder format. The importance of IgG production has been reported elsewhere, low levels of IgG are associated with higher susceptibility to TB infection, thus, stimulation of early antibody responses at the site of infection might contribute to the fight against the infection by neutralising Mtb antigens [319, 320]. Therefore, these data suggest that it is possible to incorporate antigen into NPs/MPs for dry power inhalation without any detrimental effect.

It is important to find the best particle attributes (particle size, size distribution and morphology) for the delivery systems in order to elicit the adequate immune response. However, this has been challenging as many studies evaluating the influence of the particle size on evoking immune responses are in disagreement. Studies carried out with PLGA particles with different sizes showed that administration of PLGA MPs evoked increased IgG immune responses compared to PLGA NPs [125, 321] whereas studies by Carcaboso et al. showed that similar IgG responses were obtained after administration of PLGA NPs with sizes of 110 nm and 800 – 900 nm [322]. Regarding copolymer composition, studies by San Roman et al. on PLGA MPs encapsulating OVA using copolymers 50:50 and 75:25 showed similar IgG1 responses for both formulations whereas the IgG2a responses were higher for the more hydrophobic copolymer (75:25) [323]. In this study, 4 different particle sizes were investigated along with the influence of the PLGA copolymer and the results show that neither size nor polymer choice have an impact, similar to the work of Carcaboso et al [17]. This is in contrast to the previous uptake and antigen process studies (Chapter 5) which suggested that PLGA NPs were more effective compared to PLGA MPs. *In vitro* results showed similar particle uptake for both NPs and MPs independently of the copolymer used whereas the antigen processing studies in the macrophages cell lines were significantly better for PLGA NPs.

6.4.2.2 Cellular mediated immune responses: cytokine production and T cell location

The production of Th1 and Th17 type immune responses was studied by quantification of the H56-specific IFN- γ and IL-17 cytokines respectively in the supernatants of re-stimulated splenocytes and lung lymphocytes (Figure 6.4). These cytokines were selected due to their importance in the protection against pulmonary TB [28, 34]. Results showed comparable secretion of both cytokines, IL-17 and IFN- γ , in the spleen and lungs. Stimulation was found to be independent of the PLGA booster administrated, since no significant differences between the vaccinated groups were found. All

vaccinated groups produced high and comparable cytokine responses whereas the unvaccinated group did not stimulate the production of any of the cytokines studied (Figure 6.3). Again this data confirms that antigen can be effectively formatted into a dry-powder format, suitable for pulmonary delivery without any loss of antigen efficacy.

There is a wide variety of studies using PLGA particles for vaccine delivery. Vaccine attributes such as particle size and polymer intrinsic properties influence the generated immune response. Published data generally agree that PLGA MPs produce enhanced humoral immune responses whereas PLGA NPs generate higher cellular responses [125, 324]. For example, Gutierrez et al. showed that PLGA MPs (~1 μm) loading BSA as a model antigen, produced higher IgG serum antibody titres than the PLGA:BSA NPs (200 and 400 nm) after any of the three administration routes evaluated: subcutaneous, intranasal and oral [125]. Regarding polymer properties, San Roman et al. demonstrated that PLGA 75:25 MPs encapsulating OVA produced stronger IFN- γ responses compared to PLGA 50:50 when administered intradermally [323]. This result was attributed to the hydrophobicity of the copolymer, since it is likely that the interaction of the copolymer 75:25 with the APCs resulted in superior T cell activation [323]. Moreover, Thomas et al. developed vaccine delivery systems for a hepatitis B antigen (HBsAg) based on PLGA 85:15 and 50:50 NPs (~770 and 470 nm respectively). He showed that PLGA 85:15 NPs loading HBsAg produced higher humoral and cellular immune responses compared to the other copolymer after pulmonary administration [325]. These immunological differences were attributed to the hydrophobicity of the copolymer 85:15 and its particle size [325]. However, studies on cationic PLGA 50:50 and 75:25 MPs absorbing a hepatitis B antigen (HBsAg) showed similar humoral (IgG) and cellular responses (IFN- γ and IL-2) for both copolymers after subcutaneous vaccination [326].

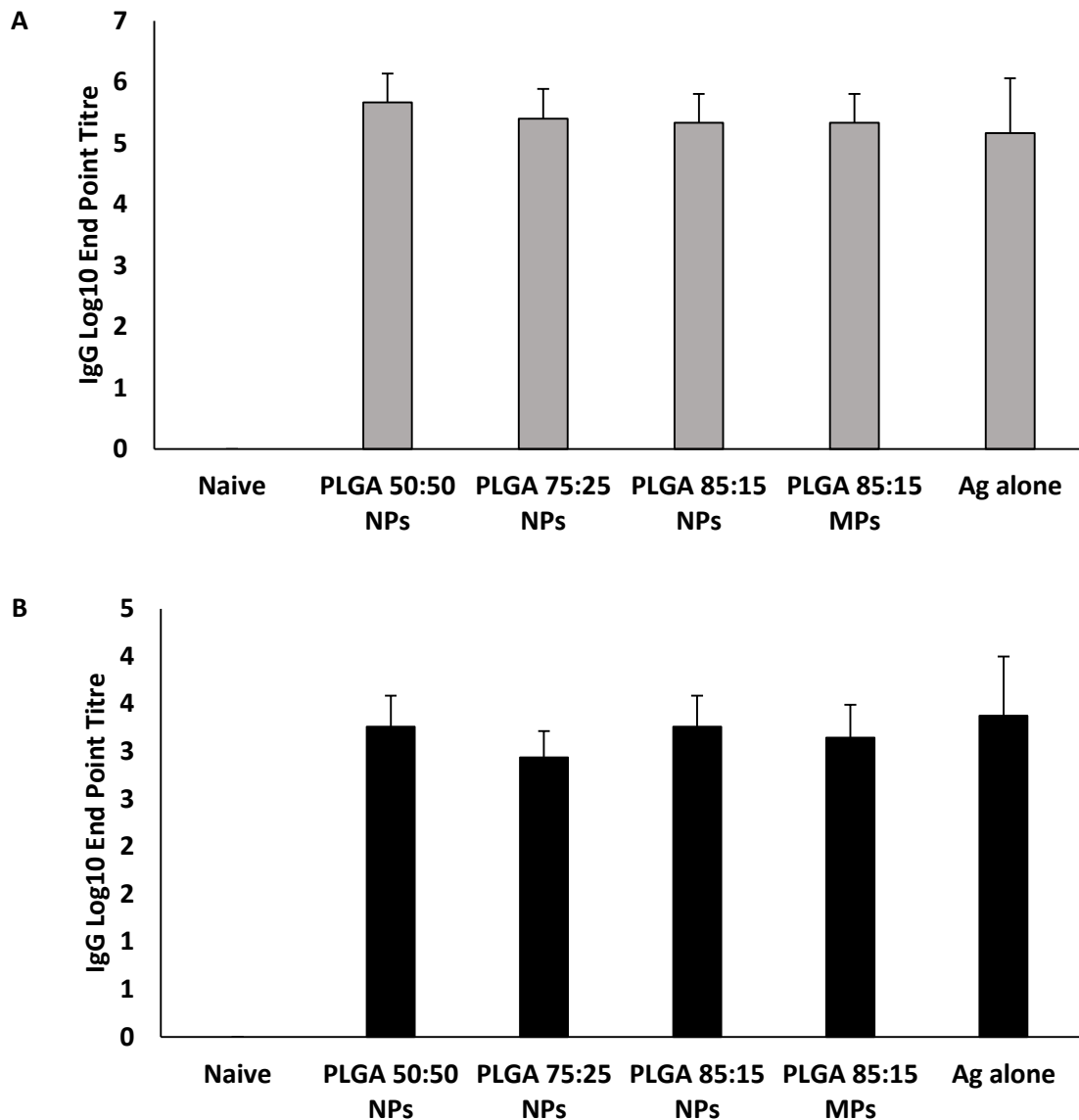


Figure 6.3 Antigen-specific humoral immune responses in (A) serum and (B) supernatants from lung lymphocytes after prime-pull immunisation (2 x s.c. CAF01:H56 and 1 x i.n PLGA:H56). Serum samples from 6 individual mice in each vaccine group were isolated 2 weeks after the booster immunization. H56-specific serum production of immunoglobulin G (IgG) was measured by ELISA. ELISA OD₄₅₀ values are represented as mean values \pm S.D, n=6.

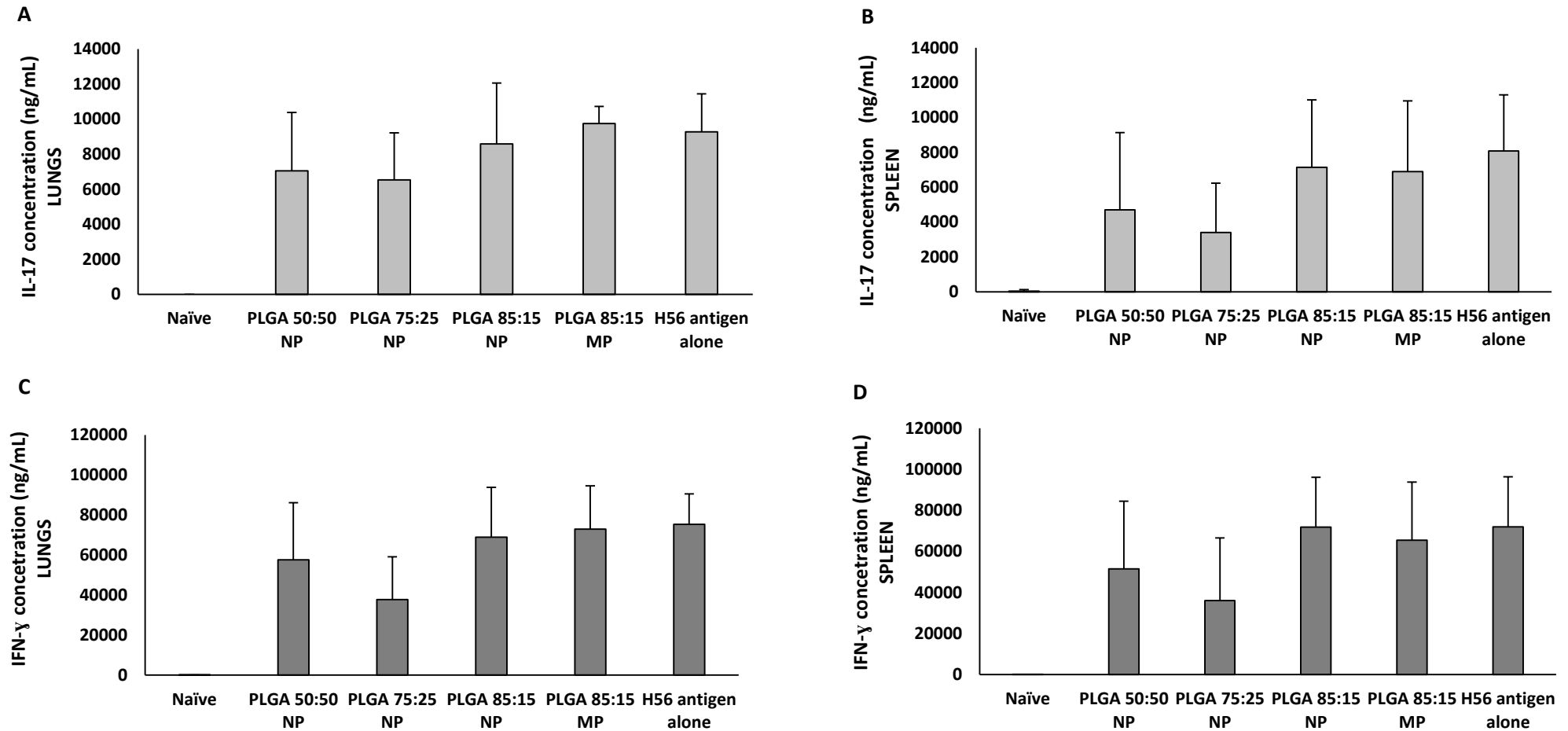


Figure 6.4 Antigen-specific cellular immune responses in supernatants from re-stimulated splenocytes and lung lymphocytes after prime-pull immunisation (2 x s.c. CAF01:H56 and 1 x i.n PLGA:H56): IL-17 concentration in the **(A)** lungs and **(B)** spleen respectively; IFN- γ concentration in the **(C)** lungs and **(D)** spleen respectively. Individual spleens and lungs were isolated 2 weeks after the booster immunization. H56-specific cellular production of cytokines was measured by ELISA. Calculated mean concentration values (bars) \pm SD are represented.

6.4.2.3 Specific location of the T-cell responses

Understanding the participation of the cells during the production of immune responses is crucial for vaccine development. Production of antigen specific CD4⁺ T cells and the homing of these cells to the lungs is of vital importance to fight against Mtb infection [327]. Their distribution is important since the cells located in the lung parenchyma and, therefore, in direct contact with the pathogen will be able to protect against the infection [328, 329]. Investigation of the distribution of the CD4⁺ T cell profiles was studied using a well-established *in vivo* staining technique described by Anderson et al [316]. FITC-labelled anti-CD45 monoclonal antibody was intravenously injected 3 minutes prior euthanasia in order to differentiate between the cells located in the vasculature and the parenchyma. By this method, blood cells will be stained (positive staining) opposite to the cells located in the parenchyma (negative staining). Therefore, the H56-specific CD4⁺CD44⁺ T cells and CD4⁺CCR6⁺ T cells cytokine profile (producing IFN- γ and IL-17) in the individual cells in the lungs, spleen and LNs (mediastinal and tracheobroncheal) were investigated using intracellular flow cytometry staining and by gating for activated CD4⁺ T cells. The *in vivo* staining technique is more noticeable for the lungs as they contain a large number of blood cells whereas the spleen and LNs contain very little. Subsequently, the amount of positive (vasculature) CD4⁺ T cells in the spleen and LNs was minimum and therefore, non-quantifiable. In contrast, as it was expected, the CD4⁺ T cell population in the lungs was differentiated between vasculature (positive staining) and parenchyma (negative staining).

6.4.2.3.1 Antigen specific CD4⁺ T cells responses in the lungs

Cells expressing CD44⁺ were measured for the identification of vaccine memory CD4⁺ T cells [330]. Analysis of the H56 specific production of IFN⁺ CD44⁺ CD4⁺ T cells and IL-17⁺ CD44⁺ CD4⁺ T cells located in the parenchyma as percentage or number of cells producing these intracellular cytokines (shown in Figure 6.5). All vaccinated groups produced significantly ($p < 0.05$) higher levels of both IFN- γ and IL-17 in the lung parenchyma compared to the unvaccinated group, independent of particle size and copolymer used. The percentage of IFN⁺ CD44⁺ CD4⁺ T cells from the groups boosted with PLGA NPs 50:50 and 75:25 as well as the group administered with PLGA MPs 85:15 produced lower levels of IFN⁺ CD44⁺ CD4⁺ T cells when compared to the groups boosted with H56 alone or PLGA NPs 85:15. On the other hand, when IL-17⁺ CD44⁺ CD4⁺ T cells levels were measured, PLGA MPs 85:15 showed the higher percentage of cytokine production alongside the group vaccinated with the antigen alone. The same quality but lower quantity was observed for the CD44⁺ CD4⁺ T cells confined in the lung vasculature (positive). In general, cytokine production in naïve mice was barely detectable and cells in the parenchyma were able to produce more cytokines than cells in the vasculature. These results confirm

the ability of PLGA to deliver H56 to the lungs with similar levels of antigen-specific cytokine producing CD4⁺CD44⁺ or CD4⁺CCR6⁺ T cells were observed for all the vaccinated groups. Expression of cytokine combinations (IL-17⁺/IFN- γ ⁺, IL-17⁺/IFN- γ ⁻ and IL-17⁻/IFN- γ ⁺) were measured and the majority of the cells were single producers of cytokines, either IL-17 or IFN- γ single-positive CD4⁺ T cells were found in the lung parenchyma (Figure 6.6). Vaccinated groups resulted in a significantly higher ($p < 0.001$) increase in antigen-specific CD4⁺ T cells compared to control mice (unvaccinated group). The expression of mucosal homing chemokine receptor CCR6 specific of Mtb was measured as a function of the mean fluorescence intensity (MFI) (Figure 6.6) [331, 332]. IL-17 and IFN- γ cytokine producing CD4⁺ T cells expressed similar levels of CCR6 in all the vaccinated groups, whereas for the unvaccinated group, higher levels of single cytokine expression was observed. Boosting with PLGA:H56 NPs and MPs induced equivalent percentages of Th1 and Th17 CD4⁺ T cells as boosting with H56 antigen alone.

The enhancement of mucosal CD4⁺ T cells producing IL-17 is important for the development of a protective vaccine against TB as well as the production of IFN- γ CD4⁺ T cells, which have been previously demonstrated to be of high importance against TB in humans. [141, 333, 334]. The current TB vaccine, BCG, does not stimulate T cells in the lungs, which has been attributed to its lack of efficacy in protecting against pulmonary TB. Studies carried out in guinea pigs showed that after mucosal vaccination with BCG, better protection against TB was found when compared to the conventional intradermal route [335, 336]. Recent studies have shown the increased local immune responses obtained by mucosal vaccination and consequently, improved protection against TB [334]. The importance of the recruitment of T cells to the lungs has recently been demonstrated for protection against TB infection. The location of these T cells is crucial for the efficacy of the vaccine since the T cells have to be in direct contact with the Mtb infected macrophages [139-144]. Therefore, respiratory mucosal vaccination is believed to be the best way to teach the lung macrophages and DCs how to fight Mtb infection and to recruit antigen specific T cells to the site of infection (lung parenchyma and airway) [145, 146]. Results from this study demonstrate that PLGA:H56 NPs and MPs can be produced in a dry powder format which can work as effectively as the administration of free antigen. This is key as it is unlikely to find an antigen that after administration alone produces these high immune responses as generally, administration of free antigen is poorly immunogenic.

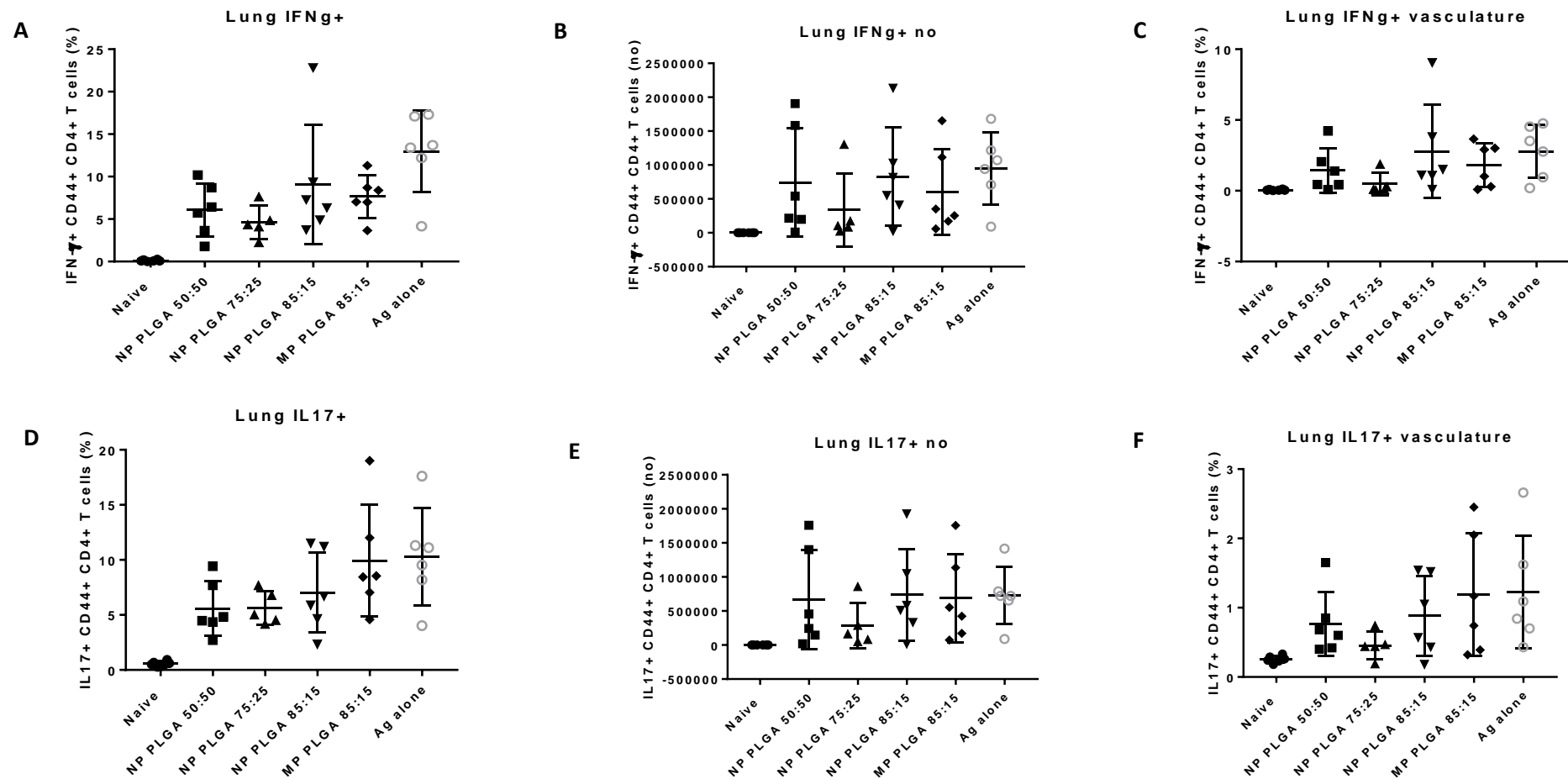


Figure 6.5 Percentage of IFN γ CD4 $^{+}$ CD44 $^{+}$ and IL-17 $^{+}$ CD4 $^{+}$ producing T cells measured by intracellular staining in the lung parenchyma (negative) and lung vasculature (positive). T cell responses following vaccination 2 x s.c. CAF01:H56 and 1 x i.n PLGA:H56 in CB6F1 mice (n = 6). Two weeks after intranasal boosting of the antigen, the cells from the lungs were stimulated with H56 antigen and cytokine production was assessed by icFACS. **(A)** Percentage and **(B)** number of H56-specific CD4 $^{+}$ T cells producing INF- γ in the lung parenchyma and **(C)** in the lung vasculature; **(D)** Percentage and **(E)** number of H56-specific CD4 $^{+}$ T cells producing IL-17 in the lung parenchyma and **(F)** in the lung vasculature.

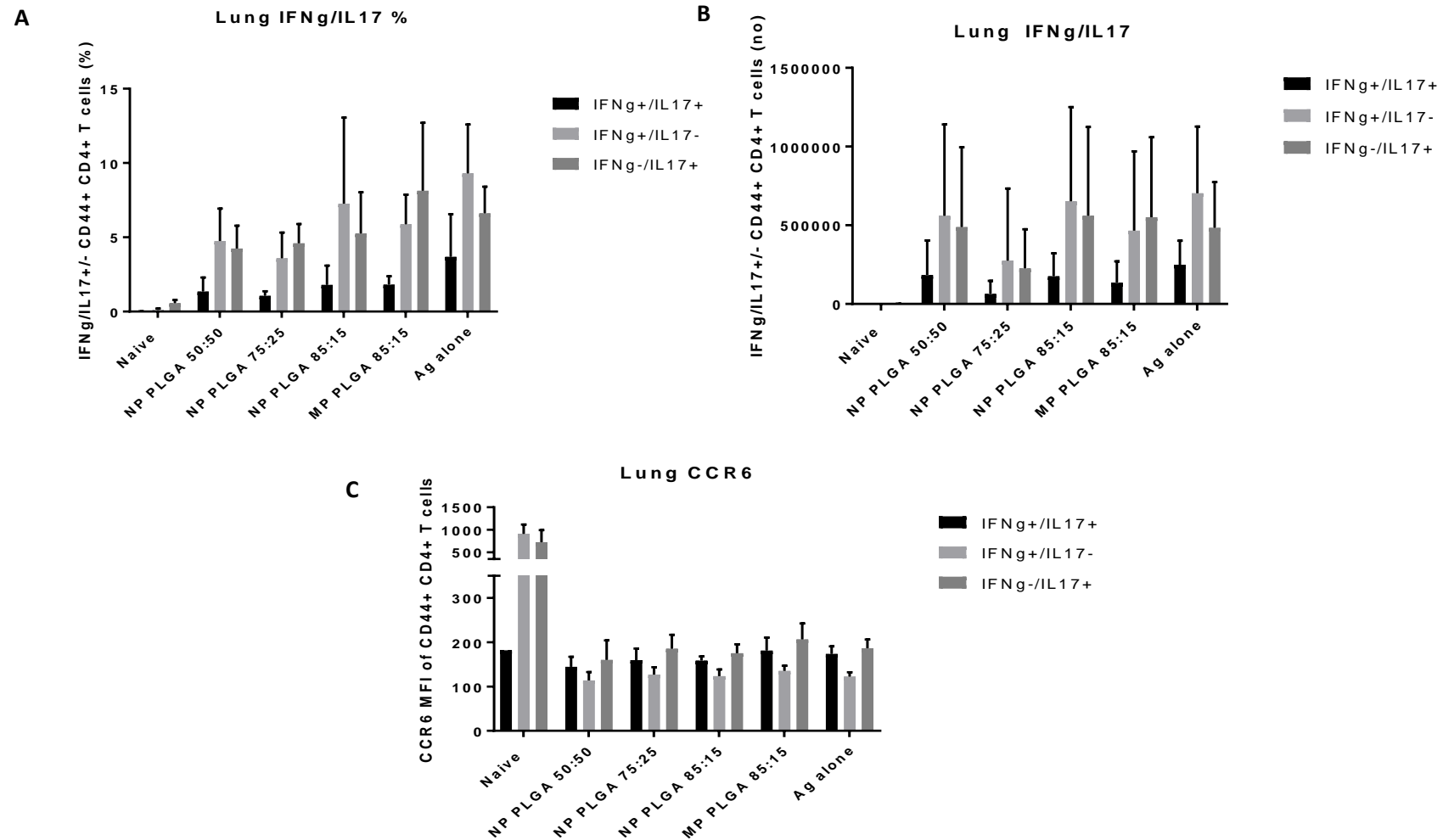


Figure 6.6 Percentage of CD4⁺CD44⁺ or CD4⁺CCR6⁺ T cells (IL-17 and IFN- γ) of the study by intracellular flow cytometry on the lung. T cell responses following vaccination 2 x s.c. CAF01:H56 and 1 x i.n PLGA:H56 in CB6F1 mice (n = 6). Two weeks after intranasal boosting of the antigen, the cells from the lungs were stimulated with H56 antigen and cytokine production was assessed by icFACS. **(A)** Percentage and **(B)** number of H56-specific CD4⁺ T cells producing INF- γ /IL-17 and **(C)** CCR6 medium fluorescence intensity cytokine production in the lung parenchyma.

6.4.2.3.2 Antigen specific CD4⁺ T cells responses in the spleen and lymph nodes

Secretion of IFN- γ and IL-17 responses in the spleen and lymph nodes was assessed. Regarding the CD4⁺ T cells responses in the spleen and lymph nodes, all the vaccinated groups secreted significantly higher ($p < 0.0001$) amounts of cytokines compared to the naïve group (Figure 6.7). Immunisation with PLGA 85:15 NPs produced increased levels of antigen specific IFN- γ producing CD4⁺ T cell responses in the splenic T cells as well as in the lymph nodes (Figure 6.7A and D). Similar numbers of H56-specific CD4⁺ T cells producing IL-17 were measured for the vaccinated groups with PLGA 85:15 copolymer, independent of the particle size (both NPs and MPs) and for the antigen alone vaccinated group (Figure 6.7B and E). It was noticeable that the production of IFN- γ ⁺ and IL-17⁺ CD4⁺ CD44⁺ T cells was significantly decreased ($p < 0.05$) for the F1 mice vaccinated with PLGA 75:25 NPs. Similar numbers of activated CD4⁺ cells expressing CCR6 were found in the spleens and LNs for all groups. Expression of CCR6 in the spleens and LNs was prominent for single IL-17 producers in all the groups (vaccinated and unvaccinated). In general, the naïve group lacked antigen specific CD4⁺ T cells secreting neither IL-17 nor IFN- γ in the lungs, spleen or LNs. Cytokine production through the stimulation of the chemokine receptor CCR6 was increased when compared to the vaccinated groups (Figure 6.7C and F).

This work demonstrates the design of a TB subunit vaccine containing the TB vaccine candidate H56 (Ag85B-ESAT6-Rv2660) as part of a prime-pull protocol where the Th1/Th17 promoting adjuvant CAF01 was administered by parenteral priming followed by a respiratory mucosal booster with PLGA:H56. Results demonstrate that the H56 vaccine candidate can be encapsulated within a well-characterised delivery system without losing its immunogenicity in a murine model. Stimulation of the adequate cell subset population in the right location and in the right quantity is believed to be a critical factor for controlling Mtb growth. Studies by Woodworth et al. [318], following a protocol based on 3 x s.c administrations of CAF01:H56 and 2 x s.c followed by 1 x i.n CAF01 in CB6F1 mice showed an improvement in the recruitment of the T cells to the lungs (parenchyma) after mucosal vaccination compared to the subcutaneous route. Regardless of the increased antigen specific responses in the lung parenchyma, the narrowed protection showed after challenge with Mtb demonstrates the limited power of the vaccine-induced T cells to regulate Mtb infection [318]. Furthermore, another recent study by Asshurst et al. for pulmonary administration of PLGA encapsulating a TB antigen also demonstrated that although the T cell immune responses were increased in the lungs, these did not enhance the protection against TB after challenge [152].

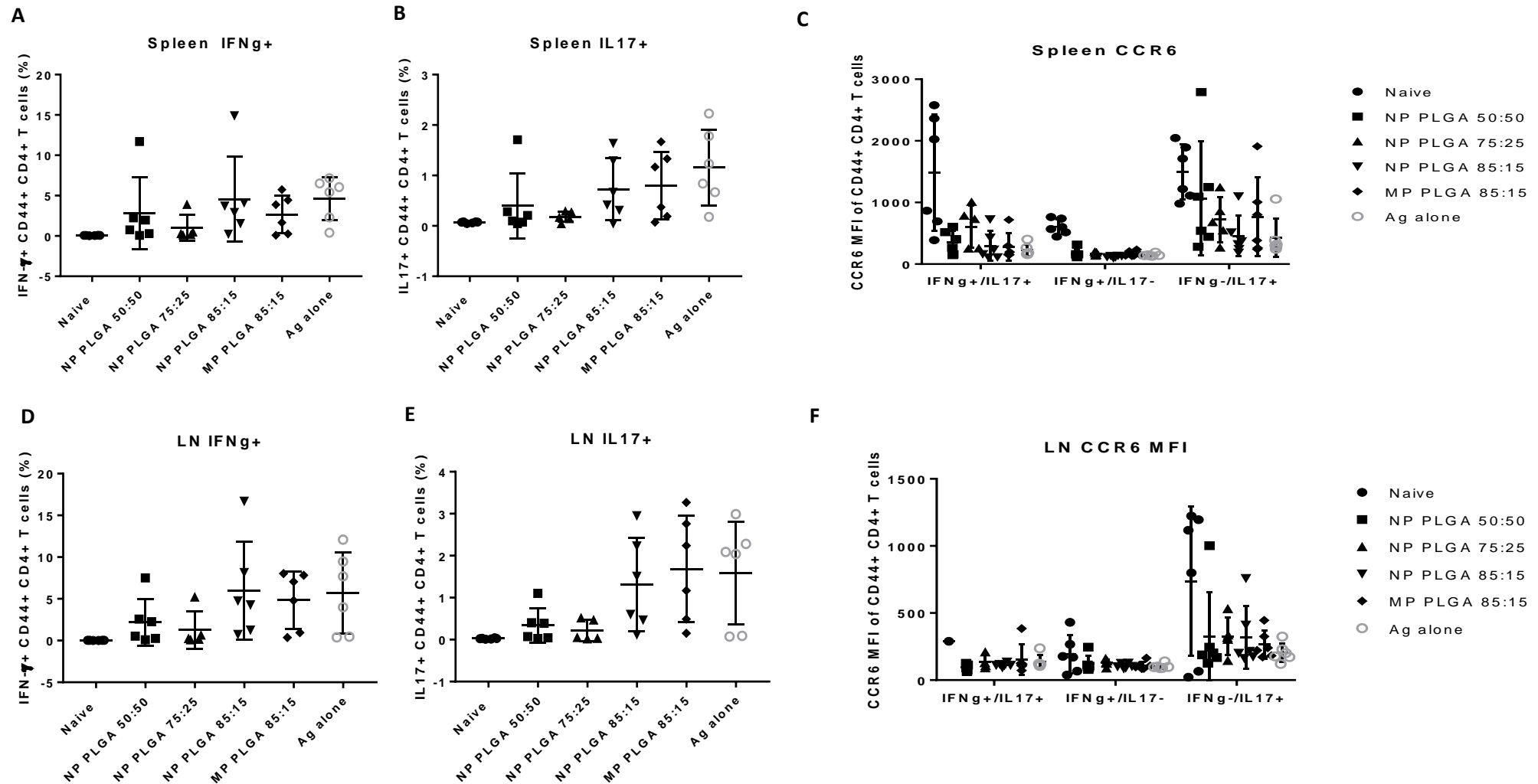


Figure 6.7 Percentage of IFN γ ⁺CD4⁺CD44⁺ and IL-17⁺CD4⁺ CD44⁺ producing T cells measured by intracellular staining in the splenocytes and lymph nodes of vaccinated mice. T cell responses following vaccination 2 x s.c. CAF01:H56 and 1 x i.n PLGA:H56 in CB6F1 mice (n = 6). Two weeks after intranasal boosting of the antigen, the cells from the lungs were stimulated with H56 antigen and cytokine production was assessed by icFACS: Percentage of (A) IFN- γ , (B) IL-17 and (C) CCR6 in the spleen. Percentage of (D) IFN- γ , (E) IL-17 and (F) CCR6 cytokines in the LNs.

6.5 Conclusions

There is still an unmet need for an efficacious TB vaccine. The current TB vaccine (BCG) has shown variable efficacy in children, while failing to elicit any protection against the main form of TB (pulmonary TB) at any age. Thus, to overcome the limitations of BCG, a wide range of vaccination strategies are being developed to stop and control TB transmission and infection. Current research has focused on the stimulation of T cell responses at the point of entry for the bacteria – the mucosa within the lungs. Here we evaluated a prime-pull immunisation approach for a vaccine against pulmonary TB, consisting of priming with CAF01:H56 followed by a mucosal boost with PLGA:H56. The inert delivery system based on PLGA encapsulating the TB vaccine candidate H56 was formulated in a scale independent manner and lyophilised to a dry powder format for aerosolisation into the lungs. Results shown here demonstrate the applicability of this manufacturing method to deliver encapsulated antigen to the lungs via the intranasal route of administration. The immune responses generated by this approach indicate the retention of the immunogenicity of the antigen encapsulated within a lyophilised PLGA delivery system. Although no enhancing effect could be observed compared to the administration of antigen alone as a boost, the work demonstrates the scale independent manufacture of polymer based delivery systems encapsulating antigens for inhalation/aerosolisation delivery to the lung mucosa. During this process the antigen remains efficacious compared to the free antigen.

Chapter 7

Overall Conclusions and Future Work

7.1 The need for a new Tuberculosis (TB) vaccine

Tuberculosis remains the leading cause of death due to an infectious disease, affecting more than one third of the population worldwide. Despite the existence of a TB vaccine (the well-known BCG vaccine) and besides being the world's most administered vaccine it fails to protect against the most common form of TB, pulmonary TB. Several initiatives are focused on the development of a TB vaccine to control and stop TB by 2035. Different approaches for vaccine development can be followed depending on the target population (children, adults, elderly, immunocompetent and so on); the vaccine backbone structure (live, attenuated or subunit vaccines); immunisation protocol (from replacement vaccines to vaccine boosters) and degree of exposure to the microorganism (prophylactic, post-exposure, and therapeutic vaccines). Due to the poor immunogenicity of highly purified peptides/antigens (subunit vaccine) and inactivated vaccines when administered by themselves, the inclusion of adjuvants in the vaccine formulation is generally necessary. Adjuvants are substances that enhance and modulate the immune response when combined with vaccine antigens and among them, lipid and polymer-based adjuvants have been extensively studied for this purpose. Independently of the vaccine approach or category selected, the same rationale for the development of any vaccine should be followed in terms of production, cost, safety and efficacy [45]. The vaccine cost should be reduced, and the method of production should be reproducible and accessible in developing countries, where the highest TB incidence occurs. The route of administration directly influences the outcome and efficacy of the vaccine. Eliciting specific immune responses at the target site can greatly enhance protection. Lungs are the port of entry of Mtb and thus, the lung mucosa is one of the first lines of defence against the bacteria, therefore, it is hypothesised that strong mucosal immune responses are required to build protection against TB.

The main aim of this thesis was to develop a prime-pull vaccine approach for protection against pulmonary TB following an immunisation protocol consisting of parenteral priming with the TB vaccine candidate (H56) alongside the cationic liposome adjuvant 01 (CAF01) followed by respiratory mucosal boosting of the H56 tuberculosis antigen within an inert delivery system (PLGA)

7.2 The use of microfluidics as a tool for the manufacture of CAF01

Initial studies were focused on the 'priming' part of the vaccination protocol. CAF01 has been extensively investigated alongside the H56 antigen for immunisation against TB. This formulation is commonly prepared by the thin film method which has several drawbacks including scale-up and

reproducibility. By this methods MLVs are produce therefore, to reduce the size and lamellarity of the formulation, a size reduction method such as high shear mixing (HSM) has to be applied to the preformed MLVs. In contrast, controllable technologies such as microfluidics have advantages in material preparation such as uniform flow and mixing, high efficiency, continuous operation, easy control and low cost [163]. Therefore, the aim of this study was to investigate the use of microfluidics as a manufacturing method for CAF01.

Results here demonstrate that cationic liposomes formulated by microfluidics can be formulated in sizes down to 65 nm depending on the parameters adopted. In general, increasing FRR reduces the size of the particles. This is in contrast to vesicles subject to HSM, where the minimum size was ~200 nm. Liposomes prepared by LH showed the biggest particle size. However, liposomes produced using microfluidics tended to be more heterogeneous in nature. Addition of cholesterol was shown to facilitate the production of liposomes by microfluidics. This might be due to the decrease of transition temperature in the formulation when cholesterol is incorporated. In terms of antigen loading, OVA was added as a model antigen to the preformed liposomes, and the results obtained showed that OVA adsorption is dependent on electrostatic interactions between the liposomal surface and the negatively charged protein. Therefore, OVA could be efficiently loaded on the positively charged membrane surface of the liposomes containing DDA (all CAF formulations gave high protein loading >90%) whereas liposomes containing DMPC were not as effective due their neutral surface charge. Lipid content of liposomal adjuvant formulations was successfully quantified using a HPLC-ELSD method. Lipid film hydration, HSM and microfluidics have shown to be suitable methods for manufacturing of liposomal adjuvants since the recovery of the lipids was high across all three of the manufacturing methods evaluated.

Production of CAF01 using the LH and HSM can be an inefficient time consuming process, especially in regards to high scale industrial manufacture. If large scale production of a TB vaccine is to be achieved for global immunisation, new manufacturing methods that can achieve this must be considered. Novel techniques to rapidly produce liposomal vesicles such as microfluidics could alleviate large scale production issues. Results demonstrated here indicate the ability of a microfluidic platform to produce CAF01 with highly similar physicochemical characteristics when compared to the traditional methods mentioned above. Additionally, the use of microfluidics allows for the control of numerous production parameters yielding a range of particle sizes for CAF01.

7.3 *In vivo* studies with CAF01 liposomal formulation manufactured by microfluidics retains its biodistribution profile and immunogenicity

CAF01 has been shown to be a potent adjuvant and produce a Th1-biased immune response in combination with a range of sub-unit vaccines including chlamydia, influenza, HIV and tuberculosis vaccine (e.g. [73, 87-90]). Its immunological profile consists of strong production of cellular and humoral immune responses based on high IFN- γ and IL-17 secretion, low IL-5 production and high IgG antibody production [98, 99]. Thus, after the successful production of CAF01 liposomes using microfluidics in the previous study, the aim of Chapter 3 was to evaluate the *in vivo* performance of CAF01 liposomes manufactured using microfluidics compared to the traditional LH method.

The pharmacokinetic and immunological profile of the microfluidic formulations (CAF01 MF) remained intact when compared with the commonly used method for the preparation of the CAF01 formulation (CAF01 LH) *in vivo*. In order to track the movement of both antigen and liposomes *in vivo*, both vaccine components were radiolabelled. High amounts of liposomes and antigen were detected at the site of injection (SOI) at all the time points studied. CAF01 biodistribution showed a sustained draining of the vaccine from the SOI independently of the manufacturing method used. Immunological studies of CAF01 LH and CAF01 MF showed no significant difference between the antibodies responses measured. Both formulations showed increasing IgG1 and IgG2c over time with strong responses after day 21. Regarding cytokine responses from re-stimulated splenocytes and lymph nodes, both CAF01 formulations showed strong Th1/Th17 responses with the CAF01 MF producing higher amounts of IFN- γ in cells from the lymph nodes.

The use of a microfluidic based manufacturing method shows potential for the production of vaccine adjuvants in a scalable process. Vaccine production is a high-cost area involving large economic investments in both research and development and vaccine manufacture. In order to bring overall costs of new vaccines down, streamlining the manufacturing process is an essential task. Novel techniques such as microfluidics offer a scale- up alternative to batch production.

7.4 Scale independent production of PLGA delivery systems

Once the production of CAF01 for the priming of the immune system was established, the manufacture of an inert delivery system to carry the H56 antigen to the lungs was investigated. Biodegradable compounds degrade into non-toxic and biocompatible products upon *in vivo* administration. Subsequently, the degradation products are removed from the system by the normal metabolic pathways. The PLGA family has been widely investigated due to its exceptional safety profile and its

FDA and EMA approval for human use [55]. These particulate delivery systems can be manufactured through a wide range of methods and therefore their physicochemical properties can be easily manipulated in order to achieve the adequate characteristics for the right interaction with biological cells. Commonly PLGA nanoparticles (NPs) and microparticles (MPs) are manufactured by using methods such as double emulsion, coacervation, nanoprecipitation, extrusion or solvent evaporation [104-111].

For the formulation design on PLGA as a vaccine delivery system, knowledge about its intrinsic properties is crucial in order to improve its efficacy. Several factors influence PLGA performance, among them, the monomer molar ratio, average molecular weight, crystallinity, size and shape are of absolute importance. PLGA polymer can be synthesized in a wide variety of lactic to glycolic monomer ratios. The main PLGA copolymers used in research are 50:50, 75:25 and 85:15, which in general contain higher lactic acid percentage. Varying the percentage of lactic or glycolic acid present in the polymer composition, influences the hydrophilicity of the polymer and thus, the degradation rate. The percentage of PGA dictates the hydrophilicity of the copolymer, therefore, PLGA copolymers with higher PGA content show accelerated degradation when compared to PLGA copolymers with higher PLA content. Antigens can be encapsulated within these PLGA particles which provide antigen protection and controlled release profiles [102, 212].

Since the aim of this thesis is to develop a prime-pull protocol for vaccination against pulmonary TB, Chapter 4 assessed the applicability of microfluidics for the preparation of PLGA delivery systems encapsulating H56 antigen and using copolymers 50:50, 75:25 and 85:15. Results have shown the successful manufacturing of polymer nanoparticles using microfluidics. In general, altering the flow rate ratio of the microfluidics system has shown to control the size of the PLGA nanoparticles obtained as well as the PLGA copolymer ratio used and the concentration of antigen loaded within these systems. In contrast, the total flow rate and therefore the output capability of the system did not impact on these parameters demonstrating the suitable scalability of this system. The formed PLGA nanoparticles were spherical and regular shaped particles with a rough outer surface suitable for pulmonary delivery. Encapsulation of the H56 tuberculosis antigen was achieved via a one-step in-line microfluidics process showing medium antigen loading (from 20 to 40%). Residual solvent was removed from the formulations to a level below the acceptable cut off point as dictated by the ICH guidelines. Microfluidics has shown to be a fast, reproducible and easy method for the production of PLGA nanoparticles. However, the microfluidics system was limited to particles below 500 nm which may require further modification for appropriate cell uptake/lung deposition. PLGA MPs were also formulated in order to have a wide range of particle sizes for further cellular uptake and deposition studies. Thus, in order to get an overview of the importance of the particle size for the delivery of the

vaccine in the deep lungs, PLGA microparticles were manufactured using the conventional double emulsion method (w/o/w). Results showed the production of micrometre range particles ($\sim 1\text{-}1.5\ \mu\text{m}$) independently of the copolymer ratio used, with lower encapsulation efficiency (from 10 to 30%) than the NPs and same physical characteristics as shown by the NPs (spherical in shape and with a rough surface).

7.5 Aerodynamic engineering of a TB vaccine for lung delivery

Formulation of an inhalable delivery system containing tuberculosis antigens to target the site of infection could be an interesting approach for the development of a subunit vaccine against this disease. PLGA particles suffer hydrolytic degradation when stored in liquid environment for prolonged periods of time. Preparation of PLGA delivery systems as dry powders can increase the stability of these particles and allow for the engineering of particles with suitable aerodynamic parameters to achieve deposition in the appropriate lung region. Besides, the exclusion of the cold-chain requirement would contribute with the reduction of the vaccine cost and it would facilitate the stability of the vaccine during transit and storage.

In this regard, particle size is one of the main factors dictating the aerosol deposition in the airways. Therefore, the rational design of delivery systems has to consider physicochemical properties such as size and shape, geometry, charge and density of the particulate system for the deposition of the inhaled particles [134]. This study aimed to develop dry powders for inhalation containing PLGA as delivery system for the delivery of the H56 tuberculosis antigen into the deep lungs (alveoli), which will be used for an *in vivo* 'pull' vaccination.

In the previous study, microfluidics was assessed for the manufacture of PLGA particles, and the production parameters were optimised. Thus, the next step was to evaluate the suitability of the PLGA nano- and microparticles produced by MF and w/o/w method to deliver the antigen to the deep lungs (alveoli). Formulations prepared at FRR 1:1 were selected for further development since using this parameter, the largest particles were obtained. Besides, formulations prepared by the double emulsion method were also included in the study to get an overview of the influence of particle size on the deposition and cellular uptake within the lungs.

A cryoprotectant screening was carried out to determine the best stabiliser and concentration to incorporate within the PLGA formulations prior to freeze drying. Sucrose (10% w/v) was selected as cryoprotectant due to its efficacy protecting the particles from agglomeration and because it is cheaper than other sugars (e.g. trehalose). The amino acid leucine (1% w/v) was also included into the

formulation due to its performance as a redispersibility enhancer. Dry powders composed of PLGA copolymers 85:15, 75:25 and 50:50, sucrose (10% w/v) and leucine (1% w/v) were produced using a freeze drying technique. All powders composed of different PLGA copolymers showed adequate particle size appropriate for deep lung delivery as shown by the aerosol performance dispersion results from the NGI (Pharmacopoeia approved airway simulator), which showed high particle deposition in the deep lungs. Besides, *in vitro* studies in three different macrophages cell lines showed the ability of these cell to take up the formulated PLGA particles and their ability to deliver the antigen to the cells for processing. Further evaluation of the developed powders is necessary to determine their ability to facilitate improved mucosal immunity without causing local side effects. Subsequently, these formulations moved on to the immunisation studies in mice as part of the prime-pull vaccination protocol.

7.6 Prime-pull immunisation stimulates cytokine production in the lung parenchyma

Alveolar macrophages can be found in multiple locations including the vasculature and the parenchyma and represent the first line of defence against Mtb. The importance of the recruitment of T cells to the lungs for protection against TB infection has recently been demonstrated. The location of these T cells is crucial for the efficacy of the vaccine since the T cells have to be in direct contact with the Mtb infected macrophages [139-144]. Therefore, respiratory mucosal vaccination is believed to be the best way to teach the lung macrophages and DCs how to fight Mtb infection and to recruit antigen specific T cells to the site of infection [145, 146].

Here we evaluated a prime-pull immunisation approach for a vaccine against pulmonary TB, consisting of priming with CAF01:H56 followed by a mucosal boost with PLGA:H56. PLGA encapsulating the TB vaccine candidate H56 was formulated in a scale independent manner and lyophilised to a dry powder format for aerolisation into the lungs. Results shown here demonstrate the applicability of this manufacturing method to deliver encapsulated antigen to the lungs via the intranasal route of administration. The immune responses generated by this approach indicate the retention of the immunogenicity of the antigen encapsulated within a lyophilised PLGA delivery system. Although no enhancing effect could be observed compared to the administration of antigen alone as a boost, the work here could provide the foundations for the scale independent manufacture of polymer based delivery systems encapsulating antigens for inhalation/aerolisation delivery to the lung mucosa.

7.7 Concluding remarks and future work

Microfluidics allows for the large-scale and reproducible preparation of liposomal and polymer-based vaccine adjuvants. These particles can be produced in a range of sizes depending on the control parameters selected. Adjuvant characteristics such as particle size, surface zeta potential and polydispersity are highly dependent on the composition of the formulation. This manufacturing process is more efficient, fast and offers a tight control of the physicochemical characteristics of the particulate systems. Furthermore, production of PLGA nano- and microparticles as dry powders for inhalation was successfully achieved. *In vitro* and *in vivo* studies in mice have shown the ability of these polymer particles to deliver H56 antigen to the deep lungs, eliciting high cellular and humoral immune responses compared to the unvaccinated group.

Further studies should focus on the administration of the PLGA:H56 vaccine as a powder for inhalation to achieve improved immune responses. Unfortunately, the lack of administration devices for powder format in mice hampered the use of the designed dry powders for mucosal boosting. Animal models used for the development of a TB vaccine include mice, rabbits, guinea pigs and non-human primates, and the mice are commonly used because they are easy to work with, low cost and their genetic background is well known. Most of the companies producing inhalation devices for animal research fabricate masks for rats as the smallest animal model. Once this problem is overcome, protection studies by challenging mice with a TB strain could be performed to offer more information with regards to the potential success of the immunisation protocol developed here. Furthermore, it is important to understand that the design and development of the CAF01 and PLGA adjuvant systems demonstrated in this thesis could be applicable for the encapsulation of antigens for the treatment and prevention against a range of other diseases.

References

- [1] World Health Organization, Global Tuberculosis report 2016.
- [2] T.M. Shinnick, R.C. Good, Diagnostic Mycobacteriology Laboratory Practices, Clinical Infectious Diseases, 21 (1995) 291-299.
- [3] L. Barksdale, K.S. Kim, Mycobacterium, Bacteriological Reviews, 41 (1977) 217-372.
- [4] J. van Ingen, M.J. Boeree, D. van Soolingen, M.D. Iseman, L.B. Heifets, C.L. Daley, Are phylogenetic position, virulence, drug susceptibility and *in vivo* response to treatment in mycobacteria interrelated?, Infection, Genetics and Evolution, 12 (2012) 832-837.
- [5] W.F. Wells, Airborne Contagion and Air Hygiene. An Ecological Study of Droplet Infections, Airborne Contagion and Air Hygiene. An Ecological Study of Droplet Infections., (1955).
- [6] W.F. Wells, ON AIR-BORNE INFECTION*STUDY II. DROPLETS AND DROPLET NUCLEI, American Journal of Epidemiology, 20 (1934) 611-618.
- [7] C. Dye, S. Scheele, P. Dolin, V. Pathania, M.C. Raviglione, W.H.O.G.S. for the, P. Monitoring, Global burden of tuberculosis: Estimated incidence, prevalence, and mortality by country, JAMA, 282 (1999) 677-686.
- [8] J.M. Gray, D.L. Cohn, Tuberculosis and HIV coinfection, in: Seminars in respiratory and critical care medicine, Thieme Medical Publishers, 2013, pp. 032-043.
- [9] L.S. Schlesinger, Entry of Mycobacterium tuberculosis into Mononuclear Phagocytes, in: T.M. Shinnick (Ed.) Tuberculosis, Springer Berlin Heidelberg, Berlin, Heidelberg, 1996, pp. 71-96.
- [10] S.-Y. Eum, J.-H. Kong, M.-S. Hong, Y.-J. Lee, J.-H. Kim, S.-H. Hwang, S.-N. Cho, L.E. Via, C.E. Barry III, Neutrophils are the predominant infected phagocytic cells in the airways of patients with active pulmonary TB, Chest, 137 (2010) 122-128.
- [11] A.J. Wolf, B. Linas, G.J. Trevejo-Nuñez, E. Kincaid, T. Tamura, K. Takatsu, J.D. Ernst, Mycobacterium tuberculosis infects dendritic cells with high frequency and impairs their function in vivo, The Journal of Immunology, 179 (2007) 2509-2519.
- [12] R.D. Berg, L. Ramakrishnan, Insights into tuberculosis from the zebrafish model, Trends in Molecular Medicine, 18 (2012) 689-690.
- [13] J.D. Ernst, A. Cornelius, L. Desvignes, J. Tavs, B.A. Norris, Limited Antimycobacterial Efficacy of Epitope Peptide Administration Despite Enhanced Antigen-Specific CD4 T-Cell Activation, The Journal of Infectious Diseases, (2018) jiy142-jiy142.
- [14] K.D. Kauffman, M.A. Sallin, S. Sakai, O. Kamenyeva, J. Kabat, D. Weiner, M. Sutphin, D. Schimel, L. Via, C.E. Barry III, Defective positioning in granulomas but not lung-homing limits CD4 T-cell interactions with Mycobacterium tuberculosis-infected macrophages in rhesus macaques, Mucosal immunology, 11 (2018) 462.
- [15] S. Srivastava, J.D. Ernst, Cutting Edge: Direct Recognition of Infected Cells by CD4 T Cells Is Required for Control of Intracellular *Mycobacterium tuberculosis* In Vivo, The Journal of Immunology, 191 (2013) 1016-1020.

- [16] J.M. Davis, L. Ramakrishnan, The role of the granuloma in expansion and dissemination of early tuberculous infection, *Cell*, 136 (2009) 37-49.
- [17] J.G. Egen, A.G. Rothfuchs, C.G. Feng, N. Winter, A. Sher, R.N. Germain, Macrophage and T cell dynamics during the development and disintegration of mycobacterial granulomas, *Immunity*, 28 (2008) 271-284.
- [18] P.S. Manzanillo, M.U. Shiloh, D.A. Portnoy, J.S. Cox, Mycobacterium tuberculosis activates the DNA-dependent cytosolic surveillance pathway within macrophages, *Cell host & microbe*, 11 (2012) 469-480.
- [19] S.A. Stanley, J.E. Johndrow, P. Manzanillo, J.S. Cox, The Type I IFN response to infection with Mycobacterium tuberculosis requires ESX-1-mediated secretion and contributes to pathogenesis, *The Journal of Immunology*, 178 (2007) 3143-3152.
- [20] D.B. Young, H.P. Gideon, R.J. Wilkinson, Eliminating latent tuberculosis, *Trends in microbiology*, 17 (2009) 183-188.
- [21] J.D. Ernst, Macrophage receptors for Mycobacterium tuberculosis, *Infection and immunity*, 66 (1998) 1277-1281.
- [22] J. Kleinnijenhuis, M. Oosting, L.A. Joosten, M.G. Netea, R. Van Crevel, Innate immune recognition of Mycobacterium tuberculosis, *Clinical and Developmental Immunology*, 2011 (2011).
- [23] D.H. Raulet, S. Gasser, B.G. Gowen, W. Deng, H. Jung, Regulation of ligands for the NKG2D activating receptor, *Annual review of immunology*, 31 (2013) 413-441.
- [24] J. Harris, J. Keane, How tumour necrosis factor blockers interfere with tuberculosis immunity, *Clinical & Experimental Immunology*, 161 (2010) 1-9.
- [25] H. Clay, H.E. Volkman, L. Ramakrishnan, Tumor necrosis factor signaling mediates resistance to mycobacteria by inhibiting bacterial growth and macrophage death, *Immunity*, 29 (2008) 283-294.
- [26] M. Fabri, S. Stenger, D.-M. Shin, J.-M. Yuk, P.T. Liu, S. Realegeno, H.-M. Lee, S.R. Krutzik, M. Schenk, P.A. Sieling, Vitamin D is required for IFN- γ -mediated antimicrobial activity of human macrophages, *Science translational medicine*, 3 (2011) 104ra102-104ra102.
- [27] E. Petruccioli, A. Romagnoli, M. Corazzari, E.M. Coccia, O. Butera, G. Delogu, M. Piacentini, E. Girardi, G.M. Fimia, D. Goletti, Specific T cells restore the autophagic flux inhibited by Mycobacterium tuberculosis in human primary macrophages, *Journal of Infectious Diseases*, 205 (2012) 1425-1435.
- [28] L. Desvignes, J.D. Ernst, Interferon- γ -responsive nonhematopoietic cells regulate the immune response to Mycobacterium tuberculosis, *Immunity*, 31 (2009) 974-985.
- [29] B. Nandi, S.M. Behar, Regulation of neutrophils by interferon- γ limits lung inflammation during tuberculosis infection, *Journal of Experimental Medicine*, 208 (2011) 2251-2262.
- [30] C.G. Feng, D. Jankovic, M. Kullberg, A. Cheever, C.A. Scanga, S. Hieny, P. Caspar, G.S. Yap, A. Sher, Maintenance of pulmonary Th1 effector function in chronic tuberculosis requires persistent IL-12 production, *The Journal of Immunology*, 174 (2005) 4185-4192.
- [31] E. Vivier, D.H. Raulet, A. Moretta, M.A. Caligiuri, L. Zitvogel, L.L. Lanier, W.M. Yokoyama, S. Ugolini, Innate or Adaptive Immunity? The Example of Natural Killer Cells, *Science*, 331 (2011) 44-49.

- [32] A. Moretta, Natural killer cells and dendritic cells: rendezvous in abused tissues, *Nature Reviews Immunology*, 2 (2002) 957.
- [33] D.M. Lewinsohn, T.T. Bement, J. Xu, D.H. Lynch, K.H. Grabstein, S.G. Reed, M.R. Alderson, Human purified protein derivative-specific CD4⁺ T cells use both CD95-dependent and CD95-independent cytolytic mechanisms, *The Journal of Immunology*, 160 (1998) 2374-2379.
- [34] T. Mogues, M.E. Goodrich, L. Ryan, R. LaCourse, R.J. North, The Relative Importance of T Cell Subsets in Immunity and Immunopathology of Airborne Mycobacterium tuberculosis Infection in Mice, *The Journal of Experimental Medicine*, 193 (2001) 271-280.
- [35] C.K. Kwan, J.D. Ernst, HIV and tuberculosis: a deadly human syndemic, *Clinical microbiology reviews*, 24 (2011) 351-376.
- [36] S.M. Behar, Antigen-specific CD8⁺ T cells and protective immunity to tuberculosis, in: *The New Paradigm of Immunity to Tuberculosis*, Springer, 2013, pp. 141-163.
- [37] H. Bruns, C. Meinken, P. Schauenberg, G. Härter, P. Kern, R.L. Modlin, C. Antoni, S. Stenger, Anti-TNF immunotherapy reduces CD8⁺ T cell-mediated antimicrobial activity against Mycobacterium tuberculosis in humans, *The Journal of clinical investigation*, 119 (2009) 1167-1177.
- [38] G. Leroux-Roels, Unmet needs in modern vaccinology Adjuvants to improve the immune response, *Vaccine*, 28 (2010) C25-C36.
- [39] L.C. Rodrigues, V.K. Diwan, J.G. Wheeler, Protective Effect of BCG against Tuberculous Meningitis and Miliary Tuberculosis: A Meta-Analysis, *International Journal of Epidemiology*, 22 (1993) 1154-1158.
- [40] P. Mangtani, I. Abubakar, C. Ariti, R. Beynon, L. Pimpin, P.E.M. Fine, L.C. Rodrigues, P.G. Smith, M. Lipman, P.F. Whiting, J.A. Sterne, Protection by BCG Vaccine Against Tuberculosis: A Systematic Review of Randomized Controlled Trials, *Clinical Infectious Diseases*, 58 (2014) 470-480.
- [41] B.R. Bloom, P.E.M. Fine, The BCG Experience: Implications for Future Vaccines against Tuberculosis, in: *Tuberculosis*, American Society of Microbiology, 1994.
- [42] P. Andersen, T.M. Doherty, The success and failure of BCG—implications for a novel tuberculosis vaccine, *Nature Reviews Microbiology*, 3 (2005) 656.
- [43] C.E. Palmer, M.W. Long, Effects of infection with atypical mycobacteria on BCG vaccination and tuberculosis, *Am Rev Respir Dis*, 94 (1966) 553-568.
- [44] R. Copin, M. Coscollá, E. Efstathiadis, S. Gagneux, J.D. Ernst, Impact of *in vitro* evolution on antigenic diversity of Mycobacterium bovis bacillus Calmette-Guerin (BCG), *Vaccine*, 32 (2014) 5998-6004.
- [45] C.J. Burrell, C.R. Howard, F.A. Murphy, Chapter 11 - Vaccines and Vaccination, in: C.J. Burrell, C.R. Howard, F.A. Murphy (Eds.) *Fenner and White's Medical Virology (Fifth Edition)*, Academic Press, London, 2017, pp. 155-167.
- [46] D.F. Hoft, A. Blazevic, A. Selimovic, A. Turan, J. Tennant, G. Abate, J. Fulkerson, D.E. Zak, R. Walker, B. McClain, J. Sadoff, J. Scott, B. Shepherd, J. Ishmukhamedov, D.A. Hokey, V. Dheenadhayalan, S. Shankar, L. Amon, G. Navarro, R. Podyminogin, A. Aderem, L. Barker, M. Brennan, R.S. Wallis, A.A. Gershon, M.D. Gershon, S. Steinberg, Safety and Immunogenicity of the Recombinant BCG Vaccine

AERAS-422 in Healthy BCG-naïve Adults: A Randomized, Active-controlled, First-in-human Phase 1 Trial, *EBioMedicine*, 7 (2016) 278-286.

[47] M.J. Brennan, B. Claggett, H. Fitzgerald, V. Chen, A. Williams, A.A. Izzo, L.F. Barker, Preclinical Evidence for Implementing a Prime-boost Vaccine Strategy for Tuberculosis, *Vaccine*, 30 (2012) 2811-2823.

[48] S.H.E. Kaufmann, J. Weiner, C.F. von Reyn, Novel approaches to tuberculosis vaccine development, *International Journal of Infectious Diseases*, 56 (2017) 263-267.

[49] Y. Perrie, A.R. Mohammed, D.J. Kirby, S.E. McNeil, V.W. Bramwell, Vaccine adjuvant systems: Enhancing the efficacy of sub-unit protein antigens, *International Journal of Pharmaceutics*, 364 (2008) 272-280.

[50] S.H. Kaufmann, Tuberculosis vaccine development: strength lies in tenacity, *Trends in immunology*, 33 (2012) 373-379.

[51] C. Aagaard, T. Hoang, J. Dietrich, P.-J. Cardona, A. Izzo, G. Dolganov, G.K. Schoolnik, J.P. Cassidy, R. Billeskov, P. Andersen, A multistage tuberculosis vaccine that confers efficient protection before and after exposure, *Nature Medicine*, 17 (2011) 189.

[52] S.A. Prabowo, M.I. Gröschel, E.D. Schmidt, A. Skrahina, T. Mihaescu, S. Hastürk, R. Mitrofanov, E. Pimkina, I. Visontai, B. de Jong, Targeting multidrug-resistant tuberculosis (MDR-TB) by therapeutic vaccines, *Medical microbiology and immunology*, 202 (2013) 95-104.

[53] P. Andersen, S.H.E. Kaufmann, Novel Vaccination Strategies against Tuberculosis, *Cold Spring Harbor Perspectives in Medicine*, 4 (2014) a018523.

[54] A.W. Olsen, L.A. van Pinxteren, L.M. Okkels, P.B. Rasmussen, P. Andersen, Protection of mice with a tuberculosis subunit vaccine based on a fusion protein of antigen 85b and esat-6, *Infection and immunity*, 69 (2001) 2773-2778.

[55] S. Jain, D.T. O'Hagan, M. Singh, The long-term potential of biodegradable poly(lactide-co-glycolide) microparticles as the next-generation vaccine adjuvant, *Expert Rev Vaccines*, 10 (2011) 1731-1742.

[56] R.A. Schwendener, Liposomes as vaccine delivery systems: a review of the recent advances, *Therapeutic advances in vaccines*, 2 (2014) 159-182.

[57] A. Bangham, M.M. Standish, J. Watkins, Diffusion of univalent ions across the lamellae of swollen phospholipids, *Journal of molecular biology*, 13 (1965) 238-IN227.

[58] A.C. Allison, G. Gregoriadis, Liposomes as immunological adjuvants, *Nature*, 252 (1974) 252-252.

[59] C. Foged, Subunit vaccines of the future: the need for safe, customized and optimized particulate delivery systems, *Ther Deliv*, 2 (2011) 1057-1077.

[60] V.P. Torchilin, Recent advances with liposomes as pharmaceutical carriers, *Nat Rev Drug Discov*, 4 (2005) 145-160.

[61] T. Kaasgaard, C.J. Drummond, Ordered 2-D and 3-D nanostructured amphiphile self-assembly materials stable in excess solvent, *Physical Chemistry Chemical Physics*, 8 (2006) 4957-4975.

- [62] J. Israelachvili, S. Marčelja, R.G. Horn, Physical principles of membrane organization, *Quarterly reviews of biophysics*, 13 (1980) 121-200.
- [63] G. Gregoriadis, B. McCormack, M. Obrenovic, R. Saffie, B. Zadi, Y. Perrie, Vaccine entrapment in liposomes, *Methods*, 19 (1999) 156-162.
- [64] G. Gregoriadis, Liposomes as immunoadjuvants and vaccine carriers: antigen entrapment, *Immunomethods*, 4 (1994) 210-216.
- [65] P. Nordly, H.B. Madsen, H.M. Nielsen, C. Foged, Status and future prospects of lipid-based particulate delivery systems as vaccine adjuvants and their combination with immunostimulators, *Expert Opin Drug Del*, 6 (2009) 657-672.
- [66] F. Ahsan, I.P. Rivas, M.A. Khan, A.I.T. Suárez, Targeting to macrophages: role of physicochemical properties of particulate carriers—liposomes and microspheres—on the phagocytosis by macrophages, *Journal of Controlled Release*, 79 (2002) 29-40.
- [67] T. Nakanishi, J. Kunisawa, A. Hayashi, Y. Tsutsumi, K. Kubo, S. Nakagawa, M. Nakanishi, K. Tanaka, T. Mayumi, Positively charged liposome functions as an efficient immunoadjuvant in inducing cell-mediated immune response to soluble proteins, *Journal of controlled release*, 61 (1999) 233-240.
- [68] A. Joseph, N. Itskovitz-Cooper, S. Samira, O. Flasterstein, H. Elyahu, D. Simberg, I. Goldwaser, Y. Barenholz, E. Kedar, A new intranasal influenza vaccine based on a novel polycationic lipid—ceramide carbamoyl-spermine (CCS): I. Immunogenicity and efficacy studies in mice, *Vaccine*, 24 (2006) 3990-4006.
- [69] Y. Perrie, P.M. Frederik, G. Gregoriadis, Liposome-mediated DNA vaccination: the effect of vesicle composition, *Vaccine*, 19 (2001) 3301-3310.
- [70] M. Henriksen-Lacey, D. Christensen, V.W. Bramwell, T. Lindenstrøm, E.M. Agger, P. Andersen, Y. Perrie, Liposomal cationic charge and antigen adsorption are important properties for the efficient deposition of antigen at the injection site and ability of the vaccine to induce a CMI response, *Journal of Controlled Release*, 145 (2010) 102-108.
- [71] D. Christensen, E.M. Agger, L.V. Andreasen, D. Kirby, P. Andersen, Y. Perrie, Liposome-based cationic adjuvant formulations (CAF): past, present, and future, *Journal of liposome research*, 19 (2009) 2-11.
- [72] E. Feitosa, F.R. Alves, A. Niemiec, M.E. Real Oliveira, E.M. Castanheira, A.L. Baptista, Cationic liposomes in mixed didodecyldimethylammonium bromide and dioctadecyldimethylammonium bromide aqueous dispersions studied by differential scanning calorimetry, Nile Red fluorescence, and turbidity, *Langmuir : the ACS journal of surfaces and colloids*, 22 (2006) 3579-3585.
- [73] J. Davidsen, I. Rosenkrands, D. Christensen, A. Vangala, D. Kirby, Y. Perrie, E.M. Agger, P. Andersen, Characterization of cationic liposomes based on dimethyldioctadecylammonium and synthetic cord factor from *M. tuberculosis* (trehalose 6,6'-dibehenate)-a novel adjuvant inducing both strong CMI and antibody responses, *Biochim Biophys Acta*, 1718 (2005) 22-31.
- [74] E. Feitosa, Kinetic asymmetry in the gel-liquid crystalline state transitions of DDAB vesicles studied by differential scanning calorimetry, *Journal of colloid and interface science*, 344 (2010) 70-74.
- [75] J. Davidsen, I. Rosenkrands, D. Christensen, A. Vangala, D. Kirby, Y. Perrie, E.M. Agger, P. Andersen, Characterization of cationic liposomes based on dimethyldioctadecylammonium and

synthetic cord factor from *M. tuberculosis* (trehalose 6,6'-dibehenate)—A novel adjuvant inducing both strong CMI and antibody responses, *Biochimica et Biophysica Acta (BBA) - Biomembranes*, 1718 (2005) 22-31.

[76] A. Bekierkunst, I. Levij, E. Yarkoni, E. Vilkas, E. Lederer, Suppression of urethan-induced lung adenomas in mice treated with trehalose-6, 6-dimycolate (cord factor) and living bacillus Calmette Guérin, *Science*, 174 (1971) 1240-1242.

[77] V.M. Lima, V.L. Bonato, K.M. Lima, S.A. Dos Santos, R.R. Dos Santos, E.D. Gonçalves, L.H. Faccioli, I.T. Brandão, J.M. Rodrigues-Junior, C.L. Silva, Role of trehalose dimycolate in recruitment of cells and modulation of production of cytokines and NO in tuberculosis, *Infection and immunity*, 69 (2001) 5305-5312.

[78] R.L. Hunter, M. Olsen, C. Jagannath, J.K. Actor, Trehalose 6, 6'-dimycolate and lipid in the pathogenesis of caseating granulomas of tuberculosis in mice, *The American journal of pathology*, 168 (2006) 1249-1261.

[79] R.L. Hunter, M.R. Olsen, C. Jagannath, J.K. Actor, Multiple roles of cord factor in the pathogenesis of primary, secondary, and cavitary tuberculosis, including a revised description of the pathology of secondary disease, *Annals of Clinical & Laboratory Science*, 36 (2006) 371-386.

[80] D. Christensen, D. Kirby, C. Foged, E.M. Agger, P. Andersen, Y. Perrie, H.M. Nielsen, α , α' -trehalose 6, 6'-dibehenate in non-phospholipid-based liposomes enables direct interaction with trehalose, offering stability during freeze-drying, *Biochimica et Biophysica Acta (BBA)-Biomembranes*, 1778 (2008) 1365-1373.

[81] D. Christensen, Chapter 17 - Development and Evaluation of CAF01, in: V.E.J.C. Schijns, D.T. O'Hagan (Eds.) *Immunopotentiators in Modern Vaccines (Second Edition)*, Academic Press, 2017, pp. 333-345.

[82] P.T. Ingvarsson, S.T. Schmidt, D. Christensen, N.B. Larsen, W.L.J. Hinrichs, P. Andersen, J. Rantanen, H.M. Nielsen, M. Yang, C. Foged, Designing CAF-adjuvanted dry powder vaccines: spray drying preserves the adjuvant activity of CAF01, *Journal of controlled release*, 167 (2013) 256-264.

[83] P.T. Ingvarsson, M. Yang, H. Mulvad, H.M. Nielsen, J. Rantanen, C. Foged, Engineering of an inhalable DDA/TDB liposomal adjuvant: a quality-by-design approach towards optimization of the spray drying process, *Pharmaceutical research*, 30 (2013) 2772-2784.

[84] D. Christensen, C. Foged, I. Rosenkrands, H.M. Nielsen, P. Andersen, E.M. Agger, Trehalose preserves DDA/TDB liposomes and their adjuvant effect during freeze-drying, *Biochimica et Biophysica Acta (BBA)-Biomembranes*, 1768 (2007) 2120-2129.

[85] A. Thakur, P.T. Ingvarsson, S.T. Schmidt, F. Rose, P. Andersen, D. Christensen, C. Foged, Immunological and physical evaluation of the multistage tuberculosis subunit vaccine candidate H56/CAF01 formulated as a spray-dried powder, *Vaccine*, 36 (2018) 3331-3339.

[86] A.R. Mohammed, V.W. Bramwell, D.J. Kirby, S.E. McNeil, Y. Perrie, Increased potential of a cationic liposome-based delivery system: enhancing stability and sustained immunological activity in pre-clinical development, *Eur J Pharm Biopharm*, 76 (2010) 404-412.

[87] C.J.-M. Martel, E.M. Agger, J.J. Poulsen, T. Hammer Jensen, L. Andresen, D. Christensen, L.P. Nielsen, M. Blixenkroner-Møller, P. Andersen, B. Aasted, CAF01 Potentiates Immune Responses and Efficacy of an Inactivated Influenza Vaccine in Ferrets, *Plos One*, 6 (2011) e22891.

- [88] G.J. Gram, I. Karlsson, E.M. Agger, P. Andersen, A. Fomsgaard, A Novel Liposome-Based Adjuvant CAF01 for Induction of CD8⁺ Cytotoxic T-Lymphocytes (CTL) to HIV-1 Minimal CTL Peptides in HLA-A*0201 Transgenic Mice, *PLOS ONE*, 4 (2009) e6950.
- [89] A. Vangala, V.W. Bramwell, S. McNeil, D. Christensen, E.M. Agger, Y. Perrie, Comparison of vesicle based antigen delivery systems for delivery of hepatitis B surface antigen, *Journal of controlled release*, 119 (2007) 102-110.
- [90] M. Henriksen-Lacey, V.W. Bramwell, D. Christensen, E.M. Agger, P. Andersen, Y. Perrie, Liposomes based on dimethyldioctadecylammonium promote a depot effect and enhance immunogenicity of soluble antigen, *J Control Release*, 142 (2010) 180-186.
- [91] D. Christensen, M. Henriksen-Lacey, A.T. Kamath, T. Lindenstrøm, K.S. Korsholm, J.P. Christensen, A.-F. Rochat, P.-H. Lambert, P. Andersen, C.-A. Siegrist, Y. Perrie, E.M. Agger, A cationic vaccine adjuvant based on a saturated quaternary ammonium lipid have different in vivo distribution kinetics and display a distinct CD4 T cell-inducing capacity compared to its unsaturated analog, *Journal of Controlled Release*, 160 (2012) 468-476.
- [92] E. Ishikawa, T. Ishikawa, Y.S. Morita, K. Toyonaga, H. Yamada, O. Takeuchi, T. Kinoshita, S. Akira, Y. Yoshikai, S. Yamasaki, Direct recognition of the mycobacterial glycolipid, trehalose dimycolate, by C-type lectin Mincle, *J Exp Med*, 206 (2009) 2879-2888.
- [93] H. Schoenen, B. Bodendorfer, K. Hitchens, S. Manzanero, K. Werninghaus, F. Nimmerjahn, E.M. Agger, S. Stenger, P. Andersen, J. Ruland, G.D. Brown, C. Wells, R. Lang, Cutting edge: Mincle is essential for recognition and adjuvanticity of the mycobacterial cord factor and its synthetic analog trehalose-dibehenate, *J Immunol*, 184 (2010) 2756-2760.
- [94] C. Desel, K. Werninghaus, M. Ritter, K. Jozefowski, J. Wenzel, N. Russkamp, U. Schleicher, D. Christensen, S. Wirtz, C. Kirschnig, The Mincle-activating adjuvant TDB induces MyD88-dependent Th1 and Th17 responses through IL-1R signaling, *Plos One*, 8 (2013) e53531.
- [95] H. Schoenen, B. Bodendorfer, K. Hitchens, S. Manzanero, K. Werninghaus, F. Nimmerjahn, E.M. Agger, S. Stenger, P. Andersen, J. Ruland, G.D. Brown, C. Wells, R. Lang, Mincle is essential for recognition and adjuvanticity of the mycobacterial cord factor and its synthetic analogue trehalose-dibehenate, *Journal of immunology (Baltimore, Md. : 1950)*, 184 (2010) 2756-2760.
- [96] K. Werninghaus, A. Babiak, O. Groß, C. Hölscher, H. Dietrich, E.M. Agger, J. Mages, A. Mocsai, H. Schoenen, K. Finger, Adjuvanticity of a synthetic cord factor analogue for subunit Mycobacterium tuberculosis vaccination requires FcR γ -Syk-Card9-dependent innate immune activation, *Journal of Experimental Medicine*, 206 (2009) 89-97.
- [97] J. Ostrop, K. Jozefowski, S. Zimmermann, K. Hofmann, E. Strasser, B. Lepenies, R. Lang, Contribution of MINCLE-SYK signaling to activation of primary human APCs by mycobacterial cord factor and the novel adjuvant TDB, *The Journal of Immunology*, (2015) 1500102.
- [98] T. Lindenstrøm, E.M. Agger, K.S. Korsholm, P.A. Darrah, C. Aagaard, R.A. Seder, I. Rosenkrands, P. Andersen, Tuberculosis subunit vaccination provides long-term protective immunity characterized by multifunctional CD4 memory T cells, *The Journal of Immunology*, 182 (2009) 8047-8055.
- [99] J. Davidsen, I. Rosenkrands, D. Christensen, A. Vangala, D. Kirby, Y. Perrie, E.M. Agger, P. Andersen, Characterization of cationic liposomes based on dimethyldioctadecylammonium and synthetic cord factor from *M. tuberculosis* (trehalose 6,6'-dibehenate)—A novel adjuvant inducing

both strong CMI and antibody responses, *Biochimica et Biophysica Acta (BBA) - Biomembranes*, 1718 (2005) 22-31.

[100] G. Crotts, T.G. Park, Protein delivery from poly (lactic-co-glycolic acid) biodegradable microspheres: release kinetics and stability issues, *Journal of microencapsulation*, 15 (1998) 699-713.

[101] N. Petrovsky, J.C. Aguilar, Vaccine adjuvants: current state and future trends, *Immunology and cell biology*, 82 (2004) 488-496.

[102] H.K. Makadia, S.J. Siegel, Poly Lactic-co-Glycolic Acid (PLGA) as Biodegradable Controlled Drug Delivery Carrier, *Polymers-Basel*, 3 (2011) 1377-1397.

[103] V.B. Joshi, S.M. Geary, A.K. Salem, Biodegradable particles as vaccine delivery systems: size matters, *The AAPS journal*, 15 (2013) 85-94.

[104] R. Arshady, Preparation of Biodegradable Microspheres and Microcapsules .2. Polyactides and Related Polyesters, *Journal of Controlled Release*, 17 (1991) 1-21.

[105] W. Chaisri, W.E. Hennink, S. Okonogi, Preparation and characterization of cephalexin loaded PLGA microspheres, *Curr Drug Deliv*, 6 (2009) 69-75.

[106] C. Thomasin, N.T. Ho, H.P. Merkle, B. Gander, Drug microencapsulation by PLA/PLGA coacervation in the light of thermodynamics. 1. Overview and theoretical considerations, *J Pharm Sci*, 87 (1998) 259-268.

[107] L. Mu, S.S. Feng, Fabrication, characterization and *in vitro* release of paclitaxel (Taxol (R)) loaded poly (lactic-co-glycolic acid) microspheres prepared by spray drying technique with lipid/cholesterol emulsifiers, *Journal of Controlled Release*, 76 (2001) 239-254.

[108] S.R. Mao, J. Xu, C.F. Cai, O. Germershaus, A. Schaper, T. Kissel, Effect of WOW process parameters on morphology and burst release of FITC-dextran loaded PLGA microspheres, *International Journal of Pharmaceutics*, 334 (2007) 137-148.

[109] I.D. Rosca, F. Watari, M. Uo, Microparticle formation and its mechanism in single and double emulsion solvent evaporation, *Journal of Controlled Release*, 99 (2004) 271-280.

[110] A. Lamprecht, N. Ubrich, M.H. Perez, C.M. Lehr, M. Hoffman, P. Maincent, Influences of process parameters on nanoparticle preparation performed by a double emulsion pressure homogenization technique, *International Journal of Pharmaceutics*, 196 (2000) 177-182.

[111] R. Yang, T.N. Chen, H.L. Chen, W.J. Wang, Microfabrication of biodegradable (PLGA) honeycomb-structures and potential applications in implantable drug delivery, *Sensor Actuat B-Chem*, 106 (2005) 506-511.

[112] K.E. Uhrich, S.M. Cannizzaro, R.S. Langer, K.M. Shakesheff, Polymeric Systems for Controlled Drug Release, *Chem Rev*, 99 (1999) 3181-3198.

[113] X.S. Wu, N. Wang, Synthesis, characterization, biodegradation, and drug delivery application of biodegradable lactic/glycolic acid polymers. Part II: biodegradation, *Journal of Biomaterials Science, Polymer Edition*, 12 (2001) 21-34.

- [114] A.L. Silva, P.C. Soema, B. Slütter, F. Ossendorp, W. Jiskoot, PLGA particulate delivery systems for subunit vaccines: Linking particle properties to immunogenicity, *Human Vaccines & Immunotherapeutics*, 12 (2016) 1056-1069.
- [115] M. van de Weert, W.E. Hennink, W. Jiskoot, Protein Instability in Poly(Lactic-co-Glycolic Acid) Microparticles, *Pharmaceutical Research*, 17 (2000) 1159-1167.
- [116] L. Lu, S.J. Peter, M.D. Lyman, H.-L. Lai, S.M. Leite, J.A. Tamada, S. Uyama, J.P. Vacanti, R. Langer, A.G. Mikos, *In vitro* and *in vivo* degradation of porous poly (DL-lactic-co-glycolic acid) foams, *Biomaterials*, 21 (2000) 1837-1845.
- [117] L. Lu, C.A. Garcia, A.G. Mikos, *In vitro* degradation of thin poly (DL-lactic-co-glycolic acid) films, *Journal of Biomedical Materials Research: An Official Journal of The Society for Biomaterials, The Japanese Society for Biomaterials, and The Australian Society for Biomaterials*, 46 (1999) 236-244.
- [118] T.G. Park, Degradation of poly (lactic-co-glycolic acid) microspheres: effect of copolymer composition, *Biomaterials*, 16 (1995) 1123-1130.
- [119] F. Alexis, Factors affecting the degradation and drug-release mechanism of poly (lactic acid) and poly [(lactic acid)-co-(glycolic acid)], *Polymer International*, 54 (2005) 36-46.
- [120] H. Tsuji, A. Mizuno, Y. Ikada, Properties and morphology of poly (L-lactide). III. Effects of initial crystallinity on long-term *in vitro* hydrolysis of high molecular weight poly (L-lactide) film in phosphate-buffered solution, *Journal of Applied Polymer Science*, 77 (2000) 1452-1464.
- [121] G. Schliecker, C. Schmidt, S. Fuchs, R. Wombacher, T. Kissel, Hydrolytic degradation of poly (lactide-co-glycolide) films: effect of oligomers on degradation rate and crystallinity, *International Journal of Pharmaceutics*, 266 (2003) 39-49.
- [122] N. Passerini, D. Craig, An investigation into the effects of residual water on the glass transition temperature of polylactide microspheres using modulated temperature DSC, *Journal of Controlled Release*, 73 (2001) 111-115.
- [123] T.G. Park, Degradation of poly (D, L-lactic acid) microspheres: effect of molecular weight, *Journal of Controlled Release*, 30 (1994) 161-173.
- [124] Y.-Y. Yang, T.-S. Chung, N.P. Ng, Morphology, drug distribution, and *in vitro* release profiles of biodegradable polymeric microspheres containing protein fabricated by double-emulsion solvent extraction/evaporation method, *Biomaterials*, 22 (2001) 231-241.
- [125] I. Gutierrez, R. Hernandez, M. Igartua, A. Gascon, J. Pedraz, Size dependent immune response after subcutaneous, oral and intranasal administration of BSA loaded nanospheres, *Vaccine*, 21 (2002) 67-77.
- [126] J.S. Patton, P.R. Byron, Inhaling medicines: delivering drugs to the body through the lungs, *Nat Rev Drug Discov*, 6 (2007) 67.
- [127] S.M. Moghimi, L. Parhamifar, D. Ahmadvand, P.P. Wibroe, T.L. Andresen, Z.S. Farhangrazi, A.C. Hunter, Particulate Systems for Targeting of Macrophages: Basic and Therapeutic Concepts, *Journal of Innate Immunity*, 4 (2012) 509-528.
- [128] Y.-Y. Huang, C.-H. Wang, Pulmonary delivery of insulin by liposomal carriers, *Journal of Controlled Release*, 113 (2006) 9-14.

- [129] M. Nasr, I. Taha, R.M. Hathout, Suitability of liposomal carriers for systemic delivery of risedronate using the pulmonary route, *Drug Delivery*, 20 (2013) 311-318.
- [130] A. Trapani, S. Di Gioia, N. Ditaranto, N. Cioffi, F.M. Goycoolea, A. Carbone, M. Garcia-Fuentes, M. Conese, M.J. Alonso, Systemic heparin delivery by the pulmonary route using chitosan and glycol chitosan nanoparticles, *International Journal of Pharmaceutics*, 447 (2013) 115-123.
- [131] Y. Kawashima, H. Yamamoto, H. Takeuchi, S. Fujioka, T. Hino, Pulmonary delivery of insulin with nebulized dl-lactide/glycolide copolymer (PLGA) nanospheres to prolong hypoglycemic effect, *Journal of Controlled Release*, 62 (1999) 279-287.
- [132] A.F. Tena, P.C. Clarà, Deposition of inhaled particles in the lungs, *Archivos de Bronconeumología (English Edition)*, 48 (2012) 240-246.
- [133] I. Gonda, Targeting by deposition, in: *Pharmaceutical Inhalation Aerosol Technology*, Second Edition, CRC Press, 2016, pp. 84-104.
- [134] G. Pilcer, K. Amighi, Formulation strategy and use of excipients in pulmonary drug delivery, *International journal of pharmaceutics*, 392 (2010) 1-19.
- [135] J. Pritchard, Particle growth in the airways and the influence of airflow, A new concept in inhalation therapy. Bussum: Medicom, (1987) 3-24.
- [136] R.V. Lourenço, E. Cotromanes, Clinical aerosols: I. Characterization of aerosols and their diagnostic uses, *Archives of internal medicine*, 142 (1982) 2163-2172.
- [137] J. Heyder, Particle transport onto human airway surfaces, *European journal of respiratory diseases. Supplement*, 119 (1982) 29-50.
- [138] A. De Boer, D. Gjaltema, P. Hagedoorn, M. Schaller, W. Witt, H. Frijlink, Design and application of a new modular adapter for laser diffraction characterization of inhalation aerosols, *International journal of pharmaceutics*, 249 (2002) 233-245.
- [139] S. Sakai, K.D. Kauffman, J.M. Schenkel, C.C. McBerry, K.D. Mayer-Barber, D. Masopust, D.L. Barber, Cutting Edge: Control of Mycobacterium tuberculosis Infection by a Subset of Lung Parenchyma-Homing CD4 T Cells, *The Journal of Immunology*, (2014) 1400019.
- [140] J.S. Woodworth, S.B. Cohen, A.O. Moguche, C.R. Plumlee, E.M. Agger, K.B. Urdahl, P. Andersen, Subunit vaccine H56/CAF01 induces a population of circulating CD4 T cells that traffic into the Mycobacterium tuberculosis-infected lung, *Mucosal immunology*, 10 (2017) 555.
- [141] R. Gopal, J. Rangel-Moreno, S. Slight, Y. Lin, H.F. Nawar, B.A. Fallert Junecko, T.A. Reinhart, J. Kolls, T.D. Randall, T.D. Connell, S.A. Khader, Interleukin-17-dependent CXCL13 mediates mucosal vaccine-induced immunity against tuberculosis, *Mucosal Immunology*, 6 (2013) 972.
- [142] T.D. Bold, N. Banaei, A.J. Wolf, J.D. Ernst, Suboptimal activation of antigen-specific CD4+ effector cells enables persistence of M. tuberculosis in vivo, *PLoS pathogens*, 7 (2011) e1002063.
- [143] A.O. Moguche, S. Shafiani, C. Clemons, R.P. Larson, C. Dinh, L.E. Higdon, C. Cambier, J.R. Sissons, A.M. Gallegos, P.J. Fink, ICOS and Bcl6-dependent pathways maintain a CD4 T cell population with memory-like properties during tuberculosis, *Journal of Experimental Medicine*, 212 (2015) 715-728.

- [144] M.A. Sallin, S. Sakai, K.D. Kauffman, H.A. Young, J. Zhu, D.L. Barber, Th1 differentiation drives the accumulation of intravascular, non-protective CD4 T cells during tuberculosis, *Cell reports*, 18 (2017) 3091-3104.
- [145] M. Jeyanathan, Y. Yao, S. Afkhami, F. Smaill, Z. Xing, New tuberculosis vaccine strategies: taking aim at un-natural immunity, *Trends in immunology*, (2018).
- [146] M. Jeyanathan, A. Heriazon, Z. Xing, Airway luminal T cells: A newcomer on the stage of TB vaccination strategies, *Trends in Immunology*, 31 (2010) 247-252.
- [147] A. Garapaty, J.A. Champion, Tunable particles alter macrophage uptake based on combinatorial effects of physical properties, *Bioengineering & Translational Medicine*, 2 (2017) 92-101.
- [148] C. He, Y. Hu, L. Yin, C. Tang, C. Yin, Effects of particle size and surface charge on cellular uptake and biodistribution of polymeric nanoparticles, *Biomaterials*, 31 (2010) 3657-3666.
- [149] K. Hirota, T. Hasegawa, T. Nakajima, H. Inagawa, C. Kohchi, G.-I. Soma, K. Makino, H. Terada, Delivery of rifampicin-PLGA microspheres into alveolar macrophages is promising for treatment of tuberculosis, *Journal of Controlled Release*, 142 (2010) 339-346.
- [150] S. Iwaoka, T. Nakamura, S. Takano, S. Tsuchiya, Y. Aramaki, Cationic liposomes induce apoptosis through p38 MAP kinase-caspase-8-Bid pathway in macrophage-like RAW264.7 cells, *Journal of Leukocyte Biology*, 79 (2006) 184-191.
- [151] M. Arisaka, T. Nakamura, A. Yamada, Y. Negishi, Y. Aramaki, Involvement of protein kinase C δ in induction of apoptosis by cationic liposomes in macrophage-like RAW264.7 cells, *FEBS Letters*, 584 (2010) 1016-1020.
- [152] A.S. Ashhurst, T. Parumasivam, J.G.Y. Chan, L.C.W. Lin, M. Flórido, N.P. West, H.-K. Chan, W.J. Britton, PLGA particulate subunit tuberculosis vaccines promote humoral and Th17 responses but do not enhance control of *Mycobacterium tuberculosis* infection, *Plos One*, 13 (2018) e0194620.
- [153] B.B. Eedara, I.G. Tucker, S.C. Das, Phospholipid-based pyrazinamide spray-dried inhalable powders for treating tuberculosis, *International Journal of Pharmaceutics*, 506 (2016) 174-183.
- [154] B.B. Eedara, B. Rangnekar, S. Sinha, C. Doyle, A. Cavallaro, S.C. Das, Development and characterization of high payload combination dry powders of anti-tubercular drugs for treating pulmonary tuberculosis, *European Journal of Pharmaceutical Sciences*, 118 (2018) 216-226.
- [155] Y. Yang, N. Bajaj, P. Xu, K. Ohn, M.D. Tsifansky, Y. Yeo, Development of highly porous large PLGA microparticles for pulmonary drug delivery, *Biomaterials*, 30 (2009) 1947-1953.
- [156] K.A. Beningo, Y.-I. Wang, Fc-receptor-mediated phagocytosis is regulated by mechanical properties of the target, *Journal of Cell Science*, 115 (2002) 849-856.
- [157] M. Henriksen-Lacey, A. Devitt, Y. Perrie, The vesicle size of DDA: TDB liposomal adjuvants plays a role in the cell-mediated immune response but has no significant effect on antibody production, *Journal of controlled release*, 154 (2011) 131-137.
- [158] D.A. Mannock, M.Y.T. Lee, R.N.A.H. Lewis, R.N. McElhaney, Comparative calorimetric and spectroscopic studies of the effects of cholesterol and epicholesterol on the thermotropic phase behaviour of dipalmitoylphosphatidylcholine bilayer membranes, *Biochimica et Biophysica Acta (BBA) - Biomembranes*, 1778 (2008) 2191-2202.

- [159] M.J. Hussain, A. Wilkinson, V.W. Bramwell, D. Christensen, Y. Perrie, Th1 immune responses can be modulated by varying dimethyldioctadecylammonium and distearoyl-sn-glycero-3-phosphocholine content in liposomal adjuvants, *Journal of Pharmacy and Pharmacology*, 66 (2014) 358-366.
- [160] A. Bangham, A correlation between surface charge and coagulant action of phospholipids, *Nature*, 192 (1961) 1197.
- [161] F. Szoka Jr, D. Papahadjopoulos, Comparative properties and methods of preparation of lipid vesicles (liposomes), *Annual review of biophysics and bioengineering*, 9 (1980) 467-508.
- [162] M.-L. De Temmerman, J. Rejman, J. Demeester, D.J. Irvine, B. Gander, S.C. De Smedt, Particulate vaccines: on the quest for optimal delivery and immune response, *Drug Discovery Today*, 16 (2011) 569-582.
- [163] G.S. Luo, L. Du, Y.J. Wang, Y.C. Lu, J.H. Xu, Controllable preparation of particles with microfluidics, *Particuology*, 9 (2011) 545-558.
- [164] G. Gregoriadis, *Liposome Technology: Liposome Preparation and Related Techniques*, CRC Press, 1993.
- [165] L.V. Andreasen, G.K. Wood, D. Christensen, Methods for producing liposomes, in, *Google Patents*, 2013.
- [166] R. Barnadas-Rodríguez, M. Sabés, Factors involved in the production of liposomes with a high-pressure homogenizer, *International Journal of Pharmaceutics*, 213 (2001) 175-186.
- [167] E. Kastner, R. Kaur, D. Lowry, B. Moghaddam, A. Wilkinson, Y. Perrie, High-throughput manufacturing of size-tuned liposomes by a new microfluidics method using enhanced statistical tools for characterization, *International journal of pharmaceutics*, 477 (2014) 361-368.
- [168] I.V. Zhigaltsev, N. Belliveau, I. Hafez, A.K.K. Leung, J. Huft, C. Hansen, P.R. Cullis, Bottom-Up Design and Synthesis of Limit Size Lipid Nanoparticle Systems with Aqueous and Triglyceride Cores Using Millisecond Microfluidic Mixing, *Langmuir*, 28 (2012) 3633-3640.
- [169] E.M. Agency, ICH guideline Q3C (R5) on impurities: guideline for residual solvents, in, 2016.
- [170] R.C. Murdock, L. Braydich-Stolle, A.M. Schrand, J.J. Schlager, S.M. Hussain, Characterization of nanomaterial dispersion in solution prior to *In vitro* exposure using dynamic light scattering technique, *Toxicol Sci*, 101 (2008) 239-253.
- [171] S. Hupfeld, A.M. Holsæter, M. Skar, C.B. Frantzen, M. Brandl, Liposome size analysis by dynamic/static light scattering upon size exclusion-/field flow-fractionation, *J Nanosci Nanotechnol*, 6 (2006) 3025-3031.
- [172] M. Instruments, *Zetasizer nano series user manual*, in, 2004.
- [173] N.J. Cho, L.Y. Hwang, J.J.R. Solandt, C.W. Frank, Comparison of Extruded and Sonicated Vesicles for Planar Bilayer Self-Assembly, *Materials*, 6 (2013) 3294-3308.
- [174] CHromacademy website, *High Performance Liquid Chromatography*, in 2016.

- [175] N.M. Belliveau, J. Huft, P.J.C. Lin, S. Chen, A.K.K. Leung, T.J. Leaver, A.W. Wild, J.B. Lee, R.J. Taylor, Y.K. Tam, C.L. Hansen, P.R. Cullis, Microfluidic Synthesis of Highly Potent Limit-size Lipid Nanoparticles for In Vivo Delivery of siRNA, *Molecular Therapy. Nucleic Acids*, 1 (2012) e37.
- [176] F. Bally, D.K. Garg, C.A. Serra, Y. Hoarau, N. Anton, C. Brochon, D. Parida, T. Vandamme, G. Hadziioannou, Improved size-tunable preparation of polymeric nanoparticles by microfluidic nanoprecipitation, *Polymer*, 53 (2012) 5045-5051.
- [177] E. Kastner, V. Verma, D. Lowry, Y. Perrie, Microfluidic-controlled manufacture of liposomes for the solubilisation of a poorly water soluble drug, *Int J Pharm*, 485 (2015) 122-130.
- [178] S. Joshi, M.T. Hussain, C.B. Roces, G. Anderluzzi, E. Kastner, S. Salmaso, D.J. Kirby, Y. Perrie, Microfluidics based manufacture of liposomes simultaneously entrapping hydrophilic and lipophilic drugs, *International Journal of Pharmaceutics*, 514 (2016) 160-168.
- [179] A.D. Stroock, S.K.W. Dertinger, A. Ajdari, I. Mezić, H.A. Stone, G.M. Whitesides, Chaotic Mixer for Microchannels, *Science*, 295 (2002) 647-651.
- [180] A. Jahn, W.N. Vreeland, M. Gaitan, L.E. Locascio, Controlled Vesicle Self-Assembly in Microfluidic Channels with Hydrodynamic Focusing, *J Am Chem Soc*, 126 (2004) 2674-2675.
- [181] A. Jahn, S.M. Stavis, J.S. Hong, W.N. Vreeland, D.L. DeVoe, M. Gaitan, Microfluidic mixing and the formation of nanoscale lipid vesicles, *Acs Nano*, 4 (2010) 2077-2087.
- [182] J.M. Zook, W.N. Vreeland, Effects of temperature, acyl chain length, and flow-rate ratio on liposome formation and size in a microfluidic hydrodynamic focusing device, *Soft Matter*, 6 (2010) 1352-1360.
- [183] T.A. Balbino, A.R. Azzoni, L.G. de La Torre, Microfluidic devices for continuous production of pDNA/cationic liposome complexes for gene delivery and vaccine therapy, *Colloids and Surfaces B: Biointerfaces*, 111 (2013) 203-210.
- [184] T.A. Balbino, N.T. Aoki, A.A. Gasperini, C.L. Oliveira, A.R. Azzoni, L.P. Cavalcanti, G. Lucimara, Continuous flow production of cationic liposomes at high lipid concentration in microfluidic devices for gene delivery applications, *Chemical engineering journal*, 226 (2013) 423-433.
- [185] M. Maeki, Y. Fujishima, Y. Sato, T. Yasui, N. Kaji, A. Ishida, H. Tani, Y. Baba, H. Harashima, M. Tokeshi, Understanding the formation mechanism of lipid nanoparticles in microfluidic devices with chaotic micromixers, *Plos One*, 12 (2017) e0187962.
- [186] D. Carugo, E. Bottaro, J. Owen, E. Stride, C. Nastruzzi, Liposome production by microfluidics: Potential and limiting factors, 2016.
- [187] J. Veeken, Purification of nanoparticles by hollow fiber diafiltration, *IOP Conference Series: Materials Science and Engineering*, 40 (2012) 012035.
- [188] G. Dalwadi, H.A. Benson, Y. Chen, Comparison of diafiltration and tangential flow filtration for purification of nanoparticle suspensions, *Pharmaceutical research*, 22 (2005) 2152-2162.
- [189] R. Kaur, M. Henriksen-Lacey, J. Wilkhu, A. Devitt, D. Christensen, Y. Perrie, Effect of incorporating cholesterol into DDA: TDB liposomal adjuvants on bilayer properties, biodistribution, and immune responses, *Molecular pharmaceutics*, 11 (2013) 197-207.

- [190] A. Milicic, R. Kaur, A. Reyes-Sandoval, C.-K. Tang, J. Honeycutt, Y. Perrie, A.V.S. Hill, Small Cationic DDA:TDB Liposomes as Protein Vaccine Adjuvants Obviate the Need for TLR Agonists in Inducing Cellular and Humoral Responses, *Plos One*, 7 (2012) e34255.
- [191] L.P.T.H.J. Liang, T.W. Chung, Y.Y.H.D.Z. Liu, Liposomes incorporated with cholesterol for drug release triggered by magnetic field, *Journal of medical and biological Engineering*, 27 (2007) 29-34.
- [192] S. Shaker, A.R. Gardouh, M.M. Ghorab, Factors affecting liposomes particle size prepared by ethanol injection method, *Research in pharmaceutical sciences*, 12 (2017) 346.
- [193] J. Lopez-Pinto, M. Gonzalez-Rodriguez, A. Rabasco, Effect of cholesterol and ethanol on dermal delivery from DPPC liposomes, *International journal of pharmaceutics*, 298 (2005) 1-12.
- [194] C. Socaciu, R. Jessel, H.A. Diehl, Competitive carotenoid and cholesterol incorporation into liposomes: effects on membrane phase transition, fluidity, polarity and anisotropy, *Chemistry and physics of lipids*, 106 (2000) 79-88.
- [195] S.E. McNeil, I. Rosenkrands, E.M. Agger, P. Andersen, Y. Perrie, Subunit vaccines: Distearoylphosphatidylcholine-based liposomes entrapping antigen offer a neutral alternative to dimethyldioctadecylammonium-based cationic liposomes as an adjuvant delivery system, *Journal of pharmaceutical sciences*, 100 (2011) 1856-1865.
- [196] R. Kaur, V.W. Bramwell, D.J. Kirby, Y. Perrie, Pegylation of DDA:TDB liposomal adjuvants reduces the vaccine depot effect and alters the Th1/Th2 immune responses, *Journal of Controlled Release*, 158 (2012) 72-77.
- [197] P.R.P. Salacinski, C. McLean, J.E.C. Sykes, V.V. Clement-Jones, P.J. Lowry, Iodination of proteins, glycoproteins, and peptides using a solid-phase oxidizing agent, 1,3,4,6-tetrachloro-3 α ,6 α -diphenyl glycoluril (Iodogen), *Analytical Biochemistry*, 117 (1981) 136-146.
- [198] M. Henriksen-Lacey, V. Bramwell, Y. Perrie, Radiolabelling of Antigen and Liposomes for Vaccine Biodistribution Studies, *Pharmaceutics*, 2 (2010) 91-104.
- [199] M. Henriksen-Lacey, V.W. Bramwell, D. Christensen, E.-M. Agger, P. Andersen, Y. Perrie, Liposomes based on dimethyldioctadecylammonium promote a depot effect and enhance immunogenicity of soluble antigen, *Journal of Controlled Release*, 142 (2010) 180-186.
- [200] M. Henriksen-Lacey, D. Christensen, V.W. Bramwell, T. Lindenstrøm, E.M. Agger, P. Andersen, Y. Perrie, Comparison of the depot effect and immunogenicity of liposomes based on dimethyldioctadecylammonium (DDA), 3 β -[N-(N', N'-dimethylaminoethane) carbonyl] cholesterol (DC-Chol), and 1, 2-dioleoyl-3-trimethylammonium propane (DOTAP): prolonged liposome retention mediates stronger Th1 responses, *Molecular pharmaceutics*, 8 (2010) 153-161.
- [201] N.L. Tilney, Patterns of lymphatic drainage in the adult laboratory rat, *Journal of Anatomy*, 109 (1971) 369-383.
- [202] D.G. Fatouros, S.G. Antimisiaris, Effect of Amphiphilic Drugs on the Stability and Zeta-Potential of Their Liposome Formulations: A Study with Prednisolone, Diazepam, and Griseofulvin, *Journal of Colloid and Interface Science*, 251 (2002) 271-277.
- [203] F.A. Sharp, D. Ruane, B. Claass, E. Creagh, J. Harris, P. Malyala, M. Singh, D.T. O'Hagan, V. Pétrilli, J. Tschopp, L.A.J. O'Neill, E.C. Lavelle, Uptake of particulate vaccine adjuvants by dendritic cells activates the NALP3 inflammasome, *P Natl Acad Sci USA*, 106 (2009) 870-875.

- [204] E.M. Agger, I. Rosenkrands, J. Hansen, K. Brahimi, B.S. Vandahl, C. Aagaard, K. Werninghaus, C. Kirschning, R. Lang, D. Christensen, M. Theisen, F. Follmann, P. Andersen, Cationic Liposomes Formulated with Synthetic Mycobacterial Cordfactor (CAF01): A Versatile Adjuvant for Vaccines with Different Immunological Requirements, *Plos One*, 3 (2008) e3116.
- [205] M. Hamborg, R. Kramer, C.E. Schanté, E.M. Agger, D. Christensen, L. Jorgensen, C. Foged, C.R. Middaugh, The Physical Stability of the Recombinant Tuberculosis Fusion Antigens H1 and H56, *Journal of Pharmaceutical Sciences*, 102 (2013) 3567-3578.
- [206] R. Kaur, V.W. Bramwell, D.J. Kirby, Y. Perrie, Manipulation of the surface pegylation in combination with reduced vesicle size of cationic liposomal adjuvants modifies their clearance kinetics from the injection site, and the rate and type of T cell response, *Journal of Controlled Release*, 164 (2012) 331-337.
- [207] L.A.T. Hilgers, H. Snippe, M. Jansze, J.M.N. Willers, Combinations of two synthetic adjuvants: Synergistic effects of a surfactant and a polyanion on the humoral immune response, *Cellular Immunology*, 92 (1985) 203-209.
- [208] K. Smith Korsholm, E.M. Agger, C. Foged, D. Christensen, J. Dietrich, C.S. Andersen, C. Geisler, P. Andersen, The adjuvant mechanism of cationic dimethyldioctadecylammonium liposomes, *Immunology*, 121 (2007) 216-226.
- [209] Y. Waeckerle-Men, N. Bruffaerts, Y. Liang, F. Jurion, P. Sander, T.M. Kündig, K. Huygen, P. Johansen, Lymph node targeting of BCG vaccines amplifies CD4 and CD8 T-cell responses and protection against *Mycobacterium tuberculosis*, *Vaccine*, 31 (2013) 1057-1064.
- [210] E.M. Agger, P. Andersen, Tuberculosis subunit vaccine development: on the role of interferon- γ , *Vaccine*, 19 (2001) 2298-2302.
- [211] E. Torrado, A.M. Cooper, IL-17 and Th17 cells in tuberculosis, *Cytokine & Growth Factor Reviews*, 21 (2010) 455-462.
- [212] M. Manish, R. Bhatnagar, S. Singh, Preparation and Characterization of PLGA Encapsulated Protective Antigen Domain 4 Nanoformulation, in: S. Thomas (Ed.) *Vaccine Design: Methods and Protocols*, Volume 2: Vaccines for Veterinary Diseases, Springer New York, New York, NY, 2016, pp. 669-681.
- [213] R.C. Mundargi, V.R. Babu, V. Rangaswamy, P. Patel, T.M. Aminabhavi, Nano/micro technologies for delivering macromolecular therapeutics using poly(D,L-lactide-co-glycolide) and its derivatives, *Journal of Controlled Release*, 125 (2008) 193-209.
- [214] G. Dalwadi, H.A.E. Benson, Y. Chen, Comparison of Diafiltration and Tangential Flow Filtration for Purification of Nanoparticle Suspensions, *Pharmaceutical Research*, 22 (2005) 2152-2162.
- [215] W. Ma, M. Chen, S. Kaushal, M. McElroy, Y. Zhang, C. Ozkan, M. Bouvet, C. Kruse, D. Grotjahn, T. Ichim, B. Minev, PLGA nanoparticle-mediated delivery of tumor antigenic peptides elicits effective immune responses, *International Journal of Nanomedicine*, 7 (2012) 1475-1487.
- [216] M.E.C. Lutsiak, G.S. Kwon, J. Samuel, Biodegradable nanoparticle delivery of a Th2-biased peptide for induction of Th1 immune responses, *Journal of Pharmacy and Pharmacology*, 58 (2006) 739-747.

- [217] M. Riehl, M. Harms, A. Hanefeld, K. Mader, Investigation of the stabilizer elimination during the washing step of charged PLGA microparticles utilizing a novel HPLC-UV-ELSD method, *Eur J Pharm Biopharm*, 94 (2015) 468-472.
- [218] C.G. Jones, Scanning electron microscopy: preparation and imaging for SEM, *Methods Mol Biol*, 915 (2012) 1-20.
- [219] D. Danino, Cryo-TEM of soft molecular assemblies, *Curr Opin Colloid In*, 17 (2012) 316-329.
- [220] H. Cui, T.K. Hodgdon, E.W. Kaler, L. Abezgauz, D. Danino, M. Lubovsky, Y. Talmon, D.J. Pochan, Elucidating the assembled structure of amphiphiles in solution via cryogenic transmission electron microscopy, *Soft Matter*, 3 (2007) 945-955.
- [221] M.O. Oyewumi, A. Kumar, Z. Cui, Nano-microparticles as immune adjuvants: correlating particle sizes and the resultant immune responses, *Expert Rev Vaccines*, 9 (2010) 1095-1107.
- [222] A.N. Martin, P. Bustamante, A.H.C. Chun, *Physical pharmacy : physical chemical principles in the pharmaceutical sciences*, Philadelphia (Pa.) : Lea & Febiger, 1993.
- [223] E. Chiesa, R. Dorati, T. Modena, B. Conti, I. Genta, Multivariate analysis for the optimization of microfluidics-assisted nanoprecipitation method intended for the loading of small hydrophilic drugs into PLGA nanoparticles, *International Journal of Pharmaceutics*, 536 (2018) 165-177.
- [224] S. Stolnik, S.E. Dunn, M.C. Garnett, M.C. Davies, A.G. Coombes, D. Taylor, M. Irving, S. Purkiss, T.F. Tadros, S.S. Davis, Surface modification of poly (lactide-co-glycolide) nanospheres by biodegradable poly (lactide)-poly (ethylene glycol) copolymers, *Pharmaceutical research*, 11 (1994) 1800-1808.
- [225] I. Limayem, C. Charcosset, H. Fessi, *Purification of nanoparticle suspensions by a concentration/diafiltration process*, 2004.
- [226] H.-Y. Kwon, J.-Y. Lee, S.-W. Choi, Y. Jang, J.-H. Kim, Preparation of PLGA nanoparticles containing estrogen by emulsification–diffusion method, *Colloids and Surfaces A: Physicochemical and Engineering Aspects*, 182 (2001) 123-130.
- [227] J.D. Robertson, L. Rizzello, M. Avila-Olias, J. Gaitzsch, C. Contini, M.S. Magoń, S.A. Renshaw, G. Battaglia, Purification of Nanoparticles by Size and Shape, *Scientific Reports*, 6 (2016) 27494.
- [228] K. Nagy, K. VÉKey, Chapter 5 - Separation methods A2 - Vékey, Károly, in: A. Telekes, A. Vertes (Eds.) *Medical Applications of Mass Spectrometry*, Elsevier, Amsterdam, 2008, pp. 61-92.
- [229] M. Halayqa, U. Domańska, PLGA Biodegradable Nanoparticles Containing Perphenazine or Chlorpromazine Hydrochloride: Effect of Formulation and Release, *International Journal of Molecular Sciences*, 15 (2014) 23909-23923.
- [230] D. Cun, D.K. Jensen, M.J. Maltesen, M. Bunker, P. Whiteside, D. Scurr, C. Foged, H.M. Nielsen, High loading efficiency and sustained release of siRNA encapsulated in PLGA nanoparticles: Quality by design optimization and characterization, *Eur J Pharm Biopharm*, 77 (2011) 26-35.
- [231] M. Morales-Cruz, G.M. Flores-Fernández, M. Morales-Cruz, E.A. Orellano, J.A. Rodriguez-Martinez, M. Ruiz, K. Griebenow, Two-step nanoprecipitation for the production of protein-loaded PLGA nanospheres, *Results in Pharma Sciences*, 2 (2012) 79-85.

- [232] X. Cao, M.S. Shoichet, Delivering neuroactive molecules from biodegradable microspheres for application in central nervous system disorders, *Biomaterials*, 20 (1999) 329-339.
- [233] B. Mukherjee, K. Santra, G. Pattnaik, S. Ghosh, Preparation, characterization and in-vitro evaluation of sustained release protein-loaded nanoparticles based on biodegradable polymers, *International journal of nanomedicine*, 3 (2008) 487.
- [234] G. De Rosa, A. Bochot, F. Quaglia, M. Besnard, E. Fattal, A new delivery system for antisense therapy: PLGA microspheres encapsulating oligonucleotide/polyethyleneimine solid complexes, *International journal of pharmaceutics*, 254 (2003) 89-93.
- [235] L. Feng, X.R. Qi, X.J. Zhou, Y. Maitani, S.C. Wang, Y. Jiang, T. Nagai, Pharmaceutical and immunological evaluation of a single-dose hepatitis B vaccine using PLGA microspheres, *Journal of controlled release*, 112 (2006) 35-42.
- [236] C. Witschi, E. Doelker, Influence of the microencapsulation method and peptide loading on poly (lactic acid) and poly (lactic-co-glycolic acid) degradation during *in vitro* testing, *Journal of controlled release*, 51 (1998) 327-341.
- [237] U. Bilati, E. Allemann, E. Doelker, Poly (D, L-lactide-co-glycolide) protein-loaded nanoparticles prepared by the double emulsion method—processing and formulation issues for enhanced entrapment efficiency, *Journal of microencapsulation*, 22 (2005) 205-214.
- [238] B. Koppolu, D.A. Zaharoff, The effect of antigen encapsulation in chitosan particles on uptake, activation and presentation by antigen presenting cells, *Biomaterials*, 34 (2013) 2359-2369.
- [239] T. Kissel, Y. Li, C. Volland, S. Görich, R. Koneberg, Parenteral protein delivery systems using biodegradable polyesters of ABA block structure, containing hydrophobic poly (lactide-co-glycolide) A blocks and hydrophilic poly (ethylene oxide) B blocks, *Journal of controlled release*, 39 (1996) 315-326.
- [240] M. Azizi, F. Farahmandghavi, M. Joghataei, M. Zandi, M. Imani, M. Bakhtiary, F.A. Dorkoosh, F. Ghazizadeh, Fabrication of protein-loaded PLGA nanoparticles: effect of selected formulation variables on particle size and release profile, *Journal of Polymer Research*, 20 (2013) 110.
- [241] J.-P. Colletier, B. Chaize, M. Winterhalter, D. Fournier, Protein encapsulation in liposomes: efficiency depends on interactions between protein and phospholipid bilayer, *BMC biotechnology*, 2 (2002) 9.
- [242] B. prasanth Koppolu, S.G. Smith, S. Ravindranathan, S. Jayanthi, T.K.S. Kumar, D.A. Zaharoff, Controlling chitosan-based encapsulation for protein and vaccine delivery, *Biomaterials*, 35 (2014) 4382-4389.
- [243] S.K. Sahoo, J. Panyam, S. Prabha, V. Labhasetwar, Residual polyvinyl alcohol associated with poly (d,l-lactide-co-glycolide) nanoparticles affects their physical properties and cellular uptake, *Journal of Controlled Release*, 82 (2002) 105-114.
- [244] L.A. Dailey, N. Jekel, L. Fink, T. Gessler, T. Schmehl, M. Wittmar, T. Kissel, W. Seeger, Investigation of the proinflammatory potential of biodegradable nanoparticle drug delivery systems in the lung, *Toxicology and Applied Pharmacology*, 215 (2006) 100-108.

- [245] B. Semete, L. Booyesen, Y. Lemmer, L. Kalombo, L. Katata, J. Verschoor, H.S. Swai, In vivo evaluation of the biodistribution and safety of PLGA nanoparticles as drug delivery systems, *Nanomedicine: Nanotechnology, Biology and Medicine*, 6 (2010) 662-671.
- [246] N. Grabowski, H. Hillaireau, J. Vergnaud, L.A. Santiago, S. Kerdine-Romer, M. Pallardy, N. Tsapis, E. Fattal, Toxicity of surface-modified PLGA nanoparticles toward lung alveolar epithelial cells, *International Journal of Pharmaceutics*, 454 (2013) 686-694.
- [247] T. Parumasivam, S.S.Y. Leung, D.H. Quan, J.A. Triccas, W.J. Britton, H.-K. Chan, Rifapentine-loaded PLGA microparticles for tuberculosis inhaled therapy: Preparation and *in vitro* aerosol characterization, *European Journal of Pharmaceutical Sciences*, 88 (2016) 1-11.
- [248] P.S. Kumar, T.R. Saini, D. Chandrasekar, V.K. Yellepeddi, S. Ramakrishna, P.V. Diwan, Novel approach for delivery of insulin loaded poly (lactide-co-glycolide) nanoparticles using a combination of stabilizers, *Drug delivery*, 14 (2007) 517-523.
- [249] J. Vandervoort, A. Ludwig, Biocompatible stabilizers in the preparation of PLGA nanoparticles: a factorial design study, *International Journal of Pharmaceutics*, 238 (2002) 77-92.
- [250] G. Dawes, L. Fratila-Apachitei, K. Mulia, I. Apachitei, G.-J. Witkamp, J. Duszczyk, Size effect of PLGA spheres on drug loading efficiency and release profiles, *Journal of Materials Science: Materials in Medicine*, 20 (2009) 1089-1094.
- [251] F.Y. Han, K.J. Thurecht, A.K. Whittaker, M.T. Smith, Bioerodable PLGA-Based Microparticles for Producing Sustained-Release Drug Formulations and Strategies for Improving Drug Loading, *Frontiers in Pharmacology*, 7 (2016) 185.
- [252] M. Tracy, K. Ward, L. Firouzabadian, Y. Wang, N. Dong, R. Qian, Y. Zhang, Factors affecting the degradation rate of poly (lactide-co-glycolide) microspheres *in vivo* and *in vitro*, *Biomaterials*, 20 (1999) 1057-1062.
- [253] M. Dunne, O. Corrigan, Z. Ramtoola, Influence of particle size and dissolution conditions on the degradation properties of polylactide-co-glycolide particles, *Biomaterials*, 21 (2000) 1659-1668.
- [254] S.P. Badri Viswanathan, JK Pandil, AK Lele, MG Kulkarni, RA Mashelkar, N, Morphological changes in degrading PLGA and P (DL) LA microspheres: implications for the design of controlled release systems, *Journal of microencapsulation*, 18 (2001) 783-800.
- [255] A. Swed, T. Cordonnier, F. Fleury, F. Boury, Protein Encapsulation into PLGA Nanoparticles by a Novel Phase Separation Method Using Non-Toxic Solvents, 2014.
- [256] H. Keles, A. Naylor, F. Clegg, C. Sammon, Investigation of factors influencing the hydrolytic degradation of single PLGA microparticles, *Polymer Degradation and Stability*, 119 (2015) 228-241.
- [257] J. Panyam, M.M. Dali, S.K. Sahoo, W. Ma, S.S. Chakravarthi, G.L. Amidon, R.J. Levy, V. Labhasetwar, Polymer degradation and *in vitro* release of a model protein from poly (D, L-lactide-co-glycolide) nano-and microparticles, *Journal of Controlled Release*, 92 (2003) 173-187.
- [258] A.R. Mohammed, V.W. Bramwell, A.G.A. Coombes, Y. Perrie, Lyophilisation and sterilisation of liposomal vaccines to produce stable and sterile products, *Methods*, 40 (2006) 30-38.
- [259] A.R. Mohammed, A.G.A. Coombes, Y. Perrie, Amino acids as cryoprotectants for liposomal delivery systems, *European Journal of Pharmaceutical Sciences*, 30 (2007) 406-413.

- [260] T.C. Carvalho, J.I. Peters, R.O. Williams III, Influence of particle size on regional lung deposition—what evidence is there?, *International journal of pharmaceutics*, 406 (2011) 1-10.
- [261] N. Tsapis, D. Bennett, B. Jackson, D.A. Weitz, D. Edwards, Trojan particles: large porous carriers of nanoparticles for drug delivery, *Proceedings of the National Academy of Sciences*, 99 (2002) 12001-12005.
- [262] W.C. Hinds, *Aerosol technology: properties, behavior, and measurement of airborne particles*, John Wiley & Sons, 2012.
- [263] F. De Jaeghere, E. Allémann, J.-C. Leroux, W. Stevels, J. Feijen, E. Doelker, R. Gurny, Formulation and lyoprotection of poly (lactic acid-co-ethylene oxide) nanoparticles: influence on physical stability and in vitro cell uptake, *Pharmaceutical research*, 16 (1999) 859-866.
- [264] W. Abdelwahed, G. Degobert, S. Stainmesse, H. Fessi, Freeze-drying of nanoparticles: Formulation, process and storage considerations, *Advanced Drug Delivery Reviews*, 58 (2006) 1688-1713.
- [265] Y.N. Konan, R. Gurny, E. Allémann, Preparation and characterization of sterile and freeze-dried sub-200 nm nanoparticles, *International Journal of Pharmaceutics*, 233 (2002) 239-252.
- [266] P. Fonte, S. Soares, A. Costa, J.C. Andrade, V. Seabra, S. Reis, B. Sarmento, Effect of cryoprotectants on the porosity and stability of insulin-loaded PLGA nanoparticles after freeze-drying, *Biomatter*, 2 (2012) 329-339.
- [267] S. Bozdog, K. Dillen, J. Vandervoort, A. Ludwig, The effect of freeze-drying with different cryoprotectants and gamma-irradiation sterilization on the characteristics of ciprofloxacin HCl-loaded poly (D, L-lactide-glycolide) nanoparticles, *Journal of pharmacy and pharmacology*, 57 (2005) 699-707.
- [268] S. Hirsjärvi, L. Peltonen, L. Kainu, J. Hirvonen, Freeze-drying of low molecular weight poly (L-lactic acid) nanoparticles: effect of cryo-and lyoprotectants, *J Nanosci Nanotechnol*, 6 (2006) 3110-3117.
- [269] X.C. Tang, M.J. Pikal, Design of freeze-drying processes for pharmaceuticals: practical advice, *Pharmaceutical research*, 21 (2004) 191-200.
- [270] S.D. Allison, M. dC Molina, T.J. Anchordoquy, Stabilization of lipid/DNA complexes during the freezing step of the lyophilization process: the particle isolation hypothesis, *Biochimica et Biophysica Acta (BBA)-Biomembranes*, 1468 (2000) 127-138.
- [271] P. Seville, T.P. Learoyd, H. Li, I.J. Williamson, J. Birchall, Amino acid-modified spray-dried powders with enhanced aerosolisation properties for pulmonary drug delivery, 2007.
- [272] N.Y.K. Chew, B.Y. Shekunov, H.H.Y. Tong, A.H.L. Chow, C. Savage, J. Wu, H.-K. Chan, Effect of Amino Acids on the Dispersion of Disodium Cromoglycate Powders, *Journal of Pharmaceutical Sciences*, 94 (2005) 2289-2300.
- [273] J. Raula, F. Thielmann, M. Naderi, V.-P. Lehto, E.I. Kauppinen, Investigations on particle surface characteristics vs. dispersion behaviour of l-leucine coated carrier-free inhalable powders, *International Journal of Pharmaceutics*, 385 (2010) 79-85.
- [274] Y.I. Jeong, Y.H. Shim, C. Kim, G.T. Lim, K.C. Choi, C. Yoon, Effect of cryoprotectants on the reconstitution of surfactant-free nanoparticles of poly(DL-lactide-co-glycolide), *Journal of Microencapsulation*, 22 (2005) 593-601.

- [275] A. Saez, M. Guzman, J. Molpeceres, M. Aberturas, Freeze-drying of polycaprolactone and poly (D, L-lactic-glycolic) nanoparticles induce minor particle size changes affecting the oral pharmacokinetics of loaded drugs, *Eur J Pharm Biopharm*, 50 (2000) 379-387.
- [276] M. Chacon, J. Molpeceres, L. Berges, M. Guzman, M. Aberturas, Stability and freeze-drying of cyclosporine loaded poly (D, L lactide–glycolide) carriers, *European Journal of Pharmaceutical Sciences*, 8 (1999) 99-107.
- [277] W. Abdelwahed, G. Degobert, H. Fessi, Investigation of nanocapsules stabilization by amorphous excipients during freeze-drying and storage, *Eur J Pharm Biopharm*, 63 (2006) 87-94.
- [278] M. Sameti, G. Bohr, M.R. Kumar, C. Kneuer, U. Bakowsky, M. Nacken, H. Schmidt, C.-M. Lehr, Stabilisation by freeze-drying of cationically modified silica nanoparticles for gene delivery, *International journal of pharmaceutics*, 266 (2003) 51-60.
- [279] F. Danhier, E. Ansorena, J.M. Silva, R. Coco, A. Le Breton, V. Preat, PLGA-based nanoparticles: an overview of biomedical applications, *J Control Release*, 161 (2012) 505-522.
- [280] I. Bala, S. Hariharan, M.R. Kumar, PLGA nanoparticles in drug delivery: the state of the art, *Critical Reviews™ in Therapeutic Drug Carrier Systems*, 21 (2004).
- [281] E. Fröhlich, The role of surface charge in cellular uptake and cytotoxicity of medical nanoparticles, *International journal of nanomedicine*, 7 (2012) 5577.
- [282] H. Takeuchi, H. Yamamoto, T. Toyoda, H. Toyobuku, T. Hino, Y. Kawashima, Physical stability of size controlled small unilamellar liposomes coated with a modified polyvinyl alcohol, *International journal of pharmaceutics*, 164 (1998) 103-111.
- [283] M. Zambaux, F. Bonneaux, R. Gref, P. Maincent, E. Dellacherie, M. Alonso, P. Labrude, C. Vigneron, Influence of experimental parameters on the characteristics of poly (lactic acid) nanoparticles prepared by a double emulsion method, *Journal of Controlled Release*, 50 (1998) 31-40.
- [284] P. Fonte, F. Araújo, V. Seabra, S. Reis, M. van de Weert, B. Sarmento, Co-encapsulation of lyoprotectants improves the stability of protein-loaded PLGA nanoparticles upon lyophilization, *International Journal of Pharmaceutics*, 496 (2015) 850-862.
- [285] J. Buske, C. König, S. Bassarab, A. Lamprecht, S. Mühlau, K.G. Wagner, Influence of PEG in PEG–PLGA microspheres on particle properties and protein release, *Eur J Pharm Biopharm*, 81 (2012) 57-63.
- [286] A. Giteau, M.C. Venier-Julienne, A. Aubert-Pouëssel, J.P. Benoit, How to achieve sustained and complete protein release from PLGA-based microparticles?, *International Journal of Pharmaceutics*, 350 (2008) 14-26.
- [287] G. Jiang, B.C. Thanoo, P.P. DeLuca, Effect of Osmotic Pressure in the Solvent Extraction Phase on BSA Release Profile from PLGA Microspheres, *Pharmaceutical Development and Technology*, 7 (2002) 391-399.
- [288] B. Amsden, Review of osmotic pressure driven release of proteins from monolithic devices, *J. Pharm. Pharm. Sci*, 10 (2007) 129-143.
- [289] S.T. Beckett, M.G. Francesconi, P.M. Geary, G. Mackenzie, A.P.E. Maulny, DSC study of sucrose melting, *Carbohydrate Research*, 341 (2006) 2591-2599.

- [290] D.W.H. Rankin, CRC handbook of chemistry and physics, 89th edition, edited by David R. Lide, Crystallography Reviews, 15 (2009) 223-224.
- [291] J.H. Flynn, Chapter 14 - Polymer degradation, in: S.Z.D. Cheng (Ed.) Handbook of Thermal Analysis and Calorimetry, Elsevier Science B.V., 2002, pp. 587-651.
- [292] H. Benson, Transdermal Drug Delivery: Penetration Enhancement Techniques, 2005.
- [293] P.W. Stott, A.C. Williams, B.W. Barry, Mechanistic study into the enhanced transdermal permeation of a model β -blocker, propranolol, by fatty acids: a melting point depression effect, International Journal of Pharmaceutics, 219 (2001) 161-176.
- [294] P.W. Stott, A.C. Williams, B.W. Barry, Transdermal delivery from eutectic systems: enhanced permeation of a model drug, ibuprofen, Journal of Controlled Release, 50 (1998) 297-308.
- [295] W. Brostow, T. Datashvili, Miscibility and thermal properties of blends of melamine-formaldehyde resin with low density polyethylene, Materials Research Innovations, 11 (2007) 127-132.
- [296] M. Adler, M. Unger, G. Lee, Surface Composition of Spray-Dried Particles of Bovine Serum Albumin/Trehalose/Surfactant, 2000.
- [297] J. Gliński, G. Chavepeyer, J. Platten, Surface properties of aqueous solutions of L-leucine, 2000.
- [298] U. Francesca, d.A. Ivana, M. Agnese, L.R.M. I., Q. Fabiana, Engineered PLGA nano- and micro-carriers for pulmonary delivery: challenges and promises, Journal of Pharmacy and Pharmacology, 64 (2012) 1217-1235.
- [299] A. Najafabadi, K. Gilani, M. Barghi, M. Rafiee-Tehrani, The effect of vehicle on physical properties and aerosolisation behavior of disodium cromoglycate microparticles spray dried alone or with L-Leucine, 2004.
- [300] N. Y K Chew, P. Tang, H.-K. Chan, J. Raper, How Much Particle Surface Corrugation Is Sufficient to Improve Aerosol Performance of Powders?, 2005.
- [301] M.Y.T. Chow, Y. Qiu, F.F.K. Lo, H.H.S. Lin, H.-K. Chan, P.C.L. Kwok, J.K.W. Lam, Inhaled powder formulation of naked siRNA using spray drying technology with l-leucine as dispersion enhancer, International Journal of Pharmaceutics, 530 (2017) 40-52.
- [302] T. Sou, L.M. Kaminskas, T.-H. Nguyen, R. Carlberg, M.P. McIntosh, D.A.V. Morton, The effect of amino acid excipients on morphology and solid-state properties of multi-component spray-dried formulations for pulmonary delivery of biomacromolecules, Eur J Pharm Biopharm, 83 (2013) 234-243.
- [303] R. L. Wolfenden, L. Andersson, P. Cullis, C. Southgate, Affinities of Amino Acid Side Chains for Solvent Water, 1981.
- [304] X. Xie, W. Lin, C. Xing, Y. Yang, Q. Chi, H. Zhang, Y. Li, Z. Li, Y. Yang, Z. Yang, M. Li, In Vitro and In Vivo Evaluations of PLGA Microspheres Containing Nalmefene, Plos One, 10 (2015) e0125953.
- [305] C.W. Liu, W.J. Lin, Polymeric nanoparticles conjugate a novel heptapeptide as an epidermal growth factor receptor-active targeting ligand for doxorubicin, International Journal of Nanomedicine, 7 (2012) 4749-4767.

- [306] M.R. Lorenz, V. Holzapfel, A. Musyanovych, K. Nothelfer, P. Walther, H. Frank, K. Landfester, H. Schrezenmeier, V. Mailänder, Uptake of functionalized, fluorescent-labeled polymeric particles in different cell lines and stem cells, *Biomaterials*, 27 (2006) 2820-2828.
- [307] R. Zhu, C.-g. Zhang, Y. Liu, Z.-q. Yuan, W.-l. Chen, S.-d. Yang, J.-z. Li, W.-j. Zhu, X.-f. Zhou, B.-g. You, X.-n. Zhang, CD147 monoclonal antibody mediated by chitosan nanoparticles loaded with α -hederin enhances antineoplastic activity and cellular uptake in liver cancer cells, *Scientific Reports*, 5 (2015) 17904.
- [308] M.S. Cartiera, K.M. Johnson, V. Rajendran, M.J. Caplan, W.M. Saltzman, The Uptake and Intracellular Fate of PLGA Nanoparticles in Epithelial Cells, *Biomaterials*, 30 (2009) 2790-2798.
- [309] T. Akagi, F. Shima, M. Akashi, Intracellular degradation and distribution of protein-encapsulated amphiphilic poly(amino acid) nanoparticles, *Biomaterials*, 32 (2011) 4959-4967.
- [310] M.G. Qaddoumi, H. Ueda, J. Yang, J. Davda, V. Labhasetwar, V.H. Lee, The characteristics and mechanisms of uptake of PLGA nanoparticles in rabbit conjunctival epithelial cell layers, *Pharmaceutical research*, 21 (2004) 641-648.
- [311] R. Nicolette, D.F.d. Santos, L.H. Faccioli, The uptake of PLGA micro or nanoparticles by macrophages provokes distinct in vitro inflammatory response, *International Immunopharmacology*, 11 (2011) 1557-1563.
- [312] P.E.M. Fine, Variation in protection by BCG: implications of and for heterologous immunity, *The Lancet*, 346 (1995) 1339-1345.
- [313] A. Roy, M. Eisenhut, R.J. Harris, L.C. Rodrigues, S. Sridhar, S. Habermann, L. Snell, P. Mangtani, I. Adetifa, A. Lalvani, I. Abubakar, Effect of BCG vaccination against Mycobacterium tuberculosis infection in children: systematic review and meta-analysis, *BMJ : British Medical Journal*, 349 (2014).
- [314] C.N. Horvath, C.R. Shaler, M. Jeyanathan, A. Zganiacz, Z. Xing, Mechanisms of delayed anti-tuberculosis protection in the lung of parenteral BCG-vaccinated hosts: A critical role of airway luminal T cells, *Mucosal Immunology*, 5 (2012) 420.
- [315] A. Pawlowski, M. Jansson, M. Sköld, M.E. Rottenberg, G. Källenius, Tuberculosis and HIV Co-Infection, *PLOS Pathogens*, 8 (2012) e1002464.
- [316] K.G. Anderson, K. Mayer-Barber, H. Sung, L. Beura, B.R. James, J.J. Taylor, L. Qunaj, T.S. Griffith, V. Vezys, D.L. Barber, D. Masopust, Intravascular staining for discrimination of vascular and tissue leukocytes, *Nature Protocols*, 9 (2014) 209.
- [317] P. Andersen, K.B. Urdahl, TB vaccines; promoting rapid and durable protection in the lung, *Current Opinion in Immunology*, 35 (2015) 55-62.
- [318] J.S. Woodworth, D. Christensen, P. Andersen, Parenteral-Mucosal prime-boost with a TB subunit vaccine enhances early lung T cells against aerosol M. tuberculosis infection with transient improved protection, *The Journal of Immunology*, 198 (2017) 73.75-73.75.
- [319] P.B. Kang, A.K. Azad, J.B. Torrelles, T.M. Kaufman, A. Beharka, E. Tibesar, L.E. DesJardin, L.S. Schlesinger, The human macrophage mannose receptor directs Mycobacterium tuberculosis lipoarabinomannan-mediated phagosome biogenesis, *The Journal of Experimental Medicine*, 202 (2005) 987-999.

- [320] H. Kohama, M. Umemura, Y. Okamoto, A. Yahagi, H. Goga, T. Harakuni, G. Matsuzaki, T. Arakawa, Mucosal immunization with recombinant heparin-binding haemagglutinin adhesin suppresses extrapulmonary dissemination of *Mycobacterium bovis* bacillus Calmette-Guérin (BCG) in infected mice, *Vaccine*, 26 (2008) 924-932.
- [321] A. Carcaboso, R. Hernandez, M. Igartua, J. Rosas, M. Patarroyo, J. Pedraz, Potent, long lasting systemic antibody levels and mixed Th1/Th2 immune response after nasal immunization with malaria antigen loaded PLGA microparticles, *Vaccine*, 22 (2004) 1423-1432.
- [322] J. Wendorf, J. Chesko, J. Kazzaz, M. Ugozzoli, M. Vajdy, D. O'hagan, M. Singh, A comparison of anionic nanoparticles and microparticles as vaccine delivery systems, *Human vaccines*, 4 (2008) 44-49.
- [323] B.S. Román, J.M. Irache, S. Gómez, N. Tsapis, C. Gamazo, M.S. Espuelas, Co-encapsulation of an antigen and CpG oligonucleotides into PLGA microparticles by TROMS technology, *Eur J Pharm Biopharm*, 70 (2008) 98-108.
- [324] C.S.W. Chong, M. Cao, W.W. Wong, K.P. Fischer, W.R. Addison, G.S. Kwon, D.L. Tyrrell, J. Samuel, Enhancement of T helper type 1 immune responses against hepatitis B virus core antigen by PLGA nanoparticle vaccine delivery, *Journal of Controlled Release*, 102 (2005) 85-99.
- [325] C. Thomas, A. Rawat, L. Hope-Weeks, F. Ahsan, Aerosolized PLA and PLGA nanoparticles enhance humoral, mucosal and cytokine responses to hepatitis B vaccine, *Molecular pharmaceuticals*, 8 (2011) 405-415.
- [326] V. Saini, V. Jain, M.S. Sudheesh, K.S. Jaganathan, P.K. Murthy, D.V. Kohli, Comparison of humoral and cell-mediated immune responses to cationic PLGA microspheres containing recombinant hepatitis B antigen, *International Journal of Pharmaceutics*, 408 (2011) 50-57.
- [327] S. Shafiani, C. Dinh, James M. Ertelt, Albanus O. Moguche, I. Siddiqui, Kate S. Smigiel, P. Sharma, Daniel J. Campbell, Sing S. Way, Kevin B. Urdahl, Pathogen-Specific Treg Cells Expand Early during *Mycobacterium tuberculosis* Infection but Are Later Eliminated in Response to Interleukin-12, *Immunity*, 38 (2013) 1261-1270.
- [328] S. Sakai, K.D. Mayer-Barber, D.L. Barber, Defining features of protective CD4 T cell responses to *Mycobacterium tuberculosis*, *Current Opinion in Immunology*, 29 (2014) 137-142.
- [329] M.D. Tameris, M. Hatherill, B.S. Landry, T.J. Scriba, M.A. Snowden, S. Lockhart, J.E. Shea, J.B. McClain, G.D. Hussey, W.A. Hanekom, H. Mahomed, H. McShane, Safety and efficacy of MVA85A, a new tuberculosis vaccine, in infants previously vaccinated with BCG: a randomised, placebo-controlled phase 2b trial, *The Lancet*, 381 (2013) 1021-1028.
- [330] B.J.G. Baaten, C.-R. Li, M.F. Deiro, M.M. Lin, P.J. Linton, L.M. Bradley, CD44 Regulates Survival and Memory Development in Th1 Cells, *Immunity*, 32 (2010) 104-115.
- [331] T. Lindenstrøm, J. Woodworth, J. Dietrich, C. Aagaard, P. Andersen, E.M. Agger, Vaccine-induced Th17 cells are maintained long-term post-vaccination as a distinct and phenotypically stable memory subset, *Infection and immunity*, (2012) IAI. 00550-00512.
- [332] C.S. Lindestam Arlehamn, A. Gerasimova, F. Mele, R. Henderson, J. Swann, J.A. Greenbaum, Y. Kim, J. Sidney, E.A. James, R. Taplitz, D.M. McKinney, W.W. Kwok, H. Grey, F. Sallusto, B. Peters, A. Sette, Memory T Cells in Latent *Mycobacterium tuberculosis* Infection Are Directed against Three

Antigenic Islands and Largely Contained in a CXCR3+CCR6+ Th1 Subset, *PLOS Pathogens*, 9 (2013) e1003130.

[333] S.A. Khader, G.K. Bell, J.E. Pearl, J.J. Fountain, J. Rangel-Moreno, G.E. Cilley, F. Shen, S.M. Eaton, S.L. Gaffen, S.L. Swain, R.M. Locksley, L. Haynes, T.D. Randall, A.M. Cooper, IL-23 and IL-17 in the establishment of protective pulmonary CD4+ T cell responses after vaccination and during *Mycobacterium tuberculosis* challenge, *Nature Immunology*, 8 (2007) 369.

[334] D. Kaushal, T.W. Foreman, U.S. Gautam, X. Alvarez, T. Adekambi, J. Rangel-Moreno, N.A. Golden, A.-M.F. Johnson, B.L. Phillips, M.H. Ahsan, K.E. Russell-Lodrigue, L.A. Doyle, C.J. Roy, P.J. Didier, J.L. Blanchard, J. Rengarajan, A.A. Lackner, S.A. Khader, S. Mehra, Mucosal vaccination with attenuated *Mycobacterium tuberculosis* induces strong central memory responses and protects against tuberculosis, *Nature Communications*, 6 (2015) 8533.

[335] L. Garcia-Contreras, Y.-L. Wong, P. Muttill, D. Padilla, J. Sadoff, J. DeRousse, W.A. Germishuizen, S. Goonesekera, K. Elbert, B.R. Bloom, R. Miller, P.B. Fourie, A. Hickey, D. Edwards, Immunization by a bacterial aerosol, *Proceedings of the National Academy of Sciences*, 105 (2008) 4656-4660.

[336] W.R. Barclay, W.M. Busey, D.W. Dalgard, R.C. Good, B.W. Janicki, J.E. Kasik, E. Ribic, C.E. Ulrich, E. Wolinsky, Protection of monkeys against airborne tuberculosis by aerosol vaccination with bacillus Calmette-Guerin, *Am Rev Respir Dis*, 107 (1973) 351-358.